DOE/ER/14208--1-9t.1

CONF-911114-774. 1



Geosciences Research Program ER-15 OFFICE OF BASIC ENERGY SCIENCES

Sedimentary Basin Geochemistry and Fluid/Rock Interactions Workshop

November 18 & 19, 1991 Norman, Oklahoma

MASTER

DISTRIBUTION OF THIS DOCUMENT IS UNLIMITED

School of Geology and Geophysics

THE UNIVERSITY OF OKLAHOMA



Jone,

Disclaimer

This document was prepared as an account of work sponsored by the United States Government. Neither the United States Government nor any agency thereof, nor the Regents of the University of Oklahoma, nor any of their employees, makes any warranty, express or implied, or assumes any legal liability or responsibility for the accuracy, completeness, or usefulness of any information, apparatus, product, or process disclosed, or represents that its use would not infringe privately owned rights. References herein to any specific commercial product, process, or service by its trade name, trademark, manufacturer, or otherwise, does not necessarily constitute or imply its endorsement, recommendation, or favoring by the United States Government or any agency thereof, or The Regents of the University of Oklahoma. The views and opinions of authors expressed herein do not necessarily state or reflect those of the United States Government or any agency thereof or The Regents of the University of Oklahoma and shall not be used for advertising or product endorsement purposes.

The University of Oklahoma is an equal opportunity employer

DISCLAIMER

Portions of this document may be illegible in electronic image products. Images are produced from the best available original document.

Proceedings of the Sedimentary Basin Geochemistry and Fluid/Rock Interactions Workshop

Norman, Oklahoma November 18 & 19, 1991

This work was supported by the Director, Office of Energy Research, Office of Basic Energy Sciences, Engineering and Geosciences Division, of the U.S. Department of Energy under Contract No. DE-FG05-91ER14208.

Foreword

Fundamental research related to organic geochemistry, fluid-rock interactions, and the processes by which fluids migrate through basins has long been a part of the DOE Geosciences program. This segment of our program was given renewed emphasis in 1987. Objectives were to emphasize those principles and processes which would be applicable to a wide range of problems associated with petroleum discovery, occurrence and extraction, waste disposal of all kinds, and environmental management. Research advances are expected to have application in a wide range of areas of immediate interest to DOE's applied technology programs related to energy and environment.

To gain a better appreciation of the progress being made in understanding basinal fluids, their geochemistry and movement, and related research, and to enhance communication and interaction between principal investigators and between DOE and other Federal program managers interested in this topic, I asked the School of Geology and Geophysics at the University of Oklahoma to organize a two-day workshop on this topic similar to one organized by LBL and LLNL at Berkeley on underground imaging last April. The extended abstracts that follow were prepared to accompany presentation made at the workshop, held November 18 and 19, 1991, in Norman, Oklahoma.

William Luth
Program Manager,
Geosciences Research Program,
ER-15
Office of Basic Energy Sciences
U.S. Department of Energy
Washington, DC 20545
301-363-5822
FTS 233-5822

Table of Contents

Abstracts in order of Presentation

Reservoir Heterogeneities of Valley Fill Sandstone Reservoirs Tillman, R.W		
Seismicity Induced by Hydrocarbon Production Segal, P., and McTigue, D		
Assessing the Role of Active and Ancient Geothermal Systems in Evolution of Oil Reservoirs in the Basin and Range Province, Eastern Nevada Hulen, J.B		
Construction of a Calibrated Eustatic Sea Level Curve: Mid-Cretaceous Through Mid-Tertiary		
Sahagian, D.L		
Ammonium Silicate Diagenesis and its Influence on the Interpretation of Fixed-Ammonium Anomalies as an Exploration Tool Ferrell, Jr., R.E., and Williams, L.B		
Organic/Inorganic Interactions of Nitrogen in Oilfields Williams, L.B. and Ferrell, Jr., R.E		
A Study of Hydrocarbon Migration Events: Development and Application of New Methods for Constraining the Time of Migration and an Assessment of Rock-Fluid Interactions Elmore, R.D. and Engel, M.H		
Dynamics of Rock Varnish Formation Raymond, Jr., R., Reneau, S.L., Guthrie, Jr., G.D., Bish, D.L. and Harrington, C.D39		
Evaporites as a Source For Oil Schreiber, B.C., Benalioulhaj, S., Philp, R.P., and Landais, P		
Organic Geochemistry of Continental Margin and Deep Ocean Sediments Whelan, J.K		

Kinetic and Compositional Model of High-Pressure Kerogen Pyrolysis	
Burnham, A.K., Braun, R.L., Reynolds, J.G., and Sweeney, J.J	9
Direct Speciation of Metal and Metalloid Ions by Optical Spectroscopies	
Tait, C.D., Janecky, D.R., Clark, D.L. Ekberg, S.A., Dixon, P.R.,	
Musgrave, J.A., and Bennett, P.C.	≀⊿
Triasgravo, 3.71., and Demiott, 1.0	, ,
Dissociation Quotients of Oxalic and Malonic Acid in Aqueouts NaCl Media	
Kettler, R.M9	8
The Stability of Hydrocarbons and C-O-H Fluids	
Bell, J.L.S., Palmer, D.A., and Drummond, S.E	2
A Search for Evidence of Comet or Asteroidimpacts at Extinction Boundaries	
Orth, C.J. and Attrep, Jr., M	5
Isotope Organic Geochemistry of the Animikie Basin (Minnesota)	
	· ^
Abrajano, T.A., and Holt, B.A	U
Organic Geochemical and Tectonic Evolution of the Midcontinent Rift System:	
Organic Geochemistry and Micropaleontology	
Hayes, J.M., Pratt, L.M., and Knoll, A.H	7
<i></i>	
An Organic Geochemical Study of Crude Oils and Source Rocks in the	
Anadarko Basin, Oklahoma	
Philp, R.P., Alam, M., Wang, H.D14	.2
Geochemistry and Origin of Regional Dolomites	
Hanson, G. N. and Meyers, W.J	1
Hallson, G. N. and Meyers, W.J	1
Stable Isotope Systematics of Burial Diagenesis in the Alberta Deep Basin:	
An Ion Microprobe Study	
Riciputi, L.R., Cole, D.R., Christie, W.H., Rossell, T.M. and Machel, H16	7
Machana Chamical Calf Organization and Northwest Description in Call and	
Mechano-Chemical Self-Organization and Nonlinear Dynamics in Sedimentary Basins	
Ortoleva, P	18

(Table of Contents Continued)

Development of an Experimental Data Base and Theories for Prediction			
of Thermodynamic Properties of Aqueous Electrolytes and Non-			
electrolytes of Geochemical Significance at Supercritical Temperatures and Pressures			
Wood, R.L., Hnedkovsky, L., Lin, C.L., and Shock, E.L	183		
Geochemistry of Crustal Processes to High Temperatures and Pressures			
Subproject: The Solubility of Calcite and Dolomite to Temperatures of			
300 °C and Pressures of 1.3 KBARS*			
Cole, D.R., Wesolowski, D.J., and Drummond, S.E	191		
Geochemistry of Crustal Processes to High Temperatures and Pressures			
Subproject: The Geochemistry of Aluminum in Sedimentary Basin			
Brines			
Wesolowski, D.J. and Palmer, D.A	199		
Stability of Natural Gas in the Deep Subsurface			
Barker, C	215		

Agenda

November 18, 1991 - Oklahoma Memorial Union - Room 6, 3rd floor		
8:00 AM	Introduction - Paul Philp and M. Charles Gilbert	
8:05	Keynote Talk Reservoir Heterogeneities of Valley Fill Sandstone Reservoirs Tillman, R.W. (Consulting Sedimentologist/Stratigrapher, Tulsa, Oklahoma)	
8:45	Seismicity Induced by Hydrocarbon Production Segal, P., (Stanford University) and McTigue, D. (Sandia National Laboratory)	
9:25	Assessing the Role of Active and Ancient Geothermal Systems in Evolution of Oil Reservoirs in the Basin and Range Province, Eastern Nevada Hulen, J.B. (University of Utah Research Institute)	
9:55	Construction of a Calibrated Eustatic Sea Level Curve: Mid-Cretaceous Through Mid-Tertiary Sahagian, D.L. (Ohio State University)	
10:15	BREAK	
10:30	Ammonium Silicate Diagenesis and its Influence on the Interpretation of Fixed-Ammonium Anomalies as an Exploration Tool Ferrell, Jr., R.E., (Louisiana State University) and Williams, L.B. (Arizona State University)	
11:00	Organic/Inorganic Interactions of Nitrogen in Oilfields Williams, L.B. (Arizona State University) and Ferrell, Jr., R.E. (Louisiana State University)	
11:30	A Study of Hydrocarbon Migration Events: Development and Application of New Methods for Constraining the Time of Migration and an Assessment of Rock-Fluid Interactions Elmore, R.D. and Engel, M.H. (University of Oklahoma)	

LUNCH - Sarkeys Energy Center - East Atrium

NOON

1:10 PM	Dynamics of Rock Varnish Formation Raymond, Jr., R., Reneau, S.L., Guthrie, Jr., G.D., Bish, D.L. and Harrington, C.D. (Los Alamos National Laboratory)
1:40	Evaporites as a Source For Oil Schreiber, B.C., (CUNY) Benalioulhaj, S., Philp, R.P., (University of Oklahoma) and Landais, P.
2:10	Organic Geochemistry of Continental Margin and Deep Ocean Sediments Whelan, J.K. (Woods Hole Oceanographic Institution)
2:40	Kinetic and Compositional Model of High-Pressure Kerogen Pyrolysis Burnham, A.K., Braun, R.L., Reynolds, J.G., and Sweeney, J.J. (Lawrence Livermore National Laboratory)
3:10	BREAK
3:25	Direct Speciation of Metal and Metalloid Ions by Optical Spectroscopies Tait, C.D., Janecky, D.R., Clark, D.L. Ekberg, S.A., Dixon, P.R., Musgrave, J.A., (Los Alamos National Laboratory) and Bennett, P.C. (University of Texas at Austin)
3:55	Dissociation Quotients of Oxalic and Malonic Acid in Aqueouts NaCl Media Kettler, R.M. (University of Nebraska Lincoln)
4:25	The Stability of Hydrocarbons and C-O-H Fluids Bell, J.L.S., Palmer, D.A., and Drummond, S.E. (Oak Ridge National Laboratory)
4:55	ADJOURN
November	19, 1991 - Oklahoma Memorial Union - Room 6, 3rd floor
8:00 AM	A Search for Evidence of Comet or Asteroid Impacts at Extinction

Orth, C.J. and Attrep, Jr., M. (Los Alamos National Laboratory)

Boundaries

8:30	Isotope Organic Geochemistry of the Animikie Basin (Minnesota) Abrajano, T.A., and Holt, B.A. (Argonne National Laboratory)
9:00	Organic Geochemical and Tectonic Evolution of the Midcontinent Rift System: Organic Geochemistry and Micropaleontology Hayes, J.M., Pratt, L.M., (Indiana University) and Knoll, A.H. (Harvard University)
9:30	An Organic Geochemical Study of Crude Oils and Source Rocks in the Anadarko Basin, Oklahoma Philp, R.P., Alam, M., Wang, H.D. (University of Oklahoma)
10:00	BREAK
10:15	Geochemistry and Origin of Regional Dolomites Hanson, G. N. and Meyers, W.J. (SUNY at Stony Brook)
10:45	Stable Isotope Systematics of Burial Diagenesis in the Alberta Deep Basin: An Ion Microprobe Study Riciputi, L.R., (University of Tennessee and Oak Ridge National Laboratory) Cole, D.R., Christie, W.H., Rossell, T.M. (Oak Ridge National Laboratory) and Machel, H. (University of Alberta)
11:15	Mechano-Chemical Self-Organization and Nonlinear Dynamics in Sedimentary Basins Ortoleva, P. (Indiana University)
11:45	LUNCH - Oklahoma Memorial Union - Dining Room 5
12:45 PM	Keynote Talk Recent Advances and Current Problems in Petroleum Geochemistry Claypool, G. (Mobil E & P Services, Inc.) no abstract
1:25	Development of an Experimental Data Base and Theories for Prediction of Thermodynamic Properties of Aqueous Electrolytes and Non-electrolytes of Geochemical Significance at Supercritical Temperatures and Pressures Wood, R.L., Hnedkovsky, L., Lin, C.L., (University of Delaware) and Shock, E.L. (Washington University)

1:55	Geochemistry of Crustal Processes to High Temperatures and Pressures Subproject: The Solubility of Calcite and Dolomite to Temperatures of 300 °C and Pressures of 1.3 KBARS*
	Cole, D.R., Wesolowski, D.J., and Drummond, S.E. (Oak Ridge National Laboratory)
2:25	BREAK
2:40	Geochemistry of Crustal Processes to High Temperatures and Pressures Subproject: The Geochemistry of Aluminum in Sedimentary Basin Brines Wesolowski, D.J. and Palmer, D.A. (Oak Ridge National Laboratory)
3:10	Stability of Natural Gas in the Deep Subsurface Barker, C. (University of Tulsa)
3:40	Luth, W., Comments (Program Manager DOE BES Geosciences)
4:00	ADJOURN

RESERVOIR HETEROGENEITIES OF VALLEY FILL SANDSTONE RESERVOIRS

Roderick W. Tillman, Consulting Sedimentologist/ Stratigrapher, Tulsa, Oklahoma

Edward D. Pittman, University of Tulsa

Valley-fill reservoirs in the Morrowan (Pennsylvanian) age Stateline Trend along the Kansas-Colorado border are heterogenous reservoirs which produce from the Stockholm Sandstone. The valleys in which the reservoirs occur were cut by rivers during drops in sea level and remained as conduits (narrow valleys trending perpendicular to the regional shoreline) until sea level began to rise. As sea level rose the valleys were filled from the landward side by rivers or from the seaward side by shoreline processes or alternately by both processes. Reservoir production properties vary greatly between the two major producing facies, river and tidal (estuarine) valley-fill sandstones in Southwest Stockholm field, Kansas. Within the approximately 150 ft thick valley-fill vertical sequence just one of the three sandstones produces. Topographic highs on the valley bottom covering an area as large as 1/2 section reduce the depositional thickness of the reservoir sandstones.

The tidal (estuarine) sands are finer grained and are more clay prone than the river sandstones and as a result have poorer producing properties. River deposits have average porosities of 17% (range from 11 to 20%) and average permeabilities of 835 md (range from 129-1890 md). Tidal channel sands have average porosities of 12% (range from 11 to 17%) and permeabilities of 90 md (range 50 to 110 md). In some wells which contain both river and tidal deposits only the river deposits are perforated. Where tidal sands interfinger with river sands vertical permeability is diminished and flow units are fragmented.

Valley-fill deposits in Southwest Stockholm field differ from deltaic deposits geologically, geometrically and in the distribution of heterogeneities. Overbank and finegrained levee deposits are absent.

Secondary, post burial, events affected the production characteristics of the reservoirs. The post depositional events which affected the reservoirs were quite different in some of the seven geological facies. Where mm thick shale lenses were deposited within sands pressure solution next to the clay has reduced porosity. Up to half of the porosity in Southwest may be leached (secondary) porosity.

SEISMICITY INDUCED BY HYDROCARBON PRODUCTION

Paul Segall

200

Department of Geophysics, Stanford University Stanford, California 94305-2215

Tel: (415) 725-7241

E-Mail segall@kilauea.stanford.edu

and

David F. McTigue
Fluid Mechanics and Heat Transfer Division 1511
Sandia National Laboratory
Albuquerque, New Mexico 87185
Tel: (505) 844-0450

Our objective is an improved understanding of the mechanisms responsible for seismic and aseismic deformation related to pore-fluid production. Specifically, we are developing physically realistic models to explain the occurrence of earthquakes in hydrocarbon fields under conditions of declining reservoir pressures.

We are concentrating our efforts on a deep gas field in southwestern France, which has been the site of hundreds of shallow, small to moderate earthquakes since 1969. This seismicity is distinctly shallower than tectonic seismicity occurring in the Pyrenees, 25 km to the southwest (Figure 1). The induced seismicity is tightly clustered near the Lacq gas field, with the majority of events occurring above the field (Figure 2). Deeper events below the field began in 1982. The reservoir pressure had declined by \sim 30 MPa at the onset of seismicity, and by \sim 55 Mpa at the onset of deep seismicity (Figure 3). Composite focal mechanisms are heterogeneous, with a tendancy for P-axes to be radially distributed. Repeated leveling shows subsidence localized above the gas reservoir reaching a maximum of 60 mm in 1989.

Previously, we suggested that poroelastic stressing, associated with volumetric contraction of the reservoir rocks, is responsible for induced seismicity associated with fluid extraction and declining pore-pressures. To test this model we make quantitative comparisons between the observations and predicted displacements and stresses.

We find that the relationship between average reservoir pressure decline and subsidence is remarkably linear, lending support to the linear poroelastic model (Figure 4). We estimate the Biot pore-pressure coeficient α by interpolating between published values for high porosity limestones and a value determined by lab measurements for the lowest porosity reservoir limestones, and find $\alpha \sim 0.25$. Using this result and known values for the reservoir depth (3.5 km), thickness (250m), pressure distribution, and elastic properties ($\mu = 2.5 \times 10^4 MPa$, $\nu = 0.25$) it is possible to predict the poroelastic fields without any free parameters. We find that the computed vertical displacements are in reasonable agreement with the observed subsidence (Figure 5). Given these same parameters we compute that poroelastic stress changes at the onset of seismicity (both above and below the reservoir) to be only a few bars!

The implication of this result is that either: (a) the pre-existing deviatoric stress is quite close to failure - even in a previously inactive area, or (b) the faults slip at remarkably low deviatoric stress. The apparent radial distribution of P-axes may support (b) since the perturbing stresses are radially distributed and the earthquake slip directions respond to the sum of the induced and tectonic stresses. It is difficult to appeal to apparent fault weakening due to elevated pore-pressures since pore-pressures above the resevoir where most of the earthquakes are located are known not to be abnormally high.

We find that while we have reasonable constraints on all of the parameters needed to compute stress change due to gas extraction, we do not, have any constraint on the state of stress prior to gas exploitation. This data is critical to a complete understanding of induced seismicity. Consider the two extreme cases: In one limit the pre-extraction deviatoric stress is small. This implies that faults at Lacq are capable of slipping at low stress. While this is now thought to be true for the San Andreas fault, it would be extraordinary if the minor faults at Lacq behaved in the same way as the San Andreas. Furthermore, it is known

from drilling data that the pore fluids in the formations overlying the gas reservoir (where most of the earthquakes occurred) were not over pressured. The alternative is that the deviatoric stress prior to gas extractionwas fairly high. The implication is that everywhere extraction induced seismicity takes place, and this includes Texas and Alberta, as well as possiblyHolland and the North Sea, the earth's crust is within a few bars of failure. This result would be equally extraordinary.

28

4

In either event we have the opportunity at Lacq to answer this question. In the next year we plan to survey existing data for possible information on the magnitude of the least principle stress. Such data could come from leak-off tests or stimulation hydrofrac tests. We will also examine caliper data to ascertain if there is useful breakout data that could be used to determine stress orientation. Finally, we plan to evaluate the feasibility of using existing boreholes for in situ stress measurements.

We will also be using the finite element method to investigate the importance of material heterogeneity on the computed stress state. There is fairly compelling evidence that the seismicity at Lacq is concentrated in the stiffer carbonate units rather than in the more compliant marls. Analytical solutions for heterogeneous media are impractical so we must turn to numerical methods to understand the importance of this effect. We believe that in order to properly analyze rock-fluid coupling when the pore fluid is a gas (as in natural gas fields and in geothermal systems) it will be important to extend the linearized theory to include realistic equations of state for gaseous pore-fluids. In the linearized, Biot theory the fluid density is a linear function of pressure. This is not a good approximation for natural gas. We will be working to extend the existing formulation to consider more realistic equations of state for the pore fluid phase. This is necessary to relate adequately the production data (net mass flux of pore fluid) to the reservoir pressure changes. These considerations may also reveal important nonlinear phenomena associated with the pressure dependent compressibility of gas.

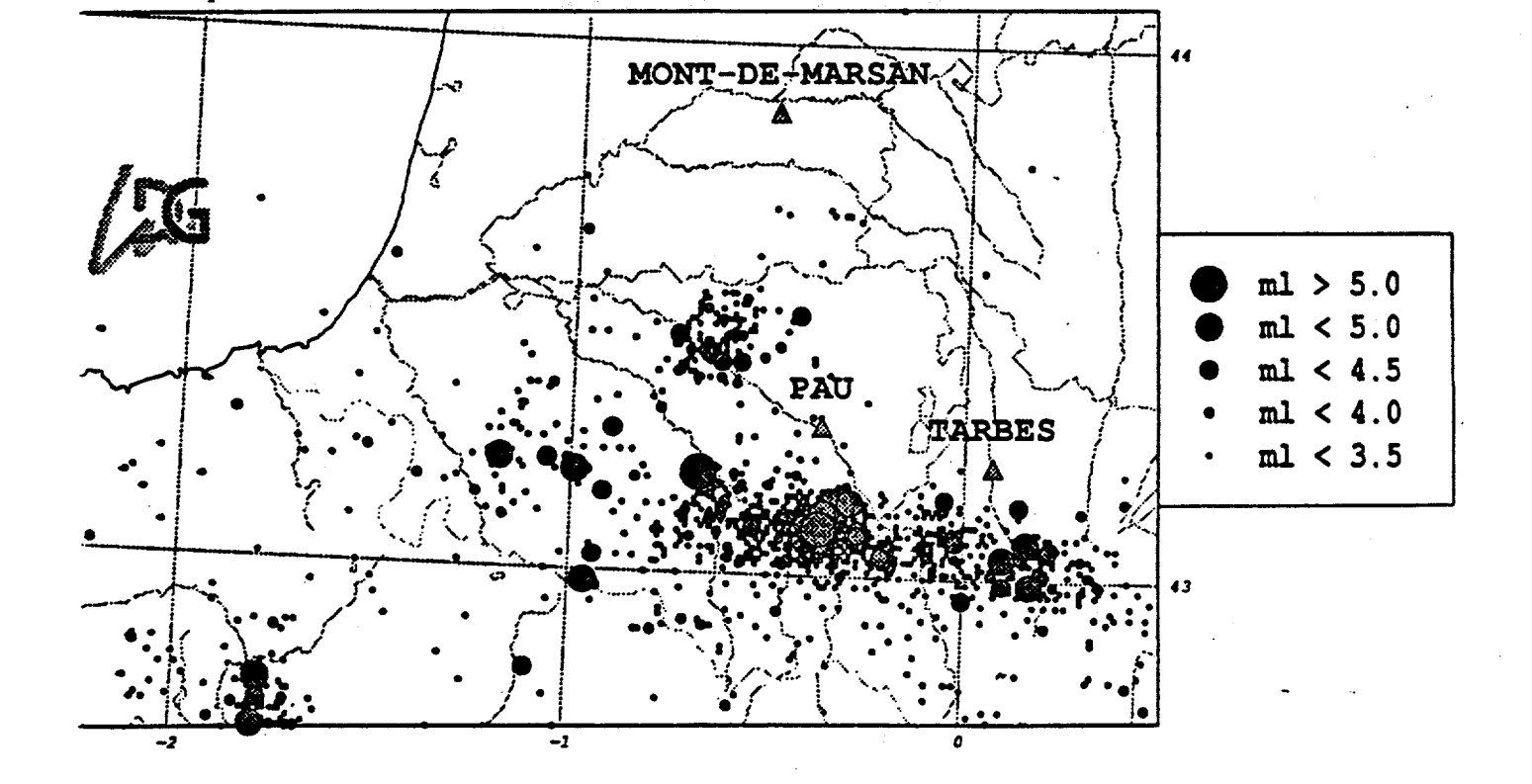


Figure 1. Seismicity in southwestern France during the time period 1962 to 1990. Data is from the national seismic networks of France and Spain. The Lacq gas field is situated in the cluster of earthquakes northwest of the city of Pau.

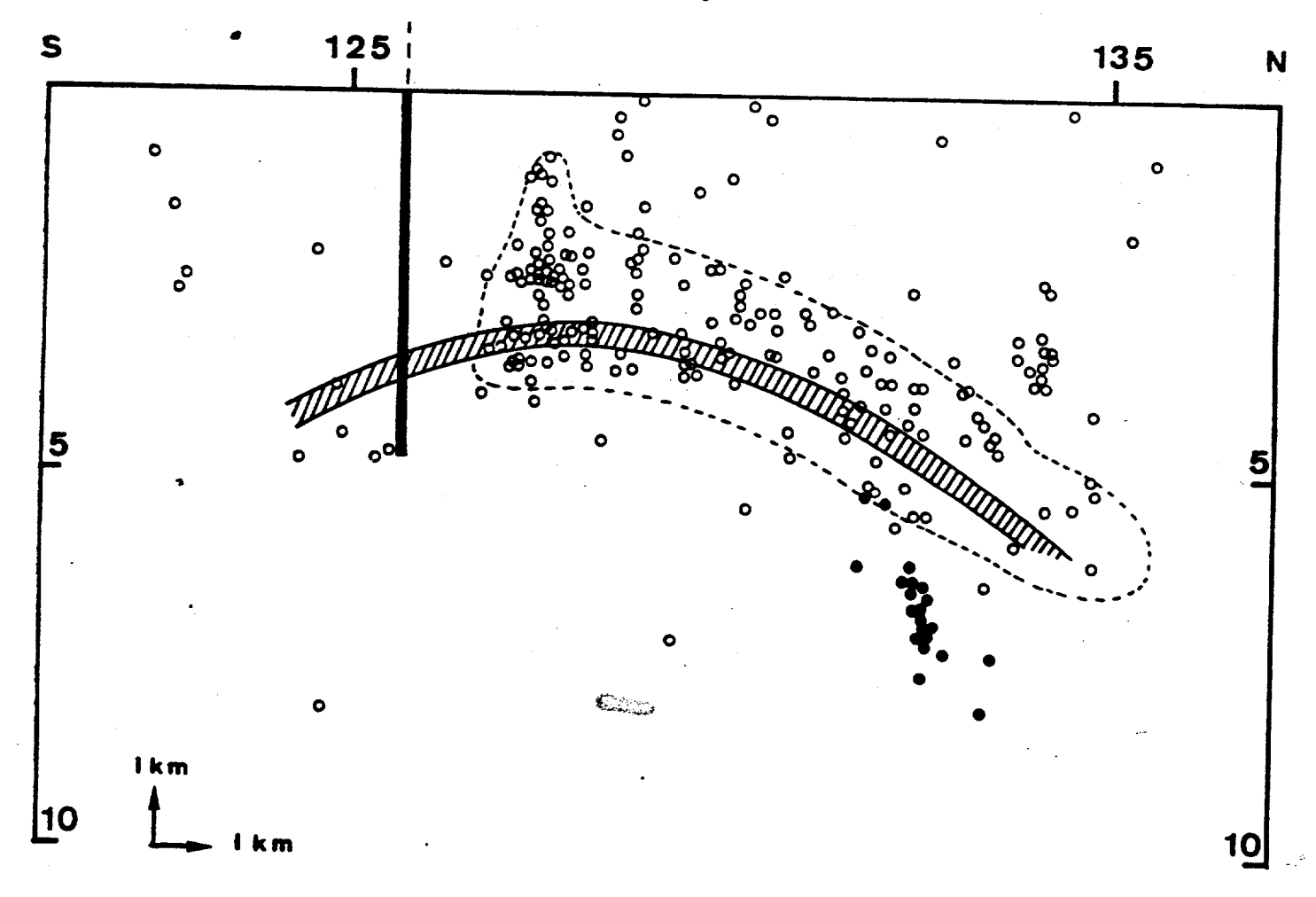


Figure 2. A cross section showing the relationship between the seismicity (circles) and the gas reservoir (cross hatched layer). After Grasso and Feignier 1001

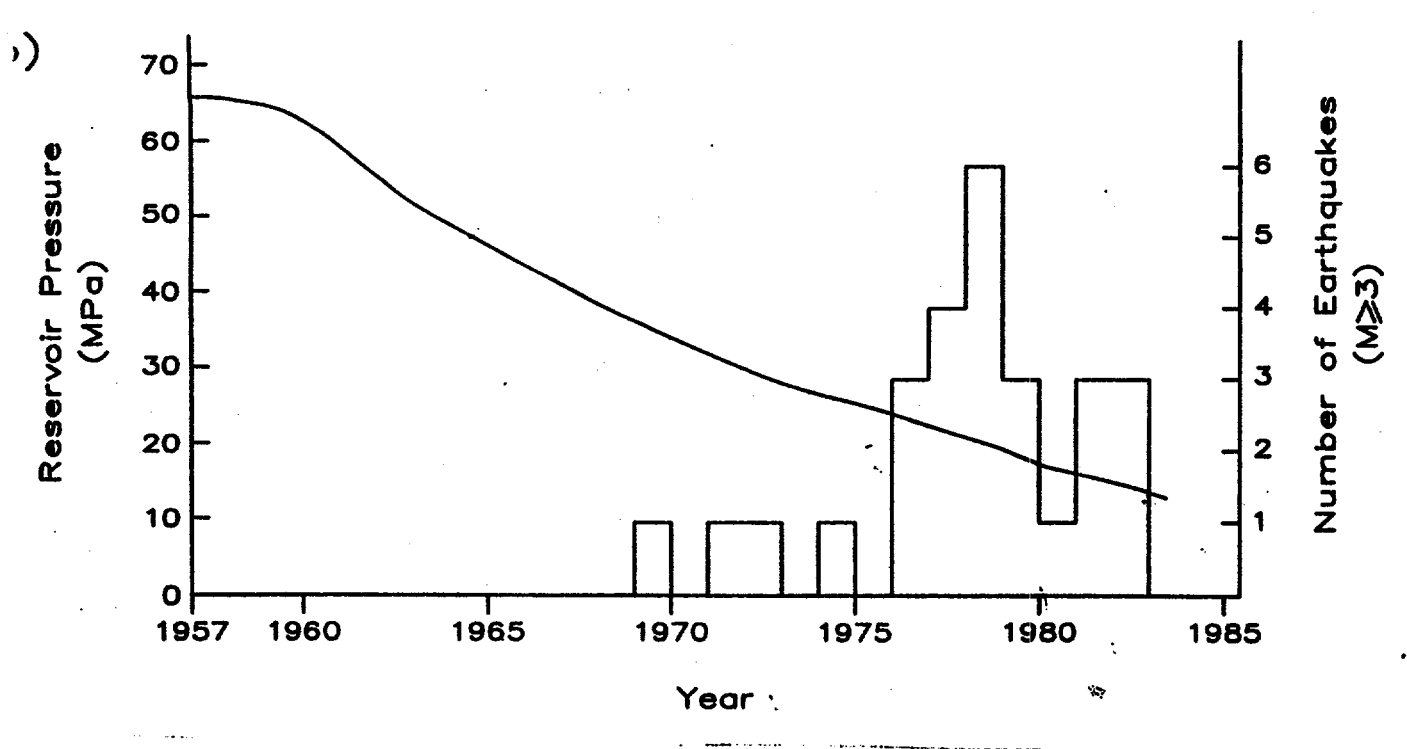


Figure 3. Number of earthquakes recorded per year (M > 3) from the Lacq local seismic network compared to the average reservoir pressure history. After Segall 1989.

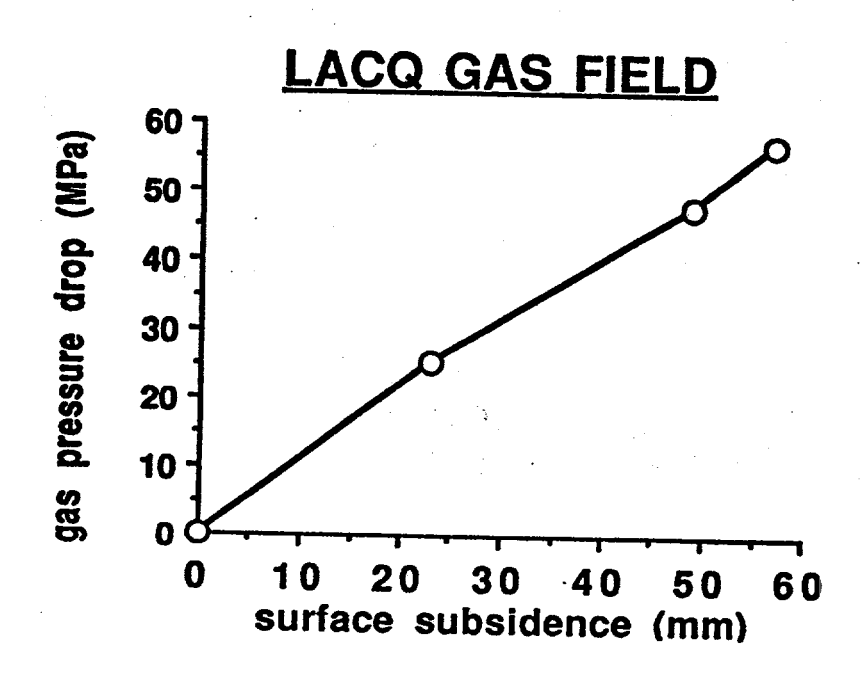


Figure 4. Relationship between average reservoir pressure change and maximum surface subsidence at the Lacq gas field.

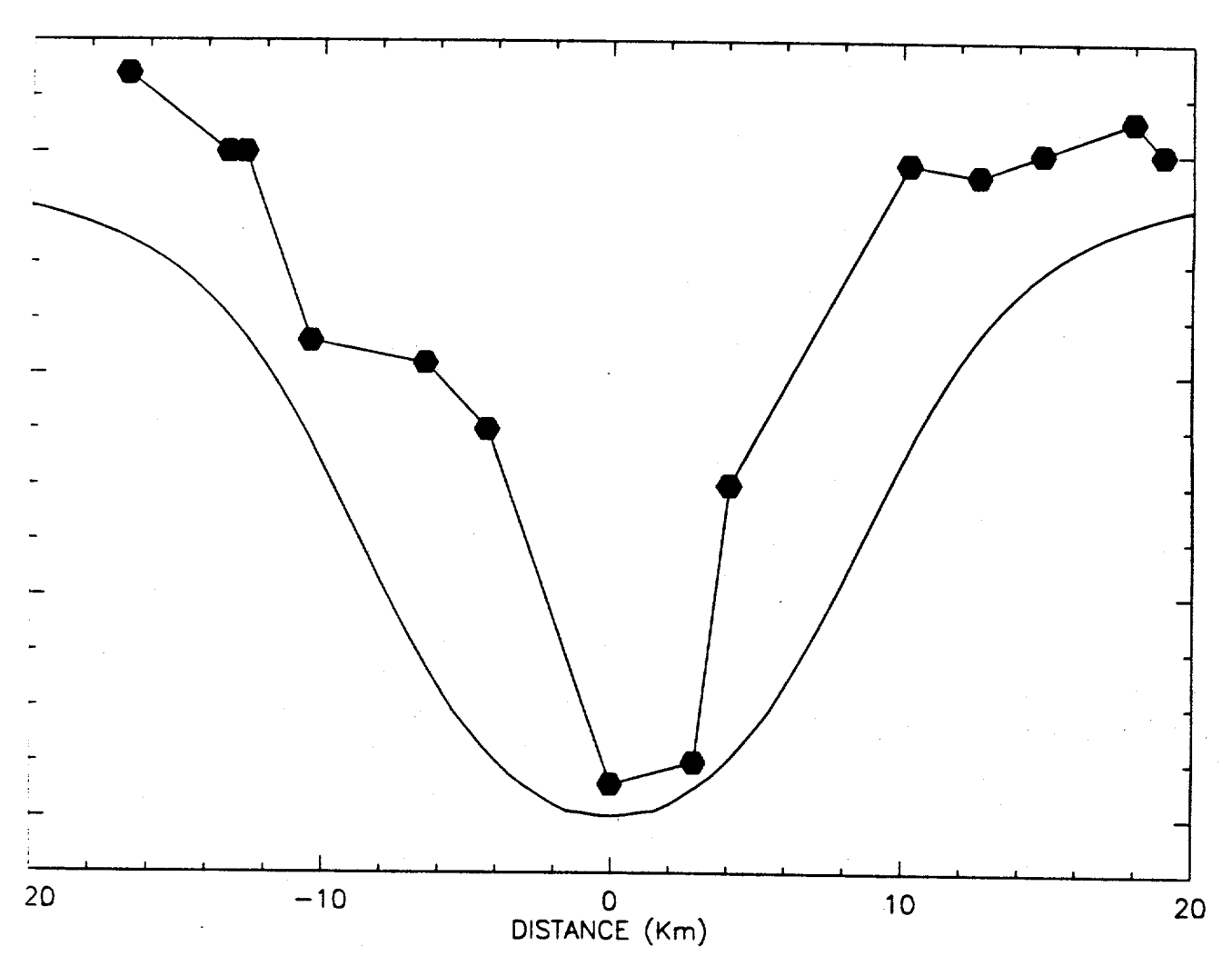


Figure 5. Observed subsidence (1886 to 1989) from releveling (closed symbols) in comparison to the predicted vertical displacement (smooth curve) based on the poroelastic model.

ASSESSING THE ROLE OF ACTIVE AND ANCIENT GEOTHERMAL SYSTEMS IN EVOLUTION OF OIL RESERVOIRS IN THE BASIN AND RANGE PROVINCE, EASTERN NEVADA

Jeffrey B. Hulen University of Utah Research Institute 391-C Chipeta Way Salt Lake City, UT 84108

INTRODUCTION: The known Basin-and-Range oilfields of eastern Nevada (Fig. 1), though small by global standards (reserves of <20 million barrels/field; Montgomery, 1988), are among the world's most intriguing and unusual. For example, many (Trap Springs, Eagle Springs, North Willow Creek, Tomera Ranch, and the newly-discovered Three-Bar field (Fig. 1)) have produced principally from welded ash-flow tuff, certainly a non-traditional petroleum reservoir rock. The Blackburn and Grant Canyon fields (Fig. 1) yield oil from deeply-concealed, intensely brecciated Devonian dolomite (Scott and Chamberlain, 1988; Veal et al., 1988), and at Blackburn these breccias were formed in part by high-temperature (>350°C), natural hydraulic fracturing related to intrusion of a Late Cretaceous granodiorite stock (Hulen et al., 1990).

Perhaps the most intriguing aspect of many of these Nevada oilfields, however, is their apparent connection with active geothermal systems. Reservoir temperature both at Blackburn and Grant Canyon, for example, is about 120°C, representing a thermal gradient several times as high as that prevailing regionally (Hulen et al., 1991; Lachenbruch and Sass, 1978). Even more surprising, at the now shut-in Bacon Flat field near Grant Canyon (Fig. 1), reservoir temperature at 1.7 km depth was measured at 171°C (Veal et al., 1988); production here was actually hampered by associated waters flashing to steam. Further evidence of this petroleum/geothermal connection is provided near the Blackburn field by the famous Bruffey hot springs (Foster et al., 1979), which yield along with near-boiling waters both oil globules and bubbling methane. Results of our research in progress suggest that moderate- to high-temperature geothermal processes may have played a critical role in development of many if not all of the eastern Nevada fields. Understanding how these systems fostered oil-reservoir evolution could enhance exploration efforts for the 100,000,000-barrel fields many believe await discovery in the Basin and Range (e.g. Bortz, 1989).

An exciting and unexpected offshoot of this research project has been discovery of "live" (theoretically producible) oil, both along fractures and as fluid inclusions in vein minerals, at the Yankee gold mine, a low-grade, sediment-hosted gold deposit midway between the Blackburn and Grant Canyon fields (Pinnell et al., 1991; Fig. 1). Results of preliminary geologic, organic geochemical, and fluid-inclusion work at Yankee suggest the possibility that disseminated gold here may have been precipitated from oil-bearing hydrothermal solutions at temperatures very close to those currently measured at both Blackburn and Grant Canyon. Confirmation of this hypothesis could have important implications for Basin-and-Range petroleum and gold exploration.

THE GEOTHERMAL CONNECTION AT GRANT CANYON OIL FIELD: The Grant Canyon oil field, at the eastern margin of Railroad Valley in northern Nye County, Nevada (Fig. 1), has produced since its discovery in 1983 over 15,000,000 barrels of oil, mostly from just two prolific wells (Montgomery, 1988; L.C. Bortz, pers. comm., 1991); one of these wells, in fact, has for years consistently been among the two or three most productive in the continental U.S., yielding over 4,000 barrels of oil per day. A new well just completed in the field (Aug. 1991) is reportedly also producing several thousand barrels per day, and may have extended the ultimate reserves of the field to more than 20,000,000 barrels. Our detailed geologic, petrographic, geochemical, hydrologic, and fluid-inclusion work at Grant Canyon continues to support a geothermal origin for this important Basin-and-Range resource.

Grant Canyon and its small (about 300,000 barrels of oil), inactive companion reservoir, Bacon Flat (Fig. 1), are located at the western margin of Railroad Valley, a broad, northerly-trending, fault-block depression. Geology in the vicinity of these fields is graphically shown on Figures 2 and 3 (on the map, geology of the immediate oil field area is subcrop beneath Tertiary and Quaternary valley-fill deposits). In this portion of Railroad Valley and the adjacent Grant Range to the east, gently folded, non-metamorphosed, mid-Paleozoic carbonate strata have been displaced westward along low-angle normal or "attenuation" faults over metamorphosed siliciclastic and carbonate rocks of Cambrian through Ordovician age (Lund et al., 1991; Kleinhampl and Ziony, 1985). Just south of the map area (Fig. 2), these rocks are intruded by Late Cretaceous granite of the Troy stock (Fryxell, 1988; Kleinhampl and Ziony, 1985. The stock and Paleozoic rocks at Grant Canyon/Bacon Flat are concealed beneath a discontinuous veneer of Oligocene ignimbrites and an overlying blanket of Miocene- to Pleistocene-age alluvial and lacustrine valley-fill deposits (Fig. 3).

Figure 3 is an interpretive east-west geologic section through the Grant Canyon and Bacon Flat fields (modified from Veal et al., 1988, who present several alternative structural interpretations). Read and Zogg (1988) and Lund et al. (1991) suggest that the high-angle Basin-and-Range normal faults shown on this section are subordinate in structural control to the attenuation faults described above, but common to all subsurface interpretations is the reservoir setting for both oil fields -- fractured Paleozoic carbonate capping buried basement highs immediately beneath and sealed by clay-rich, Oligocene- to Miocene-age volcanic and sedimentary rocks.

The principal reservoir rock at both Grant Canyon and Bacon Flat is intensely fractured, brecciated, and hydrothermally veined Devonian dolomite (Hulen et al., 1991; Veal et al., 1988; Read and Zogg, 1988). Vuggy quartz veinlets and breccia cements account for most of the reservoirs' oil-bearing secondary porosity. Our initial interest in these dolomite breccias was their striking compositional and textural similarity to those hosting oil at the Blackburn field, where the brecciation was almost certainly of high-temperature paleohydrothermal origin (Hulen et al., 1991). Unlike the Blackburn breccias, however, those at Grant Canyon have thus far yielded no high-temperature (from fluid-inclusion homogenization temperatures -- T_h) hydrothermal vein material; it may be that attenuation faulting at Grant Canyon produced the "jigsaw-puzzle" textures which at Blackburn bear witness to ancient hydrothermal rock rupture. At Grant Canyon (and Bacon Flat), however, breccia-cementing quartz does contain aqueous and oil-bearing fluid inclusions which dramatically demonstrate an ongoing geothermal influence in the field's development.

Fluid inclusions are abundant in the Grant Canyon and Bacon Flat dolomite breccia reservoir rock. The inclusions occur in both pre-breccia "saddle" dolomite and breccia-cementing quartz, which typically forms veinlets and drusy vug linings of <1-3 mm prismatic crystals. The inclusions are of both primary and secondary origin (according to criteria outlined in Roedder, 1984) and consist of aqueous solution and "live" oil in various proportions. Figure 4A plots Th's vs frequency for 102 Grant Canyon inclusions; 4B shows corresponding data only for primary inclusions (that is, those trapped as the crystals were actually growing). All inclusions homogenized at relatively low temperatures -- aqueous inclusions in saddle dolomite at 96.2-161.3°C; primary oil, water, and oil/water inclusions in quartz at 103.8-120.9°C; and secondary inclusions (or those of ambiguous origin) containing oil and water in various proportions in both dolomite and quartz at 90.4-137.8°C; in this geologic setting pressure corrections (e.g. Potter, 1977) for the quartz-hosted inclusions are considered unnecessary, and T_h's are believed to reflect true trapping temperatures; conditions of inclusion formation for dolomite-hosted inclusions are unknown, so Th's for these must be considered as minimum entrapment temperatures. Ice-melting data indicate that whereas the fluids responsible for saddle dolomite deposition were high-salinity brines, those which precipitated quartz were dilute aqueous fluids (<2.2 wt. % equiv. NaCl).

Quartz-hosted primary inclusions are of paramount significance at Grant Canyon, since these document conditions of initial oil entrapment as well as accompanying silica precipitation. As

seen in Figure 4B, primary oil, oil/aqueous, and aqueous inclusions in quartz were trapped at temperatures ranging from about 100°C to 125°C -- in other words, very close to current reservoir temperatures. If we assume that the free-flowing and fluid-inclusion oils at Grant Canyon share a common origin and evolution (an idea to be tested more rigorously with microanalysis of the inclusion oils), then the fluid-inclusion data displayed in Figure 4A also suggest that since initial oil entrapment, temperatures have never dipped much below those currently prevailing. This in turn would indicate a very young age for the oil reservoir, and suggest permissively that oil generation and entrapment might even now be taking place.

Our working model of geothermal oil migration and entrapment at Grant Canyon/Bacon Flat is shown as Figure 5. Recharge for a hypothetical, moderate- to high-temperature geothermal system is envisioned as meteoric and originating as rain and snowmelt in the Grant Range to the east. These cool recharge waters descend into Railroad Valley along faults and fracture networks of various origins and orientations, warming in response to the local geothermal gradient. As they are heated, the fluids dissolve silica and various other constituents from the rocks through which they percolate. Eventually, they rise as an upwelling geothermal plume controlled by permeable high-angle fault zones. At this point, the waters have incorporated liquid petroleum, perhaps generated by the heat source driving the geothermal system; perhaps derived from an older, deeper reservoir. As the oil- and silica-charged waters encounter porous dolomite breccias capping subvalley-fill structural highs, they begin to migrate laterally beneath a seal of argillized Tertiary ignimbrites and sedimentary rocks; the seal is probably enhanced by silicification and local sulfide and calcite mineralization. Silica precipitates in the dolomite breccias as euhedral quartz, entrapping the mineralizing fluid and contained oil as fluid inclusions. As oil continues to separate from water in the structural trap, quartz precipitation eventually ceases. The oil-depleted waters migrate laterally away from the trap, westward out into Railroad Valley, perhaps eastward and downward to rejoin fresh meteoric recharge and begin the cycle anew.

Figure 6 plots fluid-inclusion Th's for the Grant Canyon oil field relative to preliminary Th's for similar oil, oil/aqueous, and aqueous inclusions in calcite from realgar, orpiment, and goldbearing calcite veins at the "Carlin-type" Yankee gold mine in the Alligator Ridge mining district in eastern Nevada (Fig. 1; see also Pinnell et al., 1991). The mean Th of the Yankee inclusions, about 90°C, is only slightly less than the mean Th of the inclusions at Grant Canyon (note that a cooling trend, missing for Grant Canyon, is apparent in the Yankee data). Moreover, no Th's above about 112°C have been encountered in veins from the mine, yet most Carlin-type gold deposits probably formed at much higher temperatures (150-250°C; Percival et al., 1988). Although our Yankee research is just getting underway, one possible implication of our preliminary fluid-inclusion data is that in the presence of liquid hydrocarbons, gold in the Yankee area may have been transported and precipitated at unusually low temperatures.

REFERENCES

Bortz, L.C., 1989, Oil and gas potential of the Basin and Range province: 28th Int. Geol. Cong., Field Trip Guidebook T-113, p. 1-12

Foster, N.H., Howard, E.L., Meissner, F.F., and Veal, H.K., 1979, The Bruffey oil and gas seeps, Pine Valley, Eureka County, Nevada: Rocky Mtn. Assoc. of Geol. and Utah Geol. Assoc., Basin and Range Symp. and Great Basin Field Conf., p. 531-540.

Fryxell, J.E., 1988, Geologic map and descriptions of stratigraphy and structure of the west-central Grant Range, Nye County, Nevada: Geol. Soc. America, Map and Chart Series MCH064.

Hulen, J.B., Bereskin, S.R., and Bortz, L.C., 1990, High-temperature hydrothermal origin for fractured carbonate reservoirs in the Blackburn oil field, Nevada: AAPG Bull., v. 74, p. 1262-1272.

Hulen, J.B., Bortz, L.C., and Bereskin, S.R., 1991, Geothermal processes in evolution of the Grant Canyon and Bacon Flat oil reservoirs, Railroad Valley, Nye County, Nevada: Nev. Petr. Soc., 1991 Fieldtrip Guidebook, p. 47-54.

Kleinhampl, F.J., and Ziony, J.I., 1985, Geology of northern Nye County, Nevada: Nev. Bur. Mines and Geol., Bull. 99A, 172 p.

Lachenbruch, A.H., and Sass, J.H., 1978, Models of an extending lithosphere and heat flow in the Basin and Range province: Geol. Soc. America Mem. 152, p. 209-250.

Lund, K., Beard, L.S., and Perry, W.J., Jr., 1991, Structures of the northern Grant Range and Railroad Valley, Nye County, Nevada -- Implications for oil occurrences: Nev. Petr. Soc., 1991 Fieldtrip Guidebook, p. 1-6.

Montgomery, S.L., 1988, Nevada: The next great awakening? -- part 2: field summaries and exploration considerations: Petroleum Frontiers, v. 5, pt. 2, 64 p.

Percival, T.J., Bagby, W.C., and Radtke, A.S., 1988, Physical and chemical features of precious metal deposits hosted by sedimentary rocks in the western United States in Bulk-mineable precious metal deposits of the western United States (R.W. Schafer, J.J. Cooper, and P.G. Vikre, eds.): Nev. Geol. Soc., Symp. Proc. (April 6-8, 1987), p. 11-34.

Pinnell, M.L., Blake, J.G., and Hulen, J.B., 1991, Active oil seep at Nevada gold mine holds intrigue for more exploration: Oil and Gas J., Jul. 15, p. 74-79.

Potter, R.W., II, 1977, Pressure corrections for fluid-inclusion homogenization temperatures based on the volumetric properties of the system NaCl-H₂O: U.S. Geol. Survey J. Res., v. 5, p. 603-607.

Read, D.L., and Zogg, W.D., 1988, Description and origin of the Devonian dolomite oil reservoir, Grant Canyon field, Nye County, Nevada in Occurrence and petrophysical properties of carbonate reservoirs in the Rocky Mountain region: Denver, Colo., Rocky Mtn. Assoc. of Geol., p. 229-240

Roedder, E., 1984, Fluid inclusions: Min. Soc. America, Rev. in Min., v. 12, 644 p.

Scott, S., and Chamberlain, A.K., 1988, Blackburn field, Nevada — A case history <u>in</u> Occurrence and petrophysical properties of carbonate reservoirs in the Rocky Mountain region: Denver, Colo., Rocky Mtn. Assoc. of Geol., p. 241-250.

Veal, H.K., Duey, H.D., Bortz, L.C., and Foster, N.H., 1979, Grant Canyon and Bacon Flat oil fields, Railroad Valley, Nevada: The Mountain Geologist, v. 25, p. 193-209.

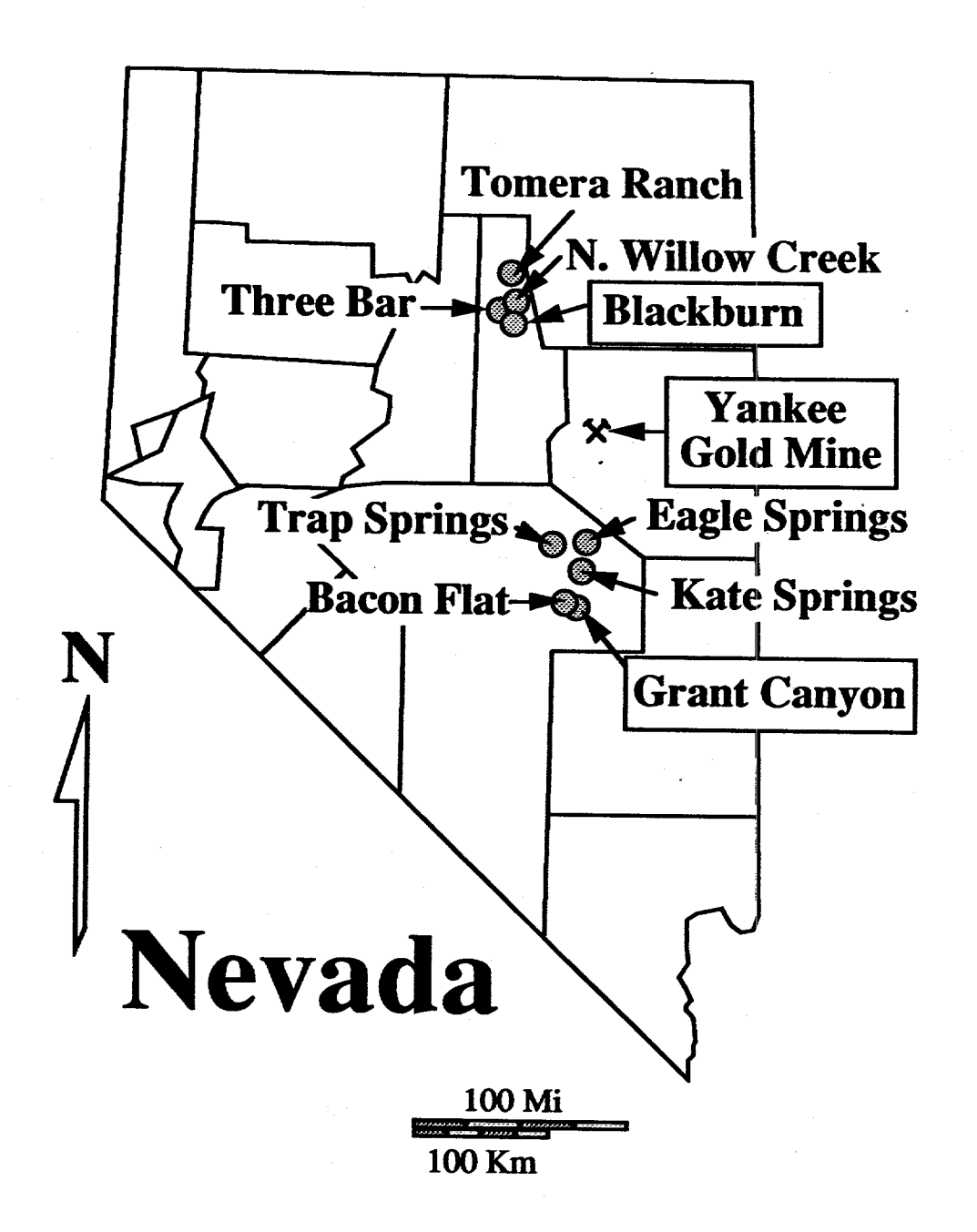


Figure 1. Location map, showing producing oil fields of Nevada and the Yankee gold mine in the Alligator Ridge mining district.

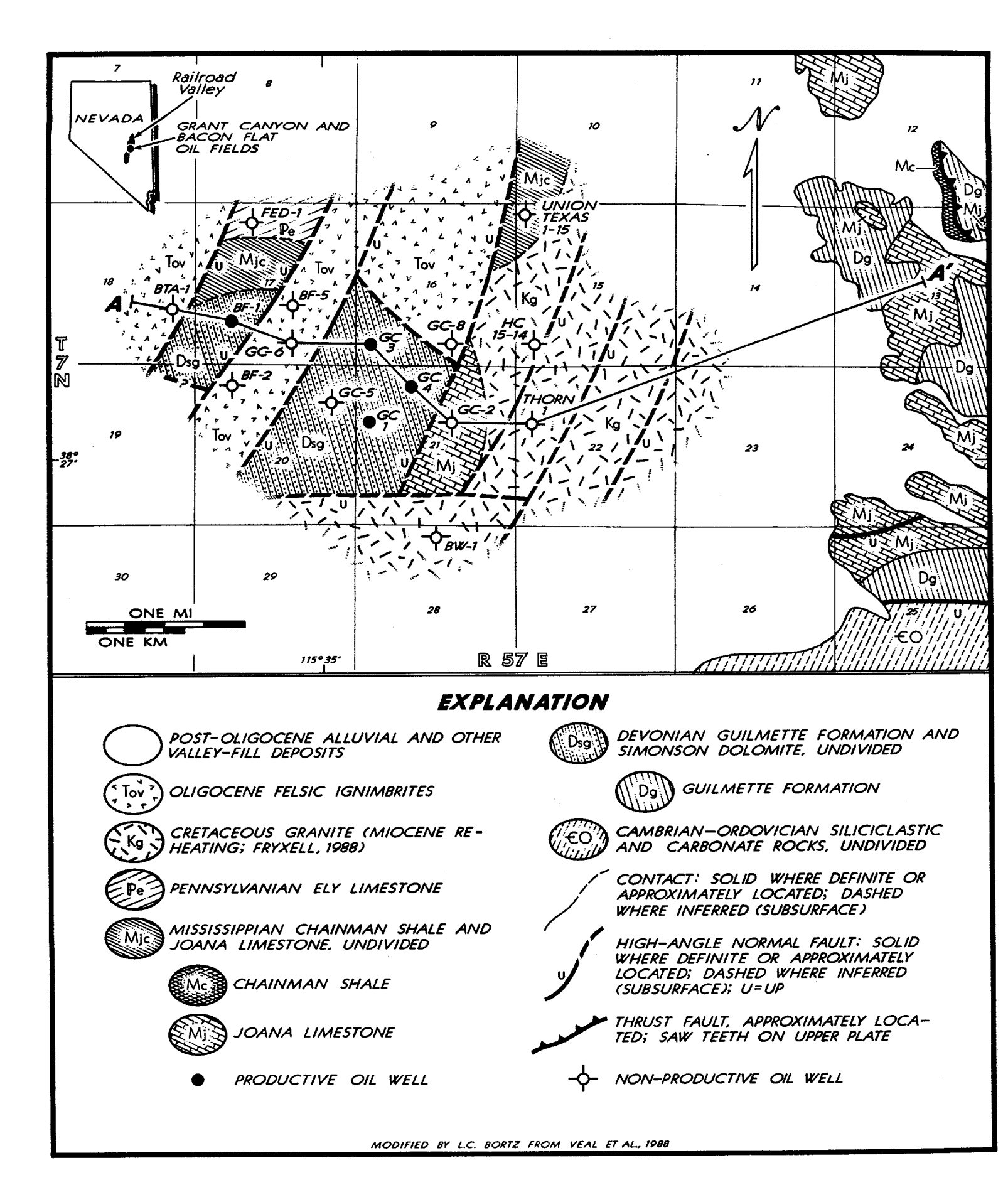


Figure 2. Geologic map of the Grant Canyon and Bacon Flat oil fields and vicinity, Nye County, Nevada.

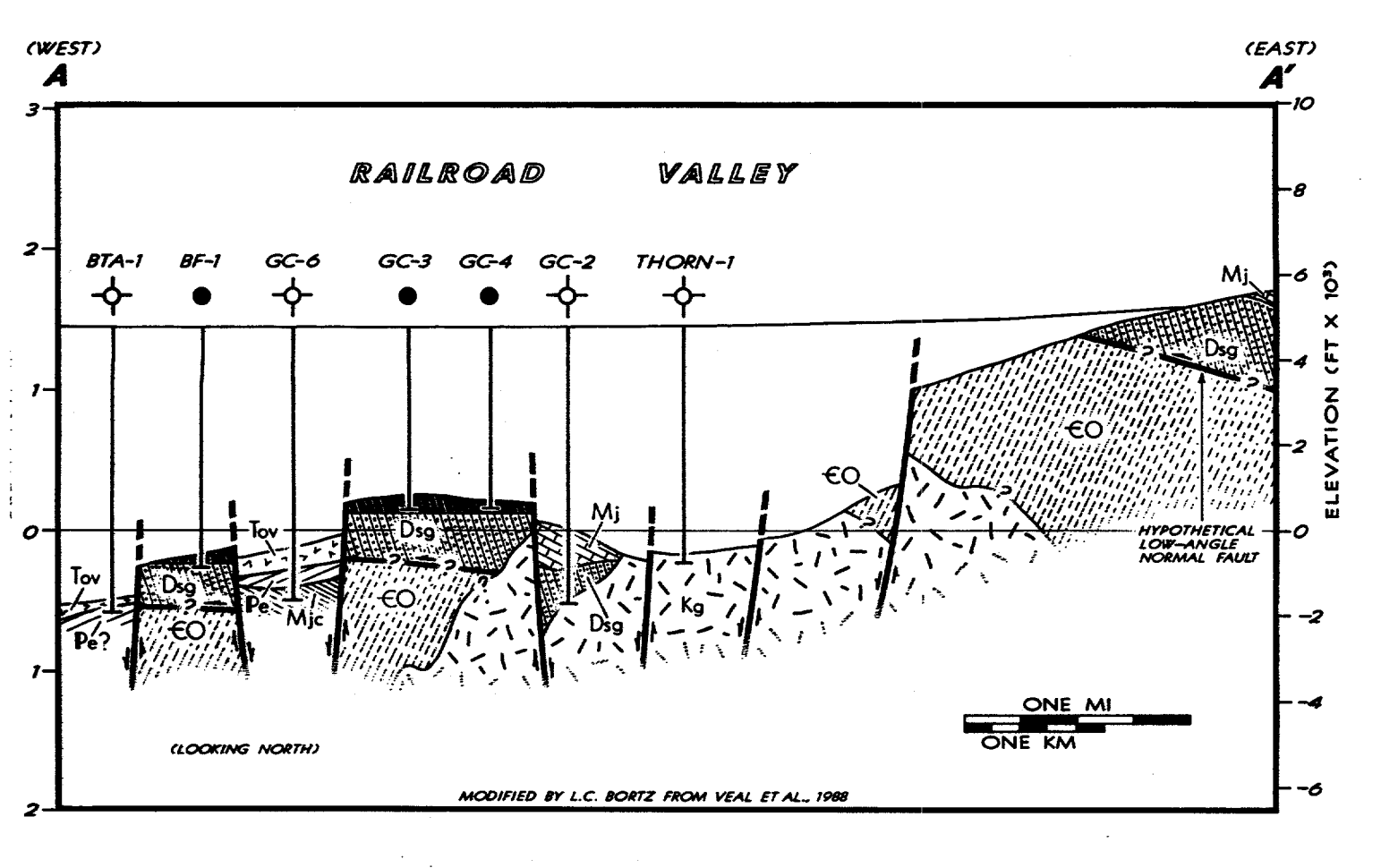


Figure 3. Interpretive west-east geologic section A-A' through the Grant Canyon and Bacon Flat oil fields.

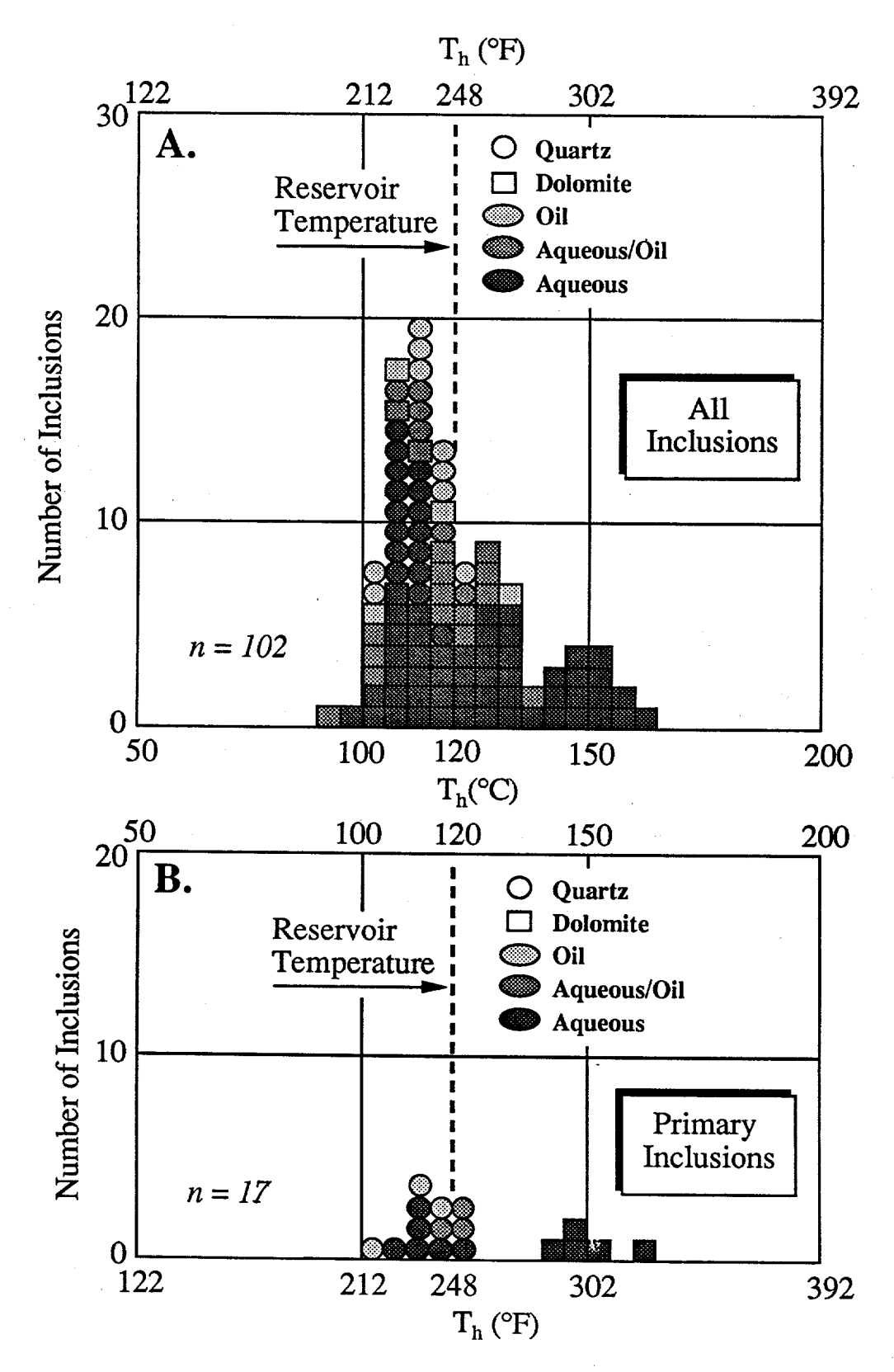


Figure 4. Plots of homogenization temperature (T_h) vs frequency for fluid inclusions from the Grant Canyon oil reservoir.

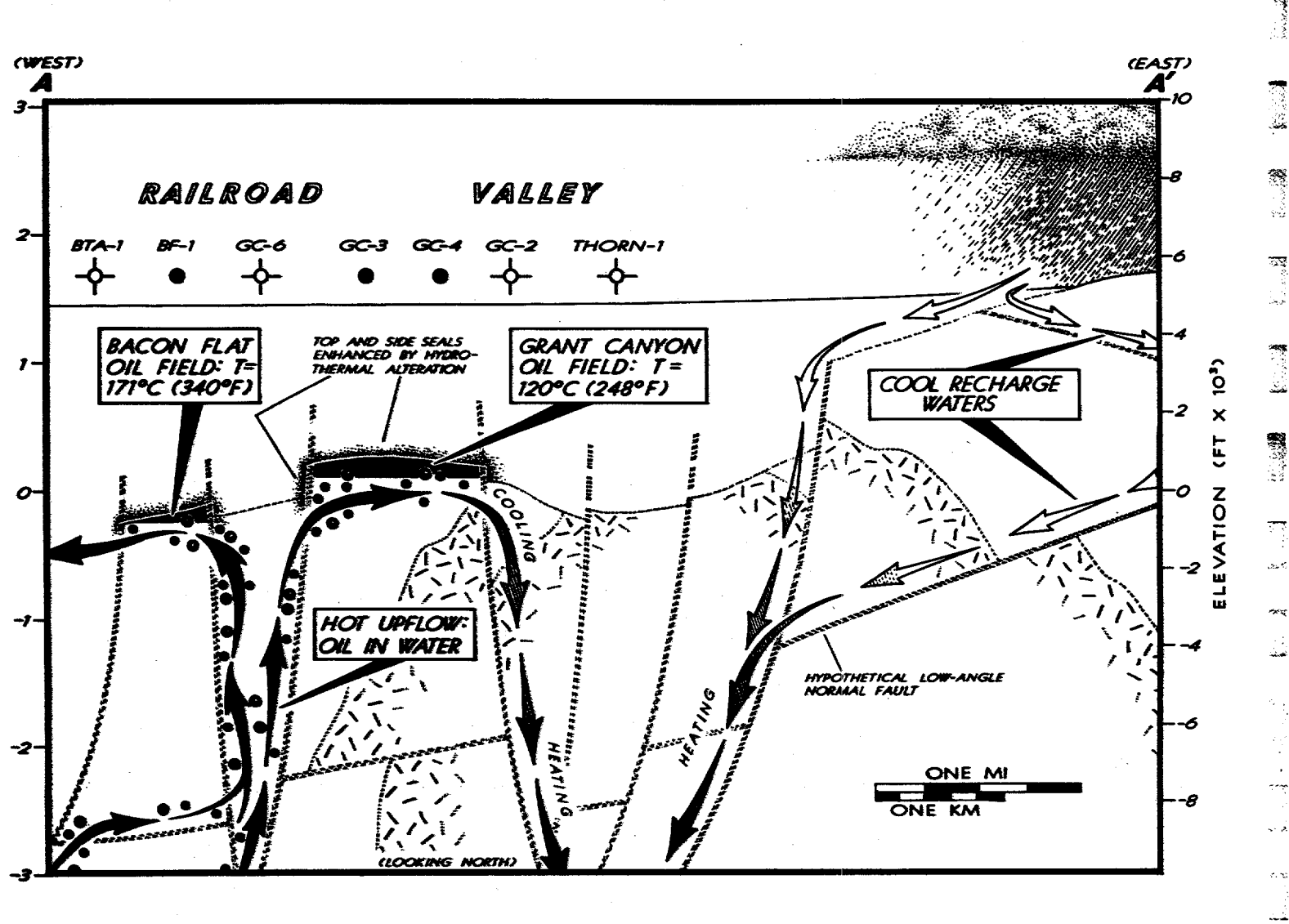
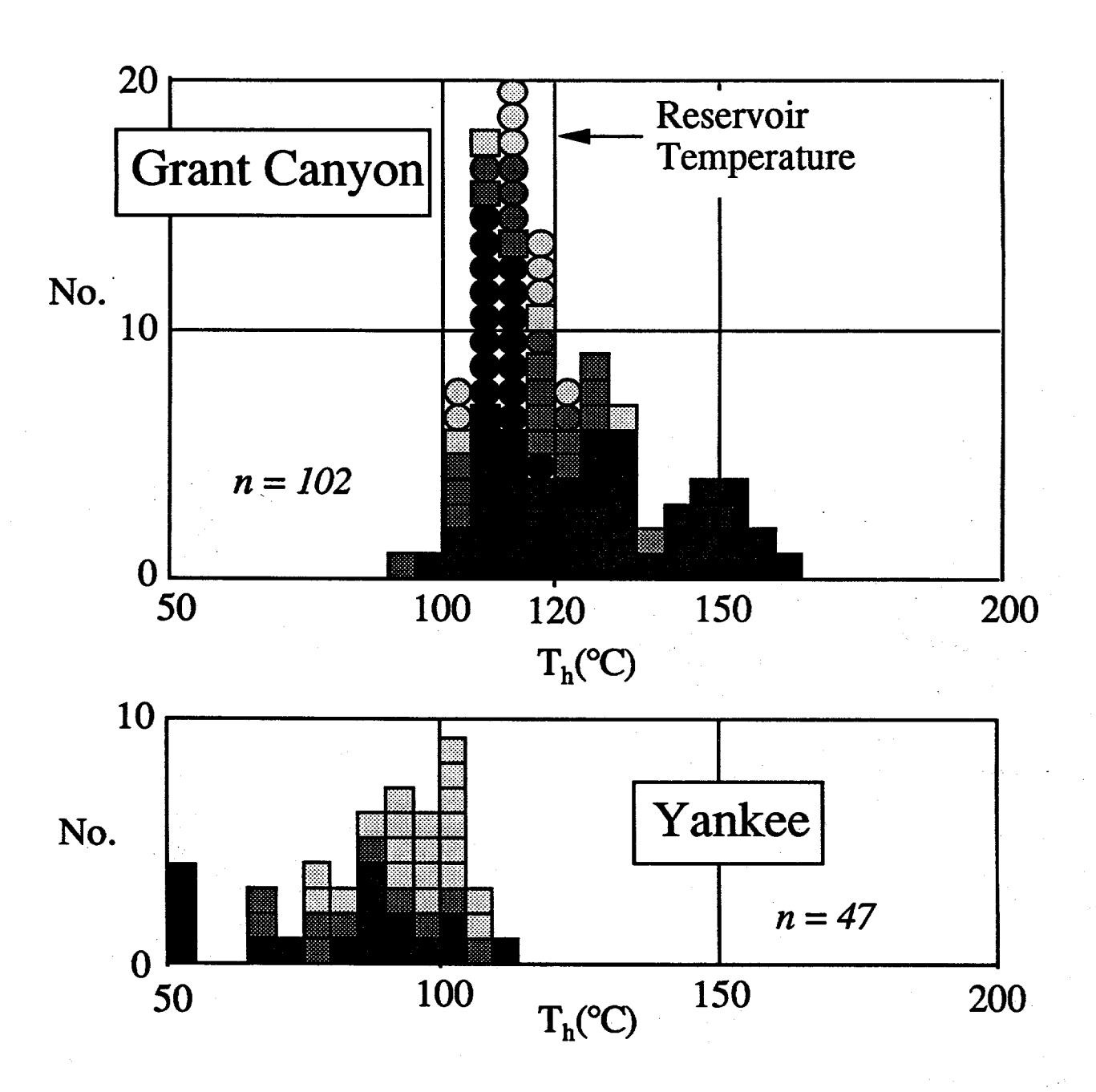
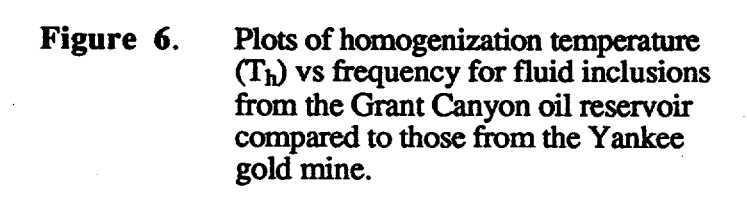
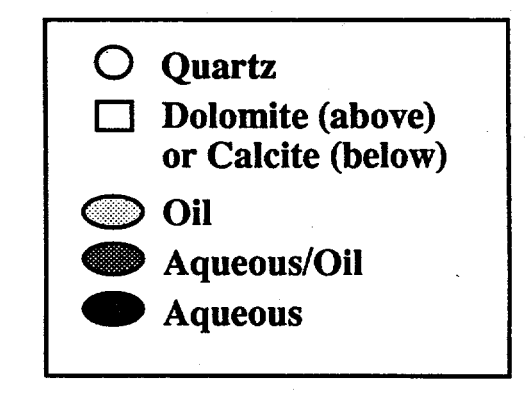


Figure 5. Working model of geothermal oil migration and entrapment at the Grant Canyon and Bacon Flat oil fields.







Construction of a calibrated eustatic sea level curve: Mid-Cretaceous through Mid-Tertiary

Dork L. Sahagian
Department of Geological Sciences
Ohio State University
Columbus, Ohio 43210

SUMMARY

A stable frame of reference is found in the Russian Platform and allows a eustatic curve to be constructed without the subsidence corrections needed for subsiding margins. The stability of the Russian Platform is indicated by flat-lying Mesozoic-Cenozoic sedimentary strata that have remained undeformed and untilted since deposition. These strata are no thicker than 200 m throughout the Russian Platform. Individual lithofacies are continuous over large distances, suggesting a very flat hypsometry in which facies types were particularly sensitive to changes in sea level. The tectonic stability of the Russian Platform allows eustatic curves to be constructed through two complementary methods. The first method, the results of which we present here, uses backstripping to calculate sea level changes from stage to stage. The second method uses the elevation of former shoreline deposits to calculate the net sea-level change from a former sea level to present sea level. Preliminary results suggest an unsteady 110 m rise in sea level from Bajocian to Albian time.

INTRODUCTION

Sea-level change and its impact on sedimentation patterns, climate, ocean chemistry and many other geologic systems have been widely discussed in recent years. The discussion has been primarily qualitative because it has been difficult to quantify sea-level change with appreciable precision. To this end, we identified a stable frame of reference based on the Russian Platform and constructed a calibrated eustatic sea-level curve for the mid-Jurassic through mid-Cretaceous.

In general, sea level is the relation between the elevation of the global sea surface and the elevation of the earth's crustal surface. However, parts of the crust as well as the sea surface have experienced variations in elevation, such that the critical question arises—"Which part of the crustal surface should be used as a reference frame against which to measure past sea levels?" A major difficulty in measuring sea-level change and in correlating sea level from locality to locality has been the lack of a universal reference frame for measurement. Relative sea level change is simply the change in sea-surface elevation relative to some local land area (such as a passive margin, ocean island, etc.). Eustatic sea level change reflects change in the relative volumes of the world's ocean basins and the world's ocean water, and can be measured by recording the change in sea surface elevation relative to some universally adopted reference frame. It is essential that eustatic measurements are obtained using a reference frame that is sensitive only to ocean water volume and ocean basin volume.

REFERENCE FRAMES

Elevation of the earth's land surface is always measured relative to sea level. We wish to measure sea level relative to the earth's land surface. This arrangement is ripe for circularity, which can be avoided by a proper choice of reference frames. Two criteria must be considered in choosing from the many available reference frames. First, the frame must be sensitive only to the relation between ocean water volume and ocean basin volume. Second, sea level must be accurately measurable in the chosen frame. Different reference frames are associated with different methods of measurement. Such frames include the center of the Earth, passive margins, flooded continental areas, the ocean floor, and continental cratonic or stable platform areas.

Each of these reference frames has advantages and disadvantages, but the most suitable frame is one against which eustasy is the only factor affecting stratigraphy, chemistry, or any other tool used for measurement. An unstable frame is useful only for local measurements of relative sea level. For instance, subsiding areas should not be used as a reference frame for eustatic measurements until

they are tied to stable regions by accurately quantifying their subsidence history.

The frame of reference least affected by factors other than eustasy is found in certain stable continental interiors. These areas have remained undeformed and untilted since deposition and may even have maintained a fixed elevation relative to the underlying mantle circulation system. Thus, transgressions and regressions on these areas are the best available measure of the relation between ocean basin volume and water volume. The stability of some interior sections is indicated by the presence of undeformed and flat-lying shoreline and shallow marine sediments. In North America, a large stable area in the region around Minnesota has been used as a frame of reference in the past. Two smaller undeformed areas are located in Africa. The largest and most reliable stable continental area for use as a sea level reference frame is found in the region of the Russian Platform in Eurasia (Fig. 1). Mesozoic and Cenozoic strata preserved over broad areas of the Russian Platform have remained untilted and otherwise undeformed since deposition. While there have been minor Mesozoic reactivations and inversions of some Paleozoic structures, these appear to have been confined to local areas and do not affect the overall stability of the Platform or the specific localities used in this analysis.

Since the undeformed part of the Russian Platform is so extensive, the region can be regarded as a reliable frame of reference for measuring long-term eustatic sea level changes. The inference of a stable Russian Platform is valid if the entire undeformed region was not epeirogenically translated as a unit. Motions of this sort are considered very unlikely, because all known or proposed epeirogenic mechanisms affecting the continental surface independently of the ocean surface act at shorter wavelengths than the observed undeformed region. Thus, the present elevation of shoreline or shallow marine sediments preserved on the Russian Platform can be completely attributed to sea level change.

APPROACH

The tectonic stability of the Russian Platform allows eustatic curves to be constructed through two complementary methods. The first method uses backstripping to calculate the sea level change during each stage or substage in a core or outcrop from data on thicknesses, lithologies, and paleoenvironments of each horizon. The second method measures the present elevation of ancient shallow marine horizons and produces a eustatic curve in which every point is measured relative to modern sea level. In effect, this fixes the position of the curve produced by the first method relative to present sea level.

With no tectonic subsidence, backstripping can be used to directly calculate eustatic variations because water depth and sediment thickness can be inferred or measured from the stratigraphic record. Thus, the large magnitude errors inherent in subsidence corrections are avoided. This method produces an internally consistent calibrated eustatic curve, but unless a continuous record exists through to the present (which it doesn't on the Russian Platform), the eustatic curve is not related to the position of present-day sea level. The curve in figure 2 is calibrated and internally consistent but is not measured relative to the position of modern sea level. However, the curve (Fig. 2) may be approximately related to modern sea level by using previous results that indicate a Cenomanian sea level about 250 meters higher than present sea level.

Because the Russian Platform has been tectonically stable, only one long core should theoretically be needed to produce a eustatic curve when the first method is used, and only one elevation per horizon would be needed to produce a eustatic curve when the second method is used. However, multiple cores and horizons have been used to cross-check the results. The observation of no tectonic subsidence can be reaffirmed by the consistency of the results: if geographically distant sections produce similar eustatic curves, the curves contain no significant tectonic component.

DATA AVAILABILITY

Abundant data are available from the Russian literature for the three principal regions of preserved Mesozoic-Cenozoic shallow-marine sediments on the Russian Platform. Figure 1 indicates the extent of Mesozoic-Cenozoic outcrops on the Russian Platform, which extends from Urals in west to Scandinavia and Polish Trough in east, and from Pechora Basin in north to Dneiper-Donets Basin and Caspian Depression in south. The three principal wells used to generate a calibrated eustatic curve are at Inza, Lomov, and Klimovka. Dark shading in figure 1 indicates regions of preserved Bajocian - Oligocene deposits; light shading indicates regions of preserved Bajocian-Cenomanian deposits. Mid-Jurassic (Bajocian) through Upper Cretaceous (Turonian) deposits are preserved in the Moscow and Kirov regions, and mid-Jurassic (Bajocian) through Oligocene deposits are found in the Penza region. Bajocian strata overlie Devonian through lower Triassic deposits, and Upper Triassic and lower Jurassic deposits are absent on the Russian Platform. Pre-Pleistocene deposits younger than mid-Oligocene are unknown from the central stable part of the Russian Platform, but they are present at the subsiding northern and southern margins of the platform.

Much of the available data consists of stage- and substage-level lithologic logs of outcrops and cores, and paleoecologic data is available for some logs. A few sections are described at the zone level and these offer the maximum time resolution available in this study. The results presented here are based on three well-described cores from Inza, Lomov and Klimovka.

DATA ANALYSIS

Changing water depths, sediment compaction, and loading by both sediments and water must be accounted for in constructing a eustatic curve. The largest potential source of error is estimating water depth during deposition. In our analysis, each horizon is classified according to one of six environments, on the basis of lithology, bedding, sedimentary structures, and fossils (e.g., benthic foraminifera and bivalves). Each environment is assigned a water depth based on an average between equivalent facies depths on modern high- and low-energy coasts. Most strata encountered

appear to have been deposited at 0 - 10 m depth.

The errors introduced by water-depth estimates on the Russian Platform should be small relative to other areas because the hypsometry of the platform was extremely flat during deposition of all Mesozoic-Cenozoic sediments, and water depths were relatively shallow. This extreme hypsometry is suggested by the widespread distribution of individual facies during any given time, and synchronous platform-wide episodes of deposition and nondeposition. Because small changes in sea level would have moved the shoreline great distances, terrigenous sources would have been flooded and exposed by relatively small sea-level changes. Since size of source areas and distances to those source areas affect lithology, small sea-level changes would have driven drastic lithologic changes, making lithology a highly sensitive indicator of sea-level change. Furthermore, a lack of siliciclastics does not necessarily suggest deeper water settings as on many hypsometrically steeper continental margins today. Even chalks may have been deposited in fairly shallow water

(<25 m) if terrigenous sources were largely flooded, as during early Turonian time. We have found no lithologic or paleontologic evidence of the deeper marine settings on the Russian Platform, and

only a few instances of offshore environments.

Corrections for compaction and loading are made through a simple Airy backstripping routine. Each horizon is assigned a sandstone, shale, or limestone compaction curve on the basis of its predominant lithology. The compaction curves were defined by the relation $\phi = \phi_0 e^{-cz}$ where and are final and initial proosities, respectively, z is depth, and c is a compaction coefficient ($c = 5 \times 10^{-4}$ for shale, 3×10^{-4} for sandstone and 7×10^{-4} for limestone). Compaction effects are integrated over the thickness of the unit. Because thicknesses of individual units are nearly constant across the stable part of the Russian Platform, a distance much greater than the lithospheric flexural wavelength, Airy isostatic response to lithospheric loading is maintained. Because of the thinness of most units (40 m or less), errors resulting from compaction and isostatic corrections are minimized.

The relatively thicker Paleozoic section is considered to be compact enough to be unaffected by the thin Mesozoic-Cenozoic overburden.

PRELIMINARY RESULTS

The eustatic sea-level curve based on three wells at Inza, Lomov, and Klimovka is illustrated in Figure 2. The curve shows an unsteady long-term rise in sea level throughout the Late Jurassic and Early Cretaceous of 110 m. The magnitude indicated for sea level fall events is a minimum, because unconformities were encountered at these horizons: the magnitude of sea level drop is at least 0.7 times water depth of the previous horizon. Error sources include water depth estimates and compaction estimates in backstripping calculations. Maximum errors due to choice of compaction coefficients range from 0 in Bajocian to 10 m in Cenomanian. Coefficients used were-sand: $3x10^{-4}$; shale: $5x10^{-4}$; limestone: $7x10^{-4}$. Errors based on water depth estimates range from 0 at unconformities, to roughly 10 m for times of greater water depth (>25 m deep).

Eustatic curves generated by backstripping the wells from Inza, Klimovka, and Lomov are very similar despite being geographically separated by hundreds of kilometers, further supporting our previous observations of a tectonically stable Russian Platform. The sea-level curves quantify sea-level changes from 170 to 97 Ma but are not tied to modern sea level. Consequently, the curves depict only the quantitative change of sea level during that time interval and not the height of sea level above present sea level. The temporal resolution of this curve is about 3-5 m.y., the average duration of the sampling intervals. The eustatic resolution is on the order of 10 m, reflecting the variation in

facies depths on modern shelves.

The Lomov well is the longest and indicates a slow, rise in long-term sea-level of 1.6 m/m.y. from Bajocian through Oxfordian, time a slower fall (0.3 m/m.y.) from the Oxfordian through Hauterivian, and a decreasingly rapid rise (2.4 m/m.y.) from the Hauterivian through the late Albian. The Inza and Klimovka wells show nearly the same magnitude and form of Hauterivian through Albian sea level rise. The discrepancies of up to 20 m between the curves during the Berriasian are

the result of a different depth interpretation for the Klimovka well.

Eustatic curves generated from all three sections indicate a prominent sea-level fall during the early Albian. The magnitude of this fall is a minimum estimate that is almost entirely dependent on water -depth estimates during the late Aptian. That is, sea level had to fall by at least as much as the water depth (minus sediment fill) in order to generate an unconformity. No early Albian deposits are present in these wells; the early Albian is marked by a presumably subaerial unconformity. Water depth estimates in all three wells during the Late Aptian are 25 m. The isostatic effect of removing 25 m of water is uplift of 7.5 meters, giving a net eustatic fall of 17.5 m. Eustatic sea level could have fallen much more, but as a result of the unconformity, we can only place a minimum estimate on the magnitude of the early Albian sea level fall. Similarly, the falls indicated during the Late Bathonian and Late Callovian are minimum estimates based on water depth estimates of the previous stages.

DISCUSSION

The Russian Platform is ideally suited for sea level quantification due to its stability and hypsometry, as described above. Further, margins with different tectonic subsidence rates may differ in the relative timing of stratigraphic responses to eustatic fluctuations. Because the Russian Platform has had no tectonic subsidence, this problem is less important, because the elevation of eustatic sea level rather than the rate of sea level change controls the location of the shoreline.

The Mesozoic-Cenozoic section on the Russian Platform is highly condensed, being only about 200 m thick. In sequence stratigraphic terms, the section consists of a stacked series of transgressive systems tracts and highstand systems tracts. Indeed, some units such as the late Bajocian and the Valanginian consist of thin phosphatic shelly sand lags, and are possibly transgressive ravinement deposits. Because it has had no tectonic subsidence, the Russian Platform is prone to unconformities and probably lacks shelf margin wedge, lowstand fan, and lowstand wedge systems tracts. During times of unconformities, the upper parts of the highstand deposits

Russian Platform contains many more unconformities than are reported in the literature.

The eustatic curve resulting from this study differs in concept as well as form from those derived by other methods. The most widely cited sea-level curve to date is that of Vail et al. (1977) and Haq et al. (1987), a curve based primarily on sequence stratigraphic analysis of passive margin data. The long-term curve drawn on the peaks of the short-term curve of Haq et al. (1987) indicates a sea level rise from Bajocian to Turonian of 200 meters, in contrast with the 120 meters obtained in this study. We attribute this difference to cumulative sequence thickness and compaction error, in addition to the long-term subsidence of the passive margins upon which the Haq et al. (1987) curve was based.

Harrison (1990) and Harrison et al (1983) constructed a curve based on hypsometry which shows a sea level rise of 80 ± 70 m in the same time period as that considered in this study. Another sea-level curve based on hypsometric analysis (Hallam, 1977; 1984) indicates a 200 m rise in the same time period. We attribute these disparate values and large standard errors associated with this technique to differential epeirogeny and tectonics of active and passive margins, erosion and paleogeographic error, and the assumption that each continent's paleohypsometry was identical to

present hypsometry.

The sea-level curve resulting from this study (Fig. 2) can be considered truly eustatic because it is based on a stable frame of reference and therefore reflects the changes in the relative volumes of global ocean basin volume and water volume. The time resolution of the curve is at the stage and substage level, so individual sequence events cannot be resolved. However, the strengths of this curve and those derived from sequence stratigraphy can be combined by "filling in" the finer stratigraphic detail using sequences from passive margins, where thicker and more complete sections are preserved. As additional data are collected, the eustatic curve can be extended throughout the upper Cretaceous and lower Tertiary. When tied to present sea level and merged with fine resolution passive margin data, this curve will represent the most accurate and precise history of sea level possible for the time period Mid-Jurassic through Mid-Tertiary.

REFERENCES CITED

Hallam, A., 1977, Secular changes in marine inundation of USSR and North America through the Phanerozoic: Nature, 269, p. 769-772.

----, 1984, Pre-Quaternary sea-level changes: Annual Reviews of Earth and Planterary Sciences, v. 12, p. 205-243.

Haq, B.U., Hardenbol, J., and Vail, P.R., 1987, Chronology of fluctuating sea levels since the Triassic: Science, v. 235, p. 1156-1167.

Harrison, C. G. A., 1990, Long-term eustasy and epeirogeny in continents, Revelle, R. ed., Sealevel change: Washington D.C., National Academy Press, p. 141-160.

Harrison, C.G.A., Miskell, K.J., Brass, G.W., Saltzman, E.S., and Sloan, J.L., 1983, Continental hypsography: Tectonics, v. 2, p. 357-377.

Vail, P.R., Mitchum, R.M., and Thompson, S., 1977, Seismic stratigraphy and global changes of sea level: American Association of Petroleum Geologists Memoir 26, p. 49-212.

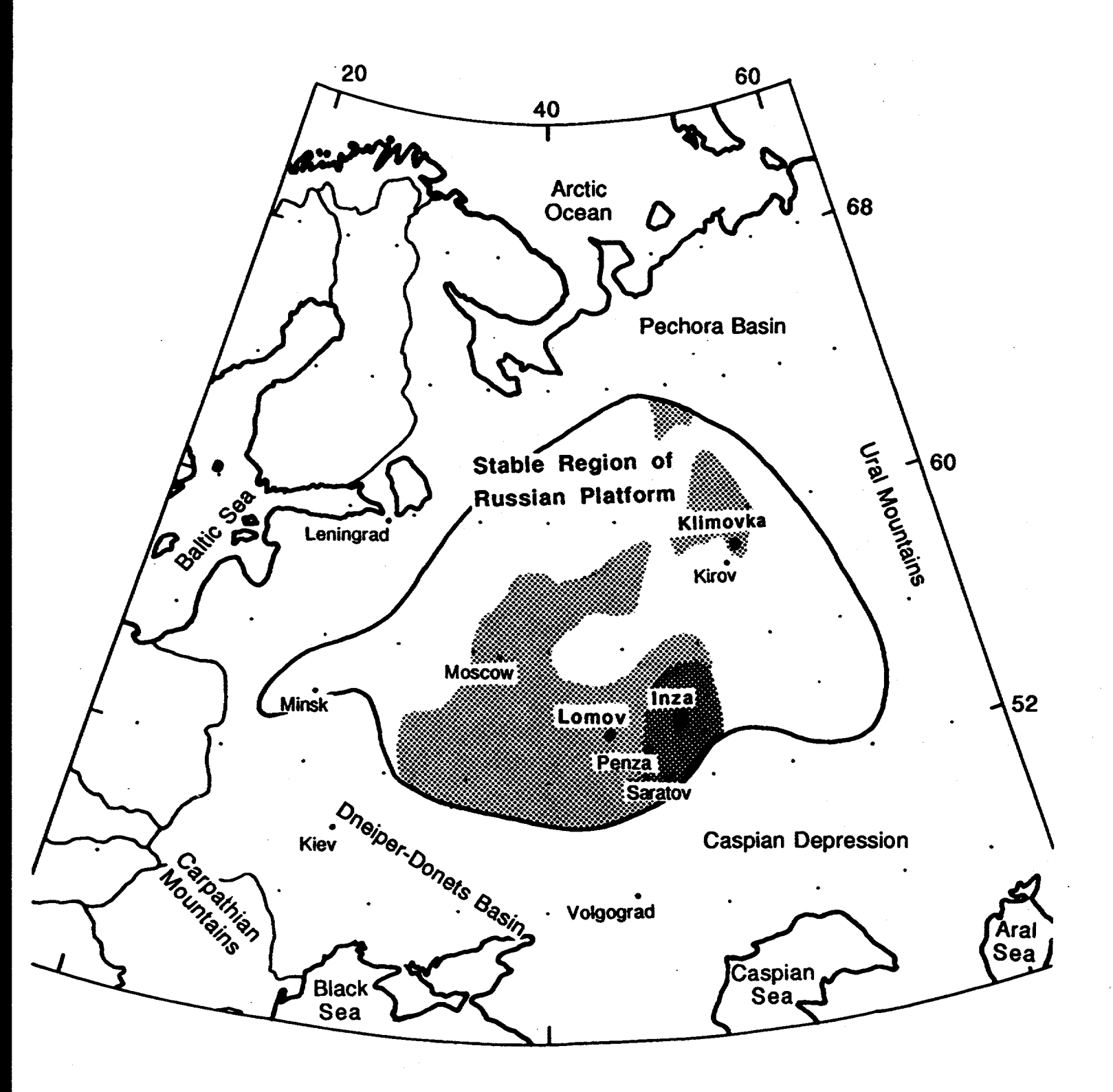


FIGURE 1

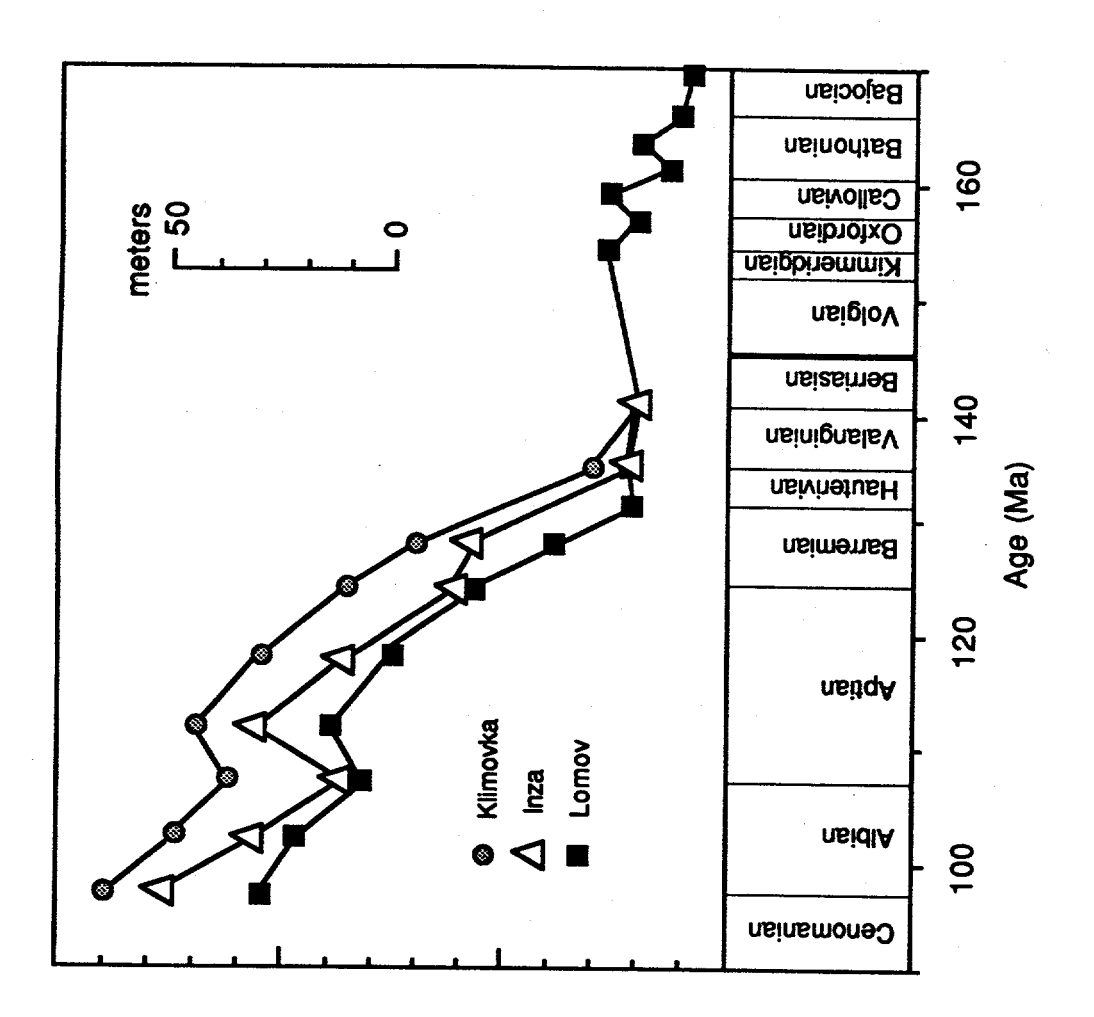


FIGURE 2

AMMONIUM SILICATE DIAGENESIS AND ITS INFLUENCE ON THE INTERPRETATION OF FIXED-AMMONIUM ANOMALIES AS AN EXPLORATION TOOL.(Grant # DE-FG05-87ER13748)

Ray E. Ferrell, Jr. and *Lynda B. Williams, Department. of Geology & Geophysics, Louisiana State University, Baton Rouge, LA

*Current address: Department of Geology, Arizona State University, Tempe, AZ.

Fixed-NH₄ in deeply buried organic-rich sediments is potentially useful in increasing our understanding of hydrocarbon maturity and migration pathways. In many of these deeply-buried, normally reducing environments, N is predominantly in the form of the ammonium ion (NH₄+), which substitutes for K+ in aluminosilicates. NH₄+ integral to a silicate structure is called "fixed-NH₄" and it is protected from environmental fluctuations that might affect dissolved, organic, and exchangeable forms of N. Once fixed, NH₄+ becomes an indicator of the chemical environment existing when the mineral formed.

In our studies, we are careful to remove soluble, organic, and readily exchangeable forms of nitrogen prior to the determination of fixed-NH₄⁺. The Kjeldahl method is employed for all of the data reported herein, however we have found IR absorption results useful in providing a semi-quantitative estimate of NH₄⁺ abundance. We have developed procedures to effectively normalize the analytical determinations with respect to the mineralogy and particle size differences among sandstones and shales. The "concentration" of fixed-NH₄ is expressed in terms of mg/kg of clay-sized (<2µm) material. Fixed-NH₄"substituted" in diagenetic illite is defined in terms of the quantity of illite in the mixed layered illite/smectite.

Our initial investigations have demonstrated that fixed-NH₄ anomalies are associated with hydrocarbon occurrences and can be used to indicate levels of hydrocarbon maturation and to trace paths of hydrocarbon migration. N-speciation and the identity of the host mineral are important to consider in all interpretations. Topics reviewed and the general findings include:

- 1.) Results of Laboratory Experiments. Three CMS reference clays were each reacted in a 0.05M NH₄Cl aqueous solution at 25, 60, and 80°C at pH 4 or 8 under reducing conditions for 128 days. The greatest NH₄-fixation occurred in mixed-layered I/S (Standard ISMT-1) at pH=4. The quantity of NH₄+ fixed is directly proportional to temperature, but equilibrium was not attained in any case. Charge heterogeneity associated with I/S mixed-layered clays and the conversion of smectite to illite are important in controlling the quantities of fixed-NH₄. Fixed-NH₄ results for the Upton, Wyoming bentonite and the Silver Hill illite were very low and erratic with respect to time, temperature, and pH.
- 2. Surface vs Subsurface Fixed-NH₄. Fixed-NH₄ concentrations in shallow cores near a Holocene oil seep in the Green Canyon area were compared to two producing reservoirs at ≈4 km depth in Fordoche Field, Pointe Coupee Parish, Louisiana. The concentrations within mudstones are twice as high at depth and intervals of the sandstone from which oil is extracted contain anomalously high fixed-NH₄ concentrations.
- 3. Fixed-NH₄ in Oil, Gas and Dry Wells. Two cores were examined from the Wilcox Group in Fordoche Field; one from a well producing crude oil, and one from an abandoned gas well at the edge of the field. Core samples from a dry hole in Hurricane Creek Field were also studied. Concentrations of fixed-NH₄ from organic-rich mudstones show a general increase with depth, coincident with increasing organic maturity. Reservoir sandstones containing crude oils show a two-fold increase over background, while fixed-NH₄

concentrations in the gaseous portion of the reservoir are three times background. High values in non-productive intervals suggest migration occurred.

4. Ammonium substitution relative to illite authigenesis. Samples from the contact aureole of the basaltic Walsen dike which intrudes the Cretaceous organic-rich Pierre Shale were studied to learn more about the fixation process. Fixed-NH₄ concentrations increase (to ≈ 1100 mg/kg clay) with the quantity of authigenic illite formed during the smectite-to-illite transformation, but the maximum NH₄-fixation per unit of illite formed occurs within the "oil window" where thermal breakdown of organic matter is rapid. Thermal destruction of the host mineral and the generally higher temperatures within 5m of the dike contribute to low fixed-NH₄ values in the most heavily altered zone.

1.00

- 5. Fixed-NH4 in a high temperature gradient: Salton Sea, California. Fixed-NH4 was analyzed in samples from the US DOE Salton Sea Scientific Drilling Project, where the geothermal gradient is steep. Fixed-NH4 concentrations in this core decrease with depth, but samples below 1200m are metamorphosed (T>300°C) and fixed-NH4 concentrations approach the minimum detection limit. Ammonia (NH3) is the dominant form of N at high temperatures and low pH, and it does not interact with silicates.
- 6. Fixed-NH4 in a high-N gas reservoir: Sorrento Field, Colorado. Analyses revealed no fixed-NH4 anomalies; samples contained fixed-NH4 concentrations approximately equal to background levels of fixed-NH4 observed in the Wilcox cores. Only background levels of fixed-NH4 are expected where N₂ gas predominates.
- 7. Fixed-NH4 in a high organic-N source area: Monterey Fm. Very high fixed-NH4 (up to 1.3% of the illite) was found in organic-rich, quartz-grade siliceous rocks of the Miocene Monterey Formation from the Santa Maria and San Joaquin basins, California. Fixed-NH4 was found to correlate with the amount of diagenetic illite layers in the I/S. Mineralization of NH4⁺ is apparently promoted by the coincident release of abundant NH4⁺ associated with oil generation and the illitization of smectite.

ORGANIC/INORGANIC INTERACTIONS OF NITROGEN IN OILFIELDS (Grant # DE FG02-91ER14218)

Lynda B. Williams, Dept. of Geology, Arizona State University Ray E. Ferrell Jr., Dept. of Geology, Louisiana State University

BACKGROUND

The study of nitrogen diagenesis associated with hydrocarbon occurrences is intended to aid in predicting favorable areas of petroleum exploration and recovery by establishing a better understanding of the interaction of organic maturation products with clastic sedimentary sequences. Our research in the Eocene Wilcox Fm, Louisiana Gulf Coast region, has indicated that fixed-NH4 in clay minerals preserves anomalous NH4+(aq) concentrations, thus recording a significant reaction in the maturation of hydrocarbons; the release of N heteroatoms from kerogen. Fixed-NH4 concentrations generally increase with organic maturity in source rocks (up to T≈150°C). We have found anomalously high fixed-NH4 concentrations in oil and gas reservoirs, and in sandstones that may have acted as migration conduits for a nearby oilfield (Williams et al., 1989; 1991).

We examined samples from the Miocene Monterey Fm, Lost Hills Oil field, San Joaquin Basin, California, to get an idea of the level of fixed-NH₄ in an entirely different basinal setting. The Monterey Fm represents a high-N source rock that produces crude oils containing some of the highest N-contents in the world. While the generated (immature) crude oils are enriched in nitrogen, the remaining kerogen (asphaltene) is also N-enriched. The high nitrogen content allows us to more easily examine the process by which nitrogen is generated from organic compounds and incorporated (as NH₄+) into diagenetic minerals.

The Monterey Fm is thought to be both the source and reservoir rock for the oil it has generated (Graham and Williams, 1985). Petroleum is thought to have migrated a very small distance, essentially accumulating "in situ". This allows examination of N-interactions in a relatively closed system. Temperatures and organic maturity in the Lost Hills field are much lower than those observed in the Louisiana Gulf Coast reservoirs, therefore the investigation of N-Mineralization in the Monterey Fm provides an interesting contrast to the results from earlier studies.

GEOLOGIC SETTING

The Monterey Fm sediments are highly siliceous shales which were deposited in a marine basinal setting of synclinal troughs and anticlinal banks. Coastal upwelling currents are thought to have caused a proliferation of diatoms. Diagenetic alteration of opal-CT to quartz in this

formation causes the unit to become brittle, and tectonic stress produces fractures which become filled with petroleum (Krudge, 1983).

Petroleum in the Lost Hills Field is trapped in an anticlinal structure trending N35°W and dipping to the SE. Drill cuttings were examined from a well drilled by Getty Oil Co. (WELL A-178), located in the SE quad. sec. 15 T27S R21E. Ten samples were provided by the California Well Sample Repository. Samples consist of rock chips collected over 30 ft (9 m) intervals between 3630 ft to 5970 ft (1106 m-1820 m). The lower 5 samples are from the Antelope shale mbr. which is a siliceous silty claystone. The upper 5 samples are from the Reef Ridge mbr. which unconformably overlies the Antelope shale and reflects a more terrestrial detrital input to the San Joaquin basin that began in late Miocene time.

METHODS

Whole rock powders were analyzed by X-ray Diffraction for bulk mineralogical determinations, and <2 μm (e.s.d.) size fractions were mounted as oriented smears in order to determine the clay mineralogy. Rock Eval pyrolysis with a TOC (total organic carbon) analyzer was used for characterization of organic matter in the whole rock samples, and estimates of total-N were made by C-H-N analyzer. Fixed-NH4 concentrations were determined by standard Kjeldahl digestion and distillation procedures described by Keeney and Nelson (1984). Nitrogen collected (as NH4SO4) by this procedure, was analyzed for isotopic composition. Kerogen and bitumen were separated from the whole rock powders by rinsing with methyl chloride, to remove bitumen, and then digesting the mineral matter with HF to isolate kerogen. These samples and a sample of petroleum were then analyzed for C and N isotopic composition.

RESULTS

Fixed-NH4 concentrations increase with depth across the stratigraphic boundary, and reach a maximum in the production interval of well A-178. A rough estimate of the quantity of diagenetic illite was made by multiplying the amount of mixed-layered illite/smectite (I/S) by the degree of illitization. Fixed-NH4 concentrations parallel the amount of diagenetic illite with a correlation coefficient of 0.88. No other mineral phase correlates with the fixed-NH4 values therefore most of the fixed-NH4 is apparently incorporated during diagenetic alteration of smectite to illite.

A Van Krevelen plot of Rock Eval pyrolysis results indicates that the Reef Ridge mbr. contains predominantly type III (terrestrial) kerogen, and the Antelope shale contains predominantly type II (marine) kerogen.

There is no significant variation in the Production Index (S1/S1+S2) or T_{max} over the interval studied. PI values are all <0.2 and T_{max} values are $\approx 410^{\circ}$ C indicating that the petroleum is immature.

A Nitrogen Index was calculated for comparison with Rock Eval pyrolysis parameters (Hydrogen Index and Oxygen Index) in describing variations in the chemistry of kerogens with depth.

Organic-N = (Total-N) - (Fixed-N) Nitrogen Index (NI) = (Organic-N / TOC) x 100

A strong correlation exists between the Nitrogen Index and Oxygen Index (r = 0.97); both decrease with increasing depth and temperature (57°-80°C). Temperature estimates were made assuming a thermal gradient of 1.8°F/100ft (from Phillippi, 1977).

The lower Nitrogen and Oxygen content of the organic matter at depth could be due to increased release of N and O from the kerogen at higher temperature, or could be a characteristic of the type II organic matter (at depth) versus the type III organic matter. Since there is a marked increase in fixed-NH₄ in the Antelope shale relative to the Reef Ridge mbr. we can infer that the type II organic matter was originally enriched in N relative to the type III organic matter. Temperatures at depth (70 - 80°C) are apparently sufficient to have broken C-N and C-O bonds in this type II kerogen, and the N was then incorporated into diagenetic minerals.

C and N-isotopic compositions were determined for the Antelope shale kerogen, bitumen, and petroleum. Fixed-NH₄-N extracted by Kjeldahl methods was also analyzed for N-isotopic composition. The results are shown in Table 1. Fixed-N isotopic values do not vary significantly over the depth interval examined. There is approximately a 1 per mil variation over 1000 m with the lightest isotopic values at depth. The isotopic composition of fixed-NH₄ is ≈3 per mil lighter than that of the petroleum, kerogen, and bitumen.

DISCUSSION

The release of N from kerogen at these temperatures (57 - 80°C) is early in catagenesis, while N is generally thought to be released in later stages of catagenesis. Apparently the type II organic matter in the Monterey Fm contains C-N bonds (aliphatic?) that are easily broken at low temperatures, coincident with the breaking of C-O bonds. The remaining kerogen is still N-enriched, and most likely holds that N in heterocyclic compounds that require higher temperatures to breakdown.

L.A. Williams (1984) suggested that a significant source of petroleum in the Monterey Fm is filamentous bacterial mats that existed in a coastal

upwelling sedimentary environment. Williams examined the bacteria by SEM and tentatively identified them as *Beggiatoa sp.*, a sulfur oxidizing bacteria that fixes nitrogen, and are high in organically bound oxygen.

We looked for these bacteria (by SEM) in several samples from the Reef Ridge and Antelope shale. Our samples were not fresh, but filamentous bacteria were found in freshly broken fragments from the larger drill chips. A few bacteria were found in the Reef Ridge mbr., but abundant bacterial colonies were found in the Antelope Shale samples. If these are Beggiatoa they could be the source of organic compounds rich in N and O bonds that are broken at low temperatures.

The lack of significant variation in fixed-NH₄ isotopic values across stratigraphic boundaries and across the production interval (1550–1700 m) is interesting. One would expect a different isotopic signature in the production interval if the petroleum had migrated any significant distance, therefore this isotopic data supports "in situ" generation of the petroleum. It is possible that the nitrogen was fixed before the introduction of petroleum into the fractured reservoir, but this is difficult to reconcile with the clear correlation between fixed-NH₄ and the amount of diagenetic illite. The petroleum is the most probable source of the high fixed-NH₄ in the production interval.

The isotopic composition of fixed-NH₄ is about 3 per mil lighter than the organic-N (petroleum, kerogen, and bitumen). This is most likely the result of two fractionation processes. Fractionation will occur upon release from organic compounds because isotopically light nitrogen is released first, leaving the organic matter enriched in ¹⁵N. (Wada et al., 1975). Secondly, fractionation may occur upon substitution into diagenetic minerals.

The light fixed-NH₄ isotopic values may also result from the proposed Beggiatoa bacterial mat source material. Beggiatoa may fix isotopically light N (Williams, 1984), thus if the nitrogen that is mineralized has come from the early breakdown of C-N-O compounds related to Beggiatoa, it would be exceptionally lighter than the remaining organic compounds.

Further investigation of fixed-NH₄-N isotopic compositions in hydrocarbon environments is planned. In Louisiana Gulf Coast sediments, where long distance migration is proposed, the fixed-NH₄ isotopic composition from reservoirs is significantly lighter than isotopic values from the enclosing mudstones. It may be possible to use the isotopic composition of fixed-NH₄ in making petroleum - source rock correlations. This will be the emphasis of our next investigation.

REFERENCES

- Graham, S.A., and Williams, L.A., 1985, Tectonic, depositional, and diagenetic history of Monterey Formation (Miocene), Central San Joaquin Basin, California. *AAPG Bull.*: 69: 385 411.
- Krudge, M.A., 1983, Diagenesis of Miocene biogenic sediments in Lost Hills Oil Field, San Joaquin Basin, California. *in Petroleum Generation and Occurrence in the Miocene Monterey Formation*, (eds C.M. Isaacs and R.E. Garrison) Calif. SEPM Special Publication 33, p. 39 51.
- Philippi, G.T., 1977, On the depth, time and mechanism of origin of the heavy to medium gravity napthenic crude oils. *Geochimica et Cosmochimica Acta*: 44: 33 52.
- Wada, E., Kadonaga, T., and Matsuo, S., 1975, ¹⁵N abundance in nitrogen of naturally occurring substances and global assessment of denitrification from isotopic viewpoint. *Geochem. J.* 9: 139-148.
- Williams, L.B., Ferrell, R.E., Jr., Chinn, E.W., and Sassen, R., 1989, Fixed-NH₄ in clays associated with crude oils. *Applied Geochemistry*: 4: 605-616.
- Williams, L.B., Wilcoxon, B.R., Ferrell, R.E., and Sassen, Nitrogen as an indicator of hydrocarbon maturation and migration. *Applied Geochemistry* (accepted).
- Williams, Loretta Ann, 1984, Subtidal stromatolites in Monterey Formation and other organic-rich rocks as suggested source contributors to petroleum formation. *AAPG Bull.*: 68: 1879-1893.

TABLE 1. STABLE ISOTOPE ANALYSIS OF ORGANIC AND INORGANIC NITROGEN IN THE MONTEREY FM, LOST HILLS OIL FIELD, CALIFORNIA

δ ¹⁵ N	δ13C
+8.9, +9.2	-22.8, -22.8
+8.7	-23.2, -23.2
+8.4	-24.1
+6.8	
+6.4	
+6.0	
+6.6, +7.0	
+6.4	
+6.1, +6.4	
+6.2	
+6.0	
+6.0	
+5.8, +5.8	
	+8.9, +9.2 +8.7 +8.4 +6.8 +6.4 +6.0 +6.6, +7.0 +6.4 +6.1, +6.4 +6.2 +6.0 +6.0

A STUDY OF HYDROCARBON MIGRATION EVENTS: DEVELOPMENT

AND APPLICATION OF NEW METHODS FOR CONSTRAINING

THE TIME OF MIGRATION AND AN ASSESSMENT

OF ROCK-FLUID INTERACTIONS

R. Douglas Elmore and M. H. Engel School of Geology and Geophysics University of Oklahoma Norman, Oklahoma 73019

Considerable effort has been made in recent years to improve our understanding of the dynamics of fluid flow through porous media and of the compositional changes in fluids and host rocks that result from this process. This type of information is critical with respect to the development of predictive diagenetic models, the refinement of petroleum exploration and production efforts, and gaining a better understanding of the subsurface transport of groundwater and hazardous waste materials. Investigations of subsurface fluid flow or migration have, from a geologic point of view, been limited by our inability to constrain the time frame in which most past migration events have occurred and by a limited understanding of compositional changes in fluids via interaction with various mineral phases encountered along migration pathways. During the past several years we have used paleomagnetic analysis to date or constrain the timing of events such as hydrocarbon migration. method of dating is based on isolation of the magnetic component carried by authigenic minerals that precipitate as a result of a migration event and comparing the pole position for the component to an independently established magnetic time scale, the Apparent Polar Wander Path. The refinement and field tests of this dating method are the primary objectives of this study.

addition, we plan to test and compare the paleomagnetic dating approach with another hydrocarbon dating method, Pb-Pb radiometric dating recently developed by John Parnell and his colleagues (Parnell and Swainbank, 1990). A secondary objective of the study is to document some of our previous observations concerning the effects of rock-fluid interactions on the composition of crude oils. One of the proposed study areas, an exposed reservoir in northwest Colorado (Schoolhouse Member, Maroon Formation), provides us with an opportunity to continue our assessment of the potential for chemical and stable isotopic alteration of crude oils resulting from fluid-rock interactions. Whereas we have conducted numerous studies of geochromatographic effects in the laboratory (e.g., Brothers et al., 1991), it is important that we continue to compare the results of this work with natural systems (e.g., Engel et al., 1991).

Previous work at the University of Oklahoma as well as other laboratories indicate a relation between magnetite and hydrocarbons. Elmore et al. (1987), as well as other workers (e.g., McCabe et al., 1987), have reported the occurrence of authigenic magnetite in samples of biodegraded bitumen, which suggests that the magnetite may have formed as a result of microbial activity during the diagenesis of the hydrocarbons. A study of hydrocarbon-saturated speleothems in southern Oklahoma also provides evidence of a relationship between hydrocarbons and a remanence residing in authigenic magnetite (Elmore et al., 1987; Elmore and Crawford, 1990). The speleothems are composed of light to dark calcite bands; the latter contain hydrocarbons in primary fluid inclusions. The speleothems are Permian in age based on interbedded fossils. Those speleothems which contain hydrocarbons have a magnetization residing in authigenic magnetite which is over an order of magnitude stronger than the magnetization in the speleothems which contain no hydrocarbons. Paleomagnetic analysis of the

speleothems indicates that the magnetization was acquired in the Permian. These results suggest that the chemical conditions created by the hydrocarbons caused precipitation of authigenic magnetite and acquisition of the associated chemical remanent magnetization (CRM). The results from the speleothems are consistent with the idea that a paleomagnetic approach can be used to date hydrocarbon migration.

The nature of the relationship between hydrocarbons and authigenic magnetite in the speleothems is also being evaluated via a detailed organic geochemical and petrographic investigation. Analysis by gas chromatography (GC) and gas chromatography/mass spectrometry (GC/MS) suggests that the most likely source of the oil was the Devonian Woodford Formation in the Anadarko Basin. Gas chromatographic analyses of the C_{15+} aliphatic fraction isolated from the speleothems indicate that the level of biodegradation is variable. Stable carbon and oxygen isotope values for the light ($\delta^{13}C_{PDB}$ -6.7 %; $\delta^{18}O_{PDB}$ -4.2 %) and dark $(\delta^{13}C_{PDB}$ -6.2 %; $\delta^{18}O_{PDB}$ -4.7 %) speleothems are consistent with a shallow depth of formation from fresh water (Elmore et al., 1987). The fact that the carbon and oxygen stable isotope values are only slightly depleted supports the interpretation that some of the hydrocarbons in the speleothems are not extensively biodegraded. Comparisons between magnetic intensity and various organic parameters suggest some interesting relationships. For example, samples with the highest magnetic intensity are apparently the least degraded. There is also a positive relationship between the amount of extracted bitumen and magnetic intensity. There is no relationship, however, between intensity and percent asphaltenes. Additional studies comparing magnetic intensity to other organic parameters (e.g., NSO's, aromatic fraction) may provide information that relates to the mechanism(s) of magnetite precipitation.

Several hydrocarbon-bearing units also contain authigenic magnetite and associated CRMs (e.g., see Benthien and Elmore, 1987; Elmore and Leach, 1990; and others). The results from these studies are consistent with the interpretation that the chemical conditions created by the hydrocarbons caused precipitation of the authigenic magnetite and acquisition of the associated CRM.

We also have some preliminary results from the Schoolhouse Member of the Maroon Formation in northwestern Colorado. The Schoolhouse Member occurs as a zone of white to gray hydrocarbon-impregnated sandstones in the top of the Maroon redbeds (Johnson et al., 1990). Samples of the Maroon sandstones contain a southeasterly and shallow negative magnetization that resides in hematite. Bleached and hydrocarbon-impregnated samples are magnetically distinct from the red samples. On average, the magnetic intensities are lower, and rock magnetic measurements suggest the magnetization resides in magnetite. At locations where the hydrocarbon-impregnated sandstones are not well cemented, they contain a weak modern component or contain no stable remanence. At several locations the sandstones are well cemented by silica and carbonate and some samples contain a northwesterly and moderate direction which suggests remanence acquisition during the Jurassic. This is consistent with a suggested time of hydrocarbon generation and migration from the underlying Belden Formation, which is interpreted to be the source of the hydrocarbons (Nuccio et al., 1989). The preliminary results are encouraging and analysis of additional samples should better constrain the time of remanence acquisition as well as the origin of the magnetization.

We have also collected a suite of samples from the Old Red Sandstone (Devonian) in Scotland and the Orkney Islands. Both hydrocarbon-impregnated sandstones/siltstones as well as organic-rich source beds were sampled. Preliminary results suggest that some samples contain a stable magnetization

residing in magnetite. Additional studies will constrain the time of remanence acquisition as well as the origin of the magnetization.

The results described above provide empirical evidence for a relationship between hydrocarbons and the precipitation of authigenic magnetite. The speleothem investigation also provides a test of the hypothesis that hydrocarbon migration can cause acquisition of a CRM. The studies of the other units are also encouraging and suggest that paleomagnetic analysis can be used to date or constrain the time of hydrocarbon migration. A better understanding of the geochemical mechanism for magnetite authigenesis is needed to fully develop the dating approach.

In addition to further studies now underway of the Schoolhouse Member and the Old Red Sandstones (including Pb-Pb dating), we also plan to sample Triassic-Jurassic redbeds in the Hartford Basin, Connecticut that contain veins with hydrocarbons. We will also determine if the units in North America we plan to study or have studied in the past are suitable for Pb-Pb dating. Laboratory studies will include additional organic geochemical and rock magnetic studies on hydrocarbon impregnated Permian calcite speleothems and laboratory simulation experiments in order to better understand the mechanism of magnetite precipitation.

Results of these studies should provide additional constraints on the mechanism(s) of magnetite precipitation (and nature of rock-fluid interactions) as well as allowing for an evaluation of the applicability of the paleomagnetic approach for dating hydrocarbon migration. In addition, the results should permit an evaluation of the Pb-Pb dating approach in comparison with the paleomagnetic approach.

REFERENCES

- Benthien, R.H. and Elmore, R.D., 1987, Origin of magnetization in the Phosphoria formation at Sheep Mountain, Wyoming, a possible relationship with hydrocarbons: Geophys. Res. Lett., v. 14, p. 323-326.
- Brothers, L., Engel, M.H. and Krooss, B.M. (1991) The effects of fluid flow through porous media on the distribution of organic compounds in a synthetic crude oil: Org. Geochem., v. 17, p. 11-24.
- Elmore, R.D. and Crawford, L., 1990, Remanence in authigenic magnetite, testing the hydrocarbon-magnetite hypothesis: Jour. Geophys. Research, v. 95, p. 4539-4549.
- Elmore, R.D., Engel, M., Crawford, L., Nick, K., Imbus, S., and Sofer, Z., 1987,

 Evidence for a relationship between hdyrocarbons and authigenic magnetite:

 Nature, v. 325, p. 428-430.
- Elmore, R.D. and Leach, M.C., 1990, Paleomagnetism of the Rush Springs Sandstone, Cement, Oklahoma, implications for dating hydrocarbon migration, aeromagnetic exploration, and understanding remagnetization mechanisms:

 Geology, v. 18, p. 124-127.
- Engel, M.H., Macko, S.A. and Leythaeuser, D. (1991) The application of stable isotopes for interpreting indigenous versus migrated hydrocarbons in a mature shale/sandstone sequence: Chemical Geology, in press.
- Johnson, S.Y., Schenk, C.J., Anders, D.L., and Tuttle, M.L., 1990, Sedimentology and petroleum occurrence, Schoolhouse Member, Maroon Formation (Lower Permian), Northwestern Colorado: Am. Assoc. Pet. Geol. Bull., v. 74, no. 2, p. 135-150.
- McCabe, C., Sassen, R., and Saffer, B., 1987, Occurrence of secondary magnetite within biodegraded oil: Geology, v. 15, p. 7-10.

- Nuccio, V.F., Johnson, S.Y., and Schenk, C.J., 1989, Paleogeothermal gradients and timing of oil generation in the Belden Formation, Eagle Basin, Northwestern Colorado: The Mountain Geologist, v. 26, no. 1, p. 31-41. The Rocky Mountain Association of Geologists.
- Parnell, J., and Swainbank, I., 1990, Pb-Pb dating of hydrocarbon migration into a bitumen-bearing ore deposit, North Wales: Geology, v. 18, p. 1028-1030.

DYNAMICS OF ROCK VARNISH FORMATION

Robert Raymond, Jr., Steven L. Reneau,
George D. Guthrie, Jr., David L. Bish, and Charles D. Harrington
Geology and Geochemistry Group
Los Alamos National Laboratory

1 INTRODUCTION

Rock varnish is a dark brown to black coating commonly less than 50 µm thick found on a variety of rock substrates in semiarid and arid environments. Rock-varnish constituents are usually of allochthonous origin, deposited by eolian or aqueous processes and then cemented in place by Mn and Fe phases (e.g., Potter and Rossman, 1977, 1979; Dorn and Oberlander, 1982). The occurrence, form, and distribution of rock varnish on geomorphic surfaces has potential for providing keys to the past, both with respect to interpreting ages of surfaces and to interpreting paleoclimatic changes.

An unresolved question concerning the genesis of rock varnish is whether its origin is abiologic or biologic (see Dorn and Oberlander, 1982, for a review). In support of a biologic origin, some researchers have used both circumstantial evidence (e.g., that biological factors are necessary to produce the Mn enhancement observed in varnish) and direct evidence (e.g., that varnish can contain bacteria and fungi which, when isolated, will oxidize Mn and presumably will do so on the varnish surface). Alternatively, other workers have proposed that Fe⁺² and Mn⁺² from wind-blown soil may be abiologically precipitated as a result of fluctuating pH or Eh conditions or that the varnish substrate can exert a significant control on the nature and occurrence of rock varnish, possibly through the creation of a chemical environment conducive to Fe and Mn precipitation. However, mineralogic data that would define thermodynamic conditions of rock varnish formation, and thereby substantiate biologic or abiologic theories of origin, are unavailable.

Early researchers concluded that rock varnish is amorphous to X-rays (e.g., Engel and Sharp, 1958). More recently, Potter and Rossman (1977, 1979) used infrared (IR) spectroscopy to conclude that birnessite and hematite are the Mn- and Fe-oxide phases, respectively, in rock varnish and that these oxides are in intimate physical association with illite, smectite, and mixed-layer illite/smectite clays. Although they proposed that the birnessite in rock varnish is characterized by a high degree of order and a small particle size, Potter and Rossman could not substantiate the presence of birnessite by XRD.

Analyses of rock varnish chemistry have been used by several workers to estimate ages of geologic or archaeologic surfaces. Cation-ratio (CR) dating of rock varnish, first proposed by Dorn and Oberlander (1981), is an empirical method for estimating the age of a surface based on decreases in the cation ratio (Ca+K):Ti over time. The premise of CR dating is that the cations such as Na, Mg, K, and Ca are gradually leached relative to less mobile cations, such as Ti. Measured decreases in the CRs over time have been used to infer the length of time that the varnish has been exposed to cation leaching.

Our research on rock varnish has clarified some aspects of varnish genesis and of its use as a dating tool. First, whether or not biomineralization processes are instrumental in the formation

of all rock varnish, they apparently affect the morphology of varnish and the distribution of Mn within the varnish. Second, X-ray Diffraction (XRD), scanning electron microscopy (SEM), and transmission electron microscopy (TEM) analyses show that the Mn phase in rock varnish is by most definitions a non-crystalline phase with an affinity for a number of cations not normally present in birnessite. And last, element distributions within varnish 1) demonstrate that the concentrations of Ca, K, and Ti are not independent of Mn concentration, as originally implied in the CR dating technique and 2) argue against significant preferential leaching of Ca and K from varnish.

2 METHODS

Samples. Samples of rock varnish were collected from Buckboard Mesa, Nye County, Nevada, from Lava Butte, Clark County, Nevada, and from the Cima volcanic field, San Bernadino County, California. The estimated ages of surfaces from which rock varnish samples were collected range from about 20,000 years before present (20 ka) at Cima to >1000 ka at Buckboard Mesa. From these samples, thin rectangular slabs were cut parallel to the surface for examination by XRD. Varnish also was removed from the substrate by scraping thicker deposits with a tungsten carbide scribe while attempting to exclude as much substrate as possible. These scraped samples were ground to < 5 µm for XRD analysis. Other samples were slabbed perpendicular to varnished surfaces, mounted on glass slides, and polished for SEM analysis. Areas of polished SEM mounts with high concentrations of Mn as determined by SEM/energy dispersive spectroscopy (EDS) analysis were cut from the SEM mounts and ion-thinned for TEM analysis.

<u>Electron Microscopy/Energy-Dispersive Analysis</u>. Backscattered electron (BSE) SEM images reveal both textural and chemical information at high resolution. Bright- and dark-field TEM images allow crystalline and non-crystalline material to be distinguished. TEM convergent-beam electron diffraction patterns can be used to identify mineral species.

During both SEM and TEM examination, elemental compositions of the samples were determined using EDS analysis. Due to the large volume of excitation from which X-rays are emitted during SEM analysis, the resolution of the SEM EDS analyses, which include X-ray maps and elemental-line profiles, can be no better than 0.5 μ m. The resolution of TEM EDS analytical points was the size of the focused electron beam, \leq 0.05 μ m. SEM X-ray maps were acquired using a 256x256 pixel array with an acquisition time of 0.05 seconds/pixel. SEM elemental line profiles were acquired with analytical points spaced at 0.5 μ m and acquisition times of 100 seconds/point (Raymond et al., 1991). Elemental compositions obtained with EDS analyses were normalized to 100%.

<u>XRD</u>. An automated θ - θ X-ray diffractometer using either Cu or Fe K α radiation, a Si(Li) detector, and count times up to 100 seconds/ 0.02^{0} 2 θ step was used to analyze rock varnish both in situ on thin rectangular rock slabs cut parallel to rock surfaces and as powders scraped from varnished rock samples. Scraped powders were mounted as slurries on "zero-background" cut quartz plates. Heating (up to 500°C) and ethylene-glycol solvation were used to facilitate identification of the broad, poorly defined X-ray reflections resulting from the varnish samples.

A buffered oxalic acid solution was used to remove Fe- and Mn-oxide components. XRD analysis of the resulting non-oxide component, coupled with ethylene-glycol solvation, provided information on the silicate components.

3 RESULTS

Varnish Morphology. The BSE image of a rock-varnish cross section and the accompanying Mn X-ray map (Fig. 1) illustrate that high atomic number and Mn concentration define small convex upward forms that share great similarities with cyanobacterially formed fossil stromatolites (5 orders of magnitude larger) reported most commonly from the Precambrian era (>600 million years ago). The morphology and scale of varnish botryoids (Fig. 2), one of two end-member surface textures of rock varnish, demonstrate that they are the surface manifestation of the microstromatolite columns seen in cross section. We have observed similar microstromatolites in varnish collected from sites in Nevada, Arizona, and California, and similar structures have been reported by others.

<u>SEM Analyses</u>. As viewed in cross section, rock varnish typically displays stratigraphic layers distinguished by varying concentrations of Mn, Fe, and Si. An examination of element distributions in Cima varnish indicates that concentrations of the minor elements used in CR dating are in turn related to these variations in major element concentration. Variations in Ca, K, and Ti concentration typically follow variations in Mn, Si, and Fe concentration, respectively. For example, the trend of varying Mn with depth in Figure 3 is strikingly similar to the trend of varying Ca with depth. Similarly, fluctuations in K closely follow fluctuations in Si, and Ti follows Fe.

The element associations shown in Fig.3 are present in the majority of our 72 Cima profiles, and are clearly evident in plots of all analyses from single rocks (Fig. 4). These associations are also present in plots of average element concentrations in each profile, equivalent to bulk varnish analyses.

In addition to the associations between minor elements and major elements discussed above, concentrations of Fe and Si in Cima varnish are typically inversely related to Mn concentration, and the minor elements used in CR dating are thus partially related, either positively or negatively, to Mn concentration. As a result, for the Cima samples, CR shows a slight positive correlation with Mn (and Ca) concentration and a stronger negative correlation with Fe (and Ti) concentration (Fig. 5), and the lowest CRs are thus at spots of relatively high Fe and low Mn concentration.

TEM Analyses. EDS spectra of Mn-rich areas of the sample from Buckboard Mesa confirm the association between Mn, Ba, and Ca, and also show an association between these elements and Fe, Al, and P in a non-crystalline phase, as determined by dark-field (Fig. 6) and bright-field (Fig. 7) imaging. Non-crystalline Mn-rich particles occur with cross sections up to 2 μm. The bright regions in the dark-field image and the dark regions in the bright-field image are crystalline iron-oxide grains. A convergent-beam electron diffraction pattern of an iron-oxide grain (indexed uniquely as hematite) 50 nm in diameter is also shown (Fig. 8).

XRD Analyses. Although Mn commonly comprises greater than 15 wt% of rock varnish within a groundmass composed primarily of clay phases that can be identified by special treatment and XRD, no crystalline Mn phase was identified by XRD (Fig. 9) for numerous samples analyzed from Nye County, Nevada, and from Cima. Peaks consistent with the presence of chloritic and kaolinitic minerals, both of which are common in rock varnish, were enhanced following chemical treatment and removal of Mn/Fe-phase(s) with oxalic acid. No peak shift was observed with heating of samples either in vacuum to 200°C or in air to 500°C, which would occur if the peaks at ~12.2° 2θ were due to birnessite. Ethylene-glycol solvation of the treated

samples showed that the predominant silicate component of varnish consists of mixed-layer illite/smectite, illite, chlorite, and kaolinite clays.

4 DISCUSSION

Although Mn-oxidizing microorganisms have been shown to occur on rock varnish surfaces, and although Mn concentration in rock varnish far exceeds its natural abundance in arid and semi-arid environments, no definitive data exist that prescribe the specific roles that microorganisms have in Mn enhancement in rock varnish or the specific mechanisms by which this enhancement occurs. However, the presence of microstromatolitic structures observed in our samples of rock varnish suggests that microorganisms affect the morphology of rock varnish textures. Based on the occurrence of present-day stromatolites, the convex upward growth of varnish microstromatolites probably results from trapping of sediments by the filamentous bodies or exudates of the microorganisms followed by recolonization of the surface. Laminations within microstromatolites would reflect past individual episodes of entrapment and recolonization. Based again on mechanisms of present-day stromatolite growth, the size of the microstromatolites in rock varnish necessitates that the colonizing microorganisms responsible for their growth be smaller than the heads of the microstromatolite columns, i.e., < 10µm in diameter.

We propose that where microstromatolites occur in rock varnish, Mn-oxidizing bacteria, less than 10 µm in diameter, are removing Mn from eolian dust that accumulates on surfaces of host rocks and are redepositing the Mn on the upper surfaces of the microstromatolite columns. The utilization of Mn by bacteria will be catalyzed by, if not restricted totally to, intermittently wet micro-environments on the rock surfaces such as pits or small depressions. However, the scarcity of rainfall in arid and semi-arid environments at times when viable bacteria are present, combined with variations in chemistry of eolian detritus and fluctuating seasonal conditions, should greatly restrict periods of microstromatolite growth. Thus, laminations that reflect incremental periods of growth and death of bacterial colonies would represent discontinuous sedimentary records, and microstromatolite columns 50-µm high may represent growth periods of 10s to 100s of thousands of years.

Although long-scan XRD methods have been carefully applied in the examination of numerous rock-varnish samples, we were unable to confirm the presence of any crystalline Mnrich phase. Earlier researchers reported that the absence of X-ray diffraction reflections for the Mn-rich phase could be accounted for by a particle size well below 0.1 µm (Potter and Rossman, 1977, 1979). Usable diffraction data are produced by materials having crystallite sizes >3-6 unit-cell repeats (e.g., see Reynolds, 1989), which translates into crystallites >2-4 nm (0.002-0.004 µm) for Mn oxides such as birnessite. Considering the ability of XRD to identify and characterize fine-grained iron-oxide and clay species at least as small as 10 nm in crystallite size, the absence of X-ray diffraction lines for a crystalline Mn mineral cannot be explained by small particle size. Furthermore, no contrast variations were observed in bright-field or dark-field TEM images of Mn-rich regions from the Buckboard Mesa sample, as would be expected if a crystalline phase were present. Although only a small area of the Buckboard Mesa sample was analyzed by TEM, the available data do not support the presence of a crystalline Mn-rich phase in this sample. However, TEM data support the presence of a non-crystalline Mn-rich phase, in agreement with the XRD data.

The SEM/EDS data suggest that the Mn-bearing component of rock varnish is not Ba-free birnessite as previously suggested by Potter and Rossman (1977, 1979), but rather a phase that contains both Ba and Ca. TEM/EDX data for the Buckboard Mesa sample confirm the association of the Mn-rich phase with Ba and Ca on a 0.1-µm scale and suggest additional associations with Al, Fe, and P. The cation-ratio dating method was proposed to work because of leaching of more mobile elements from varnish, but the validity of this model has never been demonstrated (see Reneau and Raymond, 1991 for more indepth review). Because the ratio (Ca+K):Ti of a varnish layer is related to the major element composition of that layer, variations in this ratio with depth are related to varnish stratigraphy and thus do not, by themselves, provide evidence for or against the preferential leaching of Ca and K from varnish. Instead, because Ca is generally associated with Mn, and K with Si, if Mn and Si are relatively immobile in varnish (as assumed by the cation-ratio dating method), then any significant cation leaching should be recognizable by systematic changes in the ratios Ca:Mn and K:Si with depth and with surface age. In particular, the model of cation leaching predicts that the uppermost (youngest) varnish should be least leached and have the highest relative amounts of both Ca and K.

In our Cima line profiles, there is no evidence for such systematic changes in the ratios Ca:Mn or K:Si with depth in varnish or with surface age, or for consistently higher ratios in the uppermost varnish. Data from the oldest (CMG) and youngest (CIA) sampled surfaces are presented as representative examples in Fig. 10. Although there is scatter in these data, and an apparent rise in Ca:Mn ratios toward the surface in CIA-14, Ca:Mn ratios are typically about 0.03 and K:Si ratios about 0.11 for both samples, regardless of depth. Much of the scatter and the differences between samples again is related to the varnish stratigraphy. The high Ca:Mn data points obtained near the surface of CIA-14 and deeper in CMG-103 are associated with low-Mn layers. In these layers additional Ca is commonly present in Ca-rich detritus that is infrequent in the more Mn-rich layers. Similarly, the high K:Si points at depth in CMG-103 reflect K-rich detritus incorporated into Mn-poor layers. In addition, low Ca:Mn and K:Si values at the surface of many samples conflict with the prediction that the surface layer is least leached and highest in Ca and K. In our Cima profiles, Ca:Mn and K:Si ratios near the surface may be either higher or lower than at depth, and no systematic trends are recognized that would support the model of cation leaching.

Due to the dependence of Ca, K, and Ti concentration in rock varnish on the concentrations of Mn, Si, and Fe, and due to the absence of evidence for leaching of Ca and K, an alternative explanation is required for the empirical correlation of CR with surface age which does not assume an initial CR of surficial varnish that is constant over time and does not depend on leaching. A strong possibility is that the empirical correlation is in part related to the contamination of varnish analyses with varying amounts of substrate. Microtopographic highs thinly covered with varnish and areas of high local relief along the varnish-substrate interface are particularly susceptible to the incorporation of substrate both during scraping and during SEM analyses when beam penetration depths may be $> 5 \mu m$ (Reneau et al., 1991). The ratio (Ca+K):Ti is commonly greater in substrates than in varnish, and the incorporation of substrate into analyses thus typically increases CRs. The importance of this addition of substrate should vary inversely with average varnish thickness, relatively more substrate being included in analyses of younger, thinner varnishes than of older, thicker varnishes. The incorporation of smaller amounts of high-CR substrate in analyses of thicker varnish would provide an apparent

decrease in CR with increasing varnish age that is independent of any actual changes in varnish chemistry.

5 CONCLUSIONS

The presence of Mn-rich microstromatolites suggests that microorganisms exert an influence on both the form and the chemistry of rock varnish through biomineralization. The most reasonable microorganisms for these induced processes are Mn-oxidizing bacteria, both because of size restrictions ($<10~\mu m$) and the well-documented fact that Mn-oxidizing bacteria are ubiquitous in most environments. Some rock varnish may possibly form independent of bacterial interference, but such varnish would be lacking in Mn-rich microstromatolites as described here.

Our studies of rock varnish from the southwestern United States suggest that the Mn-phase in rock varnish has neither the chemistry nor the crystal structure of birnessite. Rather, the Mn-rich phase is non-crystalline and contains Ba, Ca, Fe, Al, and P. Unknowns concerning the formation of this non-crystalline Mn phase must be resolved before researchers are able to define chemical parameters of rock varnish formation based upon conditions of formation of the Mn phase.

13

The reasons for the empirical correlation of varnish chemistry with surface age have apparently been misunderstood. No evidence for significant preferential leaching of elements from varnish is available at the Cima volcanic field; instead, variations in CR between varnish layers and between varnish collected from lava flows of different age are related to variations in major element concentration. Because of the lack of evidence for leaching, referring to the calibrated dating curves as "cation-leaching curves" is inappropriate, and interpretation of microenvironmental variations in CRs in terms of local variations in leaching environments is questionable. In addition, because the concentrations of Ca, K, and Ti in accreting varnish are related to major element compositions that vary nonuniformly with time, use of an "initial ratio" that is assumed to be constant over time is not substantiated.

Many uncertainties remain concerning CR dating of rock varnish and the nature of the empirical correlations of chemistry with age. In the absence of significant leaching, mechanisms that cause changes in calculated CRs associated with the increase in varnish thickness over time seem more reasonable. Available data suggest that the empirical correlations may in part depend on the incorporation of varying amounts of substrate into varnish analyses, the percentage of added substrate decreasing with increasing varnish thickness and therefore with increasing age.

REFERENCES

Dorn, R. I. and Oberlander, T. M. (1981): Rock varnish origin, characteristics, and usage. Z. Geomorph. 25, 420-436.

Dorn, R. I. and Oberlander, T. M. (1982): Rock varnish. Prog. Phys. Geog. 6, 317-367. Engel, C. G. and Sharp, R. P. (1958): Chemical data on desert varnish. Geol. Soc. Amer. Bull. 69, 487-518.

Potter, R. M. and Rossman, G. R. (1977): Desert varnish: the importance of clay minerals. Science 196, 1446-1448.

- Potter, R. M. and Rossman, G. R. (1979): The manganese and iron oxide mineralogy of desert varnish. Chemical Geology 25, 79-94.
- Raymond, R.Jr., Reneau, S.L., and Harrington, C.D., (1991): Elemental Relationships in rock varnish as seen with scanning electron microscopy and energy dispersive X-ray elemental line profiling. Scanning Microscopy, 5:1, 37-46.
- Reneau, S.L., Hagan, R.C., Harrington, C.D., and Raymond, R.Jr. (1991): Scanning electron microscopic analysis of rock varnish chemistry for cation-ratio dating: An examination of electron beam penetration depths. Scanning Microscopy, 5:1, 47-54.
- Reneau, S.L. and Raymond, R.Jr. (1991): Cation-ratio dating of rock varnish: Why does it work?. Geology, 19, 937-940.
- Reynolds, R. C., Jr. (1989): Diffraction by small and disordered crystals, chap 6 in Modern Powder Diffraction, D. L. Bish and J. E. Post, eds., Mineralogical Society of America, Reviews in Mineralogy 20, 145-181.

ACKNOWLEDGMENTS

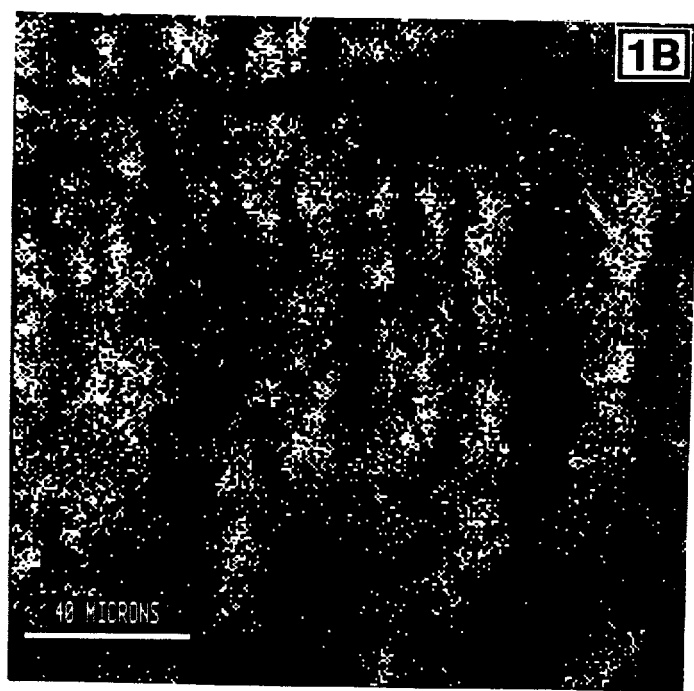
This work was conducted under the auspices of the U.S. Department of Energy's Office of Basic Energy Sciences under contract W-7405-ENG-36 and under Los Alamos National Laboratory Director's Funded Postdoctoral Fellowships to S. L. Reneau and G.D. Guthrie.

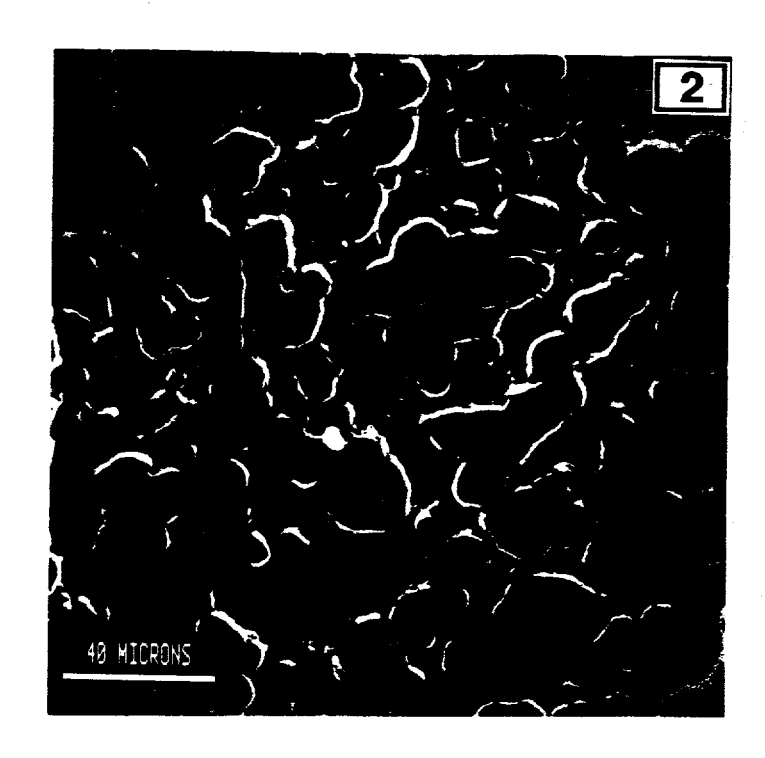
FIGURE CAPTIONS

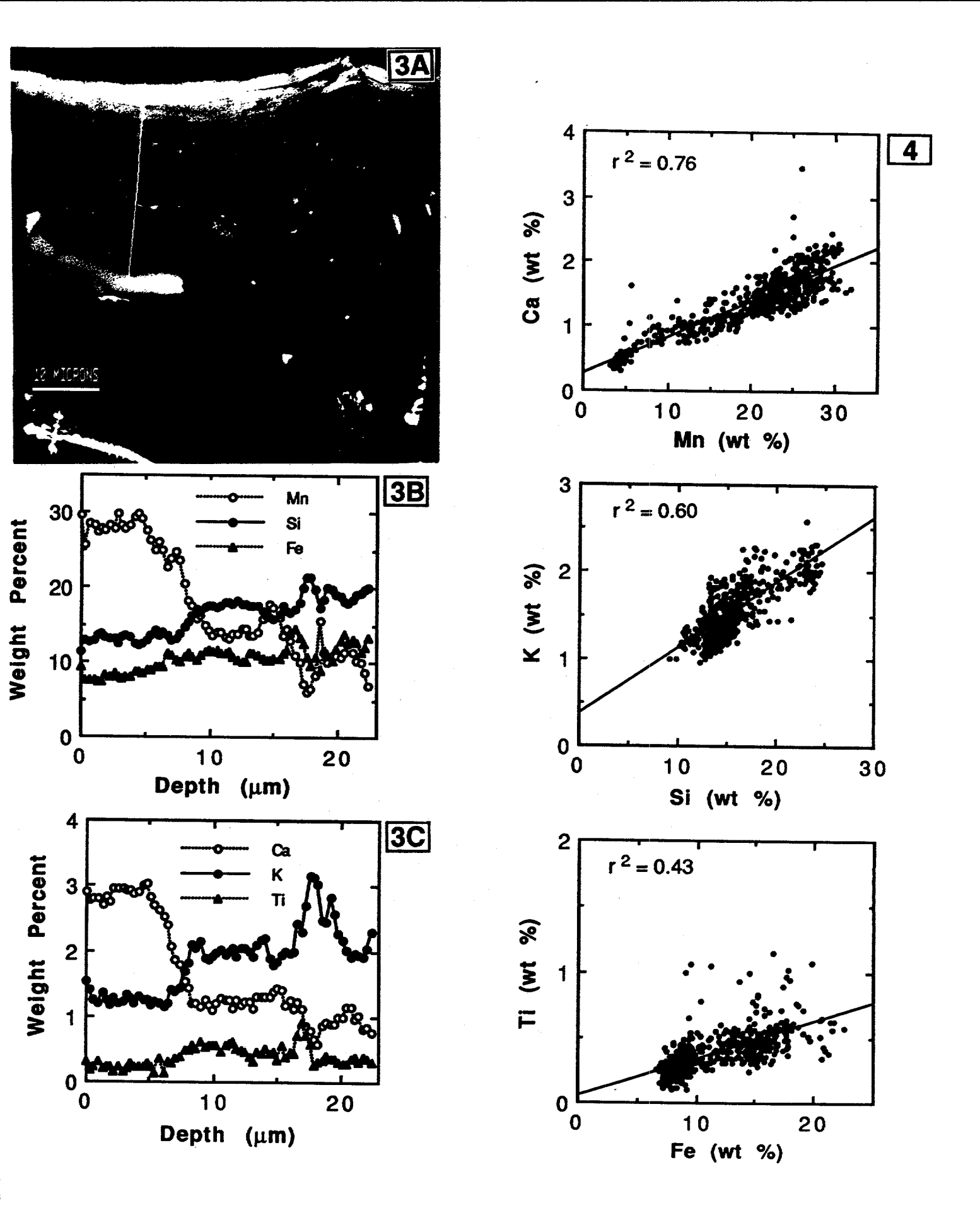
- Figure 1. a) BSE image of a polished cross-section of rock varnish on basalt substrate collected from a ~1000 ka surface on Buckboard Mesa. Note the well-laminated columns showing a combination of laterally-linked and hemispheroidal growth forms. Light-gray columns are easily differentiated from darker inter-columnar deposits by higher atomic number, reflecting greater Mn and Ba contents within the columns. b) Mn X-ray map of same area shows higher concentrations of Mn in columns relative to inter-columnar areas.
- Figure 2. Secondary electron image of the surface of rock varnish occurring on a rhyodacite substrate collected at Lava Butte. The small botryoids are the surface manifestation of the microstromatolite columns.
- Figure 3. a) BSE image of a polished cross section of rock varnish showing the position of the elemental line profile CIE-44-1, Cima volcanic field. b) Plots of Fe, Mn, and Si vs. depth, and c) Ca, K, and Ti vs. depth for line profile CIE-44-1.
- Figure 4. Plots of Ca vs. Mn, K vs. Si, and Ti vs. Fe for sample CII-17, Cima volcanic field, including all 545 analyses from eight line profiles.
- Figure 5. Plots of CR vs. Mn and CR vs. Fe for average values in all 72 Cima line profiles. Each point is average of all analyses in single profile, and is thus equivalent to bulk analysis of that profile.

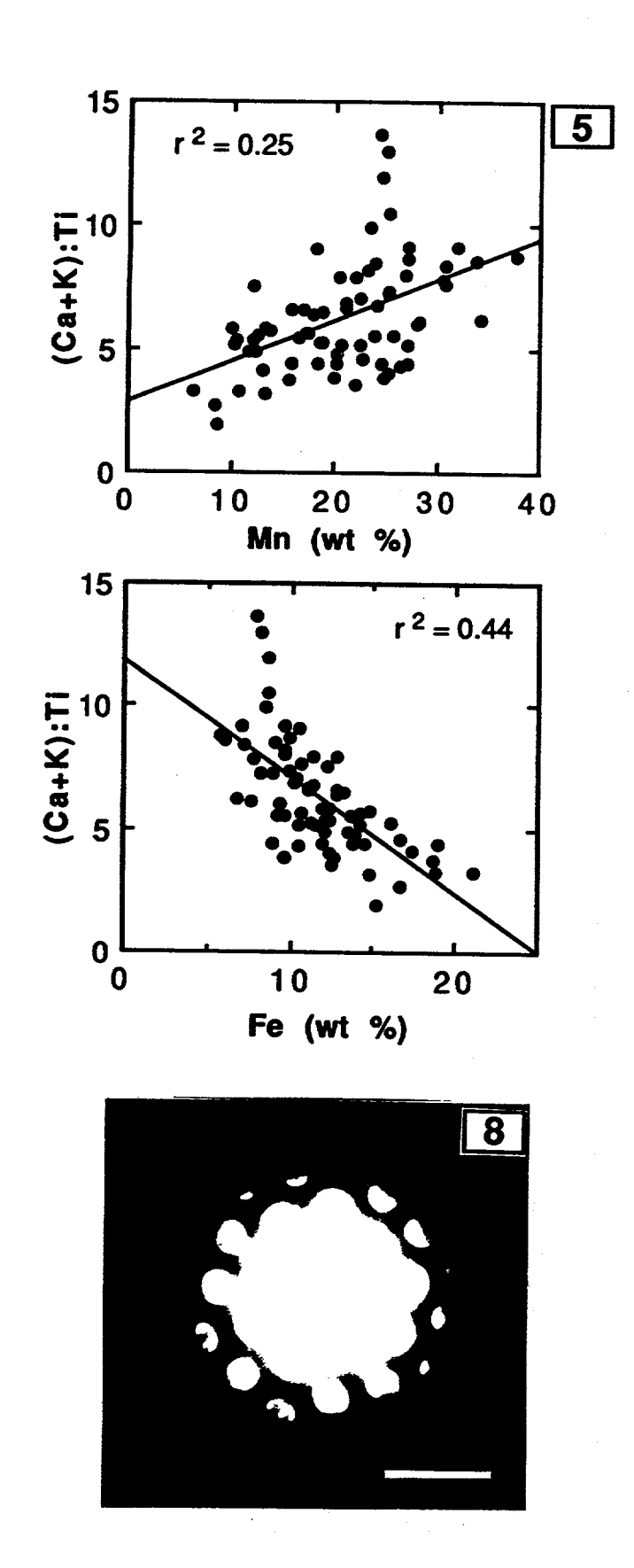
- Figure 6. Dark-field TEM image from Mn-rich band in varnish from Buckboard Mesa. Image was formed from a hematite-diffracted beam. Bright regions were Fe-rich, consistent with hematite; larger dark grains were Mn-rich and appeared amorphous to electrons. Scale bar = $1 \mu m$.
- Figure 7. Bright-field TEM image from Mn-rich band in varnish from Buckboard Mesa. Image was formed from the central beam, so any crystalline material in diffracting orientation appears darker than amorphous materials or minerals out of diffracting orientation. Regions that appeared darker were Fe-rich, Mn-poor. Tilting of sample indicated that much of the remainder was amorphous to electrons; these regions were Mn-rich. Scale bar = $0.25 \,\mu m$.
- Figure 8. Convergent-beam electron diffraction pattern of an Fe-rich hematite grain. Scale $bar = 10 \text{ nm}^{-1}$.
- Figure 9. X-ray diffraction patterns obtained from Buckboard Mesa varnish. Lower pattern is from an untreated solid rock plate covered with varnish, and upper pattern is from material removed from the varnish surface following treatment with a buffered Caoxalate solution. All Fe- and Mn-oxides were removed during this treatment. Arrow shows the position of the chlorite 002 and/or kaolinite 001 reflections that can be mistaken for the largest birnessite peak.
- Figure 10. Plots of Ca:Mn and K:Si ratios vs. normalized depth for five profiles through sample CIA-14 (including 153 analyses) and for five profiles through sample CMG-103 (including 731 analyses), both samples from the Cima volcanic field. Depths in varnish are normalized to total profile length; base of varnish is set at 1.0.

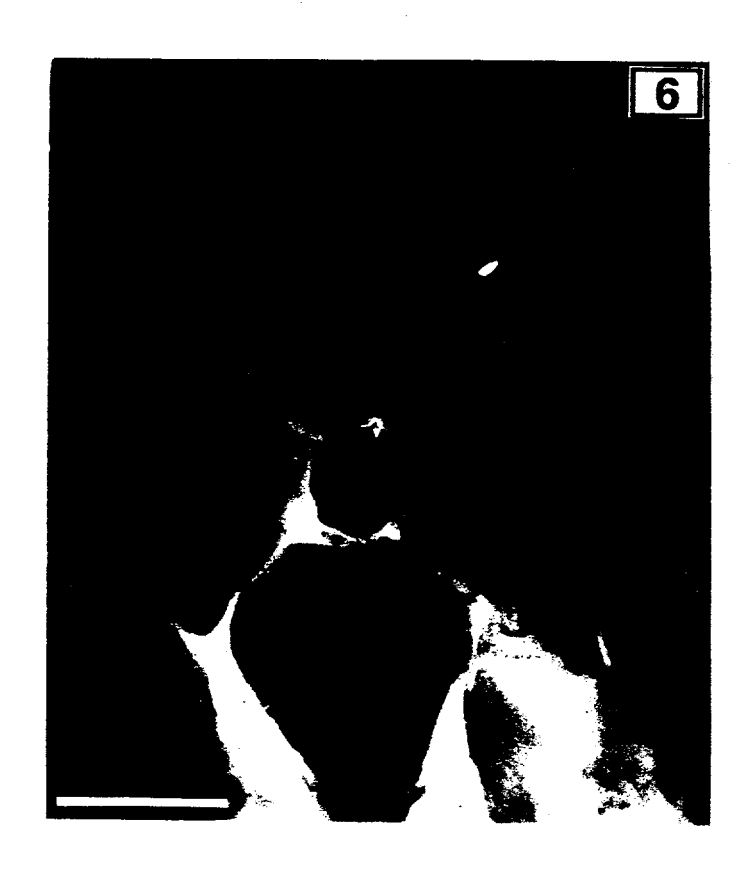


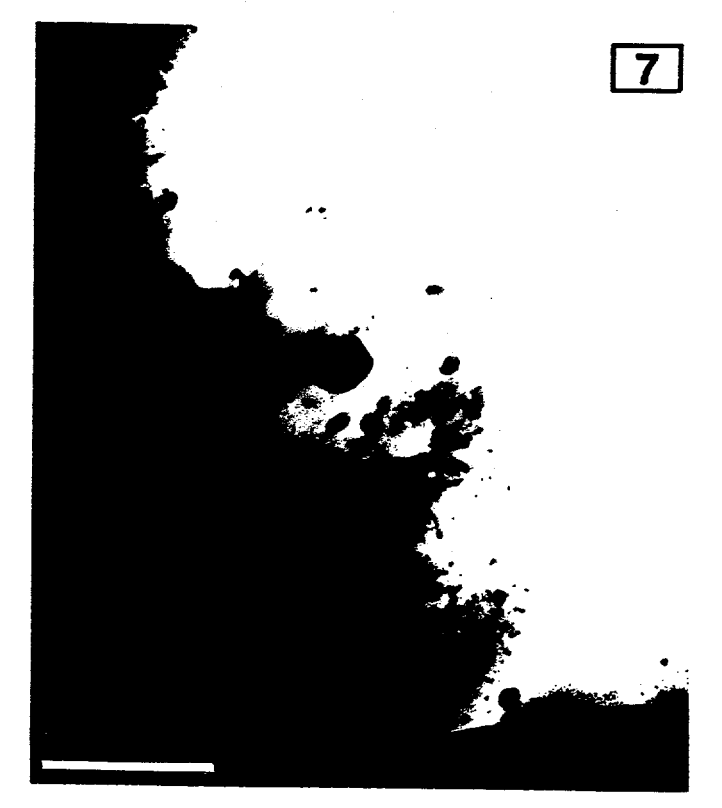


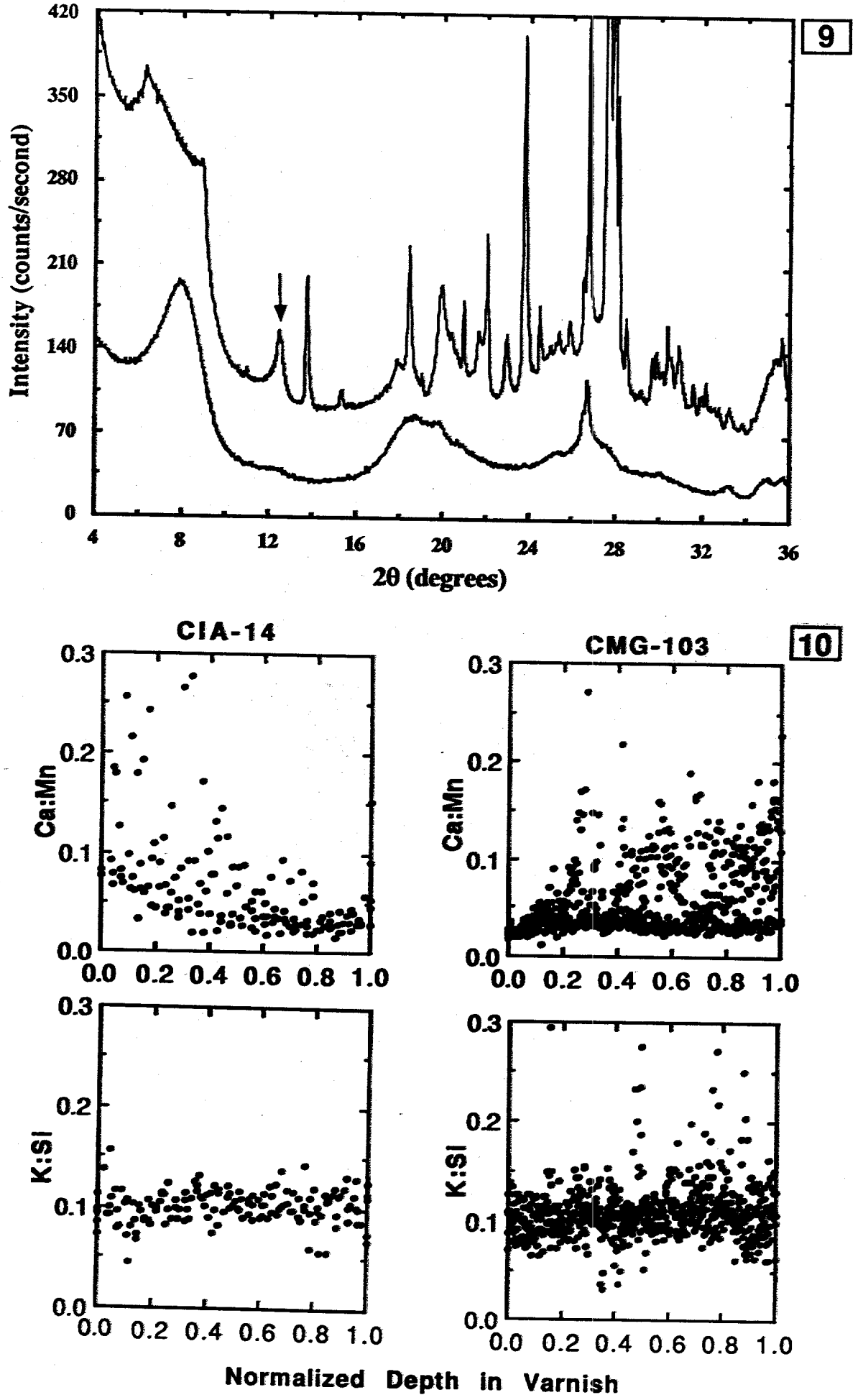












EVAPORITES AS A SOURCE FOR OIL

B.C. Schreiber, S. Benalioulhaj, R.P. Philp, and P. Landais

INTRODUCTION

In the geological record numerous evaporite deposits are intimately associated with oil accumulations. It has long been suspected that these evaporites are not only the seals to hydrocarbon accumulations, but that in some cases they also may be the sources. The Lorca Basin (Upper Miocene-Lower Pliocene) in southeastern Spain was chosen as a test model for this concept because of its diverse sediment content (Figure 1). In this basin the depositional section includes a wide range of normal marine lithologies together with several types of evaporitic carbonates and "true" evaporites, and it has been examined in great detail in terms of sedimentation, diagenesis and organic geochemistry (Figure 2). Once the depositional microfacies and early diagenetic overprints had been determined, the concomitant organic materials were then analyzed. At the same time we began a study of comparable sediments presently forming at the nearby solar salt works of Santa Pola (Figure 1). The highest amounts of organic matter, both in the Lorca section and at the salina, are found in the evaporative carbonates (up to 25% TOC), so it was decided to see if the modern sediments can be used as a geochemical model for the older deposits (Barbe et al., 1990). In order to characterize this type of Recent organic matter, to test its ability to generate oil, and to compare it to that from natural evaporitic deposits at various stages of maturation, it was decided to subject organic-rich sediment (sample SP-7, taken from the carbonatedominated salina pools), to artificial maturation, and to compare the resulting products with organic matter from sedimentologically similar Miocene sediments. In this short review, we will summarize the results we have obtained from the Lorca basin together with the artificially matured sample from the salina at Santa Pola..

EXPERIMENTAL TECHNIQUES

Confined Pyrolysis: The sample is placed in a small gold tube which is then sealed and placed in an autoclave where it is heated at different temperatures (200, 250, 300, 350, and 400°C) for 24 hours at one kilobar. Stable isotope determinations: 1 mg of sample is combusted at 550°C for 3 hours in a pyrex tube, the tube is cracked on the vacuum rack in a tube cracker and purified cryogenically and then transferred directly into the mass spectrometer (Finnigan Mat Delta E Isotope Ratio Mass Spectrometer).

 $\delta^{13}C$ was calculated by the standard definition at the $\delta^{13}C$ value with respect to the PDB international reference standard.

Gas Chromatography and Mass Spectrometry: After removal of the asphaltenes from the extract by n-pentane precipitation, the extract was fractionated into saturate, aromatic and polar fractions. Saturated and aromatic fractions were analyzed by gas chromatography using either a HP5890 or a Varian 3300 instrument. Both instruments were equipped with a J and W Scientific DB-5 Fused Silica capillary column and helium was used as the carrier gas. Oven temperature was programmed from 40°C to 130°C at 15°C/min and then to 300°C at 4°C/min and held isothermally for 25 minutes. Mass spectrometry was performed using a Finnigan Mat triple-stage quadruple mass spectrometer (TSQ 70). A Varian gas chromatograph equipped with a DB5-fused silica capillary column was interfaced to the mass spectrometer. For GC-MS/MS analysis the mass spectrometer was opereated in parent (PAR) mode.

RESULTS AND DISCUSSION

爲

The evolution of the water body in the Lorca basin throughout much of the Upper Miocene is characterized by open-marine sedimentation interspersed with zones resulting from restricted conditions, water stratification and great variation in the amount of continental input. The periods of restriction resulted in the accumulation of several different organically sourced facies (see Figure 2, at arrows). In a few instances limited quasi-evaporite deposition was initiated at the top of some of the organic-rich sections, but after a short phase of hypersalinity the basin apparently was opened again and normal marine sedimentation returned. Near the top of the Lorca section, conditions of extreme hypersalinity were established and both gypsum and halite were deposited (Ortí, 1990; Ortí and Rosell, 1990).

In the Lorca basin phases of recurrent stratification and restriction of the essentially marine water body are expressed in the earliest stages by the deposition of numerous sequences of laminar to thin-bedded diatomites with very little or no present organic content. The diatomites are variably chertified, probably due to their high porosity and permeability and from reaction with renewed, oxygenated bottom waters as marine conditions were reestablished after the restriction. In those instances where the restriction became more marked, the diatomites are overlain by exceptionally organic-rich, laminar, calcareous shale (TOC>25%), formed under hypersaline conditions. Each of the organic-rich sections corresponds to a discrete depositional environment and contains specific organic matter that still carries the marks of the original depositional conditions, particularly from the Eh and salinity of the water. This is attested to by the

low Pr/Ph ratio (Figure 3), specific distribution patterns of methylated chromans and C_{20} isoprenoid thiophenes, and the presence of extended hopanes that range from C_{32} to C_{35} with a predominance of the $C_{35}\alpha\beta$ isomer (De leeuw and Sinnghe Damste, 1990). These highly organic shales are quite perfectly laminar, suggesting very reducing bottom conditions, and this idea is supported by the high ratio of R_{22} (Figure 3) and the presence of benzohopanes ranging from C_{32} to C_{35} .

The n-alkane distribution within the organic-rich shales reveals that there was a small input of terrestrial organic matter resulting in an odd/even predominance between C_{32} and C_{35} . This odd/even predominance, the high quantity of polar compounds, the relative proportions of the isomers of the steranes and hopanes, and a low vitinite reflectance (R = 0.3) show the low level of maturation of the organics in the Lorca Basin.

Some of the calcareous shales are, in turn, overlain by slightly sandy, gypsiferous limestones. These limestones are less rich in organic matter (TOC <2%) than the underlying shales and apparently formed under more oxygenated conditions expressed by a lower R_{22} and a higher Pr/Ph ratio. The presence of displacive, lenticular gypsum and/or its pseudomorphs indicates hypersaline, evaporative conditions.

The uppermost section of the Lorca basin is characterized by greater and greater restriction associated with an increasing influx of continental water. Under these conditions the amount of preserved organic matter is greatly reduced (TOC<0.46%). The influx of continental water resulted in the accumulation of several beds of terrestrial sandstone (fluvial to nearshore tidal), containing organic matter with a markedly continental origin. The organics contain a high percentage of saturates and a predominance of high carbon number n-alkanes with a strong odd/even predominance (Figure 3). Above this continental episode the establishment of a strongly hypersaline condition with the deposition of massive gypsum (seen at outcrop) and halite (subsurface). This upper section is distinguished by the presence of unsaturated compounds among the saturated fraction: Hop-17(21)enes, fernene, sterenes, steradienes and diasterenes

Artificial Maturation

Artificial maturation has enabled us to follow the evolution of the organic matter in the SP-7 sample from deposition (0-5 years old) through to maturation (Figure 4).

While the lipid fraction of the original sample is dominated by sterols and fatty acids the lipids released during maturation closely resemble natural crude oils in their broad characteristics and composition. The changing yields of saturates, aromatics, resins, and asphaltenes (Figure 5) are accompanied by changes in isoprenoid and n-alkane distribution and

evolve progressively to an oil-like composition, with its characteristic nalkane distribution.

Cyclic hydrocarbons of the saturated fraction from pyrolyzed samples treated at different temperatures show the following:

at 200° and 250°C they are dominated by the unsaturated compounds: C_{30} Hop-17(21)ene, C_{27} , C_{28} and C_{29} sterenes, and C_{29} steradienes.

at 300°C they are represented by hopanes, diasterenes and steranes with relative proportions of isomers that are characteristic of organic matter at the threshold of maturity.

at 350° and 400°C the steroids and hopanoids are represented by diasteranes, steranes, and hopanes showing a composition and maturity parameters of natural crude oils.

The aromatic fraction of the lipid extract from pyrolyzed samples treated at different temperatures show the following:

at 200° and 250°C they contain the C_{20} isopreniod thiophenes: 3-(4,8,12 - trimethyl-tridecyl)thiophene, 3-methyl-2-(3,7,11-trimethyl-dodecyl)thiophene and 2,3-dimethyl-5-(2,6,10-trimethylundecyl)thiophene and the methylated chromans: 7,8-diMe-MTTC and 5,7,8-triMe-MTTC.

at 300°C the monoaromatic steroids and triaromatic steranes appear. at 350° and 400°C the aromatic hydrocarbons are fully aromatized, including: napthalenes (mono-, di-, trimethyl-), phenamtrenes (mono-, di-, trimethyl-), anthracenes and Diels' hydrocarbon (C₁₈).

From temperatures of 300° C and higher the δ^{13} C values diminish for all fractions (Figure 4), and the isotopic type-curves maintain the same pattern (Figure 5). This may be helpful in the understanding of the effects of maturation on the stable isotope carbon composition of the organic matter from evaporative systems and also useful in oil-to-oil and oil-to-source-rock correlations (Stahl, 1977, 1978; Lewan, 1983).

CONCLUSIONS

- 1) Many similarities can be drawn between the biomarkers in the organic-rich, calcareous shales from the Lorca basin and the SP-7 pyrolyzed calcareous sample from Santa Pola. The similarities that are indicators of paleosalinity:
 - Pr/Ph <1
 - $-R_{22} > 1$
 - Presence of methylated chromans with a MTTC ratio =

[5.78 - tri Me-MTTC] <1 [total methylated MTTC]

- Presence of C20 isoprenoidthiophenes
- Presence of Hop-17(21)enes

- Presence of hopanes ranging from C₃₂ to C₃₅
- 2) Modern solar salt works are good models for evaporative sedimentation, and we have demonstrated through the use of artificial maturation that they can be very useful in the understanding of the accumulation of associated organic matter and the generation of oil in evaporative systems.
- 3) Evaporites can be a good source for oil and the petroleum generation in these natural systems and can be simulated by using confined pyrolysis experiments.

REFERENCES

- Barbe, A., Grimalt, J.O., Pueyo, J.J. and Albaiges, J., 1990, Characterisation of model evaporitic environments through the study of lipid compenents. *Organic Geochemistry*, v. 16: 815-828.
- De leeuw, J. W. and Sinninghe Damsté, J. S., 1990, Organic sulfur compounds and other biomarkers as indicators of paleosalinity. In: *Geochemistry of Sulfur in Fossil Fuels*. American Chemical Society, Washington, D.C., 417-443.
- Hite, R., and Anders, D.E., 1991, Petroleum and evaporite. In: J. L. Melvin (ed.), Evaporites, Petroleum and Mineral Resources. Elsevier, Amsterdam, 349-411.
- Lewan, M.D., 1983, Effects of thermal maturation on stable organic carbon isotopes as determined by hydrous pyrolysis of Woodford Shale. *Geochim. Cosmochim Acta*, v.47: 1471-1479.
- Montenat, Ch., Ott, D'Estevou, Ph., De Larouzière, D., et Bedu, P., 1987, Originalité géodynamique des bassins néogènes du domaine Bétique oriental (Espagne). *Notes et Memoires*, v. 21: 11-50. TOTAL, Compagnie Française des Pétroles.
- Ortí, F, 1990, Introducción a las evaporitas de la Cuenca de Lorca. In: F. Ortí, J. M., J. Mª. Salvany Duran (eds.), Formaciones evaporíticas de la Cuenca del Ebro y cadenas periféricas, y de la zona de Levante. ENRESA, Departament de Geoquimica Petrologia i Prospecció Geològica, Universidad Barcelona, 251-256.
- Ortí, F., and Rosell, L., 1990, Yesos di Lorca (Messinienese). In: F. Ortí, J. M., J. Ma. Salvany Duran (eds.), Formaciones evaporíticas de la Cuenca del Ebro y cadenas periféricas, y de la zona de Levante. ENRESA, Departament de Geoquimica Petrologia i Prospecció Geològica, Universidad Barcelona, 297-298.
- Stahl, W.J., 1977, Carbon and nitrogen isotopes in hydrocarbon research and exploration. *Chem. Geology*, v.121-149.
- Stahl, W.J., 1978, Source rock-crude oil correlation by isotopic type curves. Geochim. Cosmochim Acta, v.42: 1573-1577.

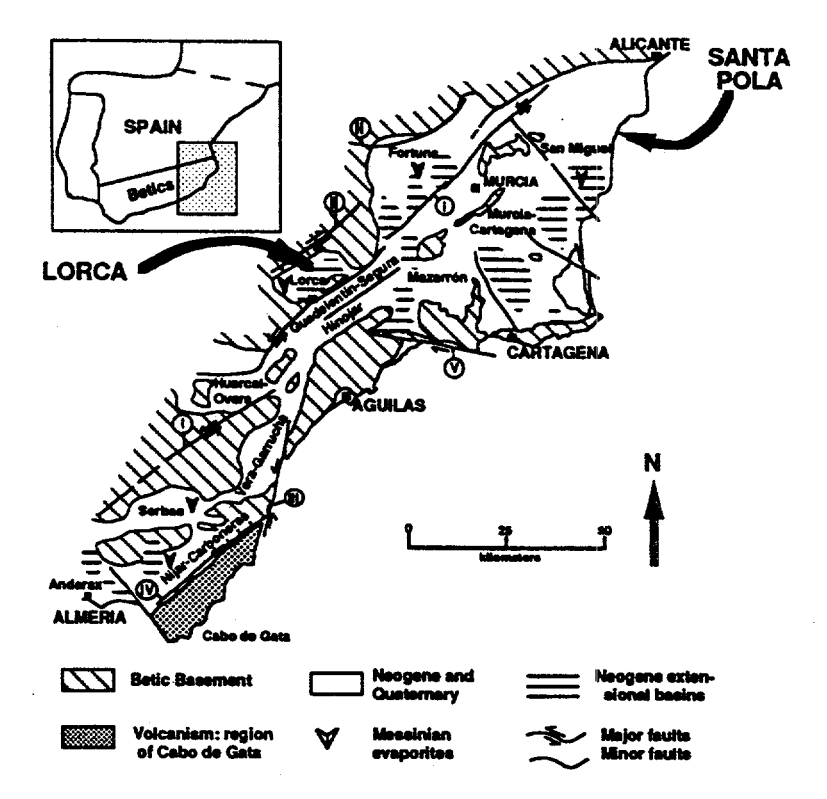


Figure 1. Location map of Neogene basins in the Betic Cordillera of southeastern Spain with indication of the position of the marine-evaporative Messinian deposits. Arrows indicate the position of the Lorca Basin (Messinian) and Santa Pola (Recent) (simplified from Montenat et al., 1987; and Orti, 1990).

GENERALIZED STRATIGRAPHIC SECTION OF LORCA BASIN

FOR THE LATE TORTONIAN THROUGH MESSINIAN (UPPER MIOCENE)

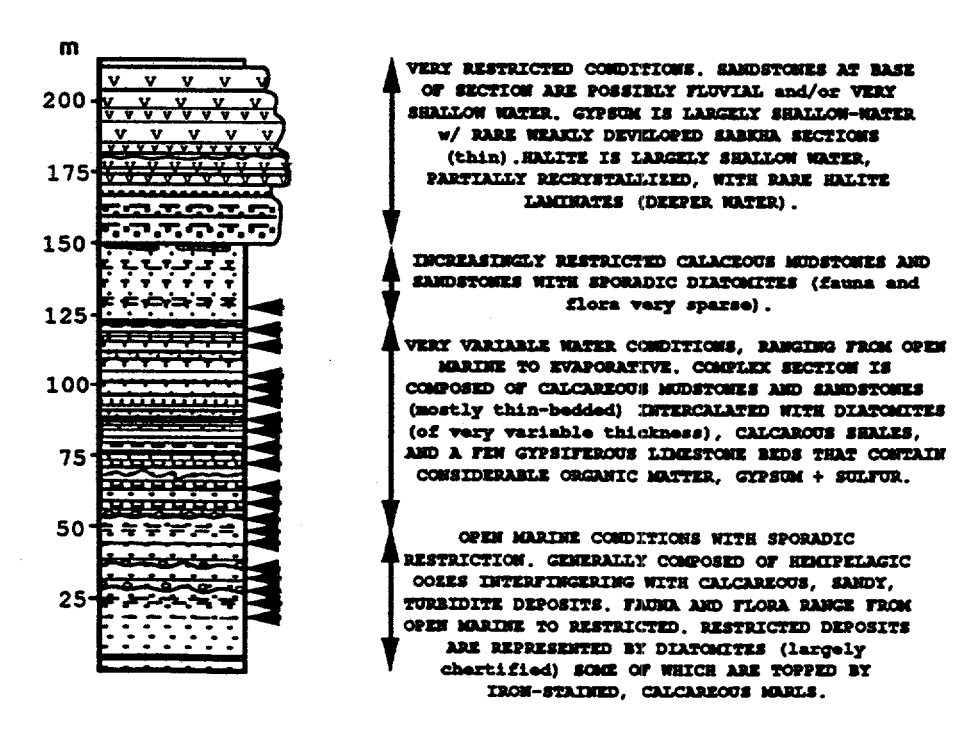


Figure 2. Stratigraphic section of the Lorca Basin with general lithologies given at right. Arrows point out diatomite layers, some of which are associated with bituminous, calcareous, shales.

56

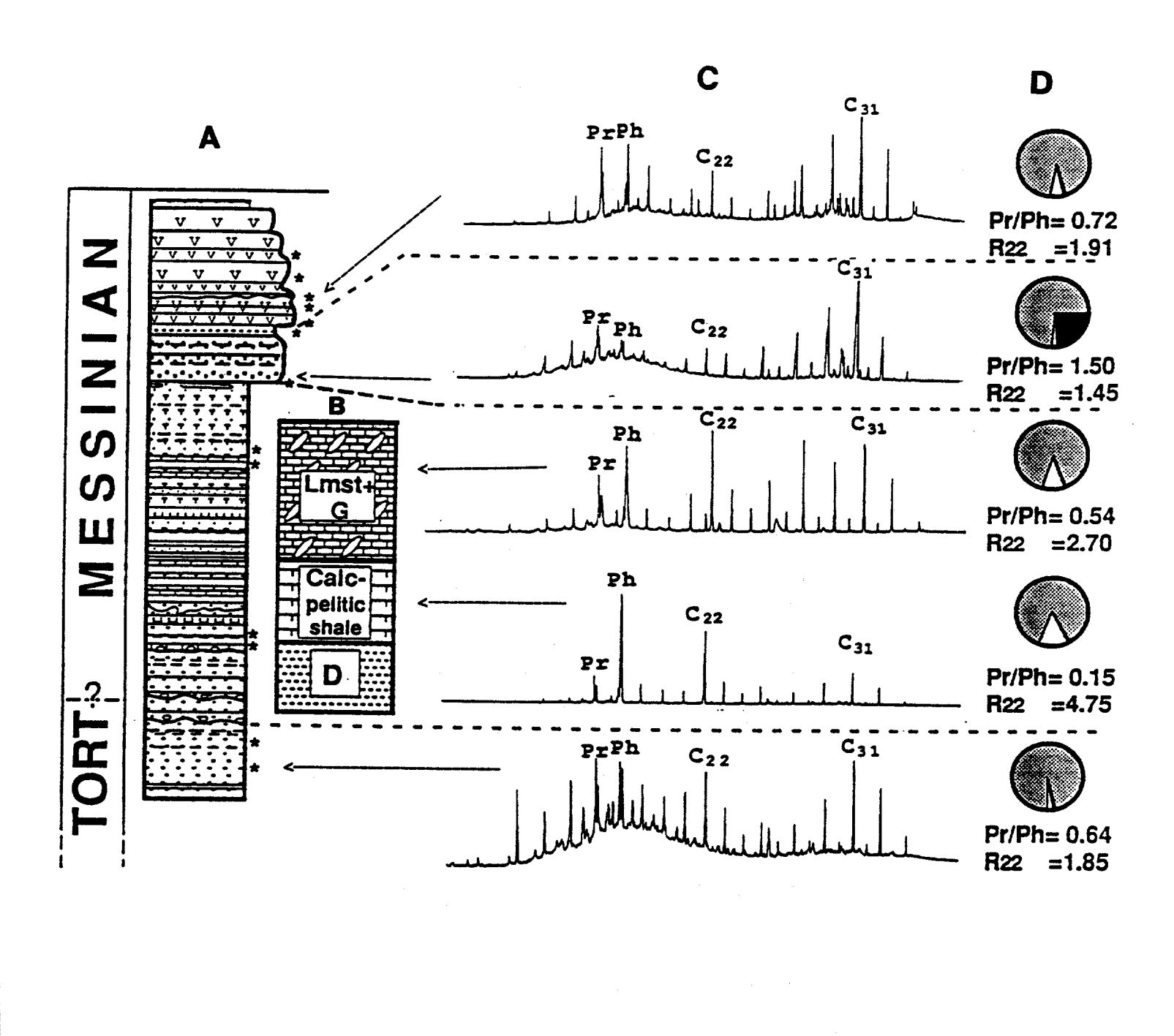




Fig.3. Correlation between lithology and biomarkers in the upper section of the Lorca basin. Column "B" represents one of many short periods of extreme restriction within generally open conditions. The basin becomes totally continental just below the gypsum (note changes in gas chromatograms (column "C" and changes in values given in column "D"), and then is of a mixed water origin within the gypsum itself.

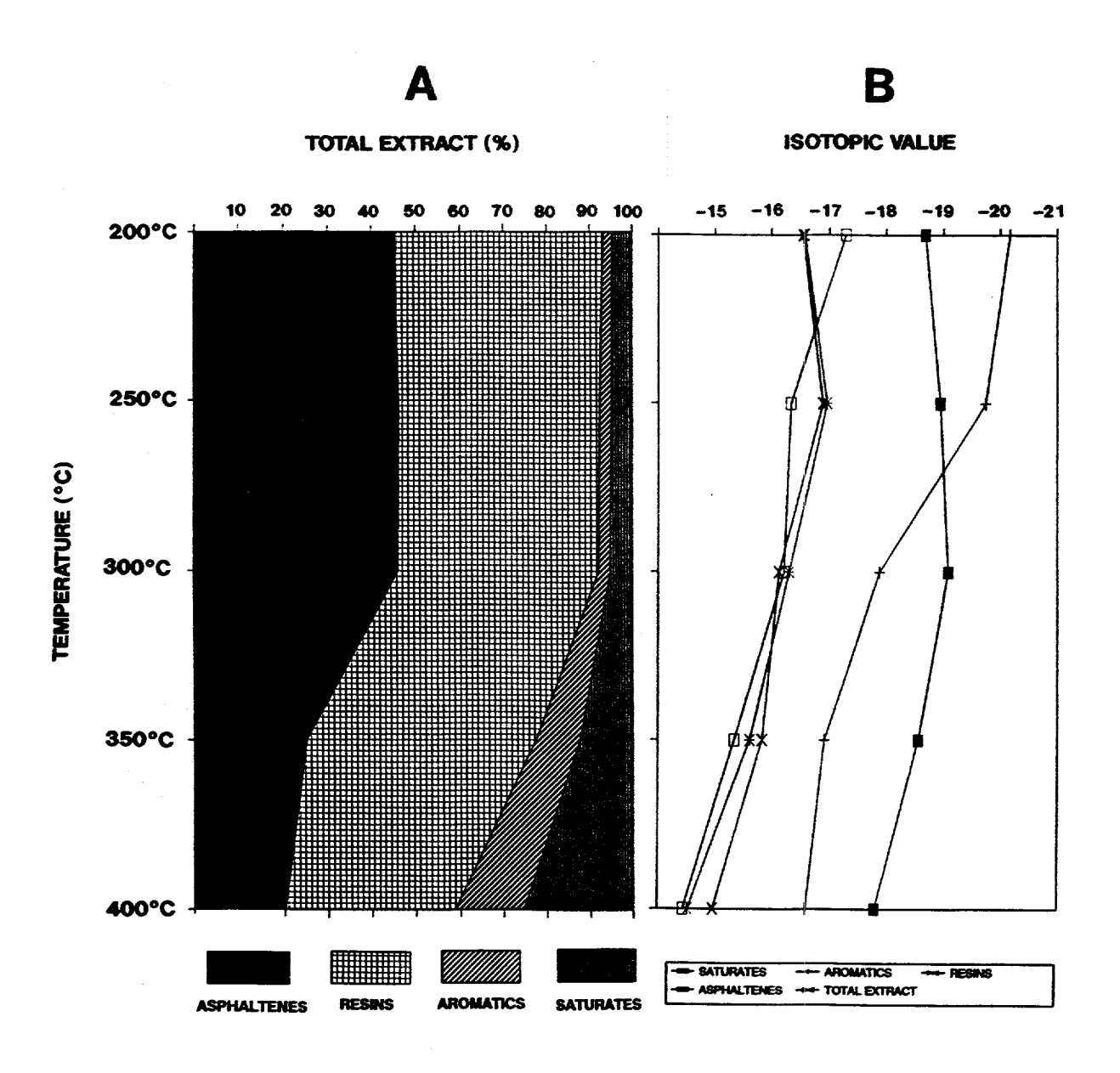


Figure 4. (A) Plot showing changes in the relative amounts of saturates, aromatics, resins and asphaltenes recovered from the Sp-7 sample pyrolysed at 200, 250, 300, 350 and 400°C, and (B) variation in δ^{13} C values of the saturates, aromatics, resins, asphaltenes and total extracts.

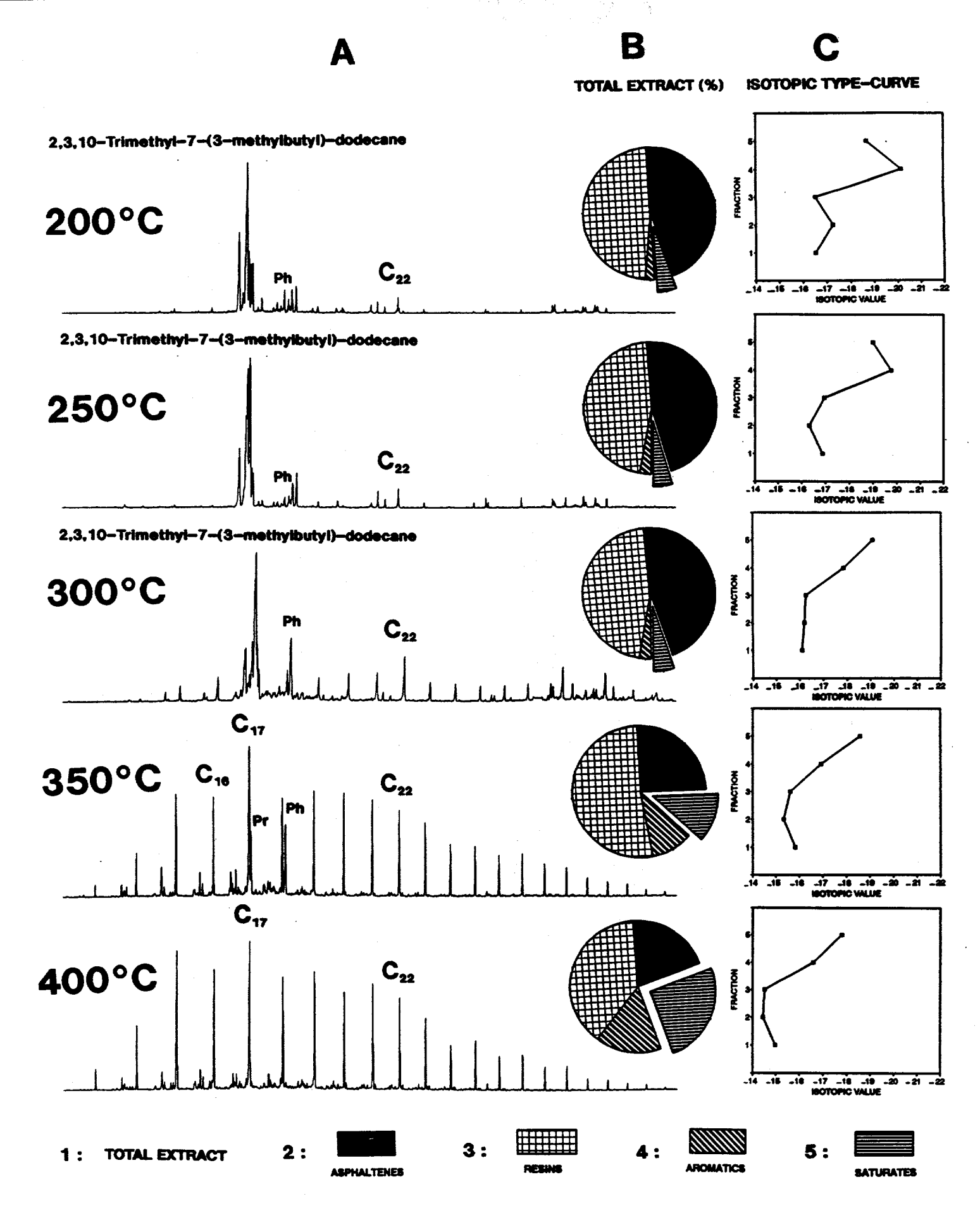


Figure 5. (A) Gas chromatograms of saturated fractions, (B) total extracts composition and (C) isotopic type-curves of the total extracts, asphaltenes, resins, aromatics and saturates, of the sp-7 sample pyrolysed at 200, 250, 300, 350 and 400°C.

Organic Geochemistry of Continental Margin and Deep Ocean Sediments

Jean K. Whelan, Principal Investigator.

Address: Department of Chemistry, Fye Building, Woods Hole Oceanographic Institution, Woods Hole, MA 02543

Background and Introduction Much of the Woods Hole DoE sponsored research has focused on basic mechanisms of gas generation and migration. During the course of this research, we became aware of "the enigma of the Gulf Coast oils". Oil and gas accumulations occur widely across the continental shelf of the entire Louisiana Ğulf Coast. These oils are distinguished by their similarity throughout much of this area (the Gulf Coast Type 1A oils in Fig 1, as defined by Thompson and Kennicutt, 1990). However, in spite of much research and speculation, identification of the source of this oil has remained elusive. In the off-shore area of the continental slope, several Tertiary rocks are currently in the oil window (vitrinite reflectance 0.6 to 1.35, Fig 2 from Dow, 1977). Most researchers currently feel that the thick sequences of Pleistocene through Miocene sediments in this area do not constitute a viable petroleum source rock (Jones 1990): that is, one rich enough in hydrogen-rich organic matter to have generated a discrete hydrocarbon phase in the source rock. Formation of such an oil phase, which largely displaces the water in the sediment, is currently thought to be the critical minimum requirement needed to overcome the energy "bottle neck" in the oil generation-expulsion process, primary expulsion of the oil from the fine-grained source rock into the initial more porous carrier beds (Lewan, 1986; Durand, 1988).

However, our past research indicates that active generation and expulsion of lighter hydrocarbons is occurring at the present time from the Miocene section of the Cost B1 well in the E. Cameron Field of the Louisiana Gulf Coast (Whelan, et al, 1984) despite the fact that these rocks are marginal to poor with respect to source rock quality (Fig 3). The vitrinite reflectance profile indicates continuous deposition through the Quaternary (Fig 4) so that a one-dimensional maturation model was run on this well (Fig 5). The experimental (Fig 6) and computed (fig 5) oil and gas generation profiles match extremely well, providing further evidence that the oil generation window has been correctly identified. The shallower maximum in the C2-C5 profile in comparison to the heavier C6-C8 profile is probably due to early expulsion and upward migration of the lower molecular weight gases as the sediments enter the oil window (Fig 5). Gas chromatograms of extractable bitumens going down the same well are shown in Fig 7. Note that compositions typical of the main phase of oil generation are starting at 12,230 ft and are well developed in sediments from 14,300 ft and deeper, in good agreement with the downhole maturation model (Fig 5). Downhole profiles of some ratios diagnostic of increasing maturation with depth, the carbon preference index (CPI) and the ratio of pristane/n-C17, are also shown in Fig 6. From the combined data, we conclude that bitumens smaller than C6 are being generated and expelled in this well, while molecules larger than C14 are being largely retained by these organic-lean sediments. For the intermediate C6-C13 hydrocarbon range, the organic geochemical information is ambiguous: Whelan, et al, 1984 is consistent with expulsion, while Fig 6 suggests retention of the C6-C8 fraction.

These data raise a number of questions concerning the Louisiana Type 1A oils (Fig 1): in spite of current wisdom, could they be sourced in "marginal" or poor source rocks similar to those occurring in E. Cameron well? The biomarker characteristics of the Type 1A oils (Comet, et al, 1990) and the position of the present day oil "kitchen" are consistent with such a source. Dow (1990) has made the argument that specific Tertiary intervals, such as a few sections with TOC >1% occurring in the Miocene section below 15,000 ft in the E. Cameron well (Fig 1), may comprise a possible source. However, it is difficult to account for the aerial extent of the Type 1A oils from such a limited source rock unit. Maybe oil can be stripped out of organic-lean rocks by gas forming either in-situ or flowing upward from deeper formations. Alternatively, a number of researchers have suggested

that Cretaceous source rocks, which have a significant terrigenous input, could be the common source of the Type 1A Gulf Coast oils (Schumacher and Perkins, 1990). However, many of the potential Cretaceous rock units also appear to be marginal with

respect to source rock quality (eg, Table 2).

If significant quantities of Type 1A oils are coming from relatively organic lean and hydrogen poor Tertiary or Cretaceous source rocks, then "non-conventional" expulsion and migration mechanisms, such as gas dissolved in oil (Solkolov, 1963; Solkolov and Mironov, 1962 and others as reviewed in Hunt, 1979, pp 2130-215) must be invoked. All of these "non-conventional" migration mechanisms require some quantity of gas to solubilize and move the oil. Therefore, quantitative data on amounts and compositions of gases potentially available to aid in these processes are key to understanding their importance both in the Gulf Coast and world-wide. Currently, very little reliable quantitative data is available on either quantities or compositions of gases generated by various kinds of rocks.

We are currently carrying out two kinds of research to address the potential role of

gas in petroleum expulsion and migration processes:

a) Laboratory experiments (hydrous pyrolysis) to better define kinetic and thermodynamic parameters of gas generation and expulsion in typical immature Tertiary and Cretaceous sediments from the Louisiana Gulf Coast and

b) Integrating laboratory and field organic geochemical data into a larger geological and geochemical framework via participation in the Global Basin Research

Network, GBRN.

This talk summarizes our progress to date in both areas. In addition, Jean Whelan recently participated as shipboard organic geochemist on Ocean Drilling Project Leg 139 to the sediment-covered Middle Valley Hydrothermal Area which is about 150 miles West of British Columbia. This research will produce an excellent sample and data set on the response of organic lean continental slope sediments, similar to those recovered from the E. Cameron well, to in-situ heating via the underlying hydrothermal system. Results and Discussion

a) Hydrous pyrolysis experiments Initial tests of an apparatus using simple pipe bombs were carried out using hydrocarbon standards in water as well as Woodford Shale standards provided by Dr Mike Lewan. These tests showed two major difficulties with this type of apparatus for studying kinetics of gas generation: a) The pipe bombs (and probably the Parr bombs which are currently widely used in hydrous pyrolysis studies) suffer from large thermal gradients and cold spots where gases condense giving anomalous results and b) it is very difficult to make an "on-line" sampling valve between the bomb and the analysis system which does not leak and pit during the experiment. These problems may explain why molecular and isotopic compositions of gases produced by hydrous pyrolysis generally do not match those found in the natural system (Lewan, in press). In addition, if kinetics of oil expulsion in Gulf Coast rocks is critically dependent on gas generation and expulsion, these cold spots may also explain why hydrous pyrolysis of potential Gulf Coast source rocks have thus far not produced oils which match compositions of the naturally occurring Type IA oils (Kennicutt, et al, 1990).

In order to overcome the problems outlined above, we are currently carrying out initial experiments with an "expandable gold bag" hydrous pyrolysis apparatus (Fig 8, Seyfried, et al, 1987). This equipment was successfully used by Jeff Seewald, a postdoctoral investigator in our laboratory, in his Ph.D. thesis work on kinetics and thermodynamics of gas evolution from organic rich Guaymas Basin sediments (Seewald, et al, 1990). On-line fluid sampling (gases, aqueous, and expelled bitumen phases) should be possible with this system, which can be run at virtually any temperature. Initial results on evolution of methane and carbon dioxide from the Woodford Shale and comparison to results of Mike Lewan using the more conventional Parr Bomb apparatus will be presented. Initial results from hydrous pyrolysis of the much more organic lean E. Cameron sediments will also be presented. Future work will involve running additional experiments

to obtain reliable activation energies, as well as carrying out similar experiments with the immature Gulf Coast rocks shown in Table 2, all of which may be potential sources for Gulf Coast gases or the Type 1A oils.

b) Global Basin Research Network (GBRN)

Over the last three years, a group of geoscientists from a number of academic institutions have worked informally to establish a research network to better understand subsurface fluid flow processes in sedimentary basins and their relation to resource accumulation (ie, petroleum and metal ores). A list of current academic and industrial participants is shown in Fig 9. The rationale for establishing the GBRN is that diverse basin phenomena, treated today by quite separate academic specialties, need to be viewed in a new way: as large-scale coupled processes in subsurface sedimentary basins which act giant thermochemical-structural reactors. These "reactors" deform and break as organic matter in them matures, generates fluid overpressures, and causes (often episodic) fluid movement that chemically alter the host sediments. These processes produce, under favorable conditions, economically valuable mineral deposits and hydrocarbon accumulations. Organic and inorganic chemical alterations interact with the basin stratigraphy and structure which control local permeability. Thus, it is the interaction of the overall basin geology and geochemistry that ultimately determine fluid migration pathways. Understanding how these subsurface fluid flows affect basin resources requires the effective joining of observations and processes that have previously been addressed by separate and largely non-communicating disciplines.

The overall goal of the GBRN is to develop a general methodology which is applicable to any sedimentary basin, as shown schematically in Fig 10. The philosophy of the approach is straightforward - i) to develop means of collecting and viewing in three-dimensions large amounts of diverse data (basin observations, placed in a "data cube" in a computer workstation, Fig 10B and ii) to develop and test integrated process models that describe diverse basin phenomena as products of operation of a single thermochemical-structural reactor ("model cube" in Fig 10A). The computer is the major tool in all phases of the work, with heavy utilization of 3-dimensional color graphics on modern computer workstations which allow comparison "snapshots" of the subsurface from the actual data (the data cube) versus that generated by the computer model (Fig10A). Thus, our approach is conceptually similar to the way science is usually done for less complex problems: a conceptual model is continuously tested and modified to fit observational data.

Initial development of the "data cube" approach to data visualization and coupled development of fluid flow models is being carried out on a 20 x 40 km area of the Louisiana Gulf Coast in the highly productive S. Eugene Island/S. Marsh Island area. The Woods Hole part of this effort is to integrate organic geochemical data (including hydrous pyrolysis data) - our own as well as that from other academic and industrial laboratories into GBRN data cubes and models. Progress to date has included: a) obtaining samples of the potential Gulf Coast Source rocks for kerogen typing and maturation studies, as well as for hydrous pyrolysis studies (Table 2); and b) insertion of organic geochemical gas and oil compositional data obtained in an extensive oil correlation study by the Geochemical and Environmental Research Group (GERG) at Texas A & M into the data cube. The latter is providing considerable insight into Gulf Coast oil and gas generation processes beyond that available by looking at either the organic geochemical data (Comet et al, in press; Thompson et al, 1990, submitted or in press) or the geological data in isolation. For example, all of the currently available organic geochemical data has been inserted into the first developmental data cube covering a very oil and gas productive 20 x 40 km area of the Gulf Coast (South Marsh Island-Eugene Island, SMI-EI). A general procedure has been worked out for contouring organic geochemical data in terms of the seismic data so that hydrocarbon distributions can be visualized in three dimensions along with the geology. This exercise alone has shown that the more terrigenous Type 1A oils occur to the north and west of the SMI-EI data cube, while the more marine Type 1B type oils (Fig 1) are found in reservoirs to the south and east. A salt ridge separates the two oil types. Thus,

"feeder" systems to the different parts of the data cube are using different plumbing systems.

Viewing this initial (and, so far, very limited) oil and gas data set together with the heat flow, salinity, and pressure data from the same area, also strongly suggests that active injection of oil and gas is currently occurring into Eugene Island reservoirs. This work together with previous results of the Texas A & M group (Thompson and Kennicutt, 1990; Thompson, unpublished results) also suggests that vertical migration of oil and gas from Cretaceous reservoirs (and, possibly source rocks) is a major process occurring at the present time. Migration of oil may be aided by upward streaming of gases and periodic rupturing of overpressured intervals. The evidence further suggests that the tops of these reservoirs are leaky and that upward migration is a steady state process. If so, we should be able to see hydrocarbon anomalies in surface sediments overlying the "leaky" intervals. To test this idea, an extensive Texas A & M surface gas data set which covers the entire Gulf of Mexico is in the process of being superimposed on the data cube in the SMI-EI area.

The academic participants in the GBRN finding that the building of the data cube brings together much very fragmented Gulf Coast data and also tells us where additional samples and analyses are required. The bi-yearly meetings between the GBRN management council and oil company participants have been very beneficial in helping to locate needed data, samples, and equipment, and in pin-pointing outstanding unsolved scientific problems. We have found that oil companies are often very willing to help when they consider a particular problem to be important and when the academic participants are able to specify exactly what resources are required. For example, through the GBRN, Chevron became aware of the need for systematic kerogen typing and maturation studies as input both to the data cube and to the models. Woods Hole currently has expert organic petrographer on its staff with extensive experience with N. Sea samples, Ms Lorraine Buxton. However, she is currently without a suitable microscope. As a result, Chevron has loaned Woods Hole a very sophisticated Zeiss petrographic microscope system so that she will be able to carry out these crucial measurements.

A videotape, made on the supercomputer at Cornell, will be shown to demonstrate the coupled processes which we currently believe are important in the S. Eugene Island/S. Marsh Island area.

c) Ocean Drilling Project Leg 139 samples and data set

Jean Whelan participated as shipboard organic geochemist on Ocean Drilling Project Leg 139 during the summer of 1991. An extensive data and core collection was obtained (see Table 1) along with excellent temperature measurements for sediments covering the Middle Valley hydrothermal area about 150 miles west of British Columbia. Shipboard analyses show that the starting mineral matrices and organic matter is very similar throughout the area. One of the major goals of the leg is to contour the heat flow and fluid flow in the 4 square mile study area. Time-temperature will be estimated in a number of different ways by several different laboratories by diverse techniques, including mineral alterations, dating of cores via shipboard paleontologists, and downhole temperature measurements. Therefore, this data set will provide an excellent lab versus "geological" comparison of various organic matter maturation reactions.

Several factors, which can complicate studies of this type, can be ruled out for the Leg 139 samples. All of these sediments contain relatively low TOC (0.5% or less), too low for efficient petroleum expulsion by "normal" petroleum expulsion processes, as described above. Thus, migration of the C14+ hydrocarbons appear to be unimportant at several of the sites (ie, 855, 856, and 857) and hydrocarbon compositions appear to reflect in-situ time-temperature conditions. Shipboard analyses also showed conditions in the sediments to be unfavorable for microbiological methanogenesis. Therefore, sediment gases, which were ubiquitous, appear to be largely thermogenic. Methane, ethane, and propane increased exponentially with increasing sediment temperature.

The further analyses of the organic geochemical material in these sediments will be a collaborative effort between:

1) Woods Hole - examination of changes in kerogen (via organic petrography, pyrolysis, and solid state NMR); examination of kinetics of gas generation (via hydrous pyrolysis).

2) Oregon State University (Dr Bernd Simoneit) -analyses of biomarkers and

maturation indicators in extractable bitumens.

3) University of British Columbia (Dr Michael Whitaker) - gas compositions and

Results will be compared with contours of heat flow, fluid circulation, and mineralogical changes being prepared by other scientists as part of the shore-based studies.

References

Comet, P.A., J.K. Rafalska and J.M. Brooks (submitted) Sterane and triterpane fingerprinting as a tool in mapping of oils, condensates and source rocks of the Gulf of Mexico region, Organic Geochemistry.

Doligez, B., Ed. (1987) Migration of Hydrocarbons in Sedimentary Basins. Colloques et

Seminaires 45, Editions Technip, Paris.

Dow, W.G. (1977) Petroleum source beds on continental slopes and rises. In: Geology of Continental Margins. AAPG Continuing Education Course Note Series 5, AAPG Continuing Education Program, AAPG, Tulsa, OK.

Dow, W.G. (1984) Oil source beds and oil prospect definition in upper Tertiary of the Gulf

Coast. Trans. Gulf Coast Assoc. Geol. Soc., v. 34, pp 329-340.

Durand, B. (1988) Understanding of HC migration in sedimentary basins (present state of knowledge). Org Geochem., v. 13, pp 445-459.

Hunt, J. M., 1979. Petroleum Geochemistry and Geology, W. H. Freeman and Co., San Francisco.

Jones, R.W. (1990) Summary.In: Schumacher, D. and Perkins, eds, Gulf Coast Oils and Gases, Their Characteristics, Origin, Distribution, and Exploration and Production Significance, Gulf Coast Section, SEPM, Earth Enterprises, Inc., Austin, TX, pp1-8.

Lewan, M.D. (1987). Petrographic study of primary petroleum migration in the Woodford Shale and related rock units. In: Doligez, et, Migration of Hydrocarbons in Sedimentary Basins. Colloques et Seminaires 45, Editions Technip, Paris., pp 113-

Lewan, M.D. (in press) Laboratory simulation of petroleum formation: hydrous pyrolysis. In: Organic Geochemistry, M.H. Engel and S.A. Macko, eds, Plenum Publishing Corp, New York.

Schumacher, D. and Perkins, eds (1990) Gulf Coast Oils and Gases. Their Characteristics. Origin, Distribution, and Exploration and Production Significance, Gulf Coast Section,

SEPM, Earth Enterprises, Inc., Austin, TX.

Seewald, J.W., Seyfried, W.E., Jr., and E.C. Thornton (1990) Organic-rich sediment alteration: an experimental and theoretical study at elevated temperatures and pressures. Applied Geochemistry, v.5, pp 193-209.

Seyfried, W.E. Jr., Janecky, D.R., and Berndt, M.E. (1987) Rocking autoclaves for hydrothermal experiments II. The flexible reaction-cell system. In: Experimental Hydrothermal Techniques, G.C. Ulmer and H.L. Barnes, eds, pp 216-240.

Solkolov, V.A. and S.I. Mironov (1962) On the primary migration of hydrocarbons and other oil components under the action of compressed gases. In: The Chemistry of Oil and Oil Deposits. Acad. Sci. USSR, Inst. Geol. and Exploit. Min. Fuels, pp 38-91.

Solkolov, V.A., T.P. Zhuse, N.B. Vassoevich, P.L. Antonov, G.G. Grigoryev, and V.P. Kozlov (1963) Migration processes of gas and oil, their intensity and directionality, World Petroleum Congress, June, Frankfurt, Maine.

Thompson, K.F. (In press) Correlations of Gulf Coast petroleums on the basis of isoprenoid biomarkers, Organic Geochemistry, Organic Geochemistry

Thompson, K.F. M. & M.C. Kennicutt (in press) Nature and frequency of occurrence of non-thermal alteration processes in offshore Gulf of Mexico petroleums, 9th Annual GCS-SEPM Research Conference, December 1988, New Orleans, LA.

Thompson, K.F.M. (1988) Gas-condensate migration and oil fractionation in deltaic

systems, Marine and Petroleum Geology, v. 5, pp 237-246.

Thompson, K.F.M. (submitted). Contrasting characteristics attributed to migration in petroleums reservoired in clastic and carbonate sequences in the Gulf of Mexico region. Petroleum Migration Symposium. 1989 Special Publication, Geological Society of London.

Thompson, K.F.M., M.C. Kennicutt, and J. M. Brooks (1990) Classification of offshore

Gulf of Mexico Oils and Gas-Condensates. AAPG Bull..

Thompson, KFM and Kennicutt, M.C. (1990) Nature and frequency of occurrence of non-thermal alteration processes in offshore Gulf of Mexico petroleums. In: Schumacher, D. and Perkins, eds, Gulf Coast Oils and Gases. Their Characteristics. Origin.

Distribution. and Exploration and Production Significance. Gulf Coast Section, SEPM, Earth Enterprises, Inc., Austin, TX., pp199-218.

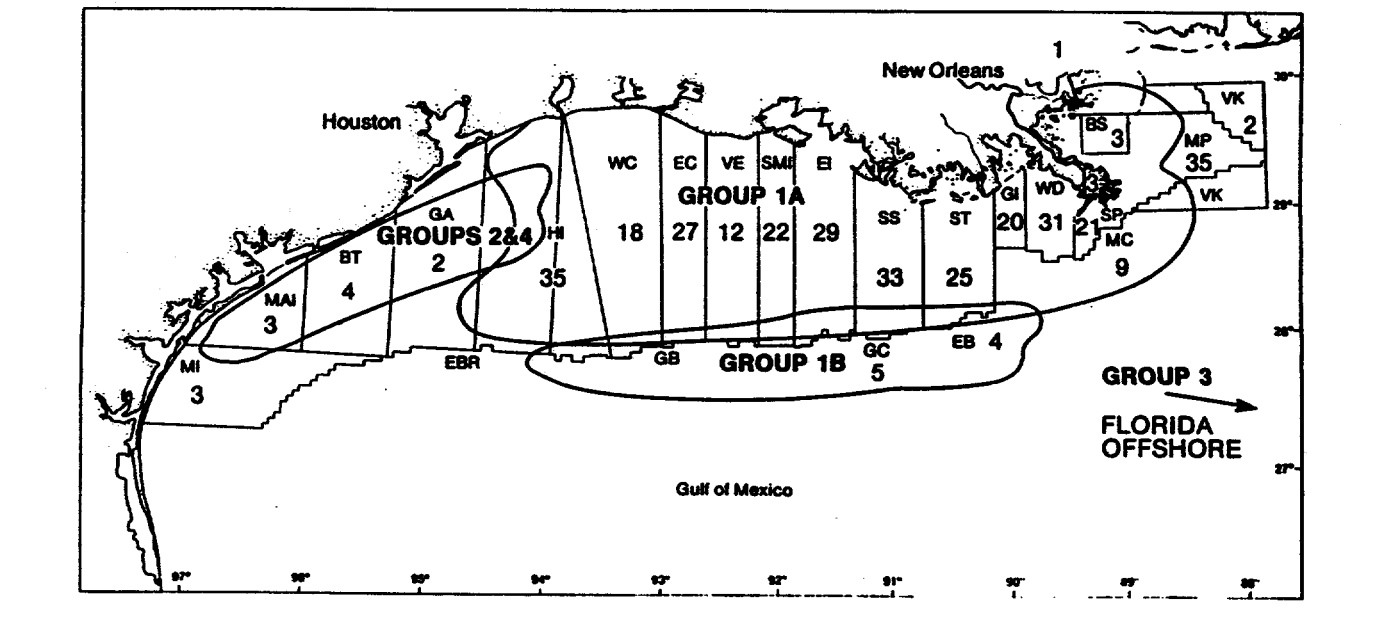
Whelan, J.K., J.M. Hunt, J. Jasper, and A. Huc (1984), Migration of C1-C8 hydrocarbons in marine sediments. Org Geochem. v.6, pp 683-694.

Figures:

- Figure 1: Location and properties of Gulf Coast Type 1A oils (from Thompson and Kennicutt, 1990)
- Figure 2: Louisiana Gulf Coast, N-S vitrinite reflectance profile, zone of Ro= 0.6 to 1.35% indicated, from Dow, 1977.
- Figure 3: Percent total organic carbon and kerogen type, E. Cameron Cost B-1 well. Kerogen typing carried out on samples shown in Fig 4.
- Figure 4: Vitrinite reflectance profile, E. Cameron Cost B-1 well. The slope of this profile matches that of the L.M. Miocene section from Dow, 1977, as indicated by arrows.
- Figure 5: One-dimensional maturation model of E. Cameron Cost B-1 well (Yukler and Whelan, unpublished data).
- Figure 6: Experimental bitumen data for E. Cameron well, including some downhole maturation indicators (%Ro, CPI, and Pris/nC17) and downhole profiles of sorbed gases, SC2-C5 and SC6-C8.
- Figure 7: Down-hole profiles gas chromatograms of solvent extractable C14 to C35 bitumens, E. Cameron Cost B-1 well.
- Figure 8: Schematic illustration of flexible cell hydrothermal equipment (from Seyfried et al., 1987). The apparatus has been adapted to use a smaller gold-titanium reaction cell in place of the one shown here.
- Figure 9: List of current active academic and industrial participants in the Global Basin Research Network.
- Figure 10: Schematic diagram of overall methodology and approach of GBRN. A)
 Schematic relationship of basin observations (i.e. data cube) and modeling; B) Building the data cube

Tables:

- Table 1: List of samples obtained from Ocean Drilling Project (ODP) Leg 139.
- Table 2: List of immature Gulf Coast samples currently in hand for hydrous pyrolysis studies.



	GROUP 1 A	GROUP 1B
§ ¹³ c § ³⁴ c	-26.5 ± 0.4 ‰ -5.6 ± 2.4 ‰	-26.5 ± 0.3 % -5.9 ± 1.2 ‰
% S	0.03 - 0.5% median ~ 0.5%	0.8 - 1.4% median ~ 1%
V/(V+Ni)	0.27 ± 0.10	0.67 ± 0.07
Sourcerock	Clastic, high Fe	Carbonate, low Fe
Pr/Phy	1.5 to 5.0	1.3

Figure 1: Location and properties of Gulf Coast Type 1A oils (from Thompson and Kennicutt, 1990)

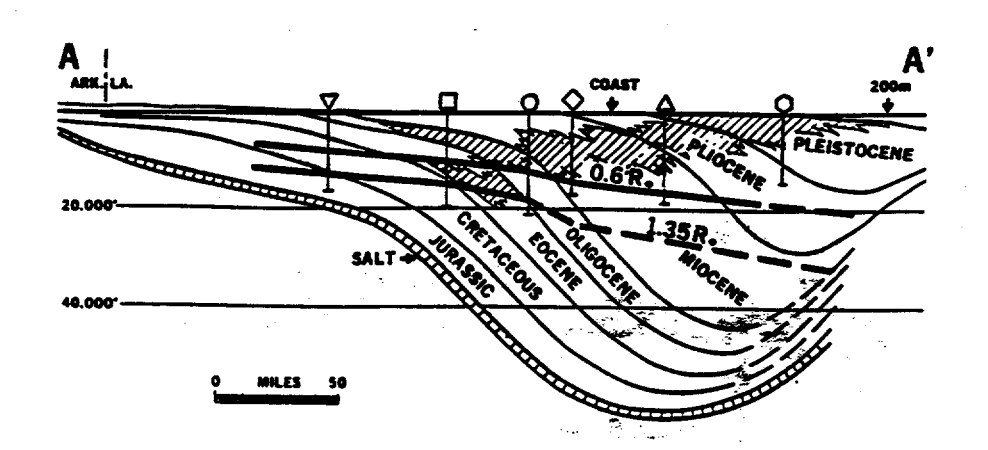
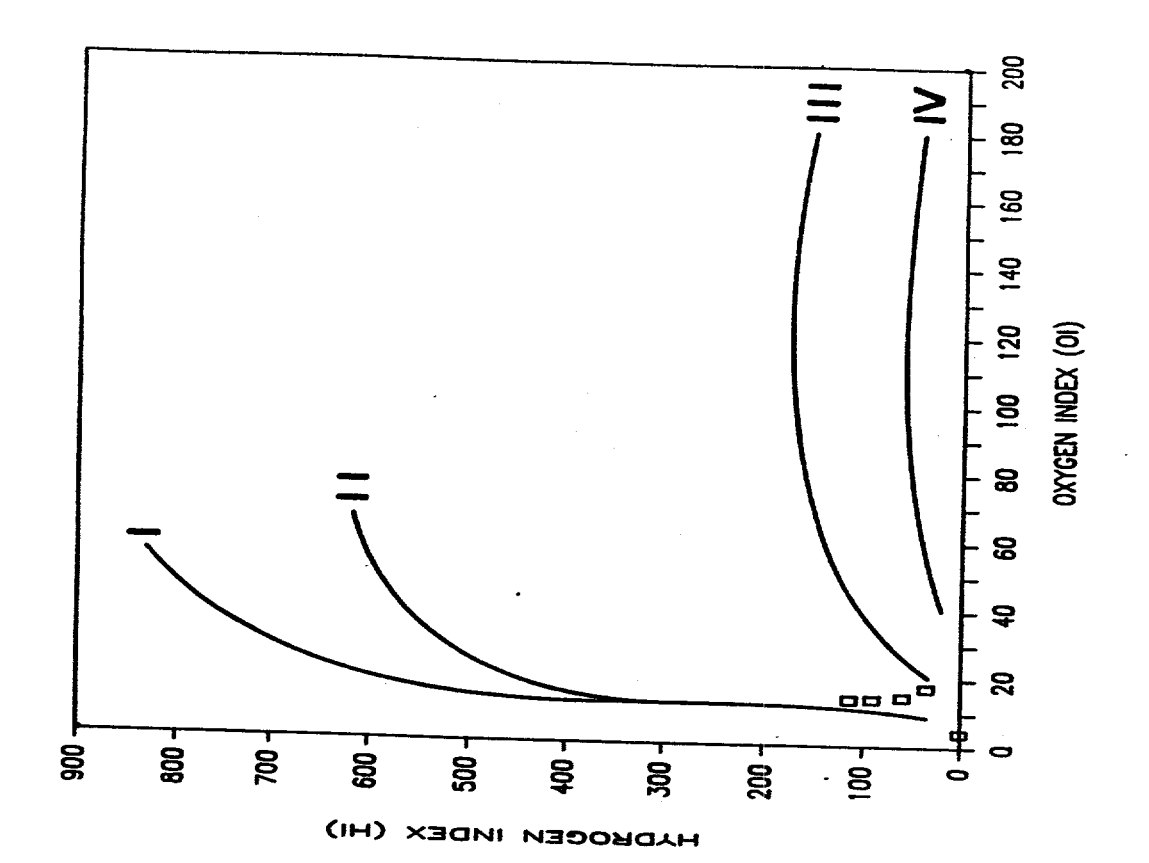


Figure 2: Louisiana Gulf Coast, N-S vitrinite-reflectance profile, zone of Ro= 0.6 to 1.35% indicated, from Dow, 1977.

6,000 6,000 8,000 6,000

Figure 3: Percent total organic carbon and kerogen type, E. Cameron Cost B-1 well. Kerogen typing carried out on samples shown in Fig



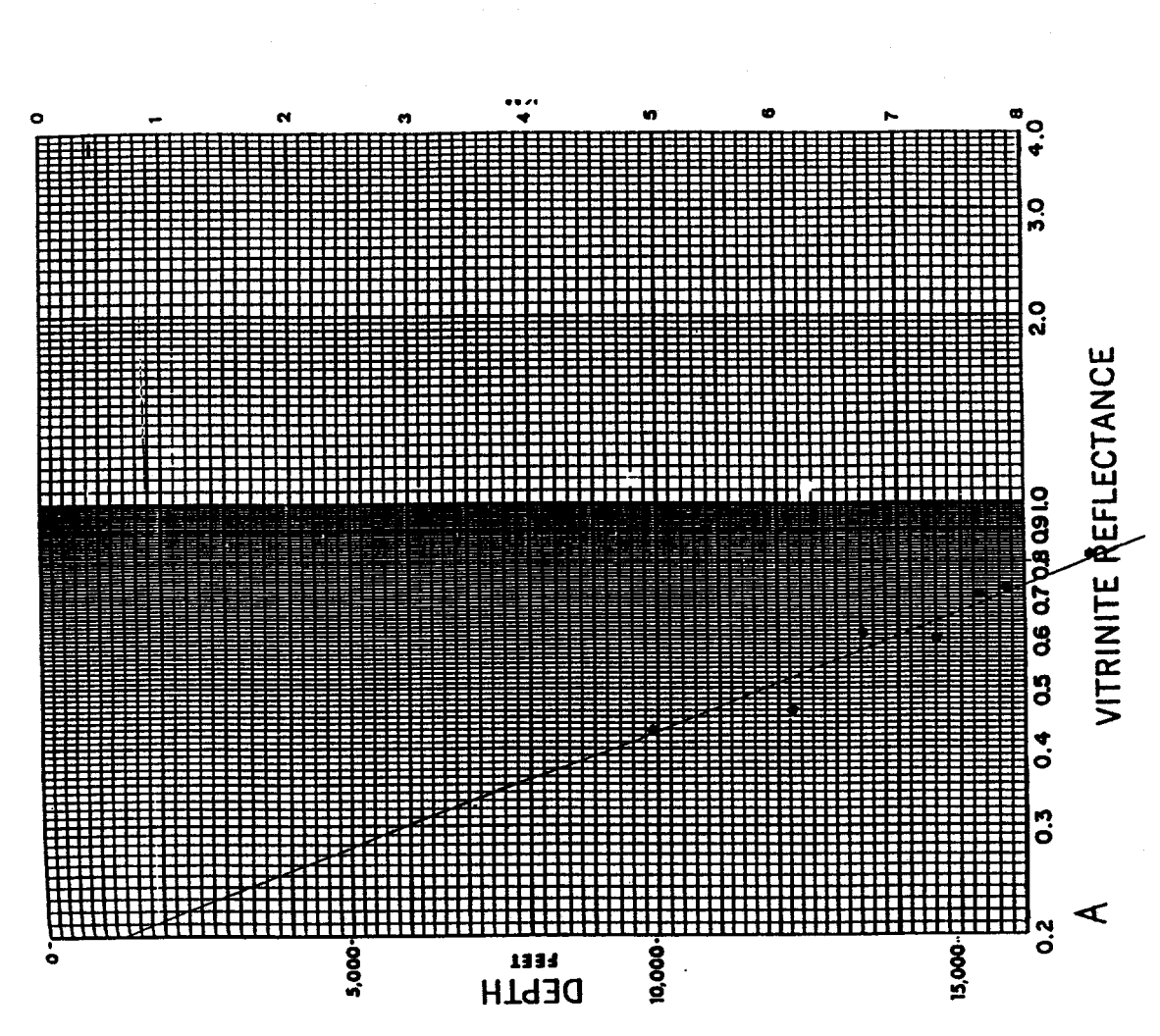
₹

7

G.0

0

18,000



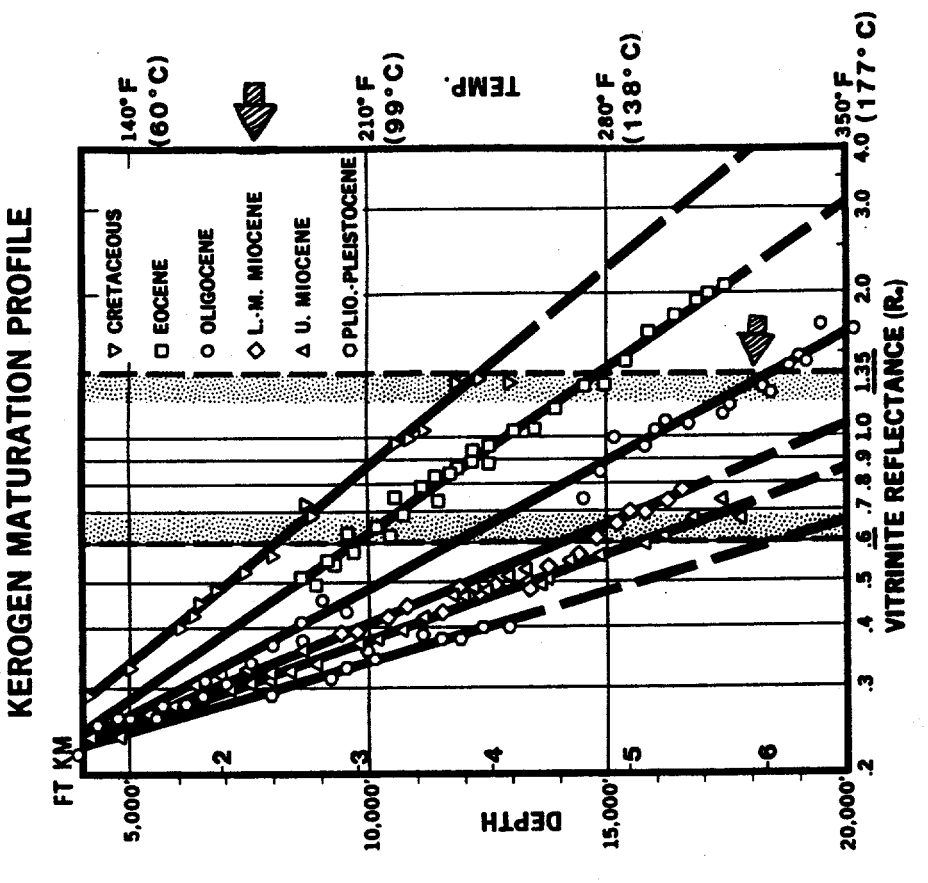


Figure 4: Vitrinite reflectance profile, E. Cameron Cost B-1 well. The slope of this profile matches that of the L.M. Miocene section from Dow, 1977, as indicated by arrows.

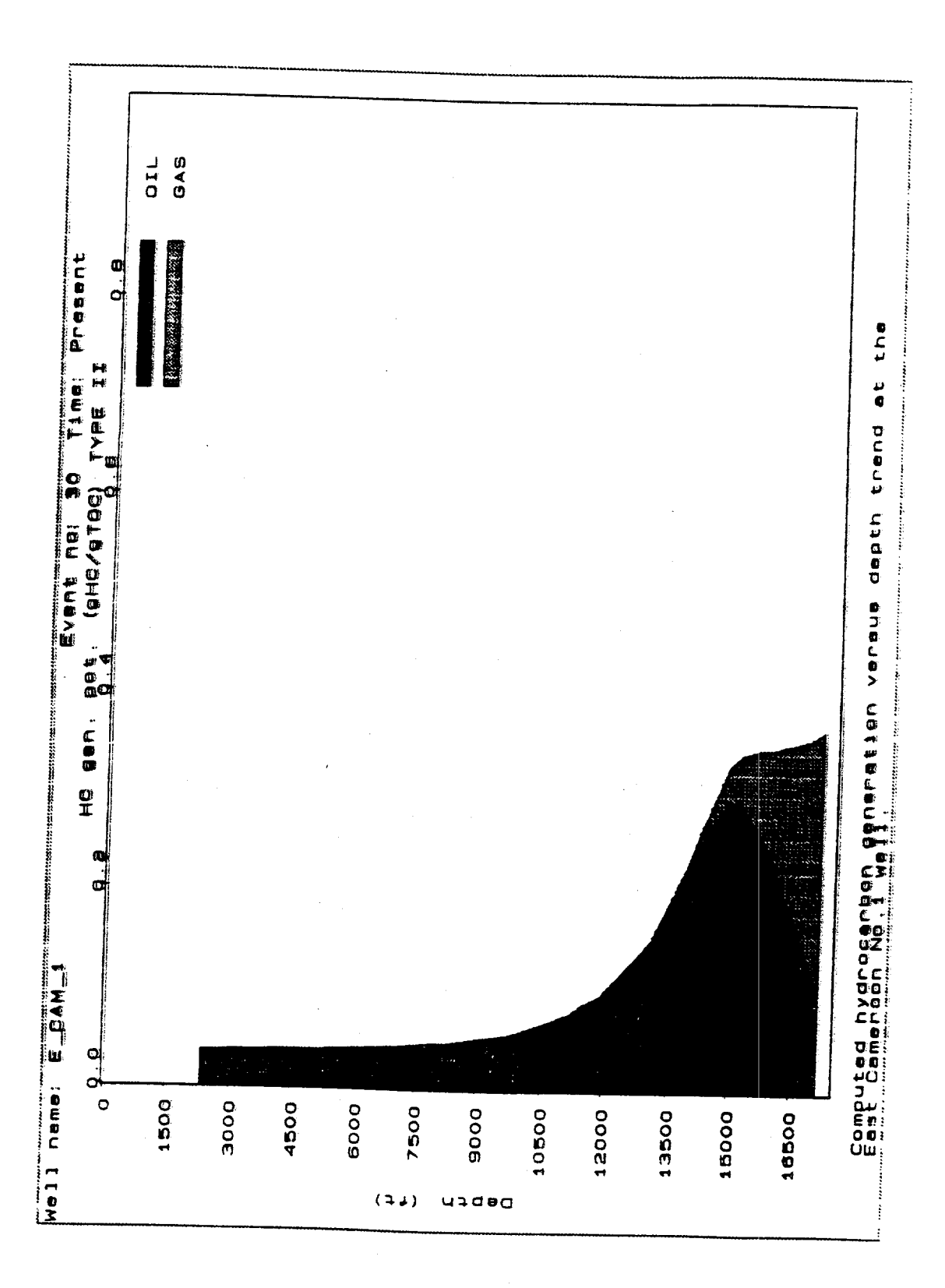


Figure 5: One-dimensional maturation model of E. Cameron Cost B-1 well (Yukler and Whelan, unpublished data).

745 1

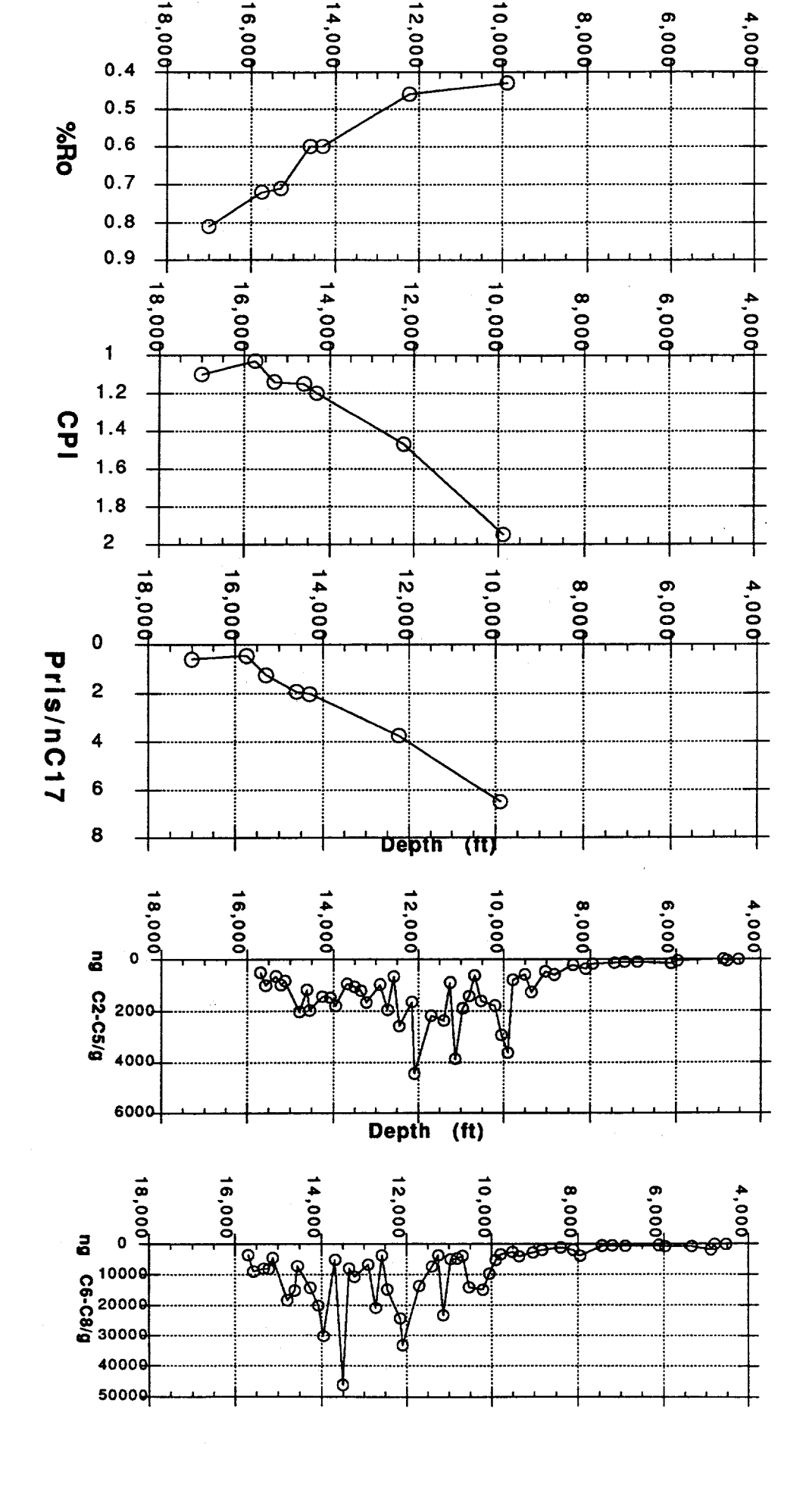


Figure 6: Experimental bitumen data for E. Cameron well, including some downhole maturation indicators (%Ro, CPI, and Pris/nC17) and downhole profiles of sorbed gases, \(\Sigma C2-C5\) and \(\Sigma C6-C8\).

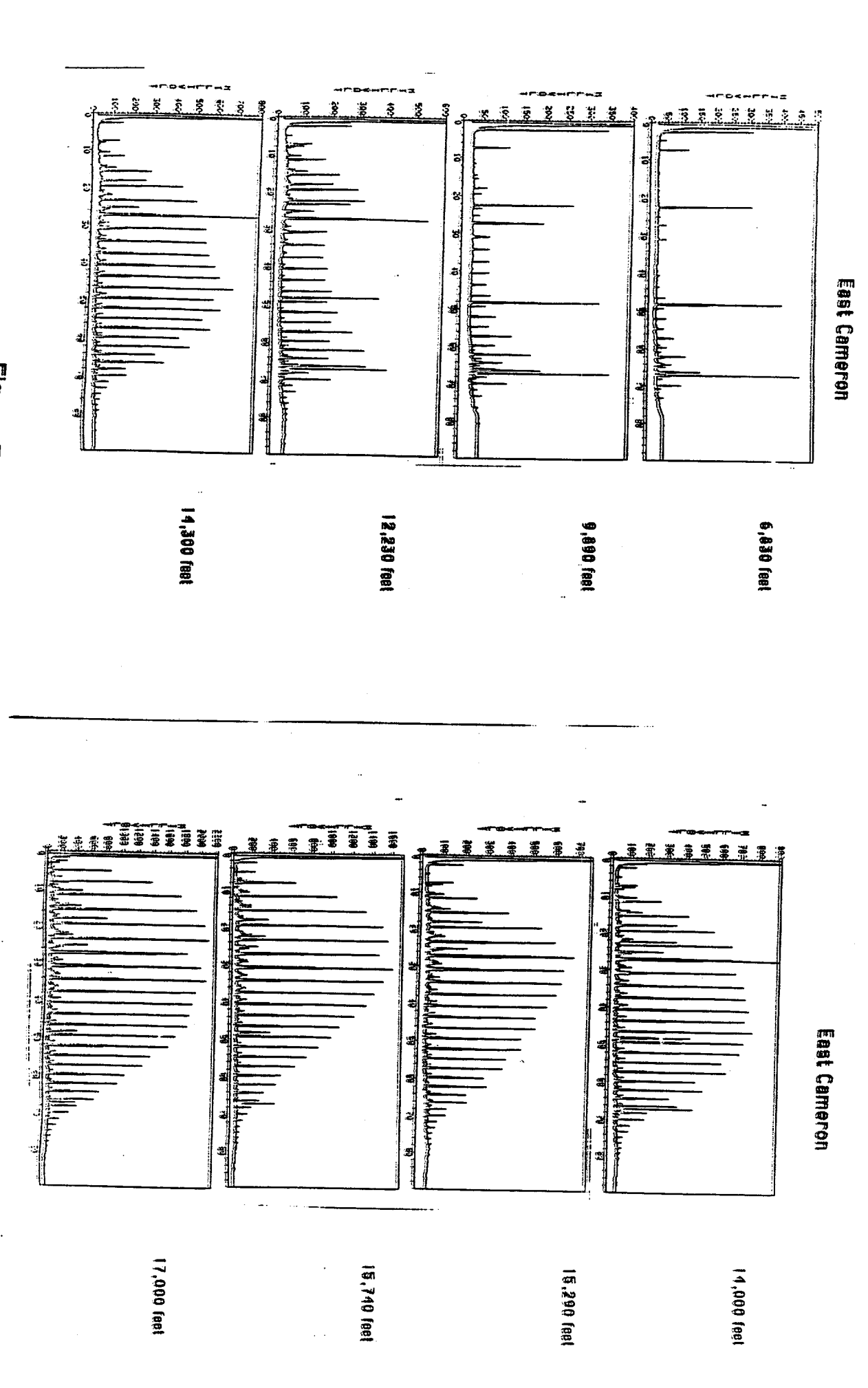


Figure 7: Down-hole profiles gas chromatograms of solvent extractable C14 to C35 bitumens, E. Cameron Cost B-1 well.

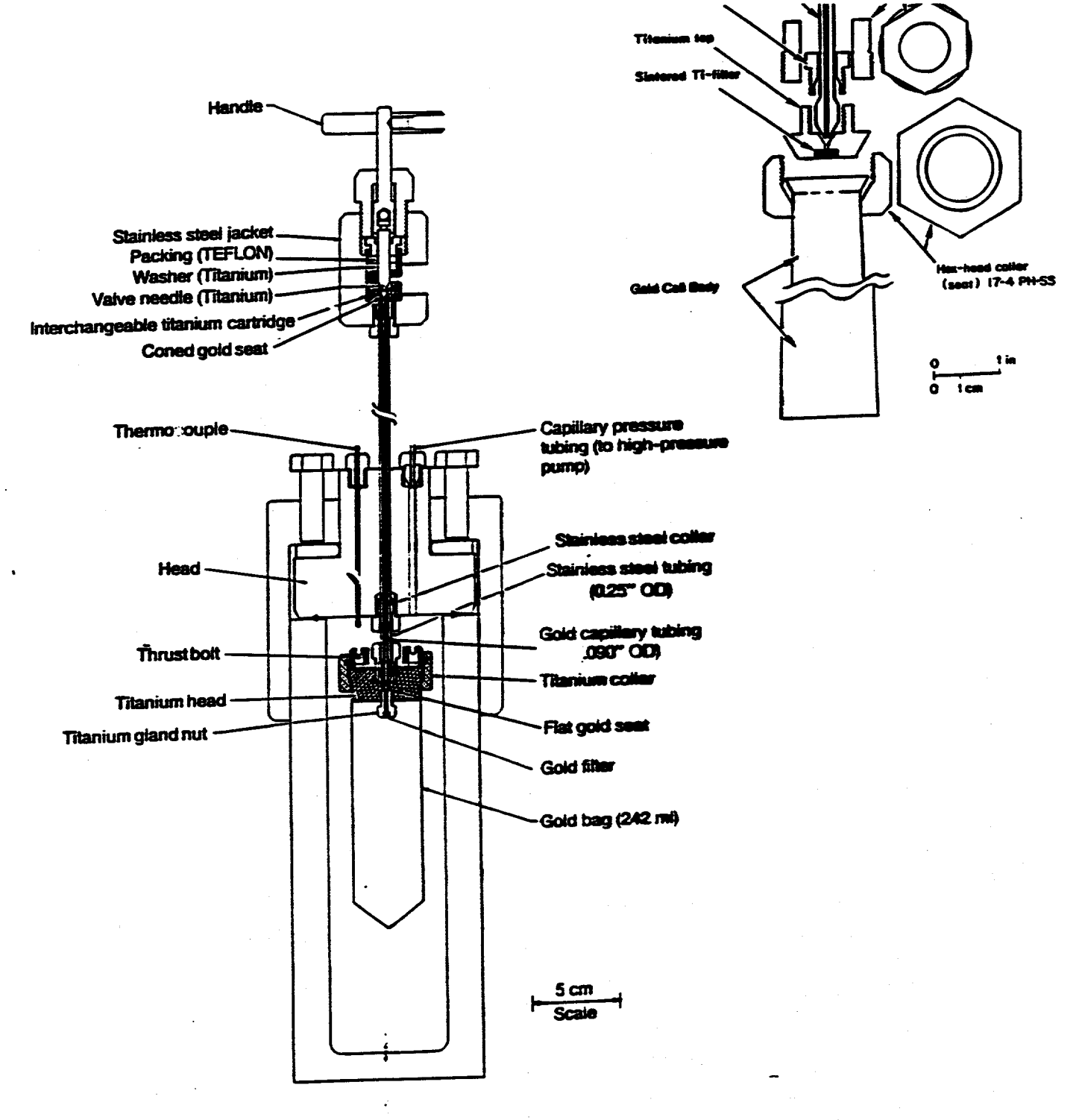


Figure 8: Schematic illustration of flexible cell hydrothermal equipment (from Seyfried et al., 1987). The apparatus has been adapted to use a smaller gold-titanium reaction cell in place of the one shown here.

Institutions:

<u>Academic</u>	Corporate Partners	Corporate Affiliates
Lamont	Landmark	Arco
Cornell	COMCO	BP
WHOI	IBM	Canad. Hunter
LSU		Chevron
U. Tenn.		Conoco
Michigan Tech.		Elf-Aquitaine
Texas A&M		Exxon
CSM		Mobil
		Shell
		Texaco
		Unocal

Figure 9: List of current active academic and industrial participants in the Global Basin Research Network.

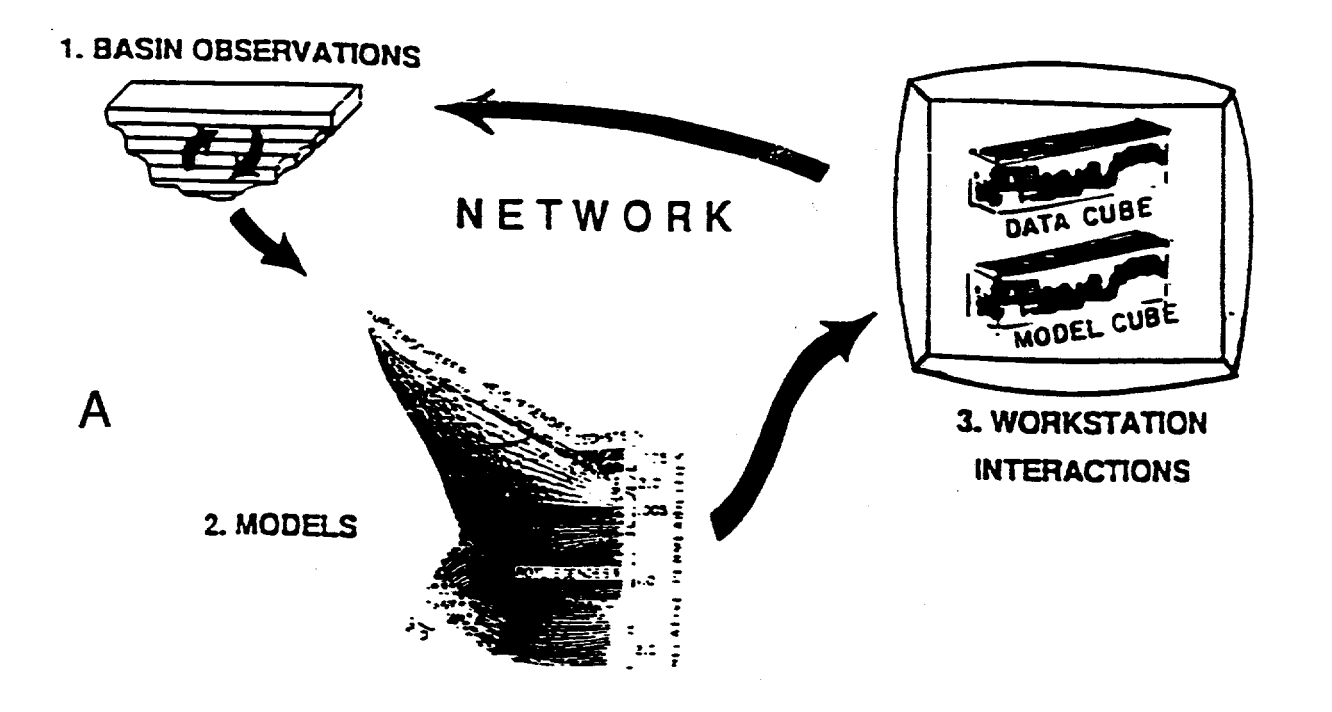


Fig. 7. Building the Data Cube

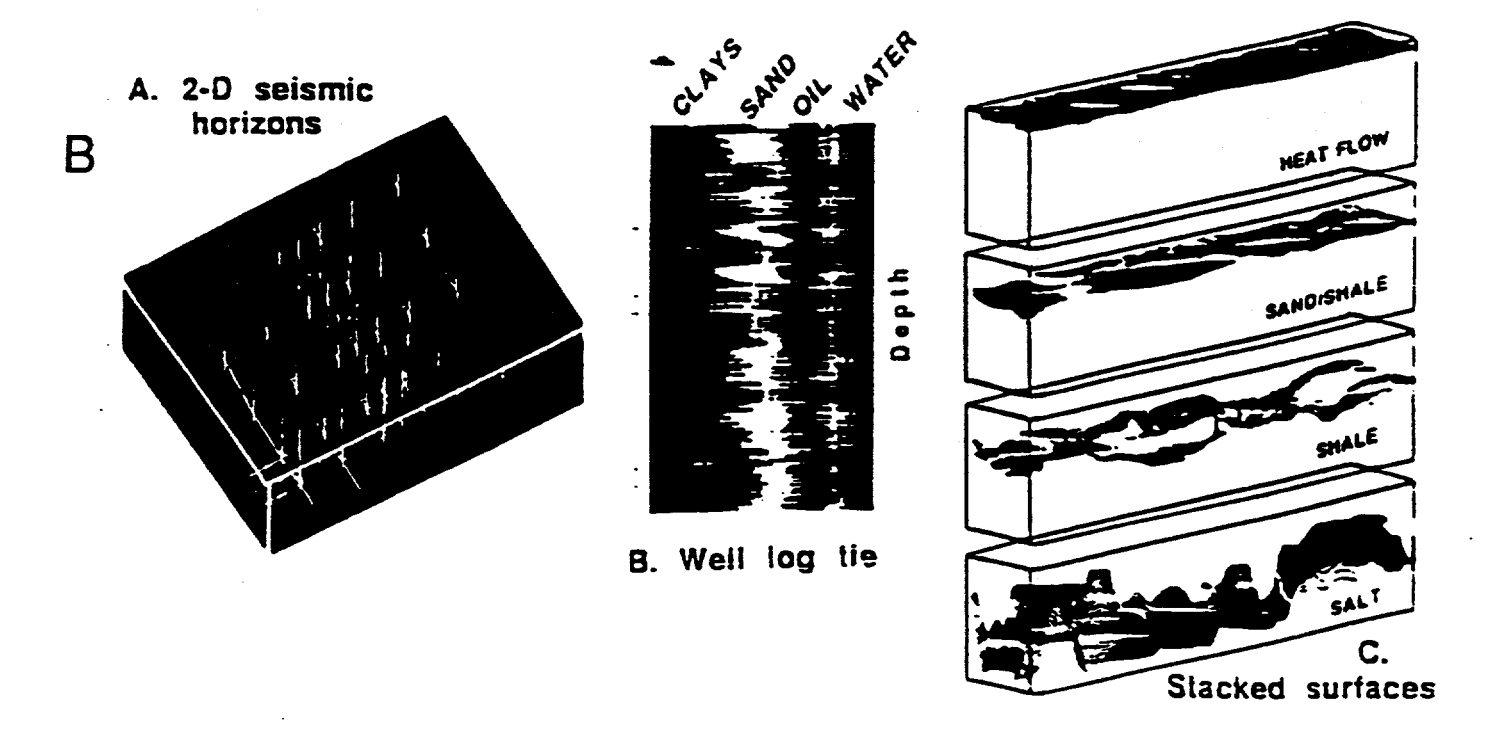


Figure 10: Schematic diagram of overall methodology and approach of GBRN. A) Schematic relationship of basin observations (i.e. data cube) and modeling; B) Building the data cube

Table 1: Frozen core samples collected for organic geochemistry at Woods Hole, ODP, Leg 139

<u>Hole</u>	Number of S	Samples for:		Description
	Hydrous pyrolysis:	Gas analysis:	Maturation:	<u> 2001 Dilon</u>
855A	2	11		Cold (4 0000)
855B	1	4	2	Cold (4-33°C); unaltered sediments;
855C	3	10	7	seawater drawdown area
855D		1	•	(Depth: 4.45-104 mbsf*)
856A	5	13	15	Gonorally and (4 ages)
856B	6	15	18	Generally cold (4-33°C) sediments;
856D		1	1	some past localized heating via magn intrusions. Sediments overlie massive sulfide deposit which has not affected the sediments. (Depth:1.45-116 mbsf)
857A 857B	8	9 3	11	Conductively heated sediments with high geothermal gradient (temperature
857C	3	65	35	4-270°C over depth range of 0-500
857D		11	7	mbsf). Evidence for cooling via horizontal fluid migration below 300 mbsf. Igneous intrusions below 470 mbsf.
858A	6	36	16	Antina fundanti.
858B	2	5	1	Active hydrothermal area; sediment
858C	4	15	3	heating via hot fluid convection.
858D	4	4	3	Measured downhole temperatures up to
858E		1	•	280°C; sediment depth range:
858F		12		0-350ft; geothemal gradient range:
858G		8	•	from 1.4°C/m in Hole 858A to 9°C/m in Hole 858B.

^{*} mbsf= meters below sea floor

Table 2: Gulf Coast samples for	If Coast sa		Hydrous pyrolysis							-		Γ
		1 3	Location									
Formation	Age	Weli	(depth)	Description	T 0C	&	Ттах	81	S 2	Ξ	ō	<u>-</u>
Smackover	Jurrassic	Amerada Hess	Clark Co, Ala	Terrigenous							1	
(upper)		#1 Scotch	(10694 ft)	and gas prone	1.43 N/A	N/A	439	0.16	96.0	67	61	0.14
		19-9N-5E										
Wilcox	Cretaceous Amoco #4	Amoco #4	Livingston, LA								\dagger	
		Barnett Hers	(13360 to 70)		1.79-	N/A	434-		4.44-206-	206-	<u> </u>	
					2.09		437		5.97	285		
Wilcox	2	Texaco #8	Pointe Coupee		1.28 N/A	N/A	435	0.16	1.93	150	23	0.08
		W.S. Duckworth	Parish, LA									
			(11939 ft)									
							1	1				
			(11985 ft)		1.73 N/A	N/A	424	0.56	5.16	298	98	0.08
Wilcox	=	Sun #8 N. Smith	Pte Coupee		1.81	1.81 0.46	441	1.52	3.81	210	8 4	0.29
			Parish, LA									
			(13129 ft)									
			Ġ							1		
Wilcox		Murexco #1	Pte Coupee		3.24	0.69	440	4.4	10.1	314	9	0.12
		Kimball	Parish, LA	and the second s				·				
		(14247 ft)	Livonia Fld.									
		- 1									1	
			Allen Ph., LA			.4467				1	1	
		Ragiey Lumber	Hurricane									
			Creek Field					-				
Sparta	Cretaceous Sun Oil,	Sun Oil, 2 O'Clock	St	Bay Environment	1.84	0.5	430	0.36	3 41	185	24	0.1
		€	Landry Ph, LA									
Sparta	*	Clayton	Pte Coupee Ph, Lagoonal	Lagoonal	1.73	0.36	432	0.63	3.19	184	17	0.16
		Williams #1	LA, Fordoche Fld)	ld)								
			(11141.7 ft)									

			Location									
Formetion	Ann	Wall	(de & L.)									
	DA		(deptn)	Description	ည	-	Tmax	S.	82	I	ō	PI
Sparta	=	•	(11182.3 ft)	Marine	3.53	0.36	430	0 03	101	212	a	70.0
						20:5	2	5	. 1		٥	0.0
Midway	Cretaceous N. Ham	N. Hampton inc			1.86to N/A		427 to low	wo	9410	94to 50 to 25 to 235	25 to	75.
		, #1 , Nelson Ball	elson Ball Pike Co, MS		6.84		432		1 38	73	30	3
		(7740 to 7874 ft)						000		1	200	6
								0.50	1		63	0.0
		1										
LUSCAIOOSA	Cretaceous		₽.	Very	5	Y/Z	429 to	429 to .01 go .56 to 70 to 16 to .02 to	.56 to	70 to	16 to	.02 to
		(10243 to 10394ft)		heterogeneous	1.8		439	0.16	2.5	105	53	0.125
Eutaw		8			α t	N/A	4 96 40	406 40 04 964		7. 1.		1
		(9813 to 0842 #)			2 ,		2	5		-	2	04 10
		2			1.62		433	0.86	1.62	235	47	0.29
•		=	=		.66 to N/A		126 to	426 to 0.02 to .55 to 46 to 31 to .03	.55 to	46 to	31 to	03 to
		(9880 to 9910 ft)			1.21		429	0.09	0.58	83	34	0.14
		-										
L. Tuscoloosa Cretaceous Diamond	Cretaceous	Diamond Core										

Kinetic and Compositional Model of High-Pressure Kerogen Pyrolysis

A. K. Burnham, R. L. Braun, J. G. Reynolds, and J. J. Sweeney

The goal of this project is to derive conceptual and mathematical models of the oil generation and expulsion process that can be used to enhance oil exploration and recovery. Laboratory pyrolysis experiments are conducted to provide information needed for model development. The models are tested by comparing their predictions with geological data. Concurrent with this process is the development of chemical indicators for thermal maturity, source, and depositional environment. The BES-supported research is closely coordinated with basic research funded by industrial sponsorship and applications funded by DOE-Fossil Energy.

A fundamental question concerning model development is whether laboratory experiments can lead to chemical kinetic rate expressions that will work on geologic time scales. There are actually two aspects to this question: (1) can the laboratory kinetics be measured accurately enough, and (2) is the mechanism sufficiently constant that the Arrhenius law is followed. Our early work determined the temperature measurement accuracy for extrapolatable kinetics (Burnham et al., 1987). Many of our insights were incorporated by a small company (Lab Instruments) into a pyrolysis kinetic analyzer called Pyromat. We tested a prototype version of this instrument with favorable results, and subsequently used it to measure pyrolysis kinetics for a variety of marine and lacustrine oil shales and petroleum source rocks (Braun et al., 1991). The kinetics from this apparatus compare favorably with oil generation in the subsurface (Sweeney et al., 1990), suggesting that both criteria can be met.

Another aspect of the extrapolatability issue is the chemical role of water. We have conducted other types of nonhydrous pyrolysis experiments in addition to the Pyromat experiments and have compared them to results from hydrous pyrolysis experiments conducted by others. Although water does inhibit coke formation and perhaps promote dealkylation reactions, it does not seem to have a clear effect on the overall reaction rate (Burnham, 1990). Less firmly established is the relationship among oil yields from open, hydrous, and geologic systems.

One important insight from the hydrous-nonhydrous pyrolysis comparisons is the distinction between bitumen and oil generation. Some proponents of hydrous pyrolysis have emphasized that hydrous pyrolysis forms an expelled, hydrocarbon-rich phase as in nature. The expulsion occurs at higher temperature (maturity) than the formation of a soluble, predominantly polar, bitumen. The volatilization kinetics determined by open-system pyrolysis correlate better with expelled oil formation than with bitumen generation. This implies that one should be cautious when using open-system kinetics to predict C_{15+} extract yields as a function of depth in sedimentary basins. A chemical kinetic model was developed that contains separate rate expressions for a soluble bitumen and a volatile, expellable oil (Braun and Burnham, 1991).

We also explored the subsequent decomposition kinetics of bitumen with the Pyromat instrument (Reynolds and Murray, 1991). Whole bitumens, asphaltenes, and maltenes were obtained from tar sands, crude oils, and source rocks. It was found that the decomposition kinetics of the asphaltenes were similar to those of the parent kerogen while the maltenes had broader decomposition profiles that extended to lower temperatures. These results

qualitatively support the approximation that the high molecular weight soluble intermediates from kerogen decomposition decompose with kinetics similar to that of the kerogen itself. A second conclusion is that thermal extraction as in a Rock-Eval machine is not equivalent to solvent extraction because much of the extracted material is non-volatile below 300 °C.

The primary focus of our mathematical model development is the computer code PMOD (Braun and Burnham, 1991). PMOD calculates oil and gas generation and cracking, rock compaction, overpressuring, and expulsion of fluids from the rock, including common geochemical diagnostics of these processes. It is faster and substantially more flexible than our previous generation-expulsion code, PYROL. PMOD is unique in that it allows the user to interactively create a custom chemical mechanism. This flexibility is important because our understanding of the pyrolysis reactions continues to evolve. We have tested its versatility by constructing a variety of maturation networks that involve various combinations of parallel and serial reactions. One moderately complex model for a generic marine shale is given in Table 1, and the model is compared to data from Monin et al. (1990) in Figure 1.

A tricky aspect of the PMOD expulsion model is how to account for previous burial and the effect of kerogen transformation on source rock porosity. We have assumed that kerogen is load bearing rather than pore filling, so conversion of kerogen to oil is accompanied by compaction. PYROL and the initial PMOD pore-pressure model had a "ratchet" that prevented porosity from increasing during oil generation or uplift, but our initial implementation caused a "loss of memory" problem upon reburial. During the past year, we reanalyzed the compaction issue and decided that it is plausible that porosity can increase from kerogen decomposition to the extent that the generated pore pressure is sufficient to support the overburden pressure. This approach still assumes that kerogen is primarily a load-bearing solid.

PMOD has been used to explore the sensitivity of various compaction and expulsion parameters. One sample result is that for a given kerogen the primary factor affecting oil expulsion efficiency, oil properties, and gas/oil ratios is the ratio of TOC to the porosity during oil generation. This is because for the bulk flow mechanism used in PMOD, the TOC/porosity ratio largely determines the residence time of the oil in the source rock, and therefore the extent of secondary maturation reactions. These predictions are being testing in applications funded by other DOE offices. While the bulk flow migration mechanism appears to explain many aspects of petroleum expulsion, it does not explain the apparent preferential expulsion of hydrocarbons from the source rock. Sorption of polar components by minerals or kerogen may be the cause, and we have started analyzing the role of the latter.

One type of information needed to construct the maturation networks for programs such as PMOD is the kinetics of gas evolution from kerogen. In a first paper, we reported a comparison of gas evolution characteristics of 15 source rocks heated at 10 °C/min using tandem mass spectrometry (Reynolds *et al.*, 1991). We have now mostly completed the derivation of gas evolution rate parameters for 7 source rocks by regression analysis of experiments at both 1 and 10 °C/min. Kinetics were derived for methane, propane, total light hydrocarbons, light saturated hydrocarbons, hydrogen, hydrogen sulfide, acetic acid, benzene, and methyl thiophene.

Three additional roles of organic geochemistry are to provide chemical indicators for thermal maturity, source, and depositional environment. Our major contributions to this aspect in the

past are improved kinetic models for the pristane formation index (Burnham, 1989) and vitrinite reflectance (Burnham and Sweeney, 1989). We are currently exploring gas evolution profiles and ultra-trace organometallic compounds for these purposes. The former is an outgrowth of pyrolysis-mass spectrometry measurements used primarily to determine gas generation kinetics for maturation modeling.

The objective of the gas evolution diagnostic method is to simultaneously measure depositional environment and maturity on the source rock. It has been long been recognized that the T_{max} for total volatile organics depends on both source and maturity. The new method is based on the observation that the relative initial T_{max} values of individual hydrocarbon gases depends on depositional conditions, providing a basis for separating source and maturity contributions to the T_{max} values. The method has only been partially tested with data gathered primarily for other purposes. Experiments to test the method more thoroughly have just begun in collaboration with Lab Instruments, Inc., which is interested in marketing a Pyromat-MS instrument to the oil industry.

Ultra-trace metals also provide the possibility of determining both source and maturity. Published analyses of digested whole oils by ICP-MS indicate both effects are present. In addition, HPLC-ICP-atomic emission spectroscopy analysis of V, Ni, and S indicate that the molecular weight and ligand type appear to change with maturity. We are currently measuring the ultra-trace metal concentrations in a variety of whole oils and rock extracts by ICP-MS analysis of organic media. Subsequent work will interface the ICP-MS to a HPLC in order to separate metal types by molecular weight, polarity, or other property, depending on the chromatographic column. So far, we have established the clean facilities needed for sample preparation, and we have modified the inlet and cooling systems of the instrument so that metals can be determined directly in organic media without plasma torch degradation. Preliminary analyses indicate the presence of many lanthanides and some actinides in bitumen extracts.

Once the analytical procedures are worked out, we will examine a variety of geochemical samples to characterize source-dependent and maturation-dependent trends. Little is known about the occurrence of ultra-trace metals in petroleum source rocks, but it is expected that the partitioning of the trace metals between kerogen and bitumen will depend on maturation. We have received samples from one of our industrial collaborators that will be useful in developing geochemically significant trends.

Work performed under the auspices of the U. S. Department of Energy by the Lawrence Livermore National Laboratory under Contract No. W-7405-Eng-48.

References

Braun R. L., Burnham A. K., Reynolds J. G., and Clarkson J. E. (1991) Energy & Fuels 5, 192-204.

Braun R. L. and Burnham A. K. (1991) PMOD: A Flexible Model of Oil and Gas Generation, Cracking and Expulsion, LLNL Report UCRL-JC-105371, submitted to Org. Geochem.

Burnham A. K., Braun R. L., Gregg H. R., and Samoun A. M. (1987) *Energy & Fuels* 1, 452-458.

Burnham A. K. (1989) Geochim. Cosmochim. Acta 53, 1693-1697.

Burnham A. K. and Sweeney J. J. (1989) Geochim. Cosmochim. Acta 53, 2649-2657.

Burnham A. K. (1990) Pyrolysis Kinetics and Composition for Posidonia Shale, LLNL Report UCRL-ID-105871.

Monin J. C., Connan J., Oudin J. L., and Durand, B. (1990) Org. Geochem. 16, 133-142.

Reynolds J. G. and Murray A. (1991) Pyromat II Micropyrolysis of Source Rocks and Oil Shales: Effects of Native Bitumen and Sample Size on T_{max} Values and Kinetic Parameters, LLNL Report UCRL-ID-106505.

Sweeney J., Talukdar S., Burnham A., and Vallejos C. (1990) Org. Geochem. 16, 189-196.

Table 1. Pyrolysis model with mass stoichiometry factors and kinetics $[A (s^{-1}), E (kcal/mol), and f (distribution fraction)]$

3

```
0.029 CH<sub>2</sub>O<sub>3</sub> -> 0.021 CO<sub>2</sub> + 0.008 H<sub>2</sub>O
   kerogen precursor of carbon dioxide and water
                  A = 5 \times 10^{+13}

E = 47 49

f = 0.25 0.50
                   → CH<sub>1.05</sub>
bitumen
  CH<sub>1.05</sub>
   keroaen
                      = 4 \times 10^{+13}
= 47 \quad 48
= 0.05 \quad 0.20
                                                      49 50 51
0.47 0.20 0.05
                  f = 0.05 0.20 0.47 0.20 0.05 0.05

→ 0.339 CH<sub>1.4</sub> + 0.088 CH<sub>2.0</sub> + 0.032 CH<sub>2.6</sub> + 0.005 CH<sub>4</sub>

heavy oil light oil gas methane

0.016 CH<sub>2.6</sub> + 0.052 CH<sub>4.0</sub> + 0.468 CH<sub>0.25</sub>
  CH<sub>1.05</sub>
  kerögen
                                                        coke-2
                                                                                   coke-3
                            3 × 10+13
                           49 50
0.05 0.20
                                                      51
0.47
                                                                  52 53 54
0.20 0.05 0.03
                      0.339 CH<sub>1.4</sub> + 0.088 CH<sub>2.0</sub> + 0.032 CH<sub>2.6</sub> + 0.005 CH<sub>4</sub> heavy oil light oil gas methane
0.016 CH<sub>2.6</sub> + 0.052 CH<sub>4.0</sub> + 0.488 CH<sub>0.25</sub>
 CH<sub>1.05</sub>
  bitumen
                            coke-1
                                                       coke-2
                           3 × 10<sup>+13</sup>
49 50
                                                                                   coke-3
                 \vec{E} = 49 50 51 52 53 54 \vec{f} = 0.05 0.20 0.47 0.20 0.05 0.03
 \text{CH}_{1.4} \rightarrow 0.223 \text{ CH}_{2.0} + 0.233 \text{ CH}_{2.6} + 0.045 \text{ CH}_4 + 0.008 \text{ CH}_{2.6}
heavy oil light oil gas methane coke-1
                  + 0.037 CH<sub>4.0</sub> + 0.454 CH<sub>0.25</sub>
coke-2 coke-2
                                                                              methane
                           2 \times 10^{+13}, E = 54, f = 0.60
                A = 2 \times 10^{+12}, E = 54, f = 0.20

A = 2 \times 10^{+11}, E = 54, f = 0.20
                → 0.565 CH<sub>2.6</sub> + 0.100 CH<sub>4</sub> + 0.001 CH<sub>2.6</sub> + 0.012 CH<sub>4.0</sub>
 CH<sub>2.0</sub>
                     gas
0.322 CH<sub>0.25</sub>
                                                   methane
                                                                               coke-1
                           coke-3
                A = 2 \times 10^{+12}, E = 54, f = 0.50
                A = 2 \times 10^{+11}, E = 54, f = 0.50
 CH<sub>2.6</sub>
                → 0.687 CH<sub>4</sub> + 0.313 CH<sub>0.25</sub>
 gas
                       methane 
                                                  coke-3
                A = 1.2 \times 10^{+12}, E = 57
CH_{2.6} \rightarrow CH_{2.6}

coke-1 gas
                A = 3 \times 10^{+13}

E = 53 \times 55
               E = 53 55 57 59 61 f = 0.38 0.38 0.12 0.08 0.04
CH<sub>4.0</sub> → CH<sub>4</sub> coke-2 methane
                    = 53 55 57 59 61 63 65 67 69
= 0.06 0.22 0.20 0.13 0.12 0.10 0.09 0.05 0.03
```

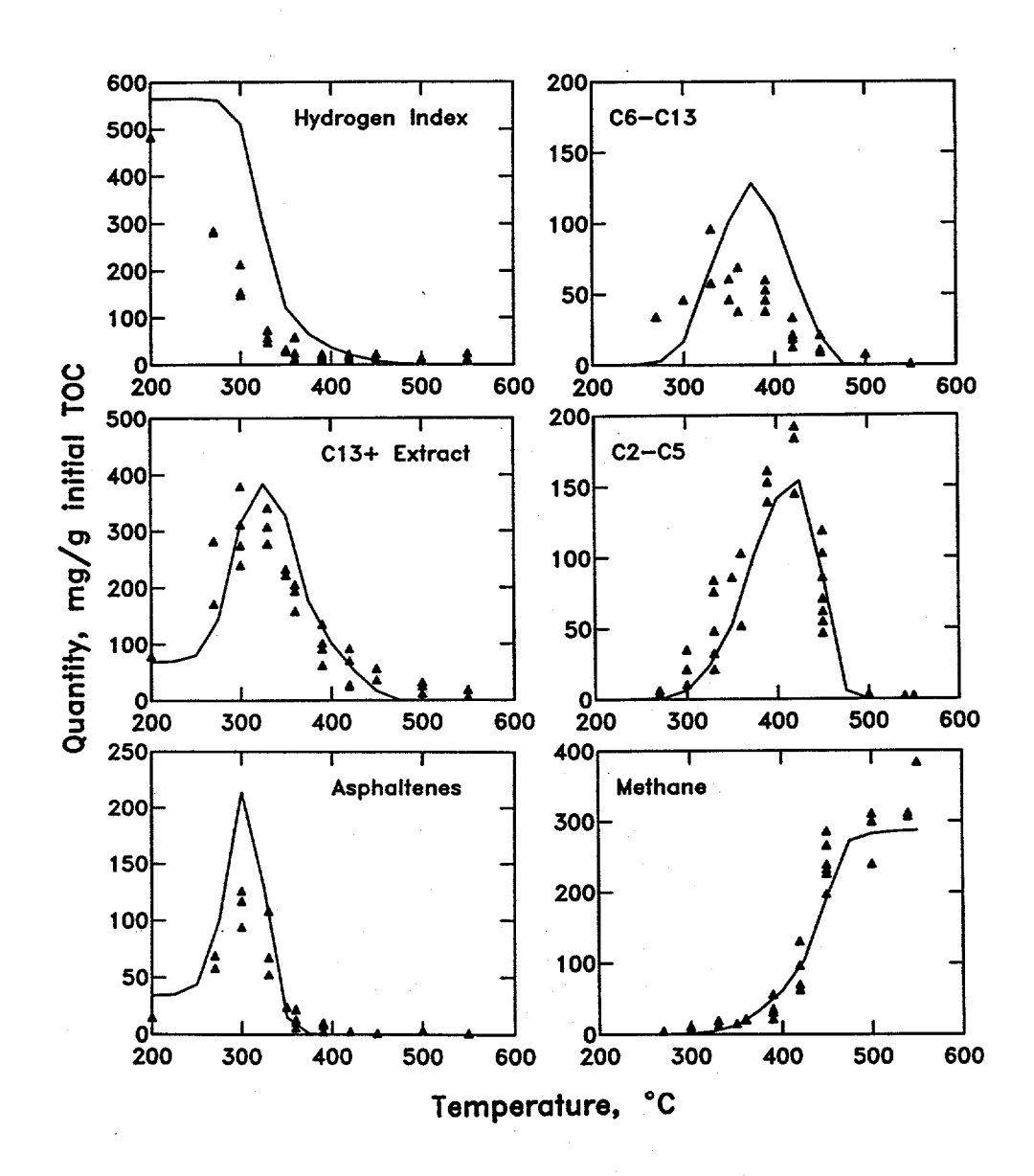


Figure 1. Comparison of calculated product yields from Table 1 model with hydrous pyrolysis data of Monin et al. (1990) for Kimmeridge clay. Because the model was not developed specifically for this data, part of the discrepancy is due to the differences in the product definitions. For example, the model is based on C₂-C₄ yields (compared to C₂-C₅) and all non-volatile, soluble products (compared to asphaltenes).

Direct Speciation of Metal and Metalloid Ions by Optical Spectroscopies

C. Drew Tait, David R. Janecky, David L. Clark, Scott A. Ekberg, Paul R. Dixon, John A. Musgrave; Isotope and Nuclear Chemistry Division, Los Alamos National Laboratory, Los Alamos, NM 87545
Philip C. Bennett; Department of Geological Sciences, University of Texas, Austin, TX 78713

Chemical interactions between dissolved organics and mineral surfaces have been increasingly the focus of investigations of diagenetic processes in sedimentary basins and in oil fields. These interactions can significantly influence the release, sequestering and transport of metals in low- to moderate-temperature hydrothermal ore systems such as the Mississippi Valley Type (MVT) deposits, and be a critical component of creation, destruction and reorganization of permeability through complex formation with the metalloids Si and Al. Our recent efforts have concentrated on organic-metalloid interactions because of their importance in rock alteration/weathering and in primary and enhanced oil recovery (EOR) processes.

Molecular level spectroscopic investigations of organic/inorganic interactions provide important new information on sedimentary geochemistry through the identification of interactions over moderate temperature and pH ranges. Although the official title of this project indicates the use of only optical spectroscopies, a combination of Uv/Vis/IR absoption, Raman scattering, and 29Si and 13C nuclear magnetic resonance (NMR) experiments are actually employed. A major advantage of integrating spectroscopic results with diagenesis studies is the ability to directly examine the mechanisms of interactions, even in complex matrices and with competing processes. Furthermore, we are extending these techniques to probe fluid inclusions with micro Raman and luminescence techniques to directly compare laboratory results with natural reservoir systems.

The mobility and transport of silica in natural waters has been a subject of debate for over a century (JULIEN, 1879; ILER, 1979). Field studies have found direct correlations between dissolved organic carbon (DOC) and dissolved silica in soil pore waters (CHESWORTH and MACIAS-VASQUEZ, 1985; WILLIAMS et al., 1985), lake and marine sediment pore waters (ASTON, 1983), shale pore waters (LERMAN, 1979), oil field formation waters (SURDAM et al., 1984), and oil-contaminated shallow groundwater (BENNETT and SIEGEL, 1987). This latter field study was especially important because it also correlated quartz etching under neutral pHs with DOC concentration. Therefore, matrixdestroying complexation of other rock-forming cationic

constituents, especially Al, could not be invoked. The DOC's implicated in these correlations consist primarily of complex organic acids, including aromatic, keto- and hydroxy-acids, and other partially oxidized carbon species (AIKEN, 1987; BAEDECKER et al., 1987). Enhanced silicon mobility is thought to involve either an increase in proton availability from these acids or significant organo-silica interactions.

Decreased pH due to organic acids cannot account for the increased silicon mobility and quartz etching found in the near neutral (pH=6 to 7) oil-contaminated groundwater site near Bemidji, MN (BENNETT and SIEGEL, 1987), thereby implicating organo-silica interactions. These interactions may include hydrogen bonded charge transfer complexes as well as covalently bonded structures (ILER, 1979), although reliable direct evidence of these interactions is rare (FARMER, 1986; EVANS et al., 1990). Laboratory work by BENNETT et al. (1988) and BENNETT (1991) show that only poly-functional organic acids increase the dissolution rate of quartz and the final solubility of the mobilized silicon, so our studies have primarily focused on oxalate and citrate anions. Oxalate is the simplest difunctional acid anion and is also found naturally in concentrations of up to 3 mM in oil field brines (KHARAKA et al., 1984, 1987), while citrate is produced in significant quantities biologically and can exist in local environments, especially in soils near rockweathering fungi. Furthermore, citrate is more active in mobilizing silica than oxalate (BENNETT et al., 1988). Other naturally occurring acids such as fulvic and humic acids are also implicated in silicon mobilization, but are too complex for these initial spectroscopic studies.

In a previous paper, Raman scattering and infrared absorption experiments purported to show spectroscopic evidence for a strong, covalently bonded silicon ester formed between oxalate and silicic acid (soluble silicon source) (MARLEY et al., 1989). As these experiments were only done at room temperature and at neutral pH, we decided to pursue them to examine the range of conditions in which this silicon ester could be expected to form. A diagnostic vibrational peak at 1305 cm $^{-1}$, both Raman and IR active and attributed to $v_{\rm C-O-Si}$ (MARLEY et al., 1989), was used as the ester marker. This marker was observed in the IR when 4 < pH < 12, and also showed no dissociation to at least 125°C. In fact, the spectrum was qualitatively unchanged to 175°C, but leakage from the cell precluded any quantitative conclusions. This temperature stability was considered especially important because organics in oil field brines and sedimentary basins in general exist between 85 and 200°C (i.e. between the temperatures at which organic-consuming bugs are significant and at which the organics decarboxylate - KHARAKA et al., 1984, 1987). Furthermore, this is also the temperature range of MVT deposit formation. However,

 $^{13}\mathrm{C}$ NMR studies performed to corroborate the bidentate nature of the oxalate interaction with silicon did not revealed a ^{13}C chemical shift between pure oxalate and oxalate/silicic acid solutions (Figure 1), implying that any complexation must be below the NMR detection limit. Subsequent IR and Raman control experiments involving oxalate-only solutions also detected the 1305 cm⁻¹ "marker" peak (Figure 1). Moreover, when we went back to the original paper (MARLEY et al., 1989), we discovered that the published control experiments involved oxalic acid rather than oxalate! Our experiments to determine the environment under which a silicon ester could exist instead turn into experiments that show where no detectable ester (or any other covalently bound Si-oxalate) is observed. Because silicon oxalate ester bond formation may be expected to strengthen at higher temperatures (see Al-oxalate data below), the negative findings from elevated temperature experiments are nonetheless a significant contribution.

In order to improve our detection limit to see if any significant organic-silicon interaction can occur, we have turned to ²⁹Si NMR experiments. These experiments probe the chemical environment of the Si atom rather than the organic carbons, and hence allow us to try to push the equilibrium toward complex formation by using excess organic species. Near-neutral solutions of ²⁹Si (introduced as enriched $^{29}\mathrm{SiO}_{2}$ below the concentration that would result in dimerization / polymerization) and oxalate/citrate ligands were allowed to sit at room temperature for two months. Figure 2 shows the room temperature spectra for 2 mM Si alone and with 50 mM citrate or oxalate. No obvious new peak appears in the organic containing solutions, although a small hump possibly appears at ~-50 ppm in the oxalate Therefore, no definitive evidence for a silicon ester is found, either because it is below the detection limit of the spectrometer, close to the detection limit (if the -50 ppm peak is real), or it is buried under the host Si peak at -116 ppm. However, these experiments are continuing, and, because they are new and an interpretational database has not yet been established, no final conclusions can yet be drawn from them . A striking feature of the spectra is the broadness of the parent Si peak (21 ppm or 1046 Hz), indicating exchange of the deuterium on $Si(OD)_4$ and D_2O solvent, where D_2O was used to provide an NMR signal "lock" to eliminate any signal drift problem. Because the broad signal implies either intermediate exchange kinetics or multiple species (dimers, trimers, etc.) with unresolved peaks, the temperature was both increased (52°C) and decreased in an effort to narrow the signal by entering the slow or fast exchange regimes. Furthermore, the $Si(OD)_4/D_2O$ sample has also been diluted by a factor of 10 with H20 to try to eliminate the possibility that dimers/polymers contribute to the peak broadness. Not all of this data has been analyzed yet. However, the fact

that 200 μ M Si species can be observed with NMR is remarkable as it is a directly relevant environmental concentration. For example, [Si] in the Rio Grande reaches concentrations of 320 μ M.

Besides silicon(IV), aluminum(III) is another major cationic constituent of rock and soil matrices. Aluminum is known to form multiligand complexes with oxalate at room temperature (BOTTARI and CIAVATTA, 1968; SJOBERG and OHMAN, 1985; THOMAS et al., 1991). In fact, oxalate solutions can leach aluminum from the relatively insoluble solid Al₂O₃ by stirring a slurrey with sodium oxalate at near neutral pH's (between 5 and 8). Aluminum-oxalate peaks are found in both IR and Raman spectra. Besides increasing the weathering of silicate minerals and consequently affecting geochemical cycles, biochemical cycles may also be affected by the simultaneous liberation of toxic Al and nutrients such as Fe, Ca, K, and Mg from mineral matrices (SJOBERG and OHMAN, 1985).

The effects of Al complexation by oxalate are easily followed spectroscopically, in contrast to the difficulty presented by Si complexation described above. Specifically, we have initiated experiments to determine the temperature dependence of Al-oxalate species, particularly to the moderate temperature regime relevant to sedimentary basins. As a pre-requisite, we first had to determine the spectroscopic signatures of the individual $Al(ox)_n^{3-2n}$ species. This process has been aided by previous room temperature speciation studies, mostly based on potentiometric results, which defined experimental conditions dominated by different complexes. Figure 3 shows the results of modifying the Al/oxalate ratio on the spectra. Since the log of the step-wise association constants for Al(ox)⁺, Al(ox)₂⁻, and Al(ox)₃³⁻ are 6.0, 5.0, and 4.0 respectively (BOTTARI and CIAVATTA, 1968; SJOBERG and OHMAN, 1985), the 1428 cm⁻¹ peak seen to dominate at oxalate/Al ratios > 3 can be assigned to Al(ox) $_3^{3-}$, while the peak at 1408 cm⁻¹ can be assigned to Al(ox) $_2^{3-}$. A peak associated with Al(ox) + can not be definitely assigned, either because it is weak or buried beneath other peaks. The assigned peaks represent coordinated oxalate vibrations (major contributions from C-O and C-C stretches) with different force constants due to Al complexation. Peak assignments are also consistent with changes in oxalate availability as a function of pH (SJOBERG and OHMAN, 1985).

The major solution effect of increasing temperature is the decrease in solvent dielectric constant (BRIMHALL and CRERAR, 1987; SEWARD, 1984). Highly charged species are therefore destabilized relative to lower charged ones, and stability constants change to reflect this. Therefore, when conditions were set for equal concentrations of $Al(ox)_3^-$ and $Al(ox)_2^-$ at room temperature, we expected an increase in

temperature to lower the concentration of the highly charged Al (ox) 3 species. However, Figure 4 shows no change in the populations of the two species, implying an increase in the association constant for Al (ox) 3 . This is even more remarkable when the lower availability of oxalate is taken into account in this pH=3 solution, as logk, for oxalic acid increases from -4.29 at 25°C to -4.42 at 50°C and -4.69 at 80°C. Therefore, our emphasis has shifted to competition studies for oxalate as temperature is changed. For sedimentary basin geochemistry, a competing cation such as zinc, calcium, or iron could be tried. The oxalates of the first two, however, are not soluble enough for spectroscopic examination, so we will continue our experiments with Al (III) and Fe (III) competition for oxalate.

With enhanced understanding of rock matrix - organic interactions and spectral signatures of these interactions provided by the laboratory analogue studies, we intend to pursue investigations of organic species in fluid inclusions in sedimentary basins such as the oil-producing Austin Geochemical issues of importance include thermal Chalk. maturation and porosity of the surrounding rock matrix, petroleum migration history, and interactions of enhanced oil recovery (EOR) techniques. Fluid inclusions allow us to study these issues because they preserve the paleo-chemistry of the fluids that led to oil field development and contain the well-equilibrated fluid/mineral surface environment that is needed to predict the effects of EOR techniques. A range of temperatures is also readily accessible. Toward this end, we are acquiring a Raman microprobe accessory to allow examination of the vibrational fingerprints of organic species in inclusions down to 5 microns in size, and also the monochromator attachments for a UV adapted microscope to allow us to use synchronously scanned fluorescence. latter technique has recently been used with macroscopic samples to add molecular specificity to sensitive luminescence measurements (PHARR et al. 1991; PHARR, 1991; CABANISS, 1991), and will be adapted here to microscopic measurements to probe the organics in fluid inclusions. combined application of Raman microprobe and fluorescence will provide important cross checks. Demonstration of microscopic scale results will allow investigations of a diverse range of problems, including paleochemistry / paleoclimate of Yucca Mountain and ore-deposits in geothermal systems such as Carlin type gold deposits with organic-rich fluid inclusions (Jeff Hulen, Univ. of Utah, personal communication). Note that organics are unexpectedly present and largely ignored components in some geothermal systems such as the Valles Caldera drillcore fluid inclusions (MUSGRAVE and NORMAN, 1991; MUSGRAVE et al. 1991). Organic species are also often discussed but little quantified in many other systems, particularly with respect to potential coupled interactions with metals and metalloids which are direct applications of this work.

REFERENCES

Aiken, G.R.; Thorn, K.A.; Brooks, M.H. (1987) Nonvolatile organic acids in ground water contaminated with crude oil. U.S. Geol. Survey Open-File Rept. 87-109.

Aston, S.R. (1985) Silicon Geochemistry and Biogeochemistry. Academic Press, New York.

Baedecker, M.J.; Cossarelli, I.M.; Hopple, J.A. (1987) The composition and fate of hydrocarbons in a shallow glacial-outwash aquifer. U.S. Geol. Survey Open-File Rept. 87-109.

Bennett, P.C. and Siegel, D.I. (1987) Increased solubility of quartz in water due to complexation by dissolved organic compounds. *Nature* **326**, 684-687.

Bennett, P.C.; Melcher, M.E.; Siegel, D.I.; Hassett, J.P. (1988) The dissolution of quartz in dilute aqueous solutions of organic acids at 25°C. Geochim. et Cosmochim. Acta 52, 1521-1530.

Bennett, P.C. (1991) Geochim. et Cosmochim. Acta 55,

Bottari, E. and Ciavatta (1968) . Gazz. Chim. Ital. 1004.

Brimhall, G.H. and Crerar, D.A. (1987) Ore fluids: Magmatic to supergene. In *Thermodynamic Modeling of Geological Materials: Minerals, Fluids, and Melts;* (eds. I.S.E. Carmichael and H.P. Eugster); Review in Mineralogy 17 pp. 255-321.

Cabaniss, S.E. (1991) Synchronous fluorescence studies of metal-fulvic acid equilibria [abs]. Conference on Metal Speciation and Contamination of Soil, May 22-24, Jekyll Island, GA.

Chesworth, W. and Macias-Vasquez, F. (1985) pE, pH, and podzolization. Amer. J. Sci. 285, 128-146.

Evans, D.F.; Parr, J.; Coker, E.N. (1990) Nuclear Magnetic Resonance studies of silicon(IV) complexes in aqueous solution - I. Tris-Catecholato complexes. *Polyhedron*, 9, 813-823.

Farmer, V.C. (1986) Sources and speciation of aluminum and silicon in natural waters. In *Silicon Biochemistry* (eds. D. Evered and M. O'Connor), pp. 4-23. J. Wiley & Sons, New York.

Iler, R.K. (1979) Chemistry of Silica. Wiley-Interscience, New York.

Julien, A.A. (1879) On the geological action of the humus acids. Amer. Assoc. Adv. Sci. Proc. 28, 311-410.

Kharaka, Y.K.; Law, L.M.; Carothers, W.W.; Goerlitz, D.F. (1984) Role of organic species dissolved in formation waters from sedimentary basins in mineral diagenesis. In The Society of Econ. Paleontologists and Mineralogists Symposium on Relationship of Organic Matter and Mineral Diagenesis (D.L. Gautier, Ed.) 38, pp. 111-122.

Kharaka, Y.K.; Maist, A.S.; Carothers, W.W.; Law, L.M.; Lamothe, P.J.; Fries, T.L. (1987) Geochemistry of metal-rich brines from Central Mississippi Salt Dome Basin, USA. Appl. Geochem. 2, 543-561.

Lerman, A. (1979) Geochemical Processes, Water and Sediment Environments. J. Wiley & Sons, Toronto.

유텇

Marley, N.A.; Bennett, P.; Janceky, D.R.; Gaffney, J.S. (1989) Spectroscopic evidence for organic diacid complexaton with dissolved silica in aqueous systems. I. Oxalic acid. Org. Geochem. 14, 525-528.

Musgrave, J.A. and Norman, D.I. (1991) Fluid inclusion evidence for the evolution of the Sulphur Springs hydrothermal system, Valles caldera, New Mexico. *Econ. Geol.* submitted.

Musgrave, J.A.; Charles, R.W.; Goff, F.; Norman, D.I. (1991) Geochemistry of hydrothermal alteration and mineralization, Sulfur Springs, Valles caldera, New Mexico, in prep.

Pharr, D.Y. (1991) Analysis for groundwater petroleum contamination using synchronous scanning fluorescence [abs]. 21st International Symposium on Environmental Analytical Chemistry, May 20-22, Jekyll Island, GA.

Pharr, D.Y.; McKenzie, J.K.; Hickman, A.B. (1991) Fingerprinting petroleum contamination using synchronous scanning fluorescence spectroscopy. J. Groundwater, submitted.

Seward, T.M. (1984) The formation of lead(II) chloride complexes to 300oC: A spectrophotometric study. Geochim. et Cosmochim. Acta 48, 121-134.

Sjoberg, S. and Ohman, L.-O. (1985) Equilibrium and structural studies of silicon(IV) and aluminium(III) in aqueous solution. Part 13. A Potentiometric and ²⁷Al nuclear magnetic resonance study of speciation and equilibria in the aluminium(III)-oxalic acid-hydroxide system. *J. Chem. Soc.*, Dalton Trans. 2665-2669.

Surdam, R.C.; Boese, S.W.; Crossey, L.J. (1984) The chemistry of secondary porosity. In *Clastic Diagenesis* (eds. D.A. McDonald and R.C. Surdam); *AAPG Memoir 37*, pp. 127-150.

Thomas, F.; Masion, A.; Bottero, J.Y.; Rouiller, J.; Genevrier, F.; Boudot, D. (1991) Aluminum(III) speciation with acetate and oxalate. A potentiometric and ²⁷Al NMR study. *Environ. Sci. Technol.* **25**, 1553-1559.

Williams, L.A.; Parks, G.A.; Crerar, D.A. (1985) Silica diagenesis. I. Solubility controls. *J. Sediment. Petrol.* 55, 301-311.

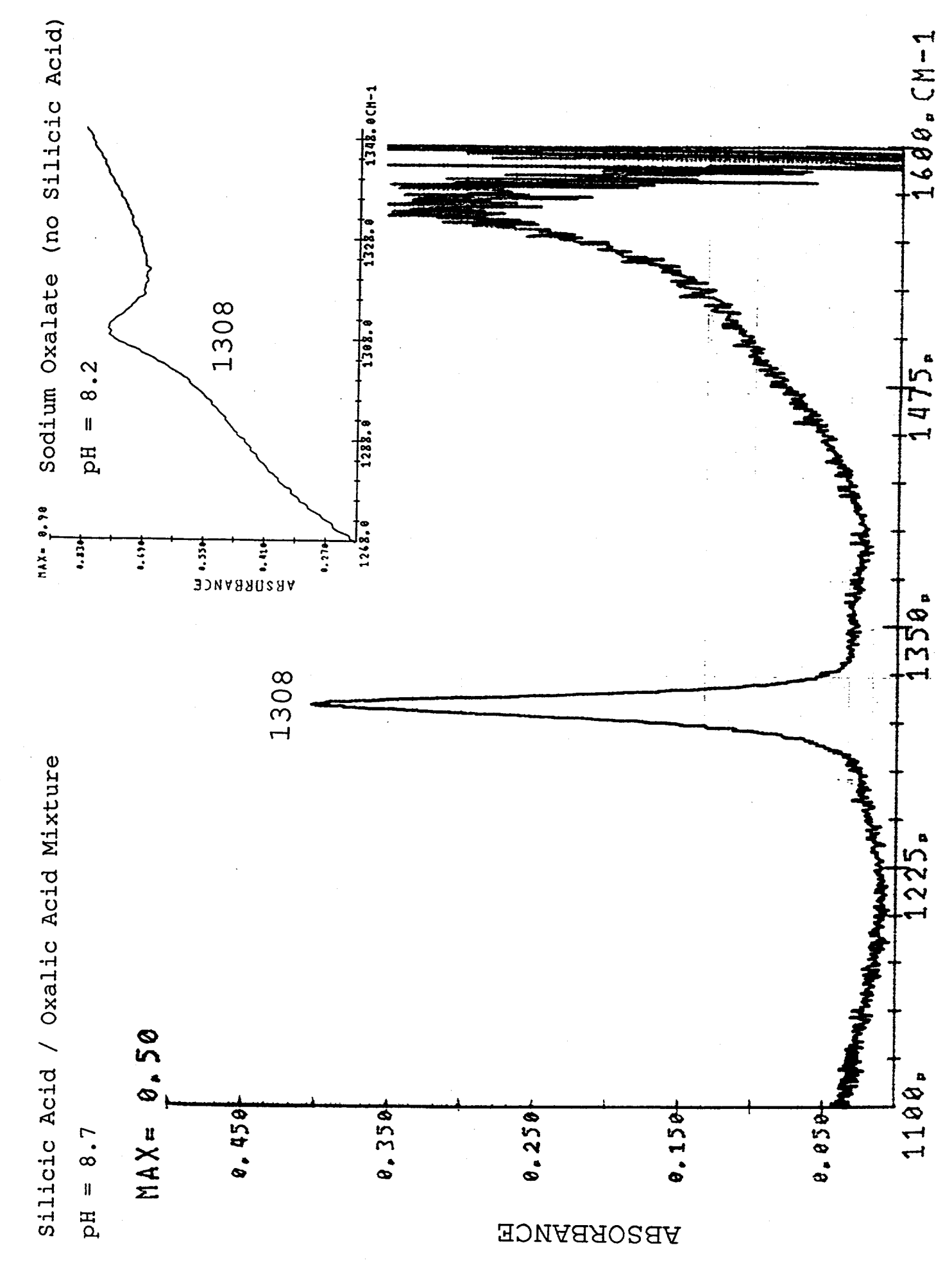
FIGURE CAPTIONS

- 1.(a) FTIR spectrum of a sodium oxalate / silicic acid mixture at neutral pH and the corresponding spectrum of sodium oxalate with no added silicon (inset, on different horizontal scale). The 1308 cm⁻¹ peak is therefore not diagnostic of silicon ester formation as concluded by MARLEY et al. (1989). (b) Carbon-13 FT-NMR spectrum of a sodium oxalate / silicic acid mixture at neutral pD and the corresponding spectrum of sodium oxalate with no added silicon. (Because the spectra were obtained in D₂O to provide a frequency lock from deuterium to prevent frequency drift, pD is noted rather than pH). The identical chemical shifts argue for identical chemical environments for the oxalate carbons namely, one not involved in a strong covalent bond with the silicon compound.
- 2. Room temperature ^{29}Si NMR spectra of (from bottom spectrum to top) 2 mM $^{29}\text{Si}(\text{OD})_4$ (from an enriched 97% $^{29}\text{SiO2}$ silicon source) with no organic ligand (pD=6.7), 2 mM $^{29}\text{Si}(\text{OD})_4$ / 50 mM sodium citrate (pD=7.4), and 2 mM $^{29}\text{Si}(\text{OD})_4$ / 50 mM sodium oxalate (pD=7.4). Note that the spectra were taken in D2O to provide a frequency lock to prevent signal drift, and that neutral D2O has a pD of 7.5. For our 250 MHz spectrometer, we used a 10 μsec pulsewidth (180° pulsewidth measurement for Si(OD)_4 was determined to be 43 μsec), a relaxation time of 90 seconds (T1 for silicon is notoriously long), and an acquisition time of 0.82 sec. The lack of significant spectral change, despite the excess organic ligand, demonstrates the weakness (or extremely slow kinetics) of any chemical reaction between the silicic acid and organic bases.
- 3. Raman vibrational spectra from solutions of different Al^{3+} / oxalate²⁻ concentration ratios at near neutral pH. Note that at near neutral pH, there is considerable precipitation for the (1:1) and (1:2) samples, as well as the presence of other Al-oxalate species such as $Al_2(OH)_2(Ox)_2$ and $Al_3(OH)_3(Ox)_3$ (SJOBERG and OHMAN, 1985) These additional species may be the cause of the 1449 cm⁻¹

peak observed only at these concentration ratios. The peaks at 1408 cm $^{-1}$ and 1429 cm $^{-1}$ are assigned to oxalate vibrations from Al(Ox) $_2$ and Al(Ox) $_3$ respectively.

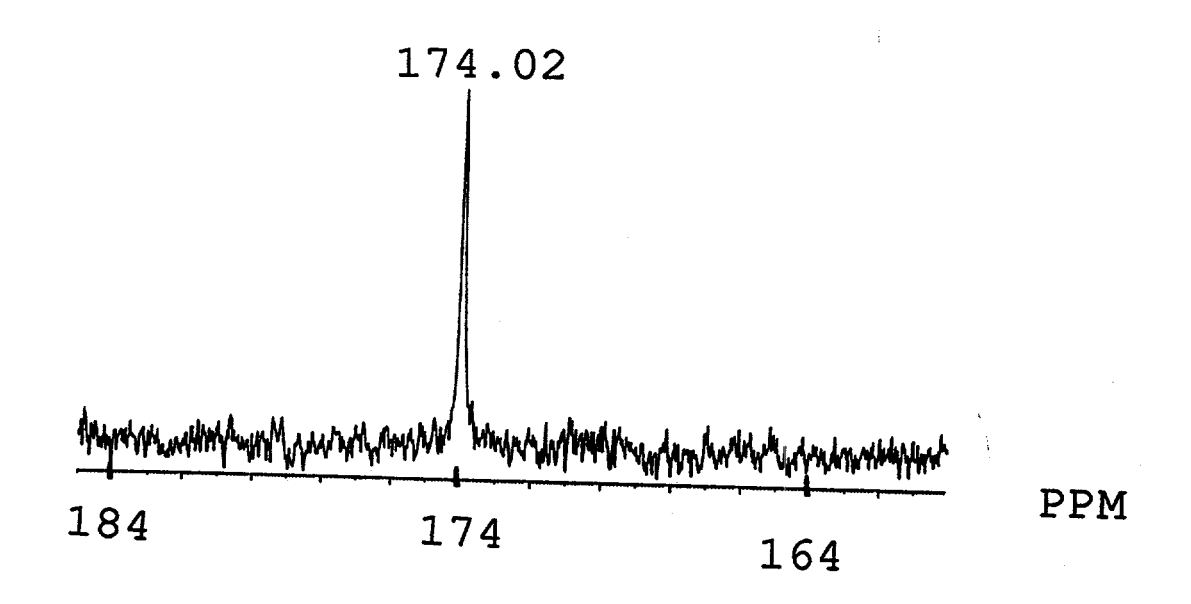
4. Temperature dependent Raman spectra for a solution of 20 mM Al $^{3+}$ / 50 mM oxalate at pH=2.9. Under these conditions, the ratio of Al $(0x)_2$ to Al $(0x)_3$ is 1 at 25°C (SJOBERG and OHMAN, 1985). Although the 1429 cm $^{-1}$ peak from Al $(0x)_3$ was expected to lose intensity relative to the 1408 cm $^{-1}$ peak of Al $(0x)_2$ as the temperature was increased, the spectra show a lack of change with temperature, indicating that the third association constant (Al $(0x)_2$ + 0x 2 --> Al $(0x)_3$) actually increases with temperature, despite the high charge of Al $(0x)_3$ and the lower availability of oxalate at higher temperatures.

INFRARED ABSORPTION SPECTRA

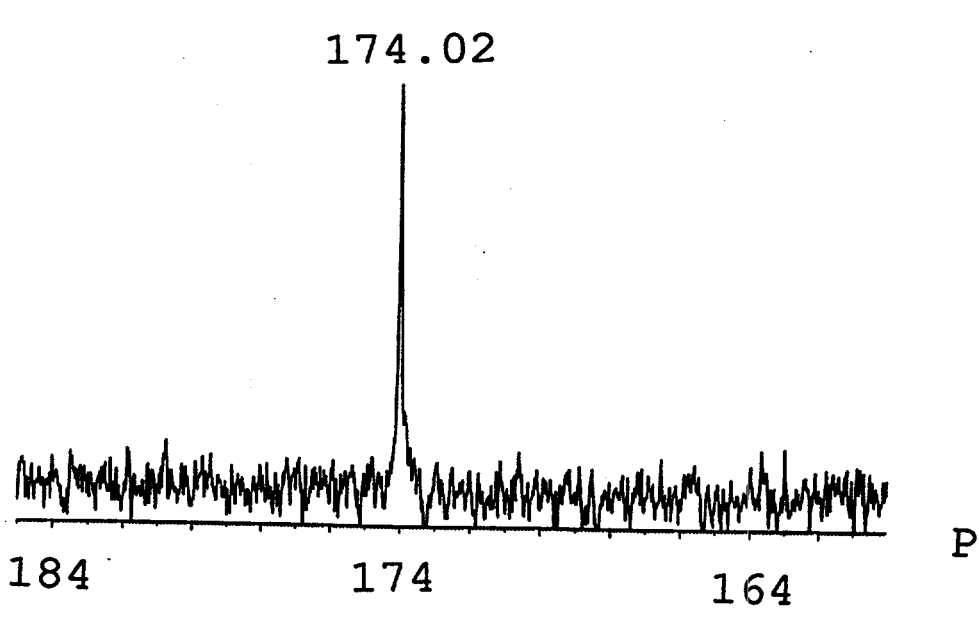


NMR SPECTRA

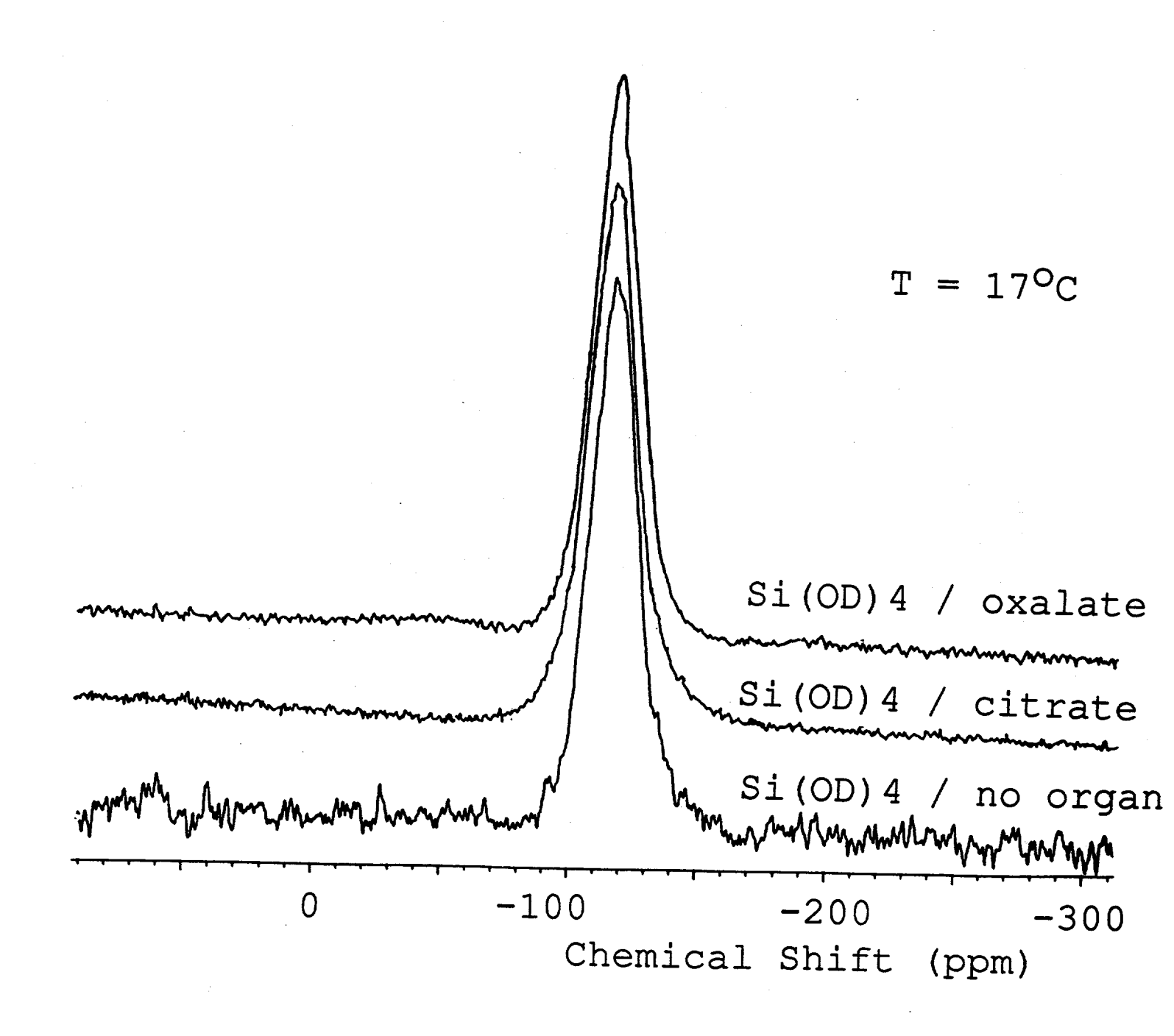
Silicic Acid / Oxalic Acid Mixture pD = 8

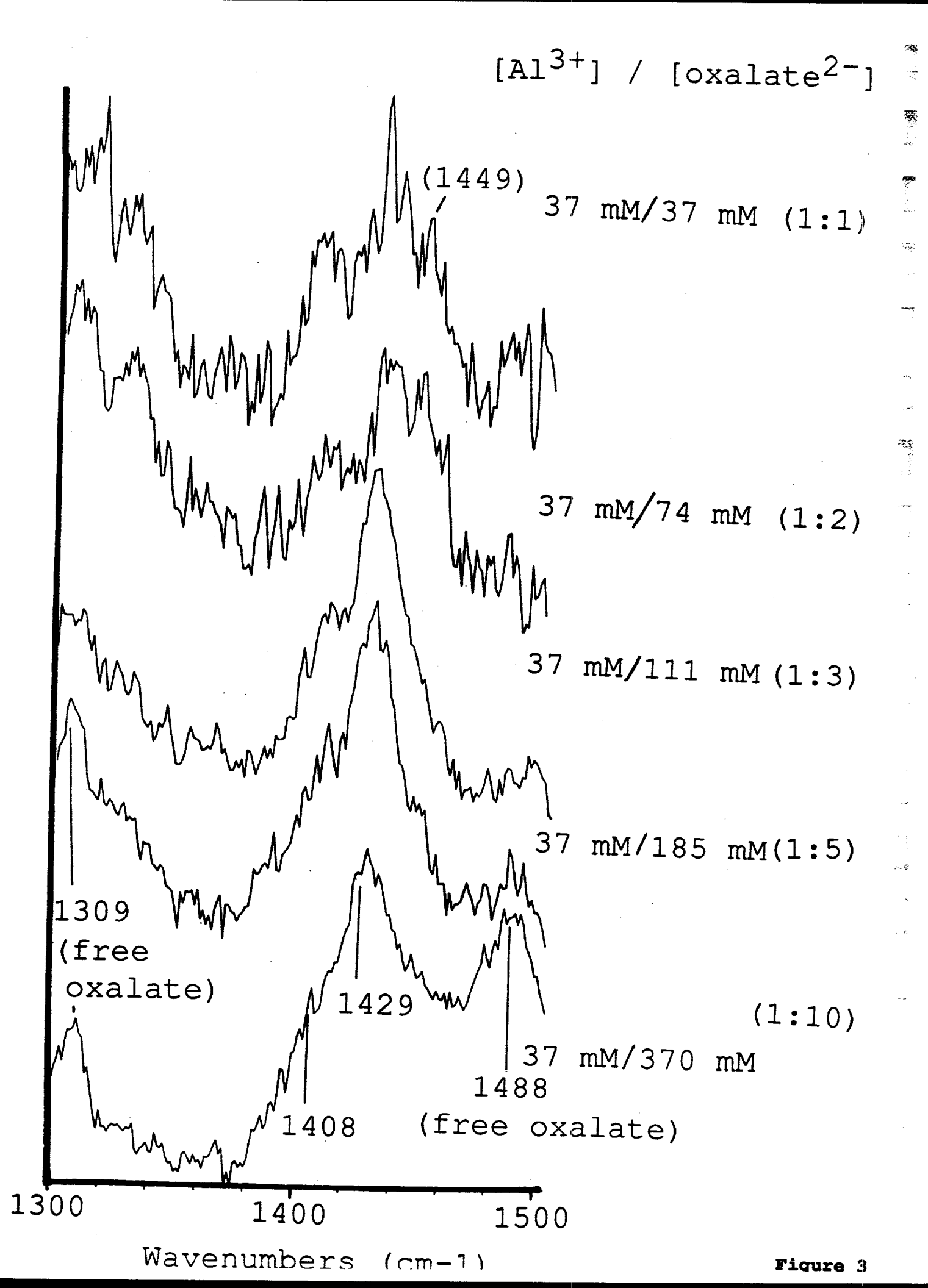


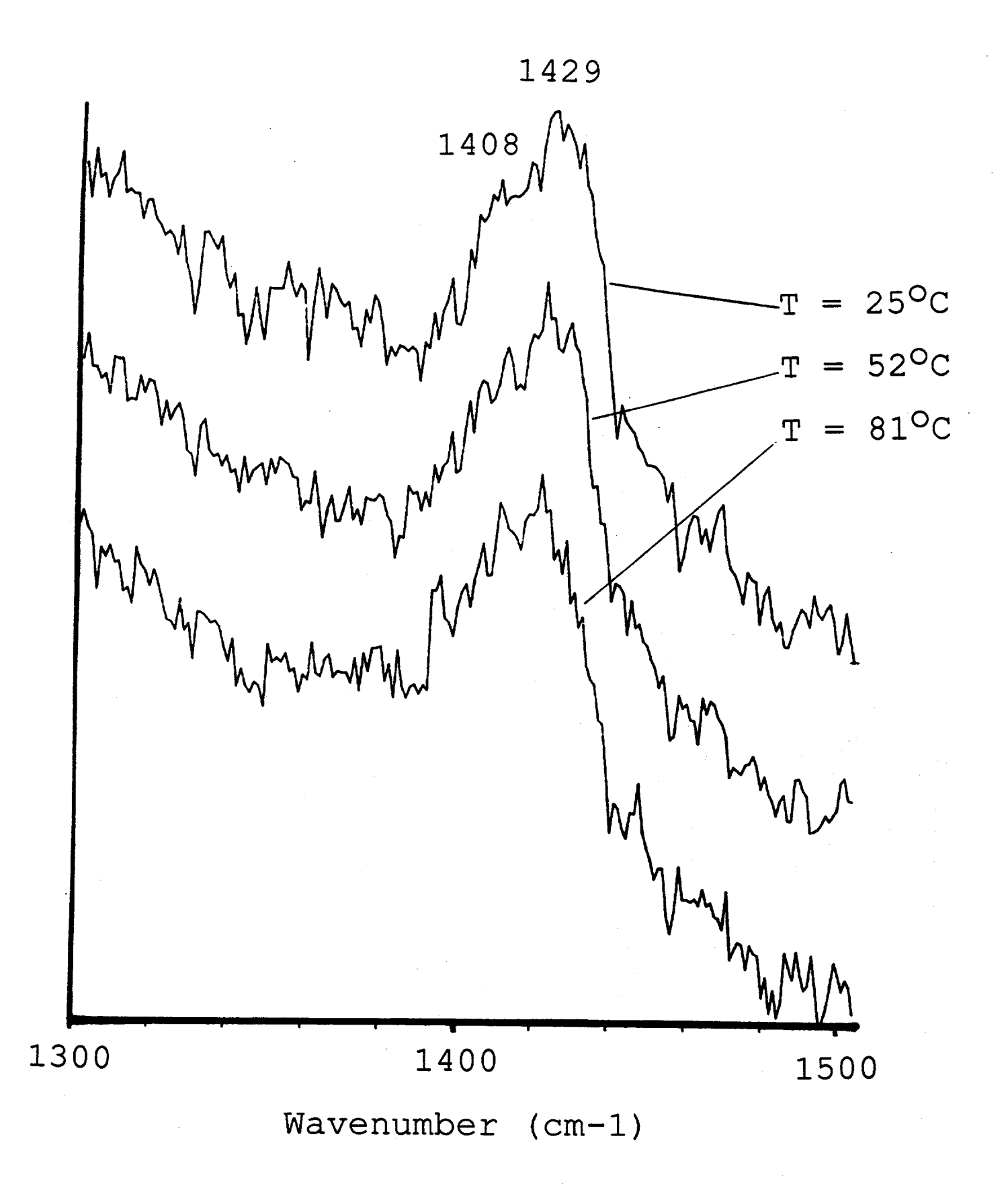
Sodium Oxalate (no Silicic Acid) pD = 8



PPM







Dissociation Quotients of Oxalic and Malonic Acid in Aqueous NaCl Media

Richard M. Kettler¹, Donald A. Palmer² and David J. Wesolowski²

¹Department of Geology University of Nebraska Lincoln, NE 68588-0340

²Chemistry Division
Oak Ridge National Laboratory
Oak Ridge, TN 37831-6110

1. Introduction

Oxalic (ethanedioic) acid and malonic (propanedioic) acid are the most important difunctional carboxylic acids in geologic systems. They are among the most abundant difunctional carboxylic acids in soils, and have received considerable attention because of their affect on nutrient availability (Traina et al., 1986), aluminum toxicity (Hue et al., 1986), and metal transport from soils to surface waters (Evans and Zelazny, 1990). Difunctional carboxylic acids may be very important in the alteration of sedimentary rocks by basinal brines. Concentrations of malonate and oxalate in excess of 2500 ppm and 400 ppm, respectively, have been reported in basinal brines (MacGowan and Surdam, 1990). The importance of difunctional carboxylic acids in geological systems results from their ability to form strong complexes with di- and tri-valent metal cations.

The thermodynamic behavior and activity/concentration relationships of the difunctional carboxylic acids in aqueous NaCl media must be understood in order to model geological systems successfully. Two of the most important equilibria are those for the dissociation of difunctional acids. Measurement of complex association constants and modelling the interaction between aqueous organic species and minerals is impossible if precise determinations of the dissociation quotients are unavailable. Experimental determinations of the dissociation quotients of oxalic acid and malonic acid at elevated temperatures (T>90°C) and high ionic strength (I>1.0 m) have not been reported.

•

2. Dissociation Quotients of Oxalic Acid

We have measured the first dissociation quotient of oxalic acid at temperatures ranging from 0° to 125°C and the second at temperatures ranging from 0° to 175°C. These limits were imposed by the thermal decomposition of oxalate. The measurements were made in NaCl solutions with ionic strengths ranging from 0.1 to 5.0 molal. The experiments were performed using a concentration emf cell that can be represented as

 $Pt, H_2 | H_2C_2O_4, NaCl, HCl | NaCl, HCl | H_2, Pt,$

for measurements of the first dissociation quotient, and as

 $Pt, H_2 | NaHC_2O_4, NaCl, NaOH | NaCl, HCl | H_2, Pt$

for measurements of the second dissociation constant.

The potentiometric data were used to calculate the equilibrium quotient for the dissociation reactions written in the base form. The equilibrium quotients were then combined with available literature data and fitted as functions of temperature and ionic strength. Regression of the data for the first dissociation quotient yielded

$$\log Q_{ox1b} = -\log a_w + p_1 + p_2 / T + p_3 \ln T + p_4 I / T + p_5 \left[1 - (1 + 2\sqrt{I}) \exp{-2\sqrt{I}}\right] / T$$

where a is the activity of water (Busey and Mesmer, 1978); p_1 (-19.8878), p_2 (4113.51), and p_3 (3.30080) determine the equilibrium constant; whereas, p_4 (12.5746) and p_5 (60.4908) have the same form as β^0 and β^1 in the ion interaction model of Pitzer (1973). Regression of the data for the second dissociation constant yielded

$$\begin{split} \log \mathcal{Q}_{ox2b} = & 2A_{\phi} \left[\sqrt{I} / \left(1 + 1.2 \sqrt{I} \right) + 2/1.2 \right) \ln \left(1 + 1.2 \sqrt{I} \right) \right] / \ln 10 - \log a_{\psi} + \\ & p_{1} + p_{2} / T + p_{3} T + p_{4} T^{2} I + p_{5} I / T + p_{6} I + p_{7} T \left[1 - \left(1 + 2 \sqrt{I} \right) \exp - 2 \sqrt{I} \right] \end{split}$$

where the first term is the Debye-Hückel expression (Dickson et al., 1990), and p_1 (-0.0262496), p_2 (3088.83), and p_3 (-2.06763x10⁻³) determine the equilibrium constant. Terms p_4 - p_8 have the form of terms in the Pitzer model with p_4 (-1.58430x10⁻⁶), p_5 (-169.301), and p_6 (0.730747) having the form of β^0 , p_7 (-7.89493x10⁻⁴) the form of β^1 .

3. Dissociation Quotients of Malonic Acid

Experiments designed to measure the first dissociation quotient used the following cell configuration

$$Pt, H_2 \mid H_2 C H_2 C_2 O_4, NaCl, NaOH \parallel NaCl, HCl \mid H_2, Pt$$

whereas, experiments using the cell configuration

$$\texttt{Pt}, \texttt{H}_2 \, | \, \texttt{NaHCH}_2 \texttt{C}_2 \texttt{O}_4, \texttt{NaCl}, \texttt{NaOH} \| \, \texttt{NaCl}, \texttt{HCl} \, | \, \texttt{H}_2, \texttt{Pt}$$

were designed to measure the second dissociation quotient. The equilibrium quotients obtained for the anionic forms of the dissociation reactions were fit as functions of temperature and ionic strength using the general equation

$$\begin{split} \log & Q_{ma1b} = -\log a_w + p_1 + p_2 / T + p_3 T + p_4 I / T + p_5 \left[1 - (1 + 2\sqrt{I}) \exp{-2\sqrt{I}} \right] / T \\ & + p_6 I + p_7 I T \end{split}$$

The equilibrium constant is determined by the first three terms and the remaining terms have the same form as terms in the ion interaction model of Pitzer. The values determined for these parameters are $p_1=-1.0652$, $p_2=3275.1$, $p_3=4.0951\times10^{-3}$, $p_4=-108.25$, $p_5=8.9741\times10^{-5}$, $p_6=0.62986$, and $p_7=-7.9435\times10^{-4}$. Similar treatment of the data for log Q_{ma2b} yields the

equation

 $\log Q_{ma2b} = 2A_{\Phi} \left[\sqrt{I} / (1+1.2\sqrt{I}) + 2/1.2 \right) \ln (1+1.2\sqrt{I}) \right] / \ln 10 - \log a_w + p_1 + p_2 / T + p_3 T + p_4 I / T + p_5 I + p_6 \left[1 - (1+2\sqrt{I}) \exp{-2\sqrt{I}} \right] T + p_7 I^2 / T$

where p_1 (-1.4093), p_2 (3038.5), and p_3 (-1.6287x10⁻³) determine the equilibrium constant. Terms p_4 - p_7 have the values p_4 =-66.210, p_5 =0.22664, and p_6 =-7.9149x10⁻⁴ and p_7 =-1.5016.

4. Conclusions

These measurements of the dissociation quotients of oxalic and malonic acid extend the existing data to 175° and 100°C, respectively. The experimental data in this study and smoothed equations produced fom those data are in excellent agreement with previously published measurements at low temperature and ionic strength. The association constants of the relevant metal carboxylate complexes can be measured using potentiometric methods (e.g. Palmer and Drummond, 1988) or through solubility measurements (e.g. Giordano, 1989).

References

- Busey, R.H. and Mesmer, R.E. (1978) Thermodynamic quantities for the ionization of water in sodium chloride media to 300°C.

 J. Chem. Engin. Data, 23, 175-176.
- Dickson, A.G., Wesolowski, D.J., Palmer, D.A. and Mesmer, R.E. (1990) The dissociation constant of bisulfate ion in aqueous sodium chloride solutions to 250°C. J. Phys. Chem., 94, 7978-7985.
- Evans, A. Jr. and Zelazny, L.W. (1990) Kinetics of aluminum and sulfate release from forest soil by mono- and diprotic aliphatic acids. Soil Sci., 149, 324-330.
- Giordano, T.H. (1989) Anglesite (PbSO₄) solubility in acetate solutions: The determination of stability constants for lead acetate complexes to 85°C. Geochim. Cosmochim. Acta, 53, 359-366.
- Hue, N.V., Craddock, G.R. and Adams, F. (1986) Effect of organic acids on aluminum toxicity in subsoils. Soil Sci. Soc. Am. J., 50, 28-34.
- MacGowan, D.B. and Surdam, R.C. (1990) The effect of organic/inorganic interactions on the progressive diagenesis of sandstones. in (Melchoir, D.C. and R. Bassett, eds.) Chemical modelling in aqueous systems II. ACS Symposium Series 416, ACS, 494-507.
- Palmer, D.A. and Drummond, S.E. (1988) Potentiometric

- determination of the molal formation constants of ferrous acetate complexes in aqueous solutions to high temperatures. J. Phys. Chem., 92, 6795-6800.
- Pitzer, K.S. (1973) Thermodynamics of electrolytes. I.
 Theoretical basis and general equations. J. Phys. Chem.,
 77, 268-277.
- Traina, S.J., Sposito, G., Hesterberg, D. and Kafkafi, U. (1986) Effects of pH and organic acids on orthophosphate solubility in an acidic, montmorillonitic soil. Soil Sci. Soc. Am. J., 50, 45-52.

THE STABILITY OF HYDROCARBONS AND C-O-H FLUIDS

SUBPROJECT:

THE STABILITY OF ORGANIC ACIDS*

J. L. S. Bell, D. A. Palmer, and S. E. Drummond Chemistry Division Oak Ridge National Laboratory Oak Ridge, TN 37831-6110

INTRODUCTION

Short-chain aliphatic acids and their anions may sometimes be present in petroleum brines and deep formation waters at relatively high concentrations. For example, the predominant acid/acid anion pair present, acetic acid/acetate (hereafter referred to as acetate), has been found at concentrations up to 0.17 mol/kg. The possibility that high concentrations of short-chain aliphatic acids may exist in solution has led to speculation as to the acids' involvement in the formation of some types of low temperature hydrothermal ore deposits, natural gas deposits, and secondary porosity in sediments. Particular attention has been given to the role of acetate in these processes. The ability of acetate to play a significant role depends in part on its hydrothermal stability under the pressure-temperature conditions prevailing in the sedimentary environment. Previous work has shown that, although short-chain aliphatic acids are extremely stable under thermal stress, they will decarboxylate if a suitable catalytic surface is present. Typical products are methane and carbon dioxide for acetic acid decarboxylation and bicarbonate and methane for acetate decarboxylation:

 $CH_3COOH_{(aq)} = CH_4 + CO_2$ $CH_3COO^- + H_2O = CH_4 + HCO_3^-$

The experiments conducted in this study had two principal goals: 1) to determine the decomposition rates of acetic acid and sodium acetate in the presence of geologically relevant catalytic surfaces, i.e. minerals commonly found in sedimentary basins and 2) to investigate the effect of pH on decomposition rate. In order to achieve acceptable decomposition rates, experiments were performed at 335°C and 355°C and the results extrapolated back to a temperature relevant to the basinal environment (100°C). Crushed and sieved mineral samples of known surface area were loaded into titanium pressure vessels along with one mol/kg acetic acid. One mol/kg sodium acetate was substituted for the reactions involving calcite since that mineral is soluble in acetic acid. Solutions having varying acetic acid to sodium acetate ratios were loaded into gold bag apparatus for experiments designed to investigate the effect of solution pH. The vessels were placed in rocking tube furnaces which had been previously heated. Approximately 1.5 ml of solution were periodically drawn off and analyzed for acetic acid or acetate by both potentiometric titration and ion exchange chromatography. Gas phase samples were collected at temperature at the termination of each experiment and analyzed for composition using mass spectrometry.

SURFACE EFFECTS

The decarboxylation reaction was consistently found to be first-order with respect to acetic acid or acetate for experiments in which the minerals acted as true catalysts. For these experiments, first-order rate plots were constructed and rate constants derived from the slope of a

This research is sponsored by the U.S. Dept. of Energy, Office of Basic Energy Sciences under contract number DE-AC05-84OR21400 with Martin Marietta Energy Systems, Inc.

line fit to the data (a typical first-order rate plot is given in Figure 1). The thermal stabilities of acetic acid and acetate in the presence of the various surfaces studied are summarized in Figure 2 in which the experimentally derived log k are plotted against 1000/T. Linear fits to these data correspond to the equation of Arrhenius in the form:

 $2.303 \log k = 2.303 \log A - E_a/RT$

where k is the rate constant at temperature T, A is the pre-exponential factor, E_a is the activation energy, and R is the gas constant. The slopes, m, of the lines are related to the activation energy, $m = -E_a/RT$, so that higher activation energies result in steeper slopes of the line. Pre-exponential factors, A, are derived from the intercept. First-order rate constants at 100°C were extrapolated using the appropriate values of A and E_a in the Arrhenius equation. Entropies and enthalpies of activation for decomposition were calculated for each surface type (for which first-order kinetics were obtained) using the Eyring-Polanyi relationship:

 $lnk = ln(k_pT/h) + (\Delta S^{\dagger}/R) - (\Delta H^{\dagger}/RT)$

where k is the observed rate constant, k_p is the Boltzman constant, T is temperature in Kelvin, h is Planck's constant, ΔH^{\dagger} is the enthalpy of activation, R is the universal gas constant, and ΔS^{\dagger} is the entropy of activation. Extrapolated low temperature rate constants were used to calculate half-lives for the reaction in the presence of the various minerals at 100°C.

Experimental rate constants, calculated rate constants at 100°C, half-lives at 100°C, and activation parameters are tabulated below. Comparison of the data for experiments where mineral surfaces were present with those for blank experiments in which no mineral was added yields a sense of the effectiveness of the mineral as a catalyst. A linear relationship was

Mineral	k _{349.6°C} (s ⁻¹)	k335°C (s ⁻¹)	k355°C (s ⁻¹)	k _{100°C} (s ⁻¹)
Blank		8.97x10 ⁻⁹	2.61x10 ⁻⁸	3.86x10 ⁻¹⁸
Quartz		1.48x10 ⁻⁸	5.16x10 ⁻⁸	1.78x10 ⁻¹⁸
Ca-Mont		4.23x10 ⁻⁸	7.22x10 ⁻⁸	1.12x10 ⁻¹²
Pyrite		3.29x10 ⁻⁷	3.97x10 ⁻⁸	8.45x10 ⁻²⁰
Magnetite		1.23x10 ⁻⁶	2.38x10 ⁻⁶	2.35x10 ⁻¹²
Blank (Na Acetate)	5.54x10 ⁻⁷	3.52x10 ⁻⁷	2.50x10	7.96x10 ⁻²³
Calcite (Na Acetate)	2.65x10 ⁻⁷	1.31x10 ⁻⁷		8.75x10-16

Mineral	E _a (kJ/mol)	ΔH [†] (kJ/mol)	ΔS [†] (J/mol K)	t _{1/2 100°С} (ут)	***********
Quartz	180	181	-102	1.2x10 ¹⁰	
Pyrite	220	210	-45.2	2.6x10 ¹¹	
Ca-Mont	85	79.5	-261	2.0x10 ⁴	
Calcite	150	147	-142	2.5x10 ⁷	
Magnetite	1.5	219	-3.95	9.4×10^3	

found to exist (see Figure 3) between the calculated activation enthalpies and entropies, which substantiates the concept of a common rate-limiting step for the surface-catalyzed decomposition reaction, presumably involving the breaking of the C-C bond. All surfaces were found to have some potential, albeit sometimes negligible, for affecting the decomposition of acetic acid and acetate. Decomposition is thought to be brought about by destabilization of the carbon-carbon bond resulting from chemisorption of the molecules onto surfaces. The success of the mineral as a catalyst depends in part on the strength of chemisorption at its available reaction sites.

Quartz, amorphous silica, and pyrite were found to have minimal catalytic effects on acetic acid decomposition. Calculated first-order rate constants for the reaction in the presence of these minerals are virtually indistinguishable from the rate constants for decomposition of acetic acid in

the absence of mineral surfaces. The dependence of the rate expression for decarboxylation on the surface area of pyrite was found to be of order 1/5 by varying the surface area to volume of solution ratio by four orders of magnitude.

Calcium montmorillonite was found to have a moderate catalytic effect on the decomposition of acetic acid. The first-order rate constant calculated for 100°C was 1.12x10⁻¹² s⁻¹ which gives t1/2 @ 20,000 years. Likewise, calcite was found to have a marginal ability to catalyze the decomposition of acetate. The first-order rate constant calculated for 100°C was 8.75x10-16 s-1 which gives t1/2 @ 25 million years. Acetate decomposition in the presence of calcite can be considered significant for only the slowest of geologic processes.

Rapid decomposition of acetic acid was observed in the presence of hematite, magnetite, and a ferric iron-bearing montmorillonite (see Figures 4 and 5). Run products analyzed by mass spectrometry indicate that acetic acid was oxidized to CO2 rather than cleaved to CO2 and CH4 as in decarboxylation. Slow conversion of hematite to magnetite during the course of experiments involving hematite, coupled with the fact that ferric iron-bearing montmorillonite and magnetite appear to have a limited ability to bring about rapid decomposition of acetic acid, suggests that the minerals in these experiments acted as reactants (oxidants) rather than catalysts. Complex kinetic behavior in these experiments meant that, except in the case of magnetite, rate constants could not be derived. Decomposition of acetic acid in the presence of magnetite followed first-order kinetics through 90% reaction. First-order rate constants given here for magnetite were calculated from initial (<90% reaction) data.

Four types of rate behavior were observed for the decomposition of acetic acid which suggest that acetic acid may undergo rapid (relative to decarboxylation) oxidative decomposition:

1) Extremely rapid decomposition rates in the presence of hematite were observed to slow dramatically after reduction of all hematite to magnetite.

2) Rapid, zero-order decomposition kinetics were observed in the presence of synthetic magnetite (Palmer and Drummond, 1986) while rapid, first-order kinetics were observed in the presence of a different synthetic magnetite (this study). In contrast, the formation of magnetite in experiments involving stainless steel (Palmer and Drummond, 1986 and Kharaka et al., 1983) and hematite (this study) did not cause an increase in rate.

3) Rapid decomposition of acetic acid was observed in the presence of an iron-bearing montmorillonite in which the iron is present in the ferric form.

4) Rapid decomposition of acetic acid was observed in the presence of synthetic pyrite which was known to have a small proportion of particles with magnetic cores that were probably low-sulfur iron sulfide or metallic iron.

These observations may be explained by the oxidation of acetic acid via reduction of Fe3+ in the available surfaces to Fe²⁺. Oxidation of acetate by Fe³⁺ has previously been proposed as an alternative to decarboxylation by Surdam et al. (1984). The marked slowing in rate observed in all four cases (see Figures 4 and 5) may be accounted for by the fact that the oxidant, which is here proposed to be Fe3+, has been consumed; e.g. the formation of magnetite in the case of hematite experiments and elimination of defects in the case of magnetite experiments and perhaps the synthetic pyrite experiment as well.

DH EFFECTS

Experiments involving solutions which were mixtures of acetic acid and acetate had significantly faster decomposition rates than solutions of either species separately (see Figures 6, 7, and 8). The rapid rate lasted only until the value for the total carboxyl species in solution (the sum of the acetic acid and acetate concentrations) had been depleted by an amount equal to the least concentrated species, after which the rate reverted to a slower one typical of the species remaining. It appears that acetic acid, not acetate, was consumed and as a result, the pH of the solution rises during the course of the reaction. The rapid initial rate did not appear to be affected by the

changing pH as the experiments proceeded; implying that the rate is not dependent on pH, but rather is dependent on, and in fact requires the presence of, both acetate and acetic acid. Rate laws may be postulated based on the above observations for three cases: 1) acetic acid only, 2) acetate only, and 3) buffer assemblages of acetic acid and acetate.

SUMMARY

Ouartz, calcite, and calcium montmorillonite do not significantly catalyze or only moderately catalyze the decomposition of acetate. This result is not surpising in that these minerals are ubiquitous -- if they significantly catalyzed acetate decomposition, there should be no acetate left in solution shortly after its formation. On the other hand, results from this study suggest that horizons within a sediment matrix which contain strongly reactive minerals such as magnetite, hematite, iron-bearing montmorillonite, and perhaps non-stoichiometric pyrite could cause a rapid loss of acetate from solutions passing through them. Rapid oxidation of acetate could, depending on initial concentration of acetate, result in local increases of fCO2 and fluctuations of pH. A given lithofacies is expected to have a finite capacity to bring about acetate decomposition by oxidative processes in that the oxidant minerals participate as reactants and are consumed. Finally, decomposition of acetate was found to be profoundly affected by solution pH. Rapid decomposition is expected in solutions having geologically reasonable pH (4 to 8). If the solutions are not pH buffered by some source other than acetic acid/acetate, or if the kinetics of pH adjustment by the external buffer are slow compared to decomposition of acetate, the decomposition of acetate may result in significant pH excursion. These observations have important implications for the participation of acetic acid in basin processes, especially those processes dependant on solution pH.

REFERENCES

- DRUMMOND, S. E. and PALMER, D. A. (1986) Thermal decarboxylation of acetate. Part II. Boundary conditions for the role of acetate in the primary migration of natural gas and the transportation of metals in hydrothermal systems. *Geochimica et Cosmochimica Acta*, 50, 825-833.
- KHARAKA, Y. K., CAROTHERS, W. W., and ROSENBAUER, R. J. (1983) Thermal decarboxylation of acetic acid: Implications for origin of natural gas. *Geochimica et Cosmochimica Acta*, 47, 397-402.
- PALMER, D. A. and DRUMMOND, S. E. (1986) Thermal decarboxylation of acetate. Part I. The kinetics and mechanism of reaction in aqueous solution. Geochimica et Cosmochimica Acta, 50, 813-823.
- SURDAM, R. C., BOESE, S. E., and CROSSEY, L. J. (1984) The chemistry of secondary porosity. In <u>Clastic Diagenesis</u> (edited by McDonald, D. A. and Surdam, R. C.) American Association of Petroleum Geologists Memoir 37, 127-149.

FIGURE CAPTIONS

- Figure 1. First-order rate plot for the decomposition of acetic acid in a titanium pressure vessel at 355°C in the presence of magnetite. The dashed line is a least squares fit to the data.
- Figure 2. Arrhenius plot of first-order rate constants for the decomposition of a) acetic acid and b) sodium acetate with linear extrapolations to relevant basin temperatures. Right vertical axis gives the half-life in years.
- Figure 3. Isokinetic plot for the decomposition of acetic acid (solid circles, the solid line represents a least squares fit) and sodium acetate (open circles, the dashed line represents a least squares fit). Note that the point for magnetite does not fall on the line for acetic acid which substantiates the proposition that another decomposition mechanism prevails in the presence of magnetite.
- Figure 4. First-order rate plot for the decomposition of acetic acid in a titanium pressure vessel at 355°C in the presence of hematite.
- Figure 5. First-order rate plot for the decomposition of acetic acid in a titanium pressure vessel at 355°C in the presence of an iron-bearing montmorillonite. The dashed line represents the least squares fit to the last six data points.
- Figure 6. The decomposition at 349.6°C of carboxyl species in a solution 0.5 mol/kg with respect to both acetic acid and acetate. A) Plot of the data for the combined, total concentration of acetic acid and acetate species versus elapsed time. B) First-order rate plot of the same data. The solid line is fit to the data plotted as the open circles, and the dashed line is fit to the data plotted as the solid circles.
- Figure 7. The decomposition at 335°C of carboxyl species in a solution which is 0.9 mol/kg acetic acid and 0.1 mol/kg sodium acetate. The solid line is the least squares fit to the solid circles.

 A) First-order rate plot showing all data. B) Exploded view of early data.
- Figure 8. The decomposition at 335°C of carboxyl species in a solution which is 0.1 mol/kg acetic acid and 0.9 mol/kg sodium acetate. A) Plot of the data for the combined, total concentration of acetic acid and acetate species versus elapsed time. B) First-order rate plot for the same data. The solid line is fit to the open circles. The dashed line is fit to the solid circles.

FIGURE 1

Decomposition of 1.0 mol/kg Acetic Acid in the Presence of Magnetite

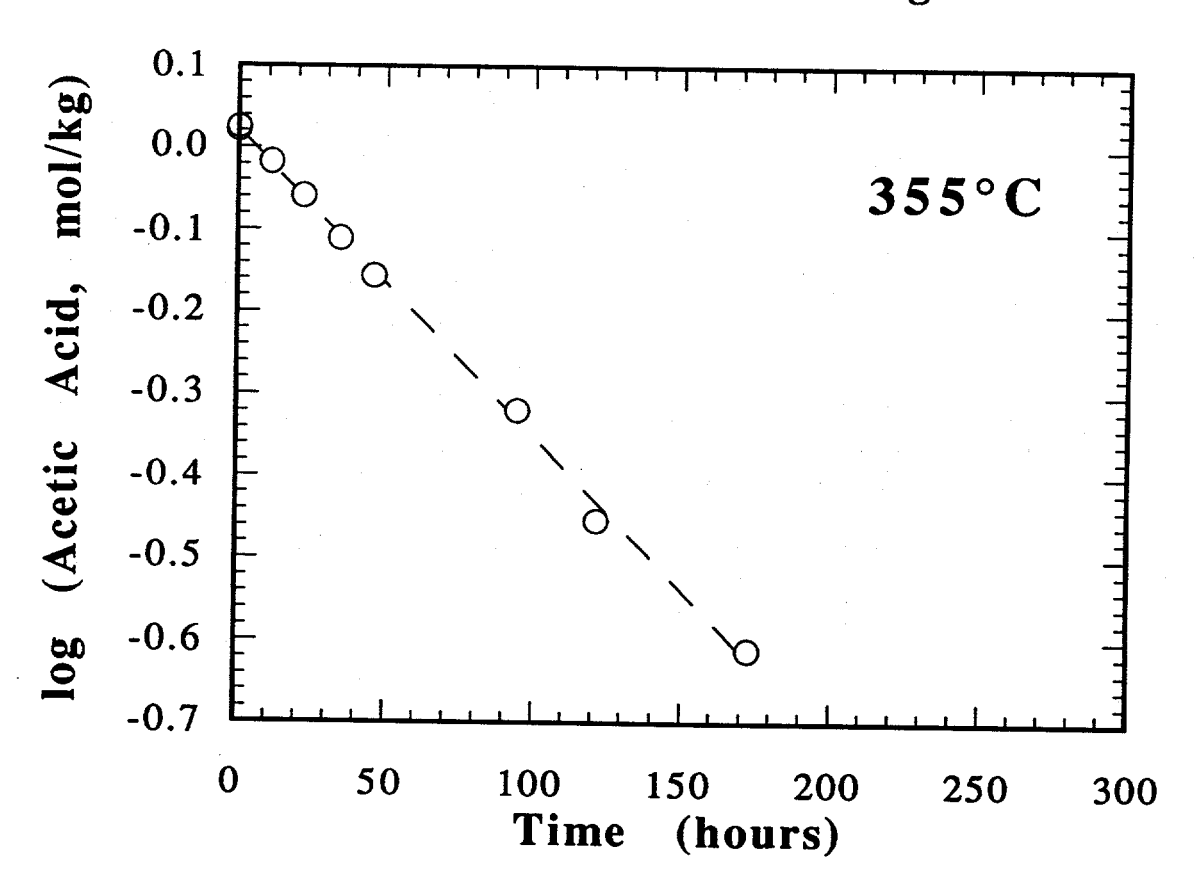
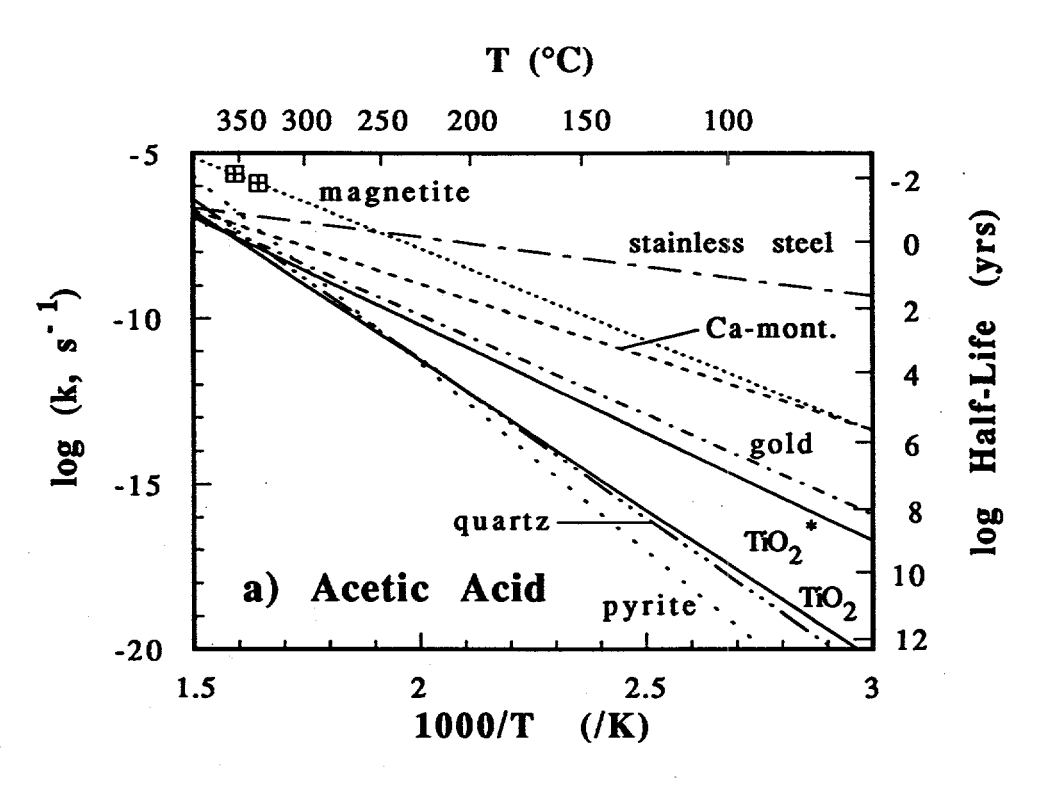


FIGURE 2



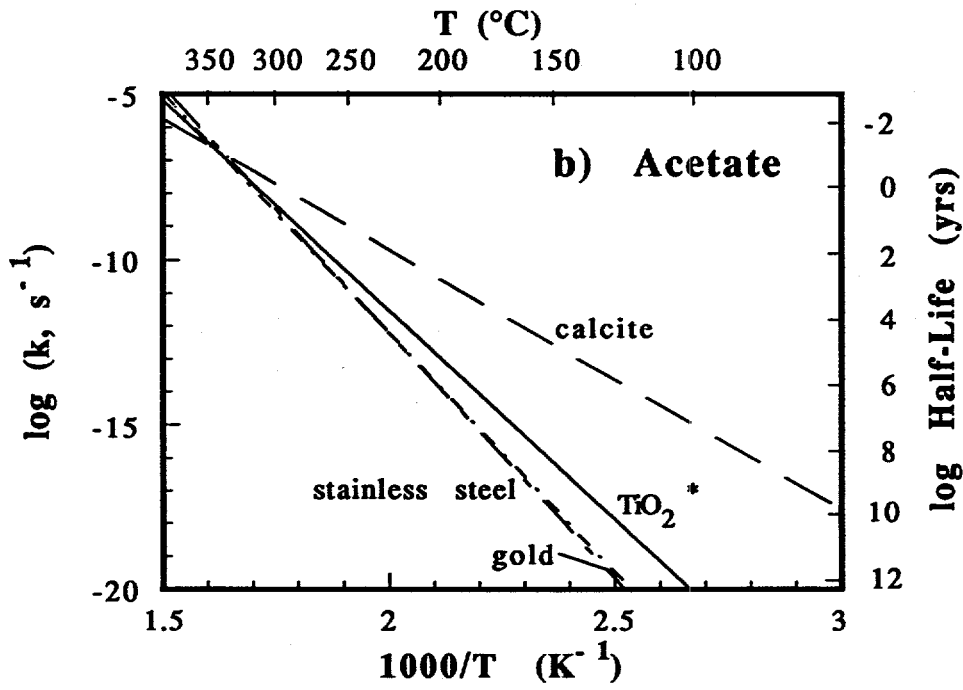


FIGURE 3

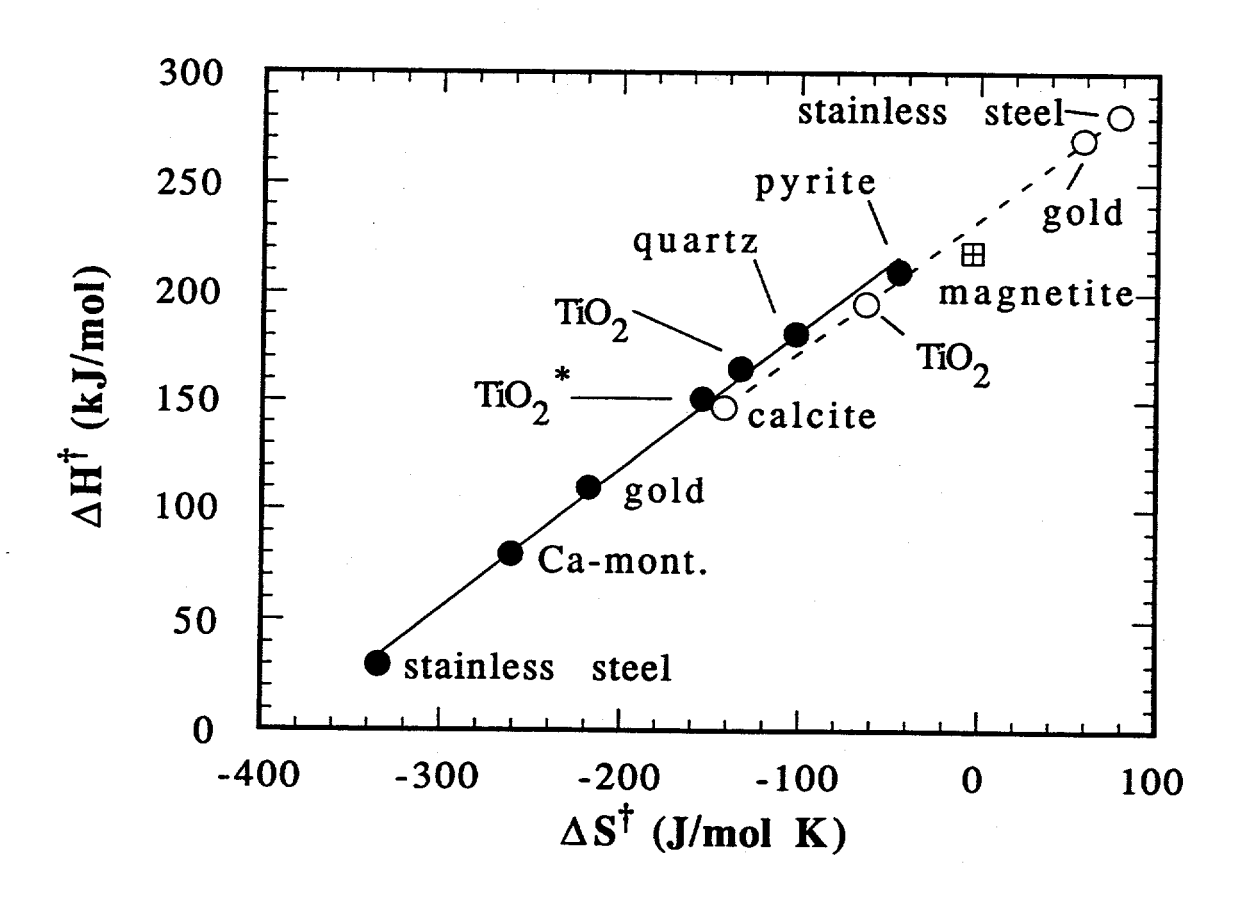


FIGURE 4

Decomposition of 1.0 mol/kg Acetic Acid in the Presence of Hematite

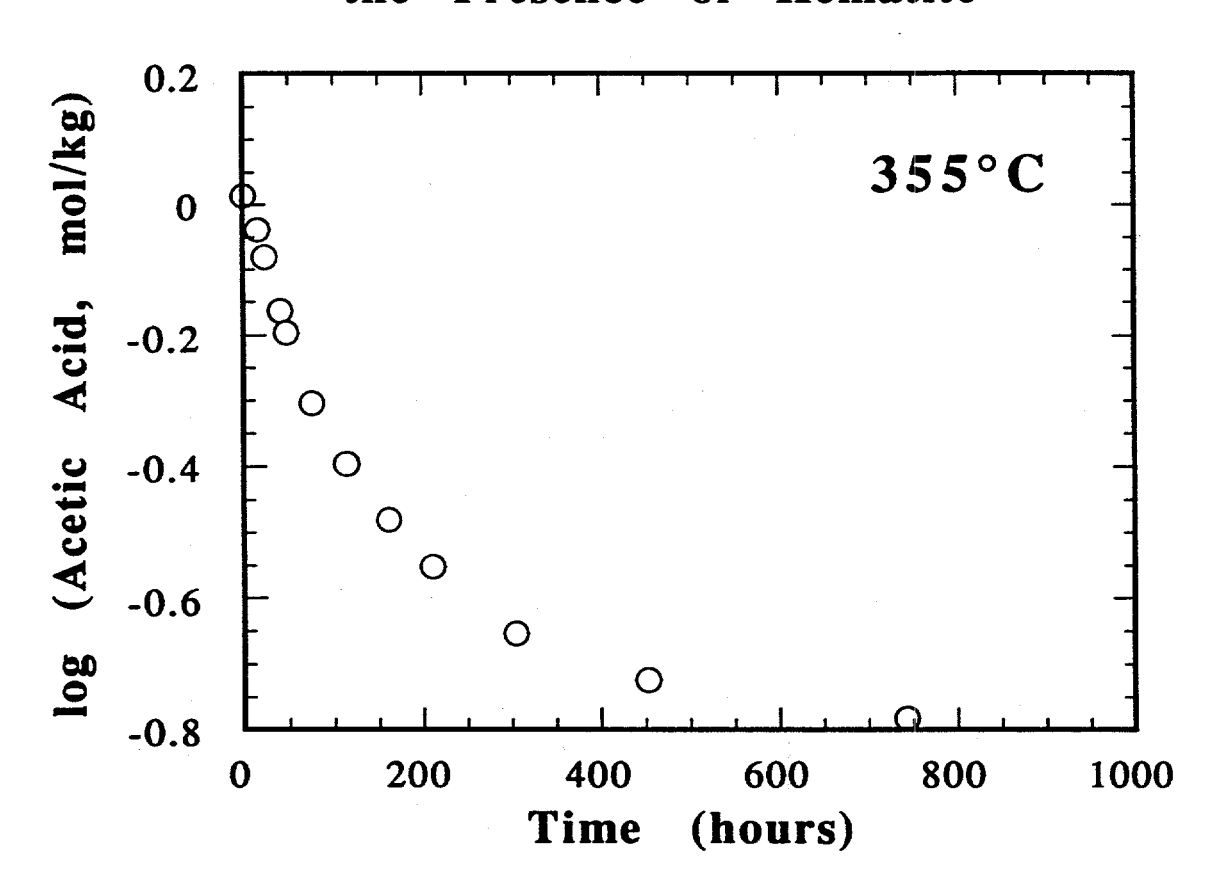


FIGURE 5

Decomposition of 1.0 mol/kg Acetic Acid in the Presence of Iron-Bearing Montmorillonite

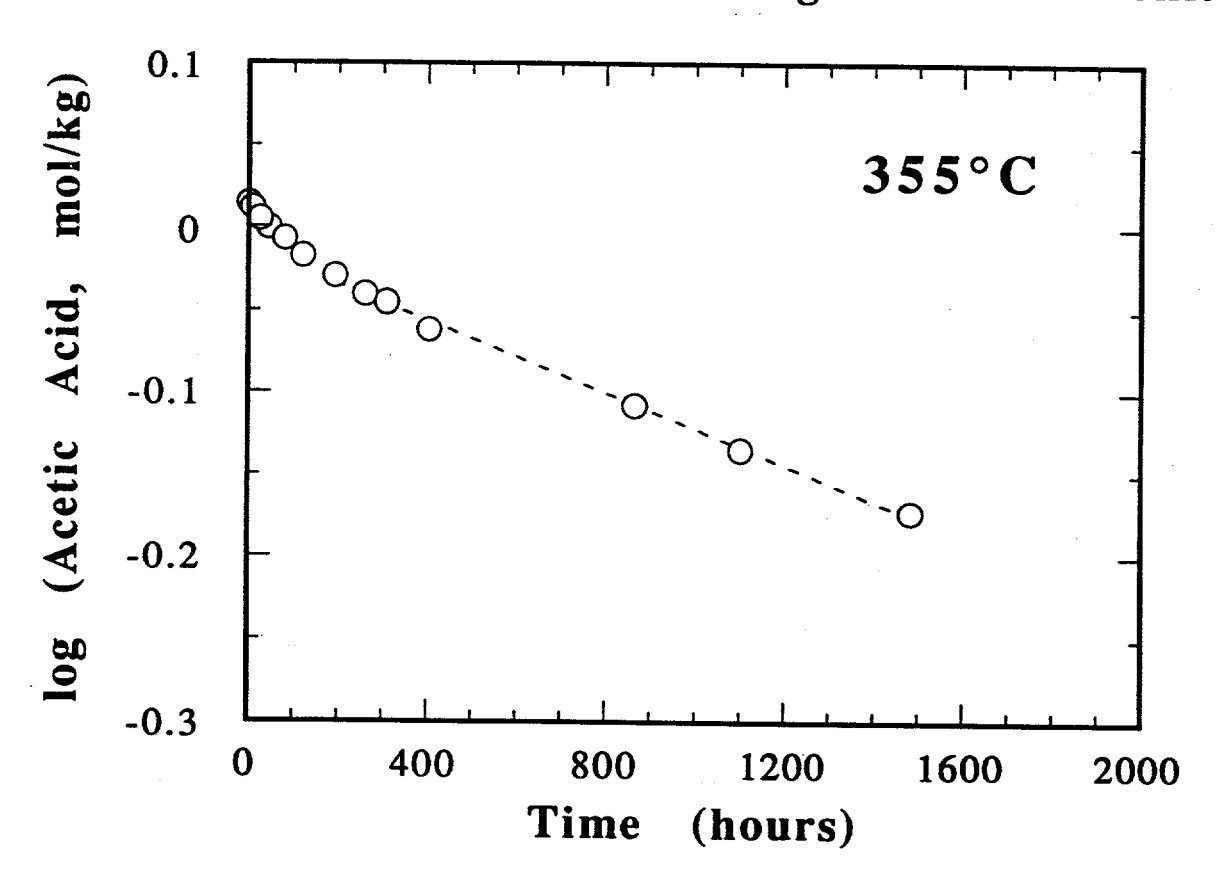
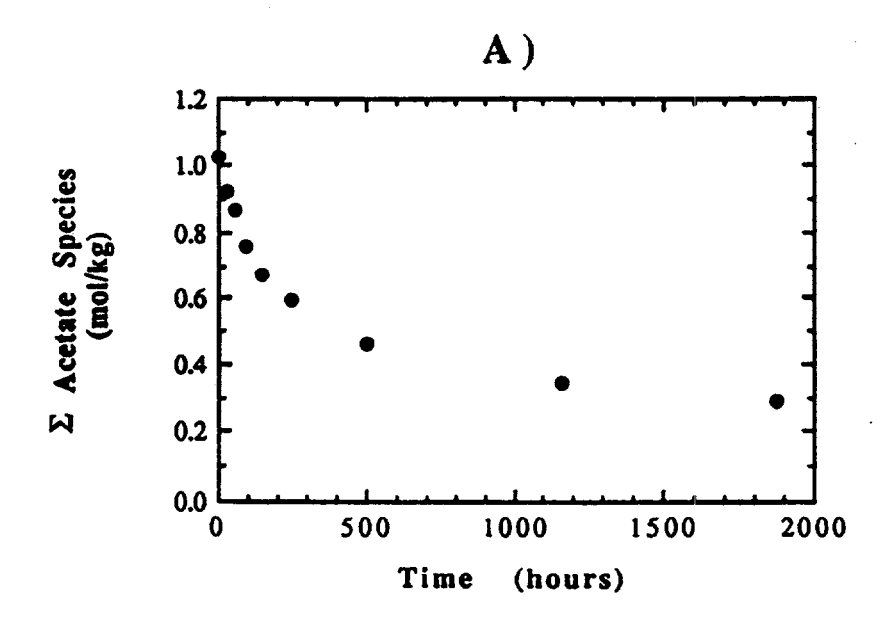


FIGURE 6



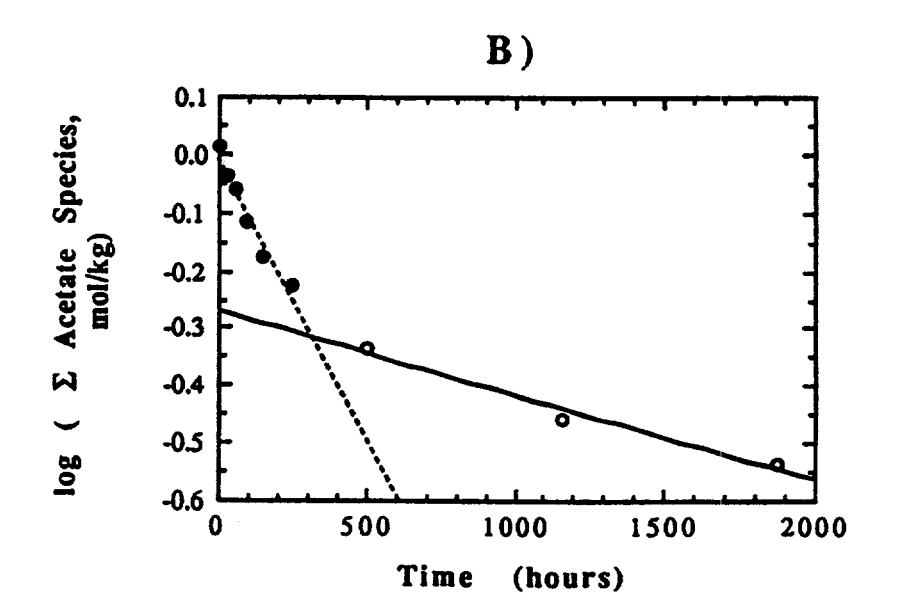
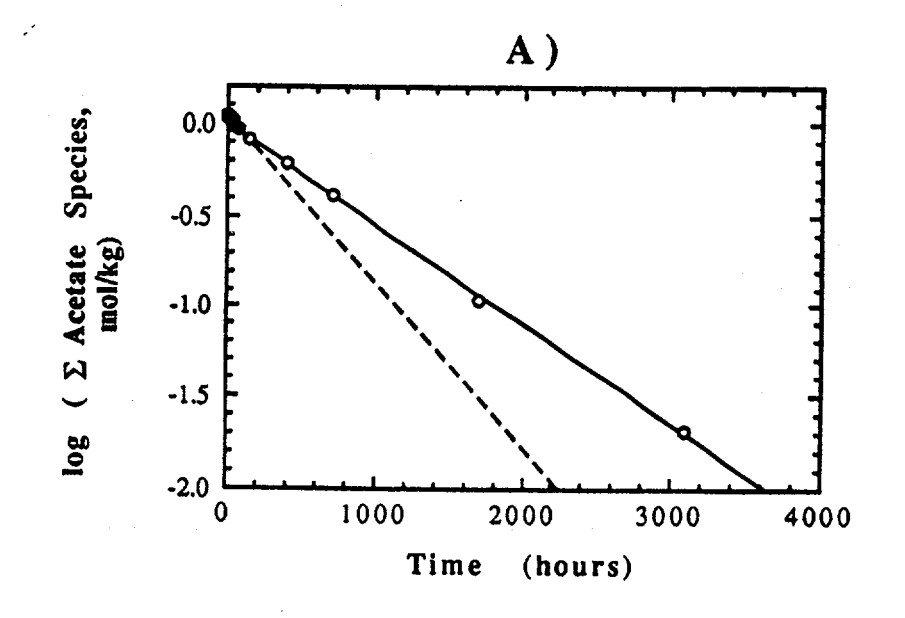
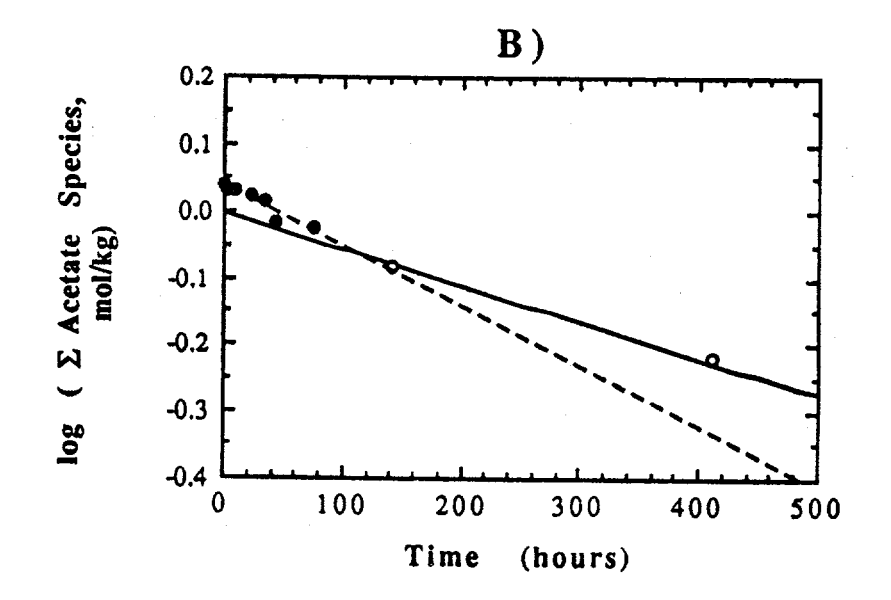
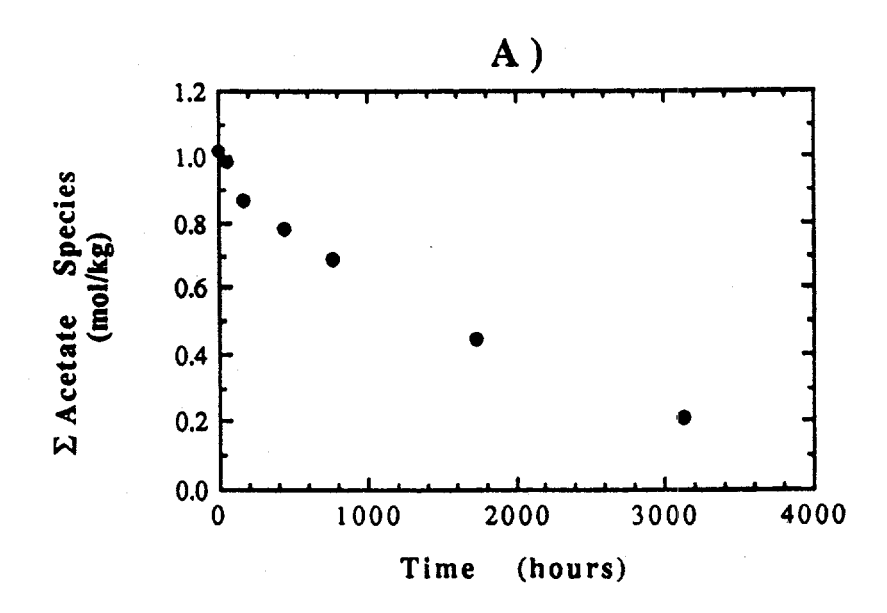


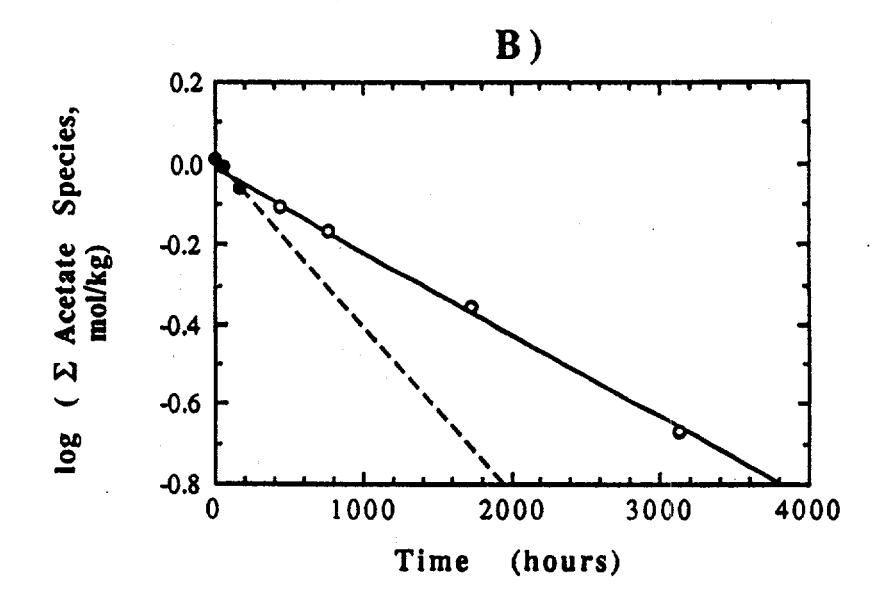
FIGURE 7











A Search for Evidence of Comet or Asteroid Impacts at Extinction Boundaries Charles J. Orth and Moses Attrep, Jr. Isotope and Nuclear Chemistry Division, Los Alamos National Laboratory, Los Alamos, New Mexico 87545

This research is primarily directed at elemental abundance measurements across the biological crisis horizons in the geologic record. We are searching for clues to the causes, such as large-body impact, massive volcanism, ocean stagnation, temperature change, and incursion of anoxic water onto platform communities. To provide answers, we also examine volcanic ash beds, storm/breccia deposits, black shales, and other significant sedimentary sequences. This research is providing a test of recent hypotheses that link large-body impacts with the periodic mass extinctions reported by Raup and Sepkoski (1984, 1986). This work is also contributing to the developing field of chemostratigraphy, a complement of biostratigraphy, to provide time markers in the geologic record.

Abundances are determined by neutron activation methods. Iridium is the element of choice to search for evidence of an impact, because it is two to four orders of magnitude more abundant in meteorites than it is in crustal rocks and it can be determined with great sensitivity by neutron activation methods. After intense irradiation in the Los Alamos Omega West Reactor, we radiochemically isolate ¹⁹²Ir in our samples from other radioactive contaminants. This procedure provides an Ir sensitivity of about 0.5 pg/g (0.5 part per trillion by weight). In appropriate samples we also radiochemically analyze for Au and the heavy platinum group elements, Os and Pt. Splits of these samples are submitted to the Reactor Group and they provide abundances for about 40 other major, minor and trace elements using their automated instrumental neutron activation analysis (INAA) system (Minor et al., 1981).

We established credibility in this research in 1981, soon after the Alvarez team (1986) announced their discovery of an Ir abundance anomaly at the Cretaceous-Tertiary (K-T) boundary in European marine sedimentary sequences. At that time skeptics claimed that the excess Ir was merely the result of chemical enrichment processes in the ocean, so we searched for the anomaly in nearby continental (fresh-water deposited) sequences. In collaboration with USGS palynologist Robert Tschudy, who had a decade earlier isolated the boundary to a three-meter interval, we soon located the anomaly in the Raton Basin of northeastern New Mexico (Orth et al., 1981). Further pollen/spore work showed the break coincided with the Ir spike (Fig. 1). These results greatly strengthened the Alvarez impact hypothesis and made it possible for stratigraphers to precisely correlate the palynological K/T boundary with the classical marine planktonic boundary.

Following the first Snowbird Conference on large-body impacts and mass extinctions, we turned our attention to the other extinction

horizons in the fossil record with emphasis on those that predate the terminal Mesozoic (K-T) event. In 1986, we received our first support from DOE/BES, which made it possible for us to expand our effort and seek further collaborations. At last count, we note that we have collaborated with more than 82 geoscientists from 37 universities, geological surveys and museums around the globe.

Current research is directed at studies of the K-T boundary in New Mexico/Colorado and Brazil, the Late Cenomanian extinction interval across the globe, the Ordovician-Silurian boundary in China and Canada, the Frasnian-Famennian boundary in China, the Late Devonian Alamo Breccia in Nevada, and international correlation of the Precambrian-Cambrian transition.

Late Cenomanian (~92 Ma) Extinction Interval

Our primary effort is currently focused on this interval. Several years ago we discoved two closely spaced Ir anomalies in the classic Cenomanian-Turonian marine sedimentary sequence in the Rock Springs anticline just west of Pueblo, Colorado (Orth et al, 1988). The Ir is accompanied by similar enrichment spikes of Sc, Ti, V, Cr, Mn, Co, Ni, Pt and Au. Chalcophile-like elements (As, Sb) are depleted in this interval as are Hf, Th and U. No change across the interval above local backgrounds is seen for the alkali metals and alkaline earth elements. Although the rare earths are somewhat depleted, heavy-to-light ratios (e.g., Yb/La and Lu/La) enhancement. Comparison with detailed paleontologic data indicates the lower abundance spike coincides with the disappearance of the foraminifers Rotalipora cushmani and R. greenhornensis. A series of molluscan extinctions and speciation events also begins near the stratigraphic level of the lower abundance anomaly. A positive excursion in δ ¹³C begins about a half meter below the lower anomaly and persists into the Lower Turonian. The abundance anomalies and the isotopic excursion may not be closely coupled. bentonite beds occur throughout the entire Cenomanian-Early Turonian interval, but have no obvious influence on the extinctions and our observations. To the contrary, the bentonitic beds are depleted in the siderophile-like elements and enriched in Hf, Th, U, Cs and rare earths, just opposite to what we observe in the two anomalies.

Following the discovery at Pueblo, we studied 15 other sections that were deposited in the Cretaceous epeiric seaway from Canada to West Texas. A section at Chispa Summit, about 30 km south of Van Horn, West Texas is our reference section, because the two anomalies are better resolved here than elsewhere in the Western Interior (Figs. 2 and 3). When we integrate the net peak areas of the 16 sections we find that the anomalies are strongest in the southern Colorado and New Mexico regions and drop off in intensity to the eastern and western margins of the seaway and especially to the north (Fig. 4), indicating that the excess elements came in from the south via the proto-Gulf of Mexico/Caribbean.

To further constrain the source location of the anomalies, sections

in the United Kingdom, Germany, Poland and South America, and Deep Sea Drilling Project (DSDP) cores from the Atlantic, Pacific and Indian Ocean basins have been and are being examined. anomalies in these sections, except for the one in South America, are quite weak. The section in South America is located near Chaparral in northwestern Colombia. The results are somewhat puzzling, because in addition to the anomaly doublet elsewhere, two other Ir peaks are present, one just below and one just above the doublet. The lowest anomaly appears to be associated with some local enrichment process, but the highest one is similar in composition to members of the doublet (Fig.5). global intensity pattern for the anomalies (Fig. 6) indicates the source location was somewhere in the proto-Caribbean/Gulf of Mexico The location might be further constrained if preserved sections could be found along the west coast of Mexico and North America, and in ODP/DSDP cores from the eastern Pacific and from the Caribbean itself.

The group of enriched elements and their interelement abundance ratios (Table 1) closely resemble those of Mid-Atlantic Ridge basalts or of Hawaiian tholeiitic lavas, but not those of C1 chondrites, black shales, average crustal rocks, or southeastern Kansas lamproites and kimberlites of comparable age. The excess Ir and other siderophiles hint of possible large body impact(s) for the source. A weak geochemical signal from comet impact(s) could be masked by the strong terrestrial-like overprint. However, we have not located any physical signatures of large impact(s) such as microspherules or shocked-mineral grains, other calcispheres of biogenic origin, and to our knowledge, micropaleontologists have not turned up any impact forms in their search for micro fossils. Less exotic, but more credible sources of these anomalies are the following:

- 1) Intense pulses of spreading center activity in the Late Cenomanian proto-Caribbean/Gulf of Mexico. Larson (1991) lists a large production of mid-ocean crust (20.4 x $10^6~\rm km^3$) in the Caribbean between 75 and 90 Ma. Age uncertainty of a few percent would give overlap.
- 2) Increased circulation of deep, metal-rich water associated with the great Late Cenomanian-Early Turonian eustatic rise and the deep-water opening of the south Atlantic. Recently, for example, Orians et al. (1990) have developed a technique for measuring dissolved Ti in the ocean at microscopic concentrations and have found that the Ti concentration is one to two orders of magnitude greater in deep water than it is near the surface.

Cretaceous-Tertiary (K-T) Boundary (Western Interior and Brazil)

Although our primary interest is in Mesozoic and older horizons, we continue to study the K-T boundary and also provide geochemical support to paleontologists and stratigraphers searching for its precise position in their sections.

After several years of correspondence, we finally received large suites of samples from seven suspected K-T sections collected by

Petrobras (Brazil) geologists/paleontologists. In none of these suites have we found any Ir concentrations above low local background levels. Therefore, if their paleontologic interpretations are correct, the boundary must not be preserved at these sites, because anywhere on the globe we have examined where it is preserved, we have observed a strong Ir anomaly.

Currently, there are at least three important, unresolved questions about the K-T event concerning: 1) Single or multiple impacts; 2) impact(s) site(s); and 3) The class of impactor(s), asteroid/comet. The first question might be best addressed by studies of North American continental sections where two visibly distinct clay (fallout) layers are preserved in quiet fresh-water swamp sequences (Fig. 7); a 1- to 3-cm thick kaolinitic clay bed overlain by a 2-to 5-mm Ir-rich mixed smectite layer containing shocked quartz grains (global layer?). Comparison of Ir content in the clays with that in meteorites indicates that > 95 % of the material is derived from target rock and the remainder from the projectile(s). Elemental abundance data also provide information about questions 2 and 3.

We are searching for similarities and differences in elemental abundance patterns in the two clay layers and we compare these results with those for local sedimentary sequences and also for similarly altered volcanic ejecta in the form of kaolinitic tonsteins. Although element migration has complicated the picture (even Ir was mobile in the acidic swamp environment), the two clay layers show similar Ti/Al and U/Th ratios, and excess chalcophile elements relative to local claystones/shales and to volcanic tonsteins (Table 2). In numerous sections we observe low rare earth concentrations, but enriched in the heavies. Despite the striking difference in the appearance of the two clay layers, the elemental data suggest that they might have come from the same general source area (a single crater should range from 150 to 300 In this scenario, the lower kaolinitic layer would have resulted from prompt, low angle ejecta mostly from the outer radius of the crater, and the upper layer, richer in projectile, would have resulted from fallout of back angle material ejected into and beyond the stratosphere. On the basis of the high U/Th ratio and excess chalcophiles, impact in or near an ocean sedimentary basin with substantial black shales should be considered in any discussions of an impact site. In other work, we have measured heavy siderophile abundances (Os, Ir, Pt and Au) and their interelement ratios are quite similar to those of C1 We have also measured Ir concentrations in Deccan chondrites. basalts and find them quite low (2 to 23 pg/g); the Deccan flood basalts are not the source of the K-T Ir anomaly. continuing to study the K-T clay(s)

Late Devonian Frasnian-Famennian (F-F) Boundary, China

In collaboration with University of Alberta paleontologists, we have studied the F-F boundary exposed near Xiangtian, Guangxi, South China. A large extinction of marine animals, a negative δ ¹³C

excursion and a moderate Ir anomaly occur at the boundary. However, many other elements, not enriched in meteorites are also enriched. Although we can not rule out a large-body impact, we suspect the excess Ir is the result of reducing conditions in the seaway; our Canadian collaborators favor an impact scenario.

Ordovician-Silurian (O-S) Boundary, Canada and China

In further work with the Alberta group, we are studying the O-S boundary exposed at three sites in South China and at a site at Avalanche Lake, Mackenzie Mountains, Northwest Territories, Canada. Thus far we have not found any compelling evidence of a large body impact at this horizon. A small Ir excess at the sites in China appears to have resulted from a change in ocean chemistry or sediment source direction. Several years ago we studied the O-S boundary at the stratotype section at Dob' Linn, Scotland (Wilde et al., 1986), and on Anticosti Island, Quebec (Orth et al., 1986), also with negative results. We feel that we have demonstrated that this massive and sharp extinction was not the result of a large-body impact, but might have been associated with some aspect of the Late Ordovician glaciation event.

Alamo Breccia, Nevada

We are currently working with John Warme (Colorado School of Mines) on the Late Devonian Alamo Breccia. He has tracked this unit over a large area of Nevada and suspects that it might have resulted from a massive tsunami wave (large rip-up clasts are incorporated), possibly from a nearby impact. Using the Brazos River K-T section as a model, we are measuring Ir abundances in the uppermost portion of the unit, where decreasing grain size suggests that the violence was damping out and undisturbed preservation of fallout might have occurred. To date, we have found only extremely low Ir concentrations. However, we are working our way up section in sediments that were laid down under increasingly quiet conditions.

Precambrian-Cambrian Transition

We are participating in the International Geological Correlation Program (IGCP) Project 303 to characterize the Precambrian-Cambian transition. We have been requested by the organizers to provide elemental abundance patterns across the transition. The purpose is to search for abundance anomalies that can be correlated on a global basis. Recently, we collaborated with paleontologists from Lund University (Sweden) to examine drill core taken near Lublin, Poland. Unfortunately, we observed no sharp peaks in over 200 meters of core, although we did observe some gradual trends in Mn content that might prove correlative. Eventually, we expect to receive large suites of samples from Russia, Morocco, Newfoundland and the Lesser Himalaya region.

References

- Alvarez, L.W., W. Alvarez, F. Asaro, and H.V. Michel, 1980, Extraterrestrial cause for the Cretaceous-Tertiary extinction, Science, v. 208, p. 1095-1108.
- Elder, W.P., 1988, Geometry of Upper Cretaceous bentonite beds: Implications about volcanic source areas and paleowind patterns, Western Interior, United States, Geology, v. 16, p. 835-838.
- Larson, R.L., 1991, Latest pulse of Earth: Evidence for a mid-Cretaceous superplume, Geology, v. 19, p. 547-550.
- Minor, M.M., W.K. Hensley, M.M. Denton, and S.R. Garcia, 1981, An automated neutron activation analysis system, Radioanalytical Chemistry, v. 70, p. 459-471.
- Orians, K.J., E.A. Boyle, and K.W. Bruland, 1990, Dissolved titanium in the open ocean, Nature, v. 348, p. 322-325.
- Orth, C.J., J.S. Gilmore, J.D. Knight, C.L. Pillmore, R.H. Tschudy, and J.E. Fassett, 1981, An iridium anomaly at the palynological Cretaceous-Tertiary boundary in northeastern New Mexico, Science, v. 214, p. 1341-1343.
- Orth, C.J., M. Attrep, Jr., X. Mao, E.G. Kauffman, R. Diner and W.G. Elder, 1988, Iridium abundance maxima in the upper Cenomanian extinction interval, Geophysical Research Letters, v. 15, p. 46-349.
- Orth, C.J., J.S. Gilmore, L.R. Quintana, and P.M. Sheehan, 1986, Terminal Ordovician extinction: Geochemical analysis of the Ordovician-Silurian boundary, Anticosti Island, Quebec, Geology, v. 14, p. 433-436.
- Raup, D.M. and J.J. Sepkoski, Jr., 1984, Periodicity of extinctions in the geologic past, Proceedings of the National Academy of Sciences, v. 81, p. 801-805.
- _____, 1986, Periodic extinctions of families and genera, Science, v. 231, p. 833-836.
- Wilde, P., W.B.N. Berry, M.S. Quinby-Hunt, C.J. Orth, and L.R. Quintana, 1986, Iridium abundances across the Ordovician-Silurian stratotype, Science, v. 233, p. 339-341.

TABLE 1. ELEMENTAL ABUNDANCE RATIOS

RATIO	LCEN	5	MARB	MARB HAWAII	KIMBER/LAMPRO (KANSAS)	EARTH'S CRUST
Cr/lr (10 ⁴)	~200	2.0	200	100	~100	500
Ni/Ir (10 ⁴)	180	7.5	190	~100	100	380
Cr/Sc	&	400	8.5	6	62	4
Cr/V	1.5	45	1.1	-	o	0.74
Cr/Co	10	9	7.5	6.5	18	4
Ti/Cr	12	0.2	24	47	12	44
Mn/Cr		0.7	3.4	3.9	1.5	တ
Cr/Ni	1.9	0.27	2.7	7	0.0	0.4
Yb/La	0.3	0.54	~0.8	0.18	0.008	0.08

LCEN - Late Cenomanian anomalies; C1 - C1 chondrite; MARB - mid-Atlantic Ridge basalts; HAWAII - Hawaiian Southeastern Kansas tholeiitic lavas; KIMBER/LAMPRO kimberlites and lamproites.

Table 2. Comparison of some abundance ratios in the K-T boundary interval for Western Interior continental sections.

LOCATION	TiO ₂ /Al ₂ O ₃	U/Th
<pre>K/T (K) Ave. Range n = 21 samples</pre>	0.051 0.045-0.059	0.96 0.54-1.8
<pre>K/T (Ir) Ave. Range n = 16</pre>	0.057 0.046-0.064	0.80 0.47-2.34
Local shale/clay Ave. Range n = 28	o.040 0.030-0.046	0.332 0.20-0.59
Volcanic tonstei Ave. Range n = 11	ns 0.020 0.016-0.030	0.26 0.19-0.80

⁽K): kaolinitic boundary clay; (Ir): Ir-rich, mixed smectite layer with shocked-quartz grains (see Fig. 7).

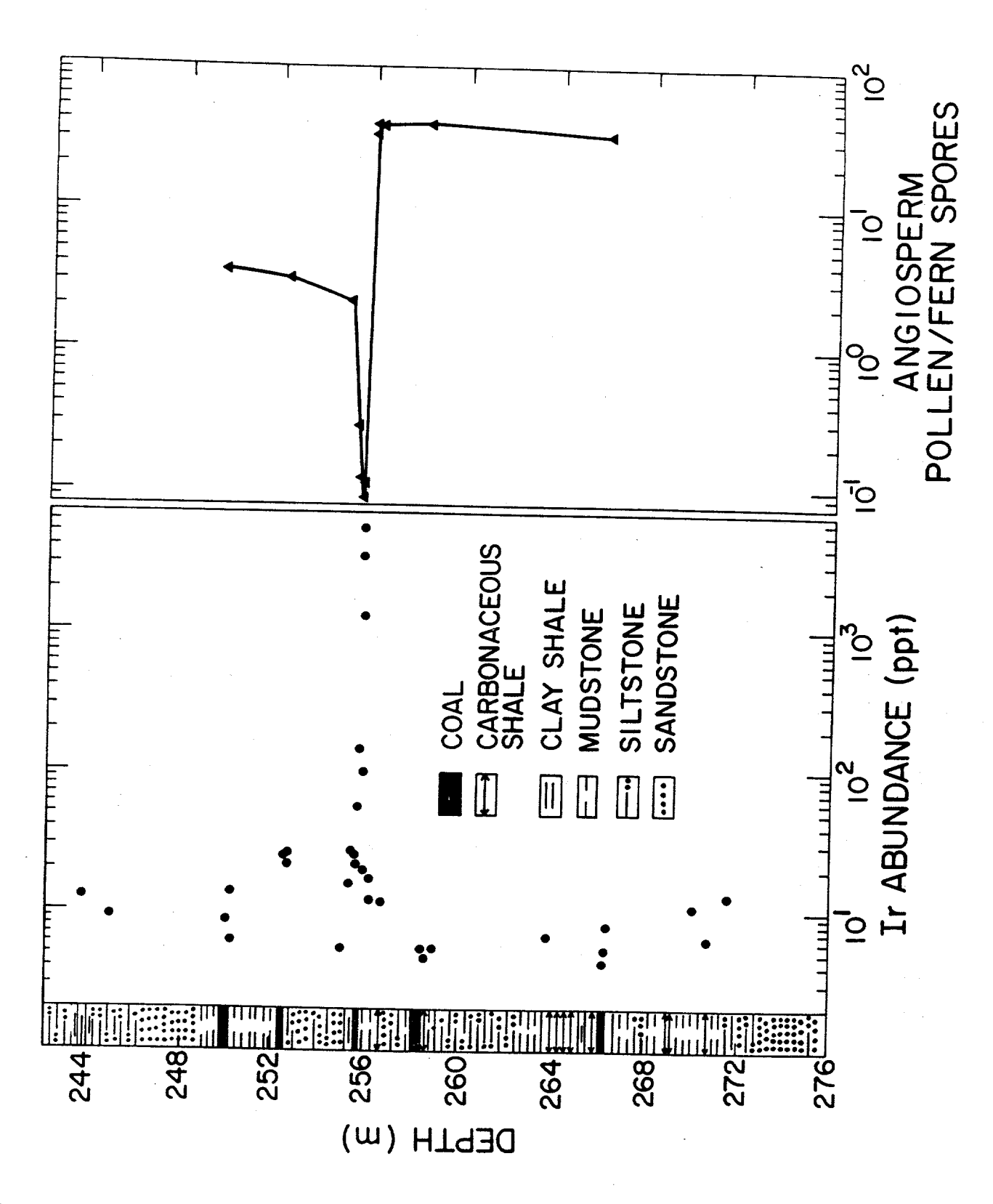


Fig. 1 Iridium abundance pattern and ratio of angiosperm pollen to fern spores in the York Canyon core as a function of core depth and lithology. Ir concentrations given in parts per trillion by weight (ppt).

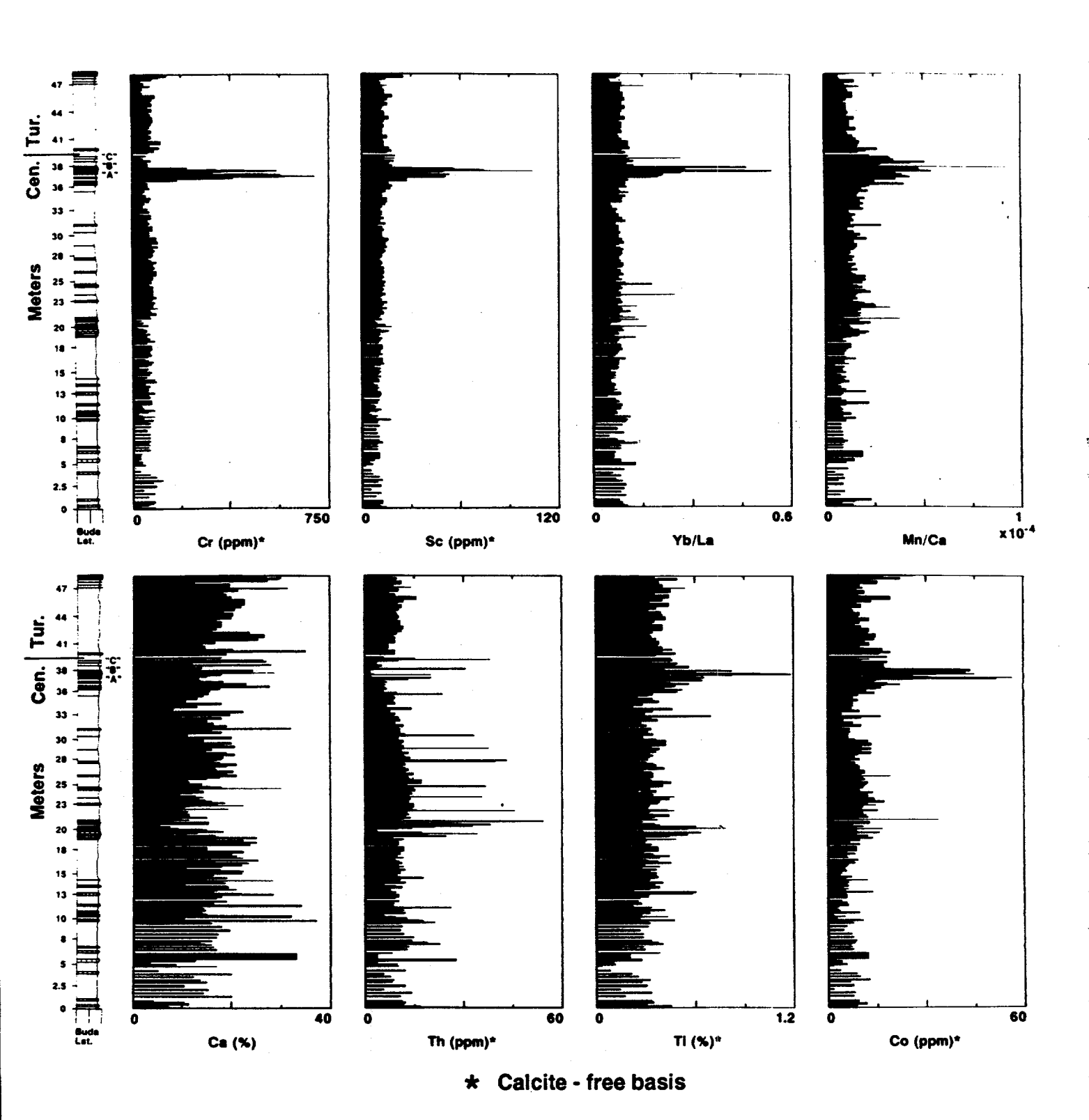


Fig. 2 Elemental abundances for the Chispa Summit measured section. Possible A, B and C volcanic ash beds of Elder (1989) are indicated, although this site is far to the south of established sequences. The Th peaks generally denote bentonitic beds from continental (silicic) volcanism. The Buda Limestone is late Early Cenomanian in age and is disconformably overlain by middle Cenomanian rocks of the Chispa Summit Formation. The section represents at least 2.5 Ma of deposition.

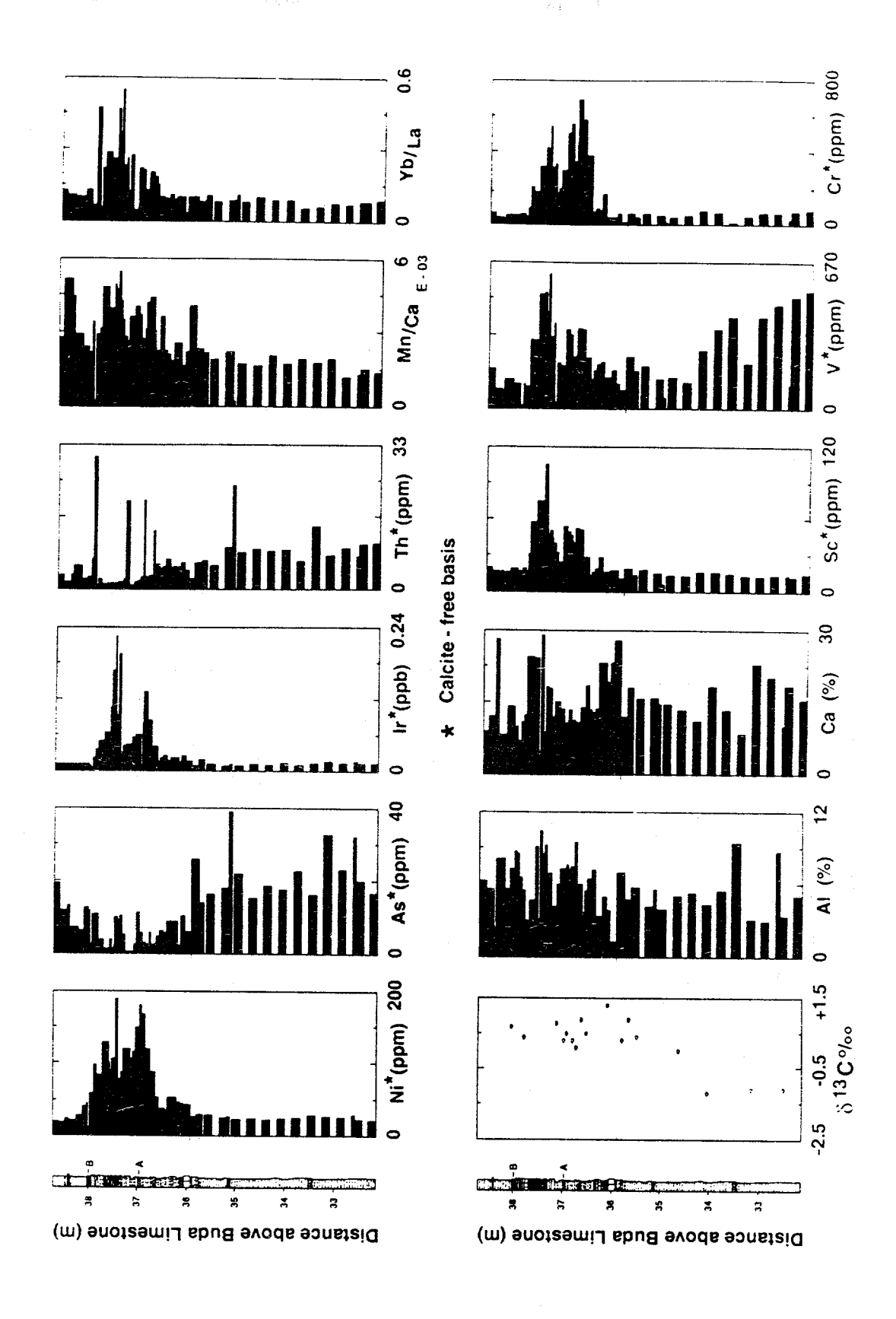
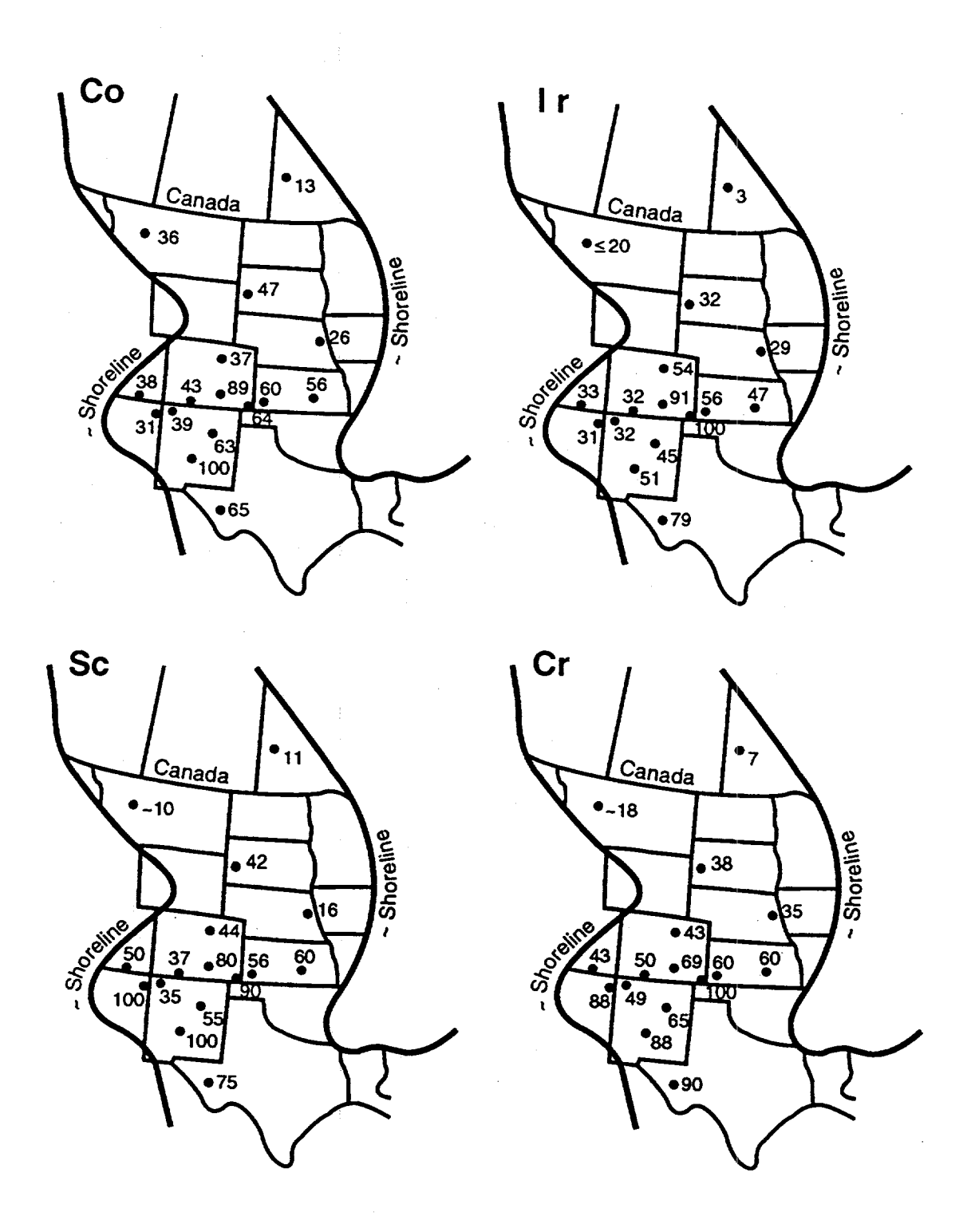


Fig. 3 Expanded view of the Chispa Summit section showing significant abundance and ratio patterns and δ ^{13}C data for calcaleous shales and marls.



~3

73

Fig. 4 Relative depositions of the Late Cenomanian elemental abundance peaks in Western Interior sections. The largest deposition (weight of element per unit area) is assigned a value of 100.

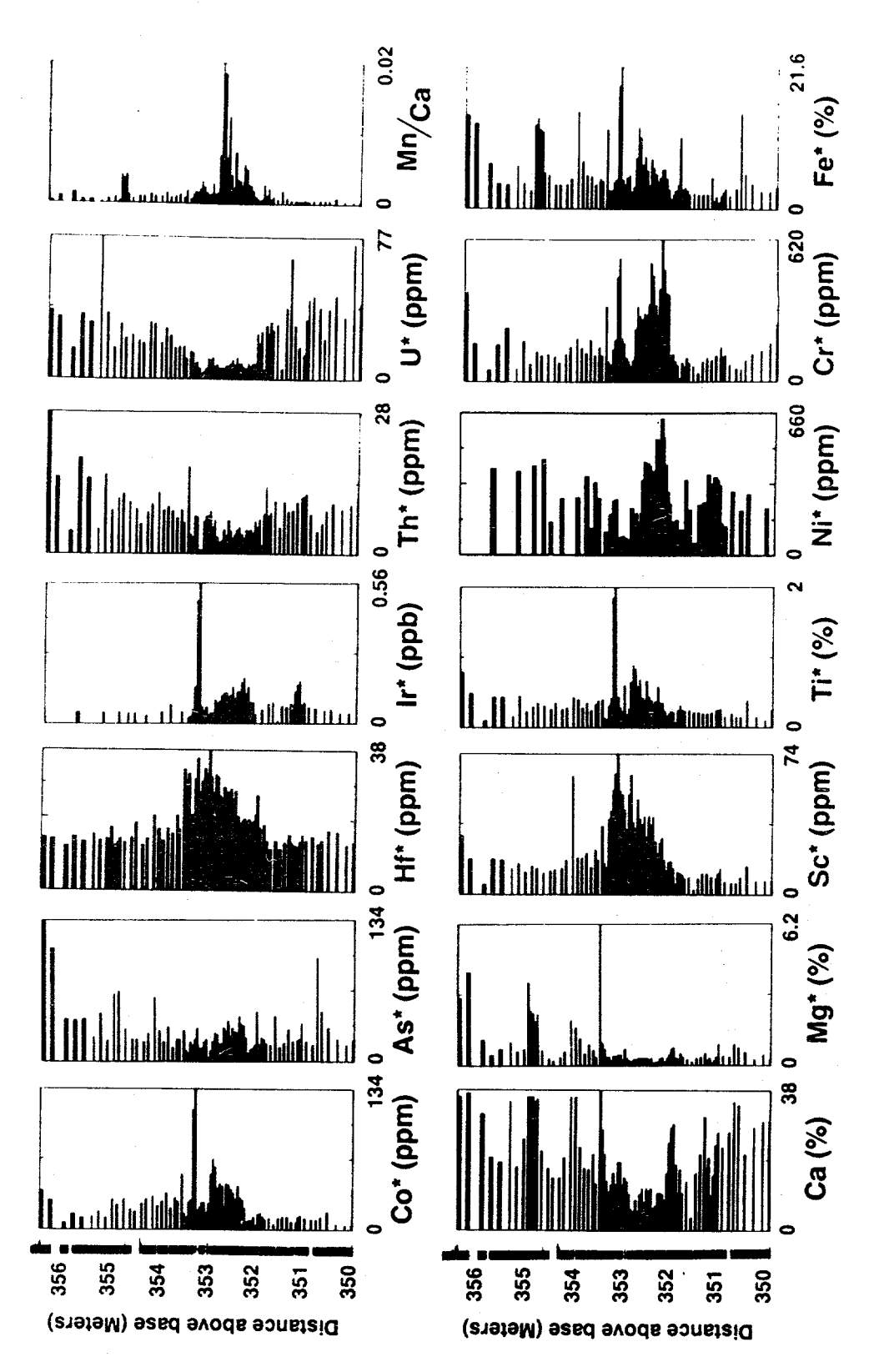


Fig. 5 Abundances and ratios for some significant elements in the Cenomanian-Turonian section near Chaparral, Colombia. The anomaly doublet, comparable to the one in North America lies between 352 and 353 meters. An extra peak, unique to this section, but similar in composition to the doublet lies at 353.4 meters. The lowest peak at 351.5 meters is probably the result of some local enrichment process. The Mg, Mn and Fe peaks near 355 meters are probably associated with a siderite phase.

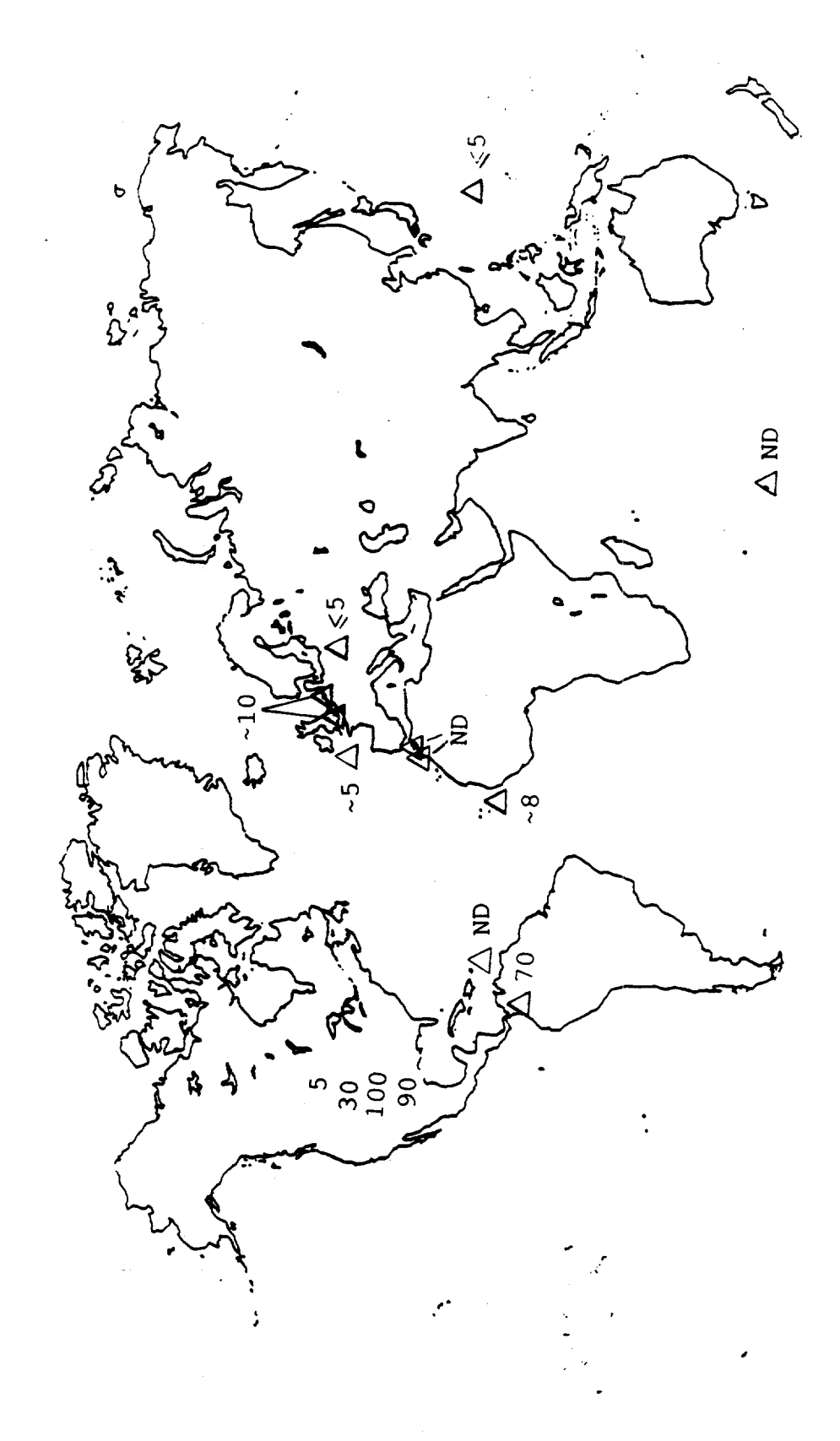


Fig. 6 Relative global distributions of the Late Cenomanian elemental anomalies. See Fig. 4 for details of the North American sites. ND: anomalies were not detected at these sites. Note that the larger depositions occur around the Caribbean and Gulf of Mexico region.



Fig. 7 Details of the K-T boundary in a well preserved section in the Raton Basin near Trinidad, Colorado. K: kaolinitic clay, ~2-cm thick, Ir: Ir-rich mixed smectite with shocked-quartz grains, ~ 3-mm thick. The K-T boundary is at the base of K.

Isotope Organic Geochemistry of the Animikie Basin (Minnesota)

T.A. Abrajano and B.D. Holt, Geoscience Group, Argonne National Laboratory, Argonne, IL 60439, USA

We present results of chemical and isotopic measurements performed on organic and carbonate carbon fractions of samples from the Proterozoic Animikie Basin (Minnesota), including the Biwabik Iron Formation. Pronounced microbanding in the Iron Formation results from alteration of siderite- and quartz-rich bands, the latter associated with slightly elevated total organic carbon (TOC) contents. This mineralogic microbanding is accompanied by isotopic microbanding; the average isotopic difference between adjacent bands are 5 % for organic carbon $\delta^{13}C$, 0.7 % for carbonate carbon $\delta^{13}C$ and 1.5 % for carbonate oxygen $\delta^{18}O$. Correlated variations in $\delta^{13}C$ and $\delta^{18}O$ in the carbonate fraction and $\delta^{13}C$ in the organic carbon fraction at larger scales (i.e. within drill cores and basin-wide) are also observed. We propose that the observed mineralogic, chemical, and isotopic patterns support a model for Banded Iron Formations origin that involves episodic mixing of waters in the sedimentary depositional environment. We have also determined TOC, total carbonate carbon (TCC), and δ^{13} C values from the Virginia and Biwabik Iron Formations that have been variably affected by the emplacement of the 1.1 by Duluth Intrusive Complex. Extensive decarbonation and limited remobilization of the organic carbon occurred within the thermal aureole of the intrusion, although the carbon isotopic compositions of the non-carbonate carbon appear to have been little affected by the metagenic alteration.

Outcrop and drill hole sampling was restricted to the northern rim of the Basin around the Mesabi Range (Figure 1). Samples from Lower Slaty and Lower Cherty Units of the Iron Formation have been dated at 2110 ± 52 Ma (Gerlach et al., 1988). The drill hole samples we examined were from the MDD-2, MDD-5 and MDD-7 holes of the Mesabi Deep Drilling Program (Pfleider et al., 1968) and from a commercial hole made available by Pickands Mather, Inc. Most outcrop samples were from open pit workings of Pickands Mather, Inc. in Aurora, Minnesota. One sample was selected for detailed isotopic analyses of the microbands. The specific sample was chosen because it is one of the least metamorphosed microbanded sample from our collection. A 3-cm cross-section of sample MDD 5-924 was sectioned to isolate the light and dark bands (Figure 2). At least nine major bands can be observed in the hand X-ray diffraction and optical microscopy revealed that the lighter bands are dominated by siderite (FeCO₃), whereas the darker bands are dominated by quartz (SiO₂). Both minerals are, however, present in both types of bands together with ubiquitous but trace amounts of dolomitic ankerite (Ca(Mg,Fe)(CO₃)₂), the latter apparently replaces siderite. diffraction analyses of demineralized (HF/HC1 dissolution) bulk samples also revealed the presence of amorphous kerogen and pyrite. Under the microscope, pyrite, kerogen and rare hematite grains are clearly associated with the quartz-rich bands and are responsible for the dark coloration. A total of 18 slices from the sample were analyzed.

Isotopic analyses followed procedures described previously (Abrajano et al. 1991). Briefly this procedure involved extraction of carbon and oxygen by reaction at 100 o with 100 per cent phosporic acid for the carbonate fraction (Rosenbaum and Sheppard, 1986) and bulk

combustion after repeated boiling HCl decarbonation of samples for the organic carbon fraction. The latter precaution was necessitated by the low levels of organic carbon in some samples. Isotopic measurements were made using a VG Prism isotope ratio mass spectrometer. All results are cast in standard delta notation $[\delta^{13}C_{*}=1000~(R_{*}/R_{PDB}-1)]$, where R represents the ratio $^{13}C/^{12}C$ and the subscripts s and PDB refers to sample and standard Pee Dee Belemnite, respectively; the $\delta^{18}O$ results are referenced to the $^{18}O/^{16}O$ of standard mean ocean water (SMOW)]. Fractionation factors used for correcting carbonate $\delta^{18}O$ measurements are from Rosenbaum and Sheppard (1986). Total carbonate and organic carbon were determined manometrically whereas chemical analyses of cations were performed by inductively coupled plasma atomic emission spectrometry after HF-aqua regia dissolution. X-ray diffraction analyses of some bulk samples were also performed.

Figure 3 summarizes the chemical and isotopic variations across sample MDD 5-924 (see Figure 2). The autocorrelation of Fe, Ca, Mn, and Mg reflects their common affinity for the carbonate-rich bands (Figure 3a-d). The Mg/Fe ratio was observed to be higher in the carbonate-rich bands than in the quartz-rich bands (Figure 3e). The Mg/Fe ratio also appears to increase systematically from the base of a quartz-rich band (e.g. band 5). The antithetic relation between total carbonate and total organic carbon (Figure 3f-g) confirms the microscopic observation already noted earlier. Distinct isotopic variations in carbonate carbon and oxygen across the bands are observed (Figure 3h-i). Carbonate-rich bands tend to be enriched in ¹³C and ¹⁸O relative to adjacent quartz-rich bands with an average difference of 0.7 per mil for δ^{13} C and 1.5 per mil for δ^{18} O. This autocorrelation between δ^{13} C and δ^{18} O was observed previously in microbanded BIF samples from the Hamersley Basin , where the average isotopic contrast between adjacent microbands is 3 per mil for δ^{13} C and 3.1 per mil for δ^{18} O . Figure 3j shows that δ^{13} C value of the organic carbon fraction is also autocorrelated to the δ^{13} C and δ^{18} O values of carbonates. This correlation has not been observed previously.

Figure 4 shows the variation of carbonate $\delta^{13}C$ and $\delta^{18}O$ and organic $\delta^{13}C$ in drill core MDD-5 as a function of depth. Autocorrelations similar to those noted between the microbands is also observed. In fact, analyses of all the drill core and outcrop samples reveal that the correlations among the same isotopic parameters occur on a regional scale (Figure 5). It appears that the thermal alteration associated with the emplacement of the Duluth intrusion represents only a minor perturbation to those isotopic relations. Nevertheless, variations in TCC and TOC close to the intrusion are observed (Figure 6), indicating that some decarbonation and organic matter remobilization must have occurred during metagenesis.

Baur et al. (1985) and Walker (1984) considered suboxic bacterial oxidation of organic matter during early diagenesis to be the primary source of 13 C- depleted carbon. Because of the autocorrelation observed between carbonate 12 C and abundance of magnetite, Baur et al. (1985) also suggested that the rhythmic pattern resulted from the dependence of the extent of 13 C-depleted CO₂ production, by in-situ bacterial oxidation, to the availability of Fe³⁺. Presumably, Fe³⁺ acted as the electron acceptor for the bacterial oxidation of organic matter (Walker, 1984; Baur et al., 1985). Although this mechanism would appear to account for the δ^{13} C pattern, no explanation has been presented for how the same process would result in a correlated δ^{13} C pattern, no explanation has been presented for how the same process would result in a correlated δ^{13} O pattern. It is noteworthy that the interbanding variations and autocorrelation of carbonate

 δ^{13} C and δ^{18} O values are both present in the Hamersley Basin and the Biwabik Iron Formation (Figure 3), although the mineralogy of the BIF in the two are quite different. In contrast to the samples analyzed by Baur et al. (1985) sample MDD 5-924 contains only trace amounts of iron oxides, yet interbanding variations of δ^{13} C and δ^{18} O (although smaller) are also observed.

The δ^{18} O value of carbonate is controlled by the δ^{18} O value of the coexisting water. The δ^{18} O value of carbonates is used extensively to determine the δ^{18} O value of the water it has last equilibrated with. In the scenario envisioned by Walker (1984) and Baur et al. (1985) where carbonate precipitation occurred below the sediment/water interface, the δ^{18} O value of the pore water would have controlled the δ^{18} O value of the carbonate. What controlled δ^{18} O variation in this pore water? If the site of in-situ bacterial oxidation proposed was shallower than about 100 meters, it is unlikely that the pore water δ^{18} O value could have been significantly different from that of the overlying water column. Deep burial diagenesis and low-temperature metamorphism are also unlikely to preserve these finer-scale isotopic variations. If diagenetic and post-diagenetic reactions were not responsible for the observed rhythmic δ^{18} O variations, processes that occurred within the water column must have been responsible. If such a mechanism can be found to explain the observed δ^{18} O rhythmic variation, can the same mechanism also account for the autocorrelated δ^{13} C variation?

The chemical and isotopic variations in BIF are most consistent with a model that involves episodic mixing between two reservoirs: resident sea water and external water. In this model, carbonate and silica precipitation occur in the water column at all times; the modal and compositional variations result primarily from the variable supply of solutes (Si, Fe, etc.) to the water column. Without input of external water, the chemical and isotopic makeup of this water column is determined by normal processes that occur in sedimentary basins. This chemical and isotopic makeup is perturbed by introduction of the external water, depending on the extent of mixing between the resident and external water. Whereas such mixing processes have commonly been proposed to explain BIF formation in general (e.g. Trendall and Blockley, 1970; Ewers and Morris, 1981; Garrels, 1987) our results indicate that specific isotopic characteristics not hitherto attributed to the mixing process are quite consistent with it. In our proposed model, the chemical and isotopic characteristics of the resident sea water and the external water are reflected by the characteristics of the carbonate- and quartz-rich bands, respectively.

An obvious contrast between the external water and the resident sea watar is the greater concentration of SiO₂ in the external water as reflected by the higher silica/carbonate ratio. A lower Mg/Fe ratio in the external water is indicated by the lower Mg/Fe ratio in the quartz-rich band. The external water is therefore more ferriferous than the resident sea water. A steady increase in the Mg/Fe ratio from the base of the quartz-rich band to the base of the next overlying quartz-rich band (Figure 3e) is suggestive of the preferential early incorporation of Fe in siderite and the consequent increase of Mg/Fe in the residual solution (Curtis et al., 1986; Longstaffe, 1987). The introduction of the next pulse of external water, marked by the appearance of the next quartz-rich band, appears to have truncated this gradual Mg/Fe variation.

The external water is more depleted in ¹⁸O and carries carbon that is more depleted in ¹³C than the resident sea water, and this difference is responsible for the rhythmic isotopic variation in the carbonates. In the model advocated here, the rhythmic variation results from

the episodic introduction of external water into a basin filled with the resident sea water. Although the resident sea water-dominated phase of carbonate precipitation cannot be assumed to tap an isotopic pool with normal (i.e. with respect to modern carbonates) 13 C/ 12 C and 18 O/ 16 O ratios, we arrive at the important conclusion that a significantly more 13 C- and 18 O-depleted pool is being provided by the external water. The autocorrelated variation in the δ^{13} C values of the organic and carbonate carbon fractions may reflect primary dependence of organic matter isotopic composition on the isotopic composition of the CO₂ substrate for carbon fixation (Hayes et al., 1989). This autocorrelation further support the suggestion that the observed rhythmic isotopic patterns were established by processes that occurred within the water column. The slight enhancement of total organic carbon content in the quartz-rich bands may also indicate that the influx of the external water is accompanied by enhanced biologic productivity.

The thermal effects of the Duluth intrusion on the Animikie Basin are most apparent very close to the intrusion. The mineralogical, TCC and TOC data, but not the isotope data, clearly manifest extensive volatile fluxes during the emplacement of the intrusive complex. The absence of carbon isotopic shifts, especially in the organic fraction, appears to indicate that labile organic components during metagenesis were isotopically similar to the residual kerogen.

References:

Abrajano, T. Jr. et al., Org. Geoch. 17, 477 (1991)
Baur M.E. et al., Econ. Geol., 80, 270 (1985)
Curtis, C.D. et al., Geochim. Cosmochim. Acta. 50, 2321 (1986)
Ewers W. E. and Morris, R.C., Econ. Geol. 76, 1929 (1981)
Garrels, R.M., Amer. Jour. Sci. 287, 81 (1987)
Gerlach, D.C. et al., EOS 69, 1515 (1988)
Hayes, J.M, et al., Geochim. Cosmochim. Acta 53, 2961 (1989)
Longstaffe, F.J., In Kyser T.K., Stable Isotope Geochemistry of Low Temperature Fluids (1987)
Rosenbaum, J. and Sheppard, S.M.F., Geochim. Cosmochim. Acta 50, 1147 (1986)
Trensdal, A. F. and Blockley, J.G., West Aust. Geol. Bull. 119, 336 (1970)
Walker, J.C.G., Nature, 309, 340.

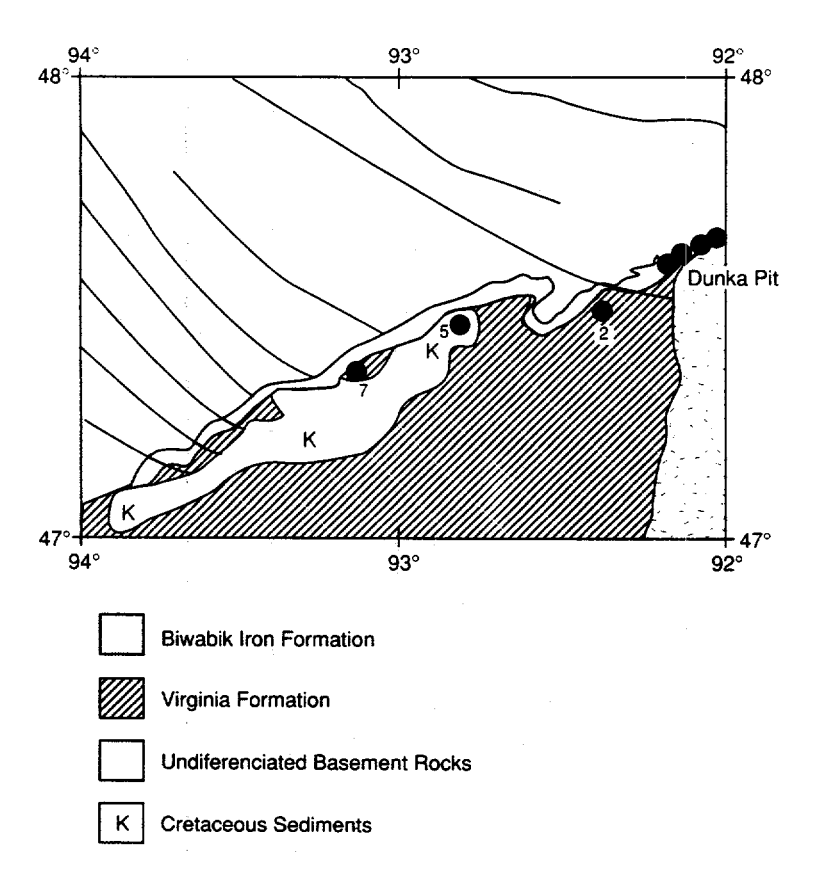


Figure 1. Schematic geological exposure map of the Animikie Basin (from Abrajano, et al., 1991). The disposition of the Duluth Complex in the eastern edge of the Basin is also shown. Filled circles are sampling locations.

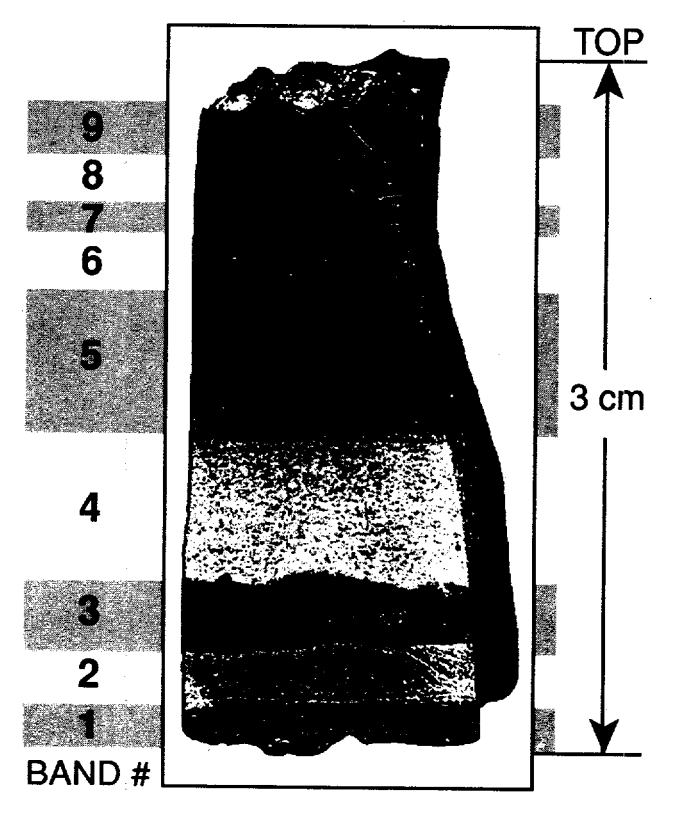


Figure 2. Photograph of microbanded sample MDD5-924. Numbers correspond to megascopically visible bands.

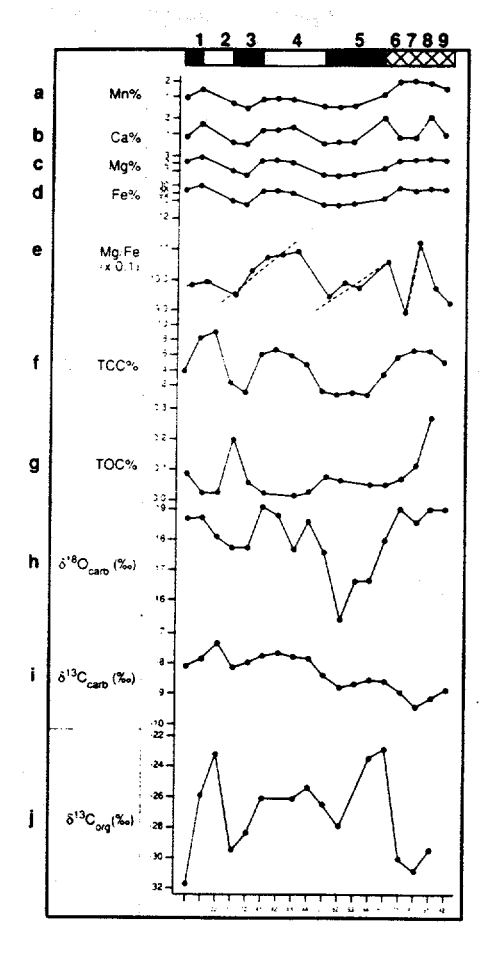


Figure 3. Chemical (wt. %) and isotopic (per mil) variations across sample MDD5-924. Band numbers correspond to those in Figure 2.

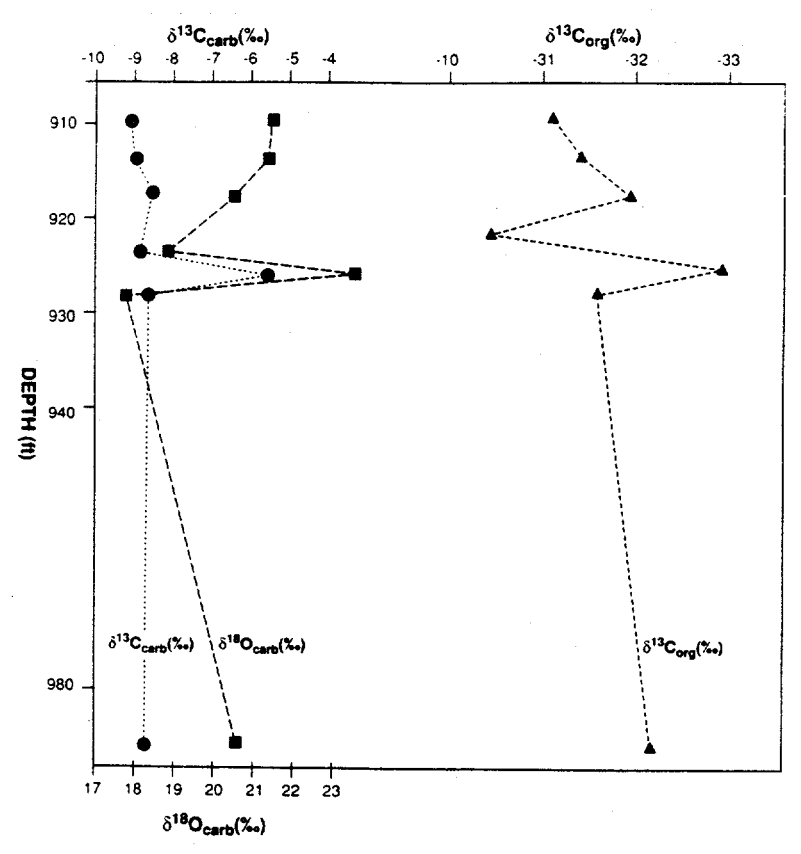


Figure 4. Variations of carbonate and organic isotopic composition with depth through the Intermediate Slate Unit in MDD5.

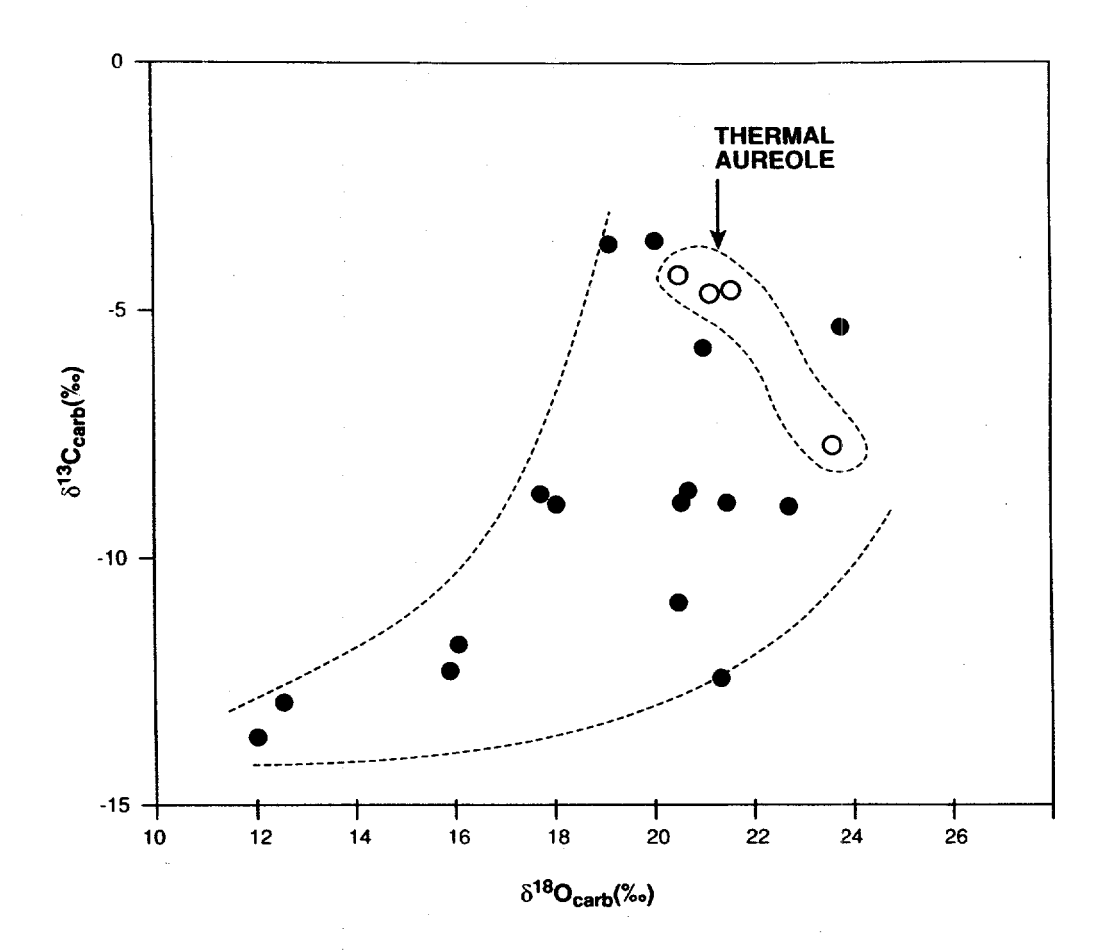


Figure 5. Regional variation in carbonate isotopic compositions. Open symbols are for samples taken from known thermal aureole of the Duluth Complex.

3.0

VIRGINIA FORMATION

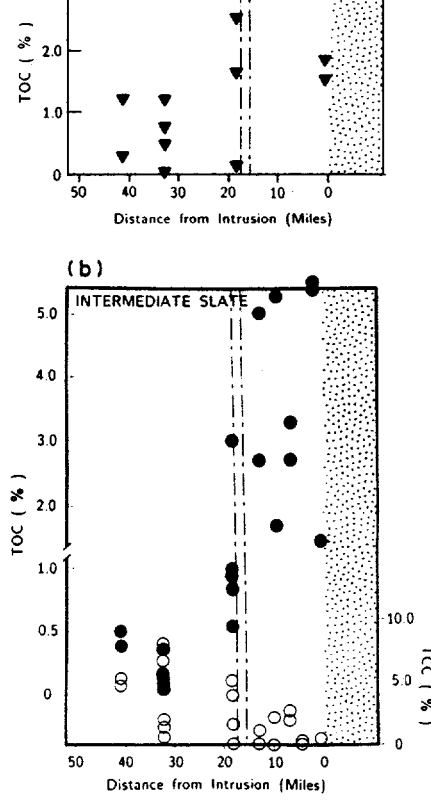


Figure 6. TOC and TCC variations as a function of distance from the Duluth Intrusion.

Organic Geochemical and Tectonic Evolution of the Midcontinent Rift System: Organic Geochemistry and Micropaleontology

J. M. Hayes and L. M. Pratt Biogeochemical Laboratories, Departments of Geological Sciences and Chemistry Indiana University, Bloomington, Indiana 47405

A. H. Knoll
Department of Earth and Planetary Sciences
Harvard University, Cambridge, Massachussetts 02139

Most organic geochemical studies of the middle Proterozoic Nonesuch Formation have focussed on petroleum seeps and stained shales from subsurface exposures in copper mines near White Pine, Michigan. Although *n*-alkanes, methyl alkanes, alkylcyclohexyl alkanes, and acyclic isoprenoids including pristane, phytane, and farnesane were found, sterane and triterpane molecular fossils were not identified in previous studies of mine samples. Recently, Imbus *et al.* (1988) utilized pyrolysis GCMS and stable-carbon-isotopic measurements to investigate core and outcrop samples of the Nonesuch from northern Wisconsin and Michigan. Pyrolysates contained predominantly *n*-alkanes and 1-alkenes with lesser amounts of alkyldienes, alkylbenzenes, phenol, methyl phenols, and diverse small polyaromatic compounds. Sterane and pentacyclic triterpane biomarkers were not identified in Nonesuch pyrolysates. The apparent absence of these polycyclic molecular fossils in the Nonesuch was problematical because the overall character of the Nonesuch petroleum, bitumen, and pyrolysates indicates only moderate thermal maturity (Imbus *et al.*, 1988; Hieshima and Pratt, in press), whereas older sedimentary rocks, in the McArthur Basin, Australia (1.4-1.7 Ga), contain both steranes and pentacyclic triterpanes (Summons *et al.*, 1988 a).

The purpose of this work was to search for steranes and pentacyclic triterpanes in extractable organic matter from unmineralized strata of the Nonesuch Formation using metastable-reaction-monitoring GCMS. This technique has substantially greater sensitivity (<0.1 ppm) than conventional GCMS (50 ppm). Additionally, greater potential for preservation of biomarker compounds is suggested for unmineralized Nonesuch strata that are of relatively lower thermal maturity than mineralized strata (Hieshima and Pratt, in press).

RESULTS

Overall hydrocarbon characterization: Extraction yields are low, ranging from 50 to 840 ppm and averaging 190 ppm of whole rock, and are not correlated with total organic carbon contents. The presence of phytane (I-20), pristane (I-19), norpristane (I-18), I-16, farnesane (I-15; Meinschein et al., 1964; Eglinton et al., 1964; Hoering, 1976) is confirmed by new analyses. Pristane to phytane ratios range from 1.33 to 5.42 and average around 2.68. Ratios of Pr/Ph, Pr/n-C₁₇, and Ph/n-C₁₈ are higher in samples from Michigan west of the White Pine Mine than in samples from Wisconsin further to the west. Variability in isoprenoid and isoprenoid/n-alkane ratios can be attributed to redox conditions of the depositional environment (Didyk et al., 1978), input from archaebacteria (Rowland, 1990), or preferential input of pristane precursors such as tocopherols (Goosens et al., 1984).

Pentacyclic triterpanes: Pentacyclic triterpanes were present in all extract samples from outside the White Pine Mine, ranging from 200 to 15,000 ng per mg of the saturated hydrocarbon fraction (ppm SAT) and averaging around 1,000 ppm SAT (Fig. 1). Compounds identified include extended hopanes (17 α (H), 21 β (H)), methyl hopanes, moretanes (17 β (H), 21 α (H)), and a pseudohomologuous series of rearranged 17 α hopanes (Moldowan, personal communication). Hopanes were the most abundant compounds, with the moretanes and rearranged hopanes secondary. Hopanes were present in extremely low concentrations in seep petroleums from the White

Pine Mine. In bitumens, hopanes were present as a pseudohomologous series from C₂₇ to C₃₅. In all samples from Michigan and in 3 of 7 samples from Wisconsin, the C₂₉ pseudohomologue was present in slightly greater concentration than the C₃₀. In 4 of 7 samples from Wisconsin, the C₃₀ homologue was the major hopane. C₃₁ to C₃₅ hopanes decreased in concentration with increasing carbon number. For C₃₁ hopanes, stereochemistry at C₂₂ is isomerized, with 22S/22S+22R ranging from 46 to 59% and averaging 54% in Wisconsin and 57% in Michigan, both close to the equilibrium value of 60% (Seifert and Moldowan, 1980).

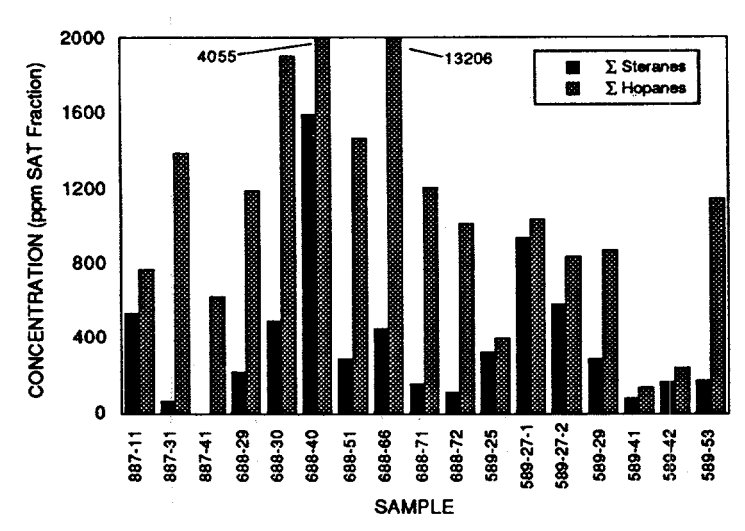


Figure 1. Histogram of concentrations of total steranes and pentacyclic triterpanes (hopanes). Concentrations of hopanes exceed those of steranes in most samples.

28,30 bisnorhopane and 29,30 bisnorhopane were detected in all samples, usually in concentrations less than 25 ppm SAT. Trisnorhopane and trisnorneohopane were present in highly variable concentrations ranging from 4 to 1650 ppm SAT but averaging around 100 ppm SAT. The trisnorhopane/trisnorneohopane ratio, proposed as a indicator of thermal maturity (Seifert and Moldowan, 1986), is highly variable, ranging from 0.06-1.51, suggesting source control. C_{31} methylhopanes were detected in 424 \rightarrow 205 MRM-chromatograms. 2-methyl and 3-methyl isomers were identified by retention time and were present in the majority of samples. In general, the 3-methyl isomer, ranging from 0 to 100 ppm SAT fraction, was present in greater concentration than the 2-methyl (0 to 18.5 ppm SAT fraction).

A series of compounds from C_{29} to C_{34} detected in MRM $M^+ \rightarrow 191$ chromatograms corresponds to rearranged 17 α hopanes recently identified by J. M. Moldowan (personal communication) and previously discussed by Summons *et al.* (1988a, b) as 18 α neohopanes. These compounds constituted between 0 and 108% of the concentration of the corresponding hopane and average between 10-30% depending on carbon number. No systematic geographic variation is apparent.

Steranes: Steranes were present in both seep petroleum from the White Pine Mine (Pratt et al., 1991) and in bitumens derived from unmineralized strata. Homologous series of C_{26} to C_{30} steranes were detected in $M^+ \rightarrow 217$ MRM chromatograms. Sterane concentrations range from 0-50% of the concentration of pentacyclic triterpanes and average about 25% (Fig. 1). Compound classes detected include $5\alpha(H)$, $14\alpha(H)$, $17\alpha(H)$ steranes, $5\alpha(H)$, $14\beta(H)$, $17\beta(H)$ steranes, and diasteranes. In unmineralized strata, C_{27} and C_{29} steranes dominated the $\alpha\alpha\alpha$ series with the C_{29} most abundant in virtually all samples. C_{27} and C_{29} $\alpha\alpha\alpha$ steranes range from <10 to 265 ppm SAT. C_{28} pseudohomologues are in general less than half as abundant as C_{27} or C_{29} compounds.

DISCUSSION

Thermal maturity of Nonesuch strata: The 20S/20S+20R ratio of C₂₉ steranes, a relatively robust indicator of thermal maturity in Phanerozoic strata (Mackenzie et al., 1980), ranges from 32 to 52% and averages around 40%. These values indicate a moderate level of thermal maturity within the zone of hydrocarbon generation and preservation. In Phanerozoic strata, the ratio equilibrates at 60% in very mature and overmature settings. The ratio of $\alpha\alpha\alpha/\alpha\alpha\alpha+\alpha\beta\beta$ C₂₉ sterane is another indicator of thermal maturity applied to Phanerozoic strata. In the Nonesuch Formation, this ratio ranges from 46 to 58% and is covariant with the sterane 20S/20S+20R ratio. The methylphenanthrene index (MPI) defined by Radke and Welte (1981; MPI = 1.5 x (2MP+3MP)/(P+1MP+9MP)) is another well documented indicator of thermal maturity based on transformations of aromatic compounds. MPI varies from 0.22 to 0.46 (average 0.32) and covaries with the sterane 20S/20S+20R ratio, confirming the moderate to low levels of thermal maturity for the Nonesuch Formation. Boreham et al. (1988) empirically derived a conversion from MPI-1 to vitrinite reflectance (Realculated = 0.7 * MPI + 0.22). The calculated vitrinite reflectance for Nonesuch strata is 0.44. This is a maximal value because the conversion is reported to overestimate Ro at MPI-1 values less than 0.7.

Overall, the thermal maturity of the Nonesuch Formation is interpreted to be low to moderate. Ratios of hopane (22S/22S+22R) and sterane (20S/20S+20R) stereoisomers suggest higher levels of thermal maturity than values of MPI-1. At very low temperatures, sterane and hopane stereoisomerization may occur more rapidly than changes in the distribution of phenanthrene and methylphenanthrene isomers. A plausible thermal history of the Nonesuch would involve rapid burial under the *circa* 4-km-thick package of sandstones of the upper Oronto and Bayfield groups (e.g., Daniels, 1982) where burial temperatures reached maximal values of around 100° C and the duration of burial was relatively short. Following erosional removal of most of the sandstones, the Nonesuch remained buried at shallow depths for nearly 1 billion years at temperatures below about 50°C.

Biological significance: The recognition of steranes and pentacyclic triterpanes (hopanes) in Nonesuch extracts establishes, respectively, eukaryotic and prokaryotic inputs to Nonesuch organic matter (e.g., Summons and Walter, 1991). The predominance of hopanes relative to steranes, however, suggests marked preferential preservation of bacterial remains. The ratio of steranes/steranes+hopanes is inversely proportional to the content of organic carbon in Nonesuch samples. This relationship is inferred to represent increasing bacterial contributions to Nonesuch sediments as increased productivity allowed greater microbial reworking of organic matter during early diagenesis.

In Nonesuch samples, moretane concentrations are correlated with hopane concentrations reflecting the origin of these compounds as alteration products of biological $17\beta(H)$, $21\beta(H)$ bacteriohopanols (Ensminger et al., 1974). Concentrations of the recently identified 17α diahopanes (Moldowan, personal communication), however, are not correlated with hopane concentrations. Therefore, diahopanes are interpreted to arise from a precursor other than $17\beta(H)$, $21\beta(H)$ bacteriohopanol. Diahopanes are not restricted to Proterozoic strata, but are present in significantly higher concentrations than in Phanerozoic strata (Summons et al., 1988a). The age-control on concentrations of these compounds suggests that lipid biochemistry has evolved significantly through time (Pratt et al., 1991).

Steranes in the Nonesuch are interpreted to be derived from eukaryotic sources, dominantly algae but possibly including heterotrophs (Summons and Walter, 1991). The C₃₀ steranes (24-n-propylcholestanes) recently have been reported to be indicators of marine organic matter and to be restricted to post-Ordovician strata (Moldowan et al., 1990). Failure to detect these compounds in Cambrian and Ordovician strata may reflect "hibernation" of the biosynthetic pathway for C₃₀ steroids. Although the marine affinity of C₃₀ steranes has not been established clearly for Proterozoic strata, the presence of this distinctive biomarker supports the interpretation of the

Nonesuch depositional environment as a marine embayment (Pratt et al., 1991; Hieshima and Pratt, in press) rather than a lacustrine basin.

The Nonesuch Formation provides a benchmark for the distribution of biomarkers around 1.1 Ga, because other organic-rich strata with preserved biological markers of this age have not been described. The Nonesuch Formation is bracketed by the 1.7-1.4 Ga McArthur Group, Australia (Summons et al., 1987a), and the 850 Ma Bitter Springs Formation, Australia (Hayes et al., 1991) and the 850 Ma Chuar Group, Arizona (Summons et al., 1987b). The paleobiological significance of biomarkers in these Middle and Late Proterozoic units has been summarized recently by Summons and Walter (1990). The distribution and variety of compounds in the Nonesuch Formation compares favorably with the composition of biomarkers in the older McArthur Group, characterized by predominance of C₂₉ steranes over other pseudohomologues, predominance of pentacyclic triterpanes over steranes, presence of monomethyl alkanes, and presence of significant concentrations of 17 α diahopanes (Summons et al., 1988b; Summons and Walter, 1990). Bitter Springs and Chuar strata contain similar suites of compounds but in different distributions including, in particular, sterane predominance over pentacyclic triterpanes and C₂₇ sterane predominance relative to other pseudohomologues (Summons and Walter, 1990). Chuar strata also contain gammacerane suggesting protozoan inputs to the sediments (Summons et al., 1988a).

REFERENCES

Barghoorn, E. S., W. G. Meinschein, and W. J. Schopf, Paleobiology of a Precambrian shale, *Science*, 148:461-472 (1965).

Boreham, C. J., I. H. Crick, and T. G. Powell, Alternative calibration of the Methylphenanthrene Index against vitrinite reflectance: Application to maturity measurements on oils and sediments, *Org. Geochem.*, 12:289-294 (1988).

Daniels, P. A., Jr., Upper Precambrian sedimentary rocks: Oronto Group, Michigan-Wisconsin, in *Geology and Tectonics of the Lake Superior Basin*, R. J. Wold and W. J. Hinze, eds., Geol. Soc. Amer. Memoir 156, pp. 107-133 (1982).

Didyk, B. M, B. R. T. Simoneit, S. C. Brassell, and G. Eglinton, Organic geochemical indicators of palaeoenvironmental conditions of sedimentation, *Nature*, 272:216-222 (1978).

Eglinton, G., P. M. Scott, T. Belsky, and M. Calvin, Hydrocarbons of biological origin from a one-billion-year-old sediment, *Science*, 145: 263-264 (1964).

Eglinton, G., P. M. Scott, T. Belsky, A. L. Burlingame, W. Richter, and M. Calvin, Occurrence of isoprenoid alkanes in a Precambrian sediment, In *Adv. in Org. Geochem.1964*, (eds. G. D. Hobson and M. C. Louis), Pergamon Press, Oxford, pp. 41-74.

Elmore, R. D., G. J. Milavec, S. W. Imbus, and M. H. Engel, The Precambrian Nonesuch Formation of the North American Mid-Continent Rift, sedimentology and organic geochemical aspects of lacustrine deposition, *Prec. Res.*, 43:191-214 (1989).

Ensminger, A., A. van Dorsselaer, Ch. Spyckerelle, and P. Albrecht, Pentacyclic triterpenes of the hopane type as ubiquitous geochemical markers: origin and significance, In *Adv. in Org, Geochem. 1973* (eds. B. Tissot and F. Bienner), Editions Technip, Paris, pp. 245-260 (1974).

B. Tissot and F. Bienner), Editions Technip, Paris, pp. 245-260 (1974).

Goosens, H., J. W. de Leeuw, P. Schenk, and S. C. Brassell, Tocopherols as likely precursors of pristane in ancient sediments and crude oils, *Nature*, 312:440-442 (1984).

Hayes, J. M., D. J. Des Marais, I. B. Lambert, J. Strauss, and R. E. Summons, Proterozoic
 Biogeochemistry, In *The Proterozoic Biosphere: A Multidisciplinary Approach*, J. W. Schopf and C. Klein, eds., Cambridge University Press, England (in press).

Hieshima, G. B. and L. M. Pratt, Sulfur/Carbon ratios and extractable organic matter of the Middle Proterozoic Nonesuch Formation, North American Midcontinent Rift, *Prec. Res.* (in press).

Hoering, T. C., Molecular fossils from the Precambrian Nonesuch Shale, Carnegie Institution of Washington Year Book, No. 75, pp. 806-813 (1976).

Hoering, T. C., Molecular fossils from the Precambrian Nonesuch Shale, In *Comparative Planetology* (ed. C. Ponnamperuma), pp. 243-255, Academic Press, New York (1978).

Imbus, S. W., M. H. Engel, R. D. Elmore, and J. E. Zumberge, The origin, distribution and hydrocarbon generation potential of organic-rich facies in the Nonesuch Formation, Central North American Rift system: a regional study, Adv. in Org. Geochem. 1987, Org. Geochem., 13: 207-219 (1988).

- Mackenzie, A. S., R. L. Patience, J. R. Maxwell, M. Vandenbroucke, and B. Durand, Molecular parameters of saturation in the Toarcian shales, Paris Basin, France. I. Changes in the configurations of acyclic isoprenoid alkanes, steranes, and triterpanes, *Geochim. Cosmochim. Acta*, 44:1709-1721 (1980).
- Meinschein, W. G., E. S. Barghoorn, and J. W. Schopf, Biological remains in a Precambrian sediment, *Science*, 145:262-263 (1964).
- Moldowan, J. M., F. J. Fago, C. Y. Lee, S. R. Jacobson, D. S. Watt, N. E. Slougui, A. Jeganathan, and D. C. Young, Sedimentary 24-n-propylcholestanes, molecular fossils diagnistic of marine algae, *Science*, 247: 309-312.
- Pratt, L. M., R. E. Summons, and G. B. Hieshima, Sterane and triterpane biomarkers in the Precambrian Nonesuch Formation, North American Midcontinent Rift, *Geochim. Cosmochim. Acta*, 55: 911-916 (1991).
- Radke, M. and D. H. Welte, The Methylphenanthrene Index (MPI): a maturity parameter based on aromatic hydrocarbons, In *Adv. in Org. Geochem. 1981* (ed. M Bjorøy et al.), Wiley, Chichester, pp. 504-512 (1983).
- Rowland, S. J., Production of acyclic isoprenoid hydrocarbons by laboratory maturation of methanogenic bacteria, Org. Geochem., 15:9-16 (1990).
- Seifert, W. K. and J. M. Moldowan, The effect of thermal stress on source-rock quality as measured by hopane stereochemistry, *In Adv. in Org. Geochem.* (ed.), Pergamon Press, Oxford, pp. 229-237 (1980).
- Seifert, W. K. and J. M. Moldowan, Use of biological markers in petroleum exploration, In *Biological Markers in the Sedimentary Record* (ed. R. B. Johns), pp. 261-290 (1986).
- Summons, R. E., Branched alkanes from ancient and modern sediments: isomer discrimination by GC/MS with multiple reaction monitoring, *Org. Geochem.*, 11: 281-290 (1987).
- Summons, R. E., S. C. Brassell, G. Eglinton, E. J. Evans, R. J. Horodyśki, N. Robinson, and D. M. Ward, Distinctive hydrocarbon biomarkers from fossiliferous sediment of the late Proterozoic Walcott Member, Chuar Group, Grand Canyon, U. S. A., *Geochim. Cosmochim. Acta*, 52: 2733-2736 (1988a).
- Summons, R. E., T. G. Powell, and C. J. Boreham, Petroleum geology and geochemistry of the Middle Proterozioc McArthur Basin, Northernm Australia. III Composition of extractable hydrocarbons, *Geochim. Cosmochim. Acta*, 52: 1747-1763 (1988b).
- Summons, R. E. and M. R. Walter, Molecular fossils and microfossils of prokaryotes and protists from Proterozoic sediments, *Amer. J. Sci.*, 290-A: 212-244 (1990).

AN ORGANIC GEOCHEMICAL STUDY OF CRUDE OILS AND SOURCE ROCKS IN THE ANADARKO BASIN, OKLAHOMA

R. P. Philp, Mahaboob Alam and Wang, Hua Di School of Geology and Geophysics University of Oklahoma, Norman, OK 73019-0628

(Submitted to DOE Workshop, November, 1991)

INTRODUCTION

The Anadarko Basin (Fig. 1) covering most of Western Oklahoma and the Texas Panhandle is the deepest sedimentary and structural basin in the cratonic interior of the United States (Johnson, 1989). The Anadarko basin, and adjacent shelf areas is one of the giant oil and gas producing provinces in North America. The sedimentary sequences started depositing during early Cambrian and ended up at the Permian (Fig. 2). The thickness of the sediment fill at north central Anadarko reaches up to 40,000 feet.

The science of organic geochemistry can be successfully used to reduce the risk associated with drilling in sedimentary basins and hence forms an integral part of all modern petroleum exploration programs. Although various aspects of the organic geochemistry of the basin have been studied over the past two decades, very few integrated studies have been undertaken to evaluate the petroleum geochemistry of the entire basin as a whole. The major aim of this study is to classify crude oils and source rocks from the Anadarko basin into genetically related families based on their geochemical characteristics. Distributions of different classes of biomarkers in both crude oils and rock extracts forms the basis of this study. Biomarkers are organic compounds whose carbon skeleton can be unambiguously related to a precursor molecule of biological origin (Philp, 1985).

CRUDE OILS

Sixty four crude oil and condensate samples ranging in reservoir age from Ordovician to Pennsylvanian have been studied (Fig. 1). In addition to the main basin area, few oil samples from the adjacent northern shelf were also included in the present study.

ROCK SAMPLES

In the Anadarko basin, oil and gas occurs in many sandstone and carbonate strata ranging in age from Ordovician to Permian. There are several organic rich formations which can qualify as source rocks (Johnson, 1989). Amongst them, Woodford shale of late Devonian to early Mississippian age is regarded as the most important source rock in the Anadarko basin (Johnson, 1989; Philp et al., 1989).

In two earlier studies Jones and Philp (1990) and Burruss and Hatch (1989) have shown that the compositions of the oils from the Anadarko basin are variable and there are multiple sources for these oils. Since the Woodford Shale is a well studied formation, the present study is aimed at evaluating possible source rocks other than the Woodford shale in the Anadarko

basin.

The major rock formations studied are as follows (Fig. 2):

- (1) Viola Group A grey to dark grey carbonate rock sequence of late Ordovician age. The formation is widely distributed all over the basin having an average thickness of about 500 feet. Twenty-five selected Viola rock samples have an average TOC value of 0.90% and the source potential can be considered as fair to good for carbonate rocks which requires comparatively lower TOC (<0.5%) to generate oil. High TOC values was recorded from the south eastern part of the basin.
- (2) Sylvan Shales- A grey to dark grey calcareous shale formation of late Ordovician age and in the subcrop section immediately overlies the Viola Formation. The Sylvan Shale is also widely distributed having an average thickness of 150 feet. Eleven selected Sylvan rock samples have an average TOC value of 0.50% and the source potential can be considered as poor.
- (3) Springer Formation- An interbedded black shale and sandstone sequence of late Mississippian to early Pennsylvanian age. The formation is restricted to the southern part of the basin. The average thickness, including the sandstones which accounts 50% of the total volume is about 500 feet thick. Twenty-seven selected Springer shale samples have an average TOC value of 2.13% and the source potential can be considered as very good.
- (4) Morrow Group- An interbedded black shale and sandstone formation of early Pennsylvanian age which unconformably overlies the Springer Formation. Twenty-seven selected Morrow shale samples have an average value of 1.17%. This formation is widely distributed over the basin having an average thickness of about 1000 feet (includes about 50% sandstones).

EXPERIMENTAL PROCEDURE

Total organic carbon (TOC) content was measured using a Leco carbon analyzer. Whole rock pyrolysis was undertaken using a PYRAN Level-I instrument. This equipment has a slightly different design than the Rock-Eval, although it gives similar parameters such as S_1 , S_2 and T_{max} which can be compared qualitatively with data obtained from Rock-Eval system. The rock samples were extracted with dichloromethane (DCM) using soxhlet extractor for forty eight hours. The details of the separation procedures and the analytical techniques involving GC, GC-MS and GC-MS/MS for both rock extracts and oil samples will be reported elsewhere. The general experimental procedure described in Jones and Philp (1990) was adapted in this study.

RESULTS AND DISCUSSION

Alkane distributions:

Gas chromatography of the saturate fractions revealed significant differences in composition of the oils. Fig. 3a to 3c shows the gas chromatograms for three oil samples from Ordovician, Pennsylvanian and Silurian/Devonian reservoirs. Oils produced from reservoirs of a given geologic age (or stratigraphic interval) are not compositionally similar in all the cases recorded by Burruss and Hatch (1989). Only two oils (Fig. 3a) have the characteristics of Ordovician oils found throughout the Midcontinent region. These oils are characterized by an odd carbon predominance in the C_{13} to C_{19} molecular weight range. The oils contain an unusually low amount of C_{20} + components, and very low abundance to complete absence of pristane and phytane. Reed et al. (1986) and Jacobson et al. (1988) concluded that organic-walled microfossil Gloeocapsamorpha prisca provided the unusual distribution of low molecular

weight n-alkanes and isoprenoids for most Ordovician oils. The remaining oil samples (Fig. 3b,c) shows a regularly decreasing n-alkane abundance with increasing carbon number with no odd-carbon predominance. The pristane/phytane ratio is usually more than unity and does not show any significant variation amongst the analyzed samples. However, it was observed that oils from the Pennsylvanian reservoirs has slightly higher pristane/ $n-C_{17}$ ratio (>0.6) compared to the Ordovician to Devonian reservoirs.

Fig. 4a to 4d shows the gas chromatograms of four rock extracts from Viola, Sylvan, Springer and Morrow Formations. The chromatograms of the Viola extracts (Fig. 4a) exhibit an abundance of low molecular weight n-alkanes with a broad distribution up to C₃₅. In contrast to this, the Sylvan (Fig. 4b) and Springer (Fig. 4c) extracts shows regularly decreasing n-alkane abundance with increasing carbon numbers. The Pennsylvanian Morrow Formation extracts (Fig. 4d) shows a bimodal distribution. The second maxima at C₂₅ to C₂₉ range suggest a dual lipid input from paralic depositional environments.

Terpane distribution:

The terpane distributions obtained by monitoring m/z 191 yielded the greatest amount of information for these oils. Fig. 5a to 5c shows the distribution of m/z 191 fragmentograms for three oil samples. On the basis of the terpane distribution the oils can be classified into three different groups. Group I (Fig. 5a) shows relatively low abundance of tricyclic terpanes up to C₃₀ and contains pentacyclic hopanes up to C₃₅. Contrary to this, Group II (Fig. 5b) shows a distribution of tricyclic terpanes up to C₃₆ in addition to various pentacyclic hopanes. The most characteristic is Group III (Fig. 5c) which contains a series of extended tricyclic terpanes from C₂₀ to at least C₄₁. These group has very little or no pentacyclic hopanes. The C₁₉ tricyclic terpane is present in low concentrations, if at all. It is noteworthy that the C₃₀ and higher homologues are in relative high abundance in Group III. The high molecular weight tricyclic terpanes have previously been recognized in a terpane concentrate prepared from a Californian oil and by metastable ion GC-MS analyses of the same sample (Moldowan et al. 1983). Kruge et al. (1989), reported the occurrences of extended tricyclic terpanes from C₂₀ to C₄₁ in the sediment extracts of Lower Jurassic synrift lacustrine black shales from the Hartford Basin, Connecticut.

It is interesting to note that in most of the cases, except two Pennsylvanian reservoirs, the Group I type oil is produced from the Ordovician to Devonian reservoirs and they are located almost exclusively in the eastern and south eastern corner of the basin. On the contrary, the Group III oils are restricted only to the Pennsylvanian reservoirs from the east central part of the basin (mainly Canadian, Caddo and Grady counties). Group II or mixed oils are mainly from the Pennsylvanian reservoirs. In few cases, the reservoirs of Ordovician to Devonian age also contain Group II oils but is restricted mainly to the northern shelf of the basin (Woods and Major counties).

Fig. 6a to 6d shows representative m/z 191 fragmentograms of the rock extracts. In Viola and Sylvan extracts (Fig. 6a,b) of Ordovician age the m/z 191 mass chromatograms are dominanted by the abundance of pentacyclic hopanes and the tricyclic terpanes, which occur up to C_{30} , have a relatively low abundance. Contrary to this, the Mississippian and Pennsylvanian Springer and Morrow rock extracts (Fig. 6c,d) shows a very high abundance of tricyclic terpanes in the range of C_{19} to C_{26} . However, none of the rock samples show the distribution of extendend tricyclic terpane series observed in the Pennsylvanian oils.

The tricyclic terpane series in the C₁₉ to C₂₉ range is commonly recognized in many rock

extract and oil samples. The origin of extended tricyclic terpane series particularly the C₃₀ and higher homologues is somewhat enigmatic. Aquino Neto *et al.* (1982) suggested a C₃₀ precursor for the C₁₉ to C₃₀ range, probably a tricyclic hexaprenol formed anaerobically from an universal cell constituent, the hexaprenol. Recently, De Grande *et al.*(1991) proposed that the extended series of tricyclic terpanes could be derived from polyprenol precursors with variable chain length such as C₃₅, C₄₀, C₄₅ and so on. The overall terpane distribution and occurrence of extended tricyclic terpane series and the absence of the hopanes in Group III oils from the Anadarko basin may be explained by (1) preferential depletion of hopanes due to long distance migration, (2) production of tricyclic terpane precursors by specific organisms favored by highly specific paleoenvironment of deposition, or (3) due to high thermal stress experienced by the samples.

Fractionation of migrating hydrocarbons, in a process similar to liquid chromatography in the laboratory may have preferentially depleted the pentacyclic hopanes in Group III oils. Migration simulation experiments conducted in the laboratory using an alumina column suggests that tricyclic terpanes and $5\alpha,14\beta,17\beta$ steranes elute faster than hopanes and $5\alpha,14\alpha,17\alpha$ steranes (Fan and Philp, 1987; Jiang et al.,1988). Keep it in mind that the Group III oils occur only in the Pennsylvanian reservoirs and migration has certainly occurred, as documented by the shallow reservoirs and regional geology. The Group III oils can be considered as an 'end-member' in composition which had migrated the furthest distance compared to mixed type Group II and Group I the other 'end-member' which had experienced very little migration certainly, documented by their association with the reservoirs of Ordovician to Devonian age.

However, for terpanes in source rocks under natural conditions, the situation may be different. They could be derived from unusual procaryotes favored by highly specific environmental conditions which may have synthesized tricyclic terpane precursors, the polyprenols. In a lacustrine environment of deposition the algal remains would include large polyprenols, which anaerobes might cyclize (Heisler et al., 1984) to form extended tricyclic terpanes. The high abundance of tricyclic terpanes in Springer and Morrow sediment extracts (Fig. 6c,d) also suggest that there may be some source dependence of this biomarker group.

It has been observed that thermal alteration of crude oil under laboratory conditions does increase the tricyclic to pentacyclic terpane ratio (Aquino Neto et al., 1983). It was noted in this study that the Group III oils are of a higher maturity level (to be reported elswhere) than the Group II and Group I oils. Thermal maturity may have resulted in preferential destruction of pentacyclic hopanes, leaving the more thermally stable tricyclic terpanes. However, thermal effects alone do not fully account for the lack of hopanes in Group III oils where all the steranes are preserved.

Sterane distribution:

Although sterane distributions in the Anadarko Basin oil samples were not particularly characteristic like the tricyclic terpane distribution, some evidence was obtained to substantiate the uniqueness of the marine input to these oils. These data were obtained using both GC-MS and GC-MS/MS analyses. Fig. 7a to 7c demonstrates the typical distribution of steranes (obtained by monitoring the m/z 217 ion) found in branched/cyclic fractions of Anadarko basin crude oils. Fig. 7d shows the partial chromatogram of the parent ion at m/z 414 which produce the daughter ion at m/z 217. The C_{30} steranes having molecular ion at m/z 414 are fragmenting to yield an intense ion at m/z 217, implying that the additional methyl group is on the side chain. The peaks labelled in Figure 7d have been tentatively identified as 24-n-propylcholestanes

by comparing the retention time and elution pattern to that of Moldowan *et al.* (1990). In a recent study, these authors have stated that C_{30} -propyl steranes originate from chrysophyte algae and thus imply that C_{30} sterane biomarkers in sedimentary rocks and crude oils have a marine origin.

Fig. 8a to 8d show the m/z 217 mass chromatograms of four rock extracts. The Viola and Sylvan extracts of Ordovician age are fairly similar, dominated by C_{29} steranes and minor amount of C_{27} diasteranes. The C_{30} propyl steranes are also present indicating marine source input. In contrast to this, the Springer and Morrow samples of Mississippian and Pennsylvanian age are dominated by C_{27} diasteranes consistent with their clay lithology compared to the Viola carbonates. The C_{29} steranes are not as abundant as this Viola and Sylvan extracts and small amounts of C_{30} steranes occur only in the Springer samples whilst in Morrow Formation they are not present.

One of the most significant features of the m/z 217 fragmentograms (Fig. 7a and 7b) is the high abundance of C_{29} steranes. Distribution of $5(\alpha)14(\alpha)17(\alpha)$ -(20R) steranes of C_{27} , C_{28} and C_{29} was thought to be source specific (Huang and Meinschein, 1976), considering the fact C_{27} $\alpha\alpha\alpha$ (20R) comes from an algal source and C_{29} $\alpha\alpha\alpha$ (20R) is a contribution from terrigenous input. The presence of C_{30} propyl steranes in oils derived from terrigenous source material is conflicting. It is becoming evident, however, that C_{29} steranes are not exclusive indicators of terrigenous organic input. In an earlier study on the Anadarko basin crude oils Jones and Philp (1990) suggested that caution should be taken in interpreting the terrigenous source input using C_{29} steranes.

Oil-source rock correlation:

The main target in the geochemical classification of oils is to determine the possible source rocks for the oils. Amongst the four group rock extracts the Viola and Sylvan samples shows a close similarity in both m/z 191 (Fig. 6a,6b and Fig. 5a) and 217 (Fig. 8a,8b and Fig. 7a,7b) mass chromatograms with that of Ordovician to Devonian oils from south eastern part of the basin. Despite the occurrence of additional peaks (Fig. 6a) in the branched/cyclic fraction, the Viola extracts shows the closest distribution with the Ordovician oils. The average Viola carbonates contain 0.9% TOC which can be regarded as a good source rock for the Group I oils reservoired in the south and south eastern part of the basin. In an earlier study on the Pauls valley area of the south eastern Anadarko basin Jones and Philp (1990) have proposed Viola Formation as source rock for those oils reservoired in the Viola Formation. Although the Springer and Morrow extracts have good source potential they do not correlate well with any of the oil groups. It was observed that the Springer and Morrow Formations have very high concentration of tricyclic terpanes in the range of C₁₉ to C₂₆ similar to Group III, Pennsylvanian oils. However, they lack the extended series of tricyclic terpanes which are common to Group III and III oils.

Source rock evaluation:

A semi-quantitative source potential evaluation of the analyzed rock samples has also been attempted. Structural maps and isopachs of sediment thickness were prepared using published geological data (Boler,1959; Jones,1959; Gibbons, 1960 and Bellis, 1961). The R_o (calculated vitrinite reflectance) equivalent maps were prepared using the equation $R_o = 0.32$ e $^{z/9580}$ (Schmoker, 1986). The percentage of shale or carbonate lithology was calculated for each data point and the source rock richness was estimated by summing up the S_1 and S_2 peak

obtained from pyrolysis experiment. Combining all the oil generation factors together, the petroleum potential index (PPI) of a rock unit can be defined as follows:

$$PPI = R \times T \times A \times S$$

where, R is the maturity factor, at 0.5% R_o, at the beginning of oil window the R value is 1 and at 1.3% R_o at the end of oil window the R value equals to 10. T is the thickness factor, a T value of 10 equals to 500 feet of sediment thickness. A is the richness factor, when a sum of S_1+S_2 is 200 it equals to a value of 10. S is the percentage of shale or carbonate present in the rock unit. Now considering all the factors together, if a rock unit has $R_o=1.3\%$, thickness=1000, $A(S_1+S_2)=300$ and S=100%. The PPI value for this rock unit can be calculated using the above equation as follows: PPI = 10 X 20 X 15 x 100 = 3000. PPI value is a relative parameter and can only be used for comparison with other rock units. High values indicates higher petroleum potential for the rock unit.

Fig. 9 and Fig. 10 shows the calculated PPI map for the Viola, Sylavan, Springer and Morrow Formations. The Viola Limestone (Fig. 9a) shows a very good petroleum source potential in the south eastern part of the basin consistent with its good correlation with the Group I oils. The Sylvan Shale (Fig. 9b) shows some potential in the eastern part of the basin but this formation has very poor source potential in the remaining areas. In contrast to this, the Morrow Formation (Fig. 10a) shows some source petroleum potential in the north western corner and in the south central part of the basin. However, the Springer Formation (Fig. 10b) of Mississippian age shows good source potential only in the south eastern part of the basin.

CONCLUSIONS

- (1) Anadarko Basin oils can be classified into three groups on the basis of terpane distribution (i) Group I, those occurring in the eastern and south eastern corner of the basin mainly in the Ordovician to Devonian reservoirs, (ii) Group II, those occurring in the Ordovician to Pennsylvanian reservoirs mainly in the western and northern part of the basin, and (iii) Group III oils, occurring exclusively in the Pennsylvanian reservoirs in the east central part of the basin.
- (2) The Group I oils occurring in Ordovician to Devonian reservoirs in the eastern and south eastern part of the basin most probably generated from Viola Limestone with a possible contribution from other Ordovician or older source rocks.
- (3) Although the exact origin of tricyclic terpane is not clearly understood it could be used as a correlation as well as migration parameter for these oils.
- (4) The occurrence of C_{30} -propyl steranes which are indicative of marine organic input in apparently C_{29} rich crude oils suggest that caution be used in interpretation of terrigenous input based on the presence of C_{29} steranes.
- (5) It is evident that in addition to Woodford Shale, multiple source rock units such as Viola Limestone and Springer Formation has generated and contributed to the oils reservoired in the Anadarko basin.

REFERENCES

- Aquino Neto F.R., Restle A., Connan J., Albrecht P. and Ourisson G. (1982) Novel tricyclic terpanes (C₁₉, C₂₀ in sediments and petroleums. Tetrahedon Letters, 23, 2027-2030.
- Aquino Neto F.R., Trendel J.M., Restle A., Connan J. and Albrecht P. (1983) Occurrence and formation of tricyclic and tetracyclic terpanes in sediments and petroleums. In: Advances in Organic Geochemistry (Edited by M.Bjoroy et al.), pp 659-667, Wiley & Sons, London.
- Bellis W.H. (1961) Distribution and thickness of Pre-Desmoinesian rock units in South-central Oklahoma. Master's Thesis, Univ. of Oklahoma, 39p.
- Boler M.E. (1959) Pre-Desmoinesian isopach and paleogeologic study of north-western Oklahoma. Master's Thesis, Univ. of Oklahoma, 53p.
- Burruss R.C. and Hatch J.R. (1989) Geochemistry of oils and hydrocarbon source rocks, greater Anadarko basin: evidence for multiple sources of oils and long-distance oil migration. In: Oklahoma Geological Survey Circular, 90, 53-64.
- De Grande S.M.B., Aquino Neto F.R. and Mello M.R. (1991) Extended tricyclic triterpanes in sediments and petroleums. 15th Int. Meeting on Org. Geochem, Manchester, Psoter abstracts, 181-183.
- Fan Z. and Philp R.P. (1987) Laboratory biomarker fractionations and implications for migration studies. Org. Geochem., 11, 169-175.
- Gibbons K.E. (1960) Pennsylvanian of the north-flank of the Anadako Basin, Master's Thesis, Univ. of Oklahoma, 46p.
- Heissler D., Ocampo R., Albrecht P., Riehl J.J. and Ourisson G. (1984) Identification of long-chain tricyclic terpane hydrocarbons (C₂₀-C₃₀) in geological samples. J. Chem. Soc., Chem. Commun., 496-498.
- Huang W. and Meinschein W.G. (1976) Sterols as source indicators of organic materials in sediments. Geochim. Cosmochim. Acta 40, 323-330.
- Jacobson S.R., Hatch J.R., Teerman S.C. and Askin R.A. (1988) Middle Ordovician organic matter assemblages and their effect on Ordovician-derived oils. AAPG Bull.,72,1090-1100.
- Jiang Z., Philp R.P. and Lewis C.A. (1988) Fractionation of biological markers in crude oils during migration and the effects on correlation and maturation parameters. Org. Geochem., 13,561-571.
- Jones P.J. and Philp R.P. (1990) Oils and source rocks from Pauls Valley, Anadarko Basin,

- Oklahoma, U.S.A. Applied Geochem., 5, 429-448.
- Jones C.L.Jr. (1959) An isopach, structural and paleogeologic study of Pre-Desmoinesian units in North Central Oklahoma, Master's Thesis, univ. of Oklahoma, 81p.
- Kruge M.A., Hubert J.F., Akes R.J. and Meriney P.E. (1989) Extended tricyclic terpanes: melecular markers in Lower Jurassic synrift lacustrine black mudstones of the Hartford Basin, Connecticut. AAPG Bull., 73, 375.
- Kruge M.A., Hubert J.F., Akes R.J. and Meriney P.E. (1990) Biological markers in Lower Jurassic synrift lacustrine black shales, Hartford Basin, Connecticut, U.S.A., Org. Geochem., 15, 281-289.
- Moldowan J.M., Seifert W.K. and Gallegos E.J. (1983) Identification of an extended series of tricyclic terpanes in petroleum. Geochim. Cosmochim. Acta 47, 1431-1534.
- Moldowan J.M., Fago F.J., Lee C.Y., Jacobson S.R., Watt D.S., Slougui N.E., Jeganathan A. and Young D.C. (1990) Sedimentary 24-n-propylcholestanes, Molecular fossils diagonostic of marine algae. Science, 247, 309-312.
- Philp R.P., Jones P.J., Michael G.H. and Lewis A.C. (1988) An organic geochemical study of oils, source rocks, and tar sands in the Ardmore and Anadarko Basin. Anadarko Basin Symposium, 1988, OGS Circular 90,3-12,65-76.
- Philp R.P. (1985) Fossil Fuel Biomarkers, Application and Spectra, Elsevier.
- Reed J.D., Illich H.A. and Horsfield B. (1986) Biochemical evolutionary significance of Ordovician oils and their sources. Org. Geochem., 10, 347-358.
- Schmoker J.W. (1986) Oil generation in the Anadarko Basin, Oklahoma and Texas: Modeling using Lopatin's method. Oklahoma Geological Survey special publication, 86-3.

Table 1. identification of steranes present in the Anadarko Basin crude oils based on Jones and Philp (1990) and Moldowan *et al.* (1990)

Peak No.	Compound			
1	13β , 17α - diacholestane (20S)			
2	13β , 17α - diacholestane (20R)			
3	$13\alpha,17\beta$ - diacholestane (20S)			
4	$13\alpha,17\beta$ - diacholestane (20R)			
5	24-methyl-13 β ,17 α - diacholestane (20S)			
6	24-methyl-13 β ,17 α - diacholestane (20R)			
7	24-methyl- 13α , 17β - diacholestane (20S)			
	+ 14α - cholestane (20S)			
8	24-ethyl-13 β ,17 α -diacholestane (20S)			
	+ 14β , 17β - cholestane (20R)			
9	14β , 17β -cholestane (20S)			
	+ 24-methyl- 13α , 17β - diacholestane (20R)			
10	14α , 17α - cholestane (20R)			
11	24-ethyl-13 β ,17 α - diacholestane (20R)			
12	24-ethyl-13 α ,17 β - diacholestane (20S)			
13	24-methyl-14 α , 17 α - cholestane (20S)			
14	24-ethyl-13 α ,17 β - diacholestane (20R)			
	+ 24-methyl-14 β ,17 β - cholestane (20R)			
15	24-methyl-14 β ,17 β - cholestane (20S)			
16	24-methyl-14 α , 17 α - cholestane (20R)			
17	24-ethyl-14 α , 17 α - cholestane (20S)			
18	24-ethyl-14 β ,17 β - cholestane (20R)			
19	24-ethyl-14 β ,17 β - cholestane (20S)			
20	24-ethyl-14 α ,17 α - cholestane (20R)			
21	24-propyl-14 α , 17 α - cholestane (20S)			
22	24-propyl-14 β ,17 β - cholestane (20R)			
23	24-propyl-14 β ,17 β - cholestane (20S)			
24	24-propyl-14 α ,17 α - cholestane (20R)			

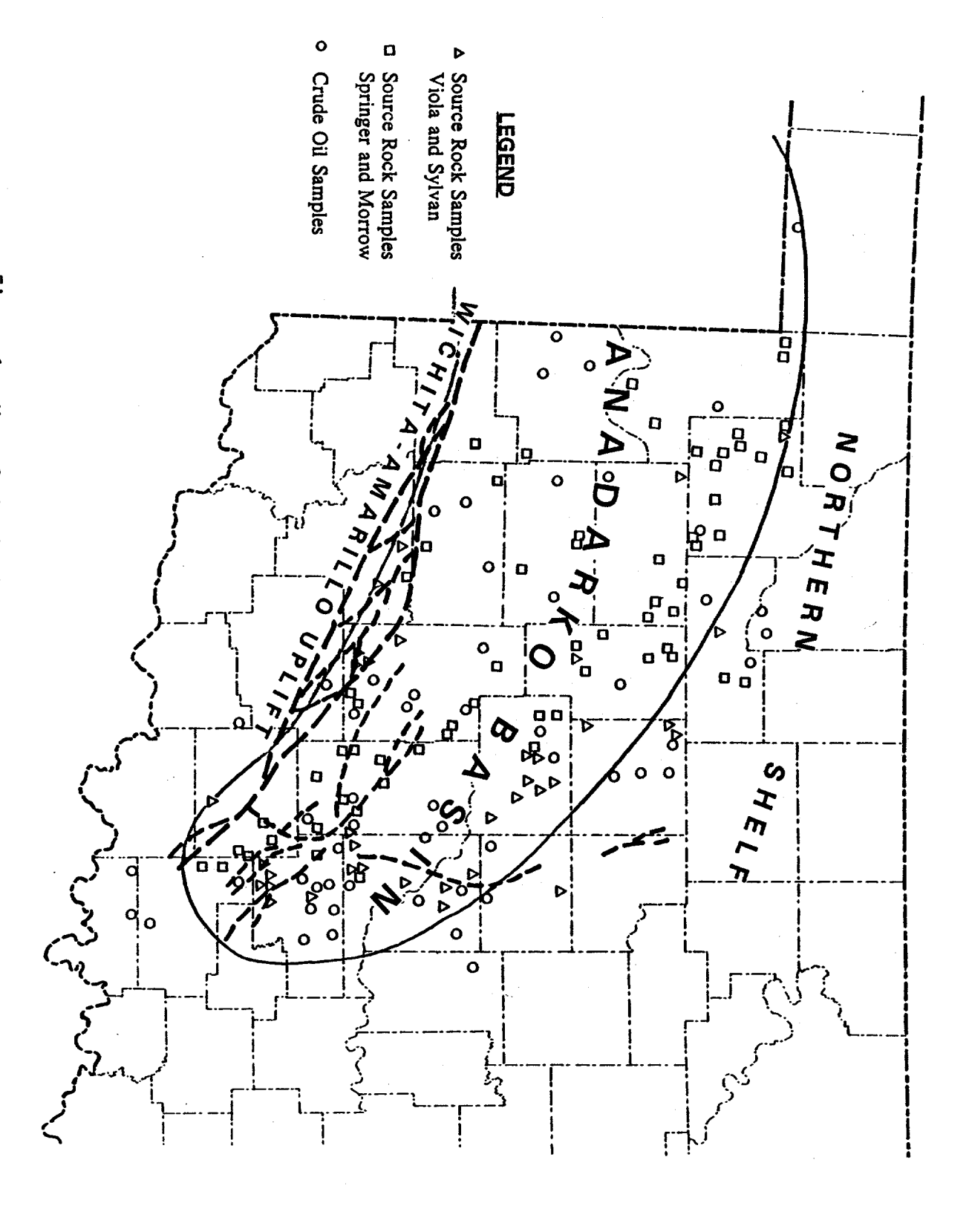


Figure 1. Map of the Anadarko Basin, showing the locations of oil and rock samples.

	GENERALIZED STRATIGRAPHIC COLUMN FOR ANADARKO BASIN								
878 TEL		S. MIC.S.	LITH-	, , , , , , , , ,	ATION KER BED	POTENTIAL RESERVOIR TYPE			
a E	19	:		H CLINTON LAN E S 13 FINGER LM	UPPER DORNICX	Atobe - Herrow - Springer offshere ber sendslence in cast, Produminantly			
	MORROM			UPPER MORROW "SQUAW BELL" SS." LOWER MORROW	MORROW	anter-truncation frapa associated with Seringer Uncenformitys also stratigraphic and updip plachaut trups. Multiple thin channel and tenticular bar sendstanes in west, Chart facies important in Texas Panhandle.			
	ERAN	1		:	PRIMROSE	Sheer sandstones			
N A	SPRINGERAN			SPRINGER	CUMMINGHAM BRITT SPIERS	in west with peroperm verietien end updep pinchoud trape Occesional tenticular carbonate reservoirs.			
SISSIPPI	CHESTERIAN			LOWER CHESTER LM.	SOATWRIGHT CANEY SHALE				
S I W	************			STE GENEVIEVE ST. LOUIS SPENSEN- WARSON	MAYES	Occasional carbonale reservous.			
	1 2 2	L		OSAGE EMBERHOOK SM	SYCAMORE				
SILURIAN		HUNTON		WOODFORD BOIS d'ARC HEMTHOUSE HARAGAN CHIMNEY HILL		Predominately delamite reservoirs with peraperm variations and fracture peresity in structural trape. Sub-unconformity traps			
CIAN	NAI		VIOLA L			in seet. Occesionet limestone reservoirs.			
ORDOVICIAN	CHAMPL AINIAN	SIMP SON		SIMPSON DOL. SIMPSON SO.	BROMIDE MeLISH OIL CREEK JOINS	Occasional sandstono reservoirs in Mountain Front area,			
		1		ARBUCKLE (ELLENBURGER)		Carbonete reservoirs usually in structural traps.			

Figure 2. Generalized stratigraphic column for Early to Middle Paleozoic rocks in the Anadarko Basin.

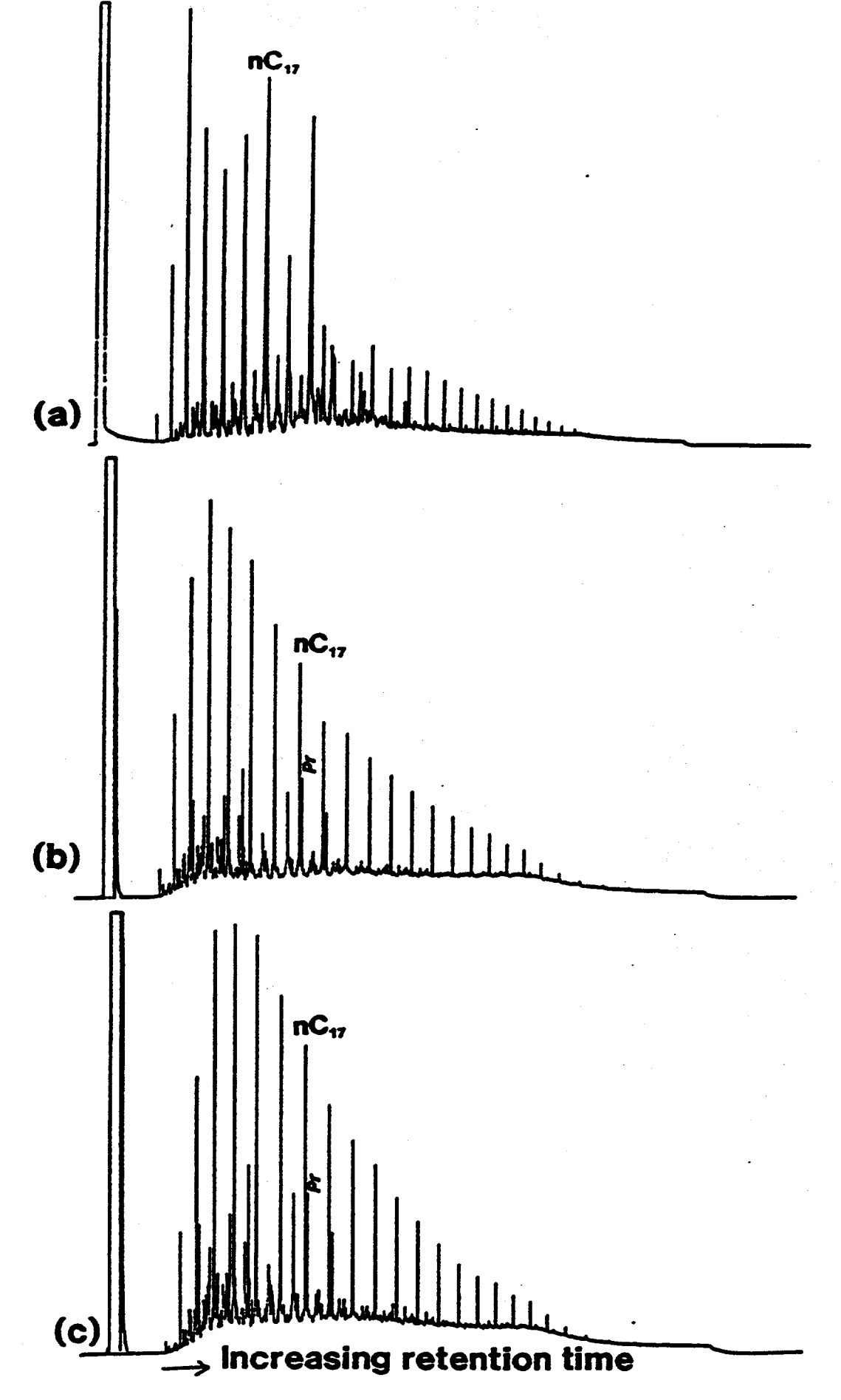


Figure 3. Representative gas chromatograms of saturated hydrocarbon fractions (a) Ordovician reservoir, (b) Pennsylvanian reservoir, (c) Silurian/Devonian reservoirs.

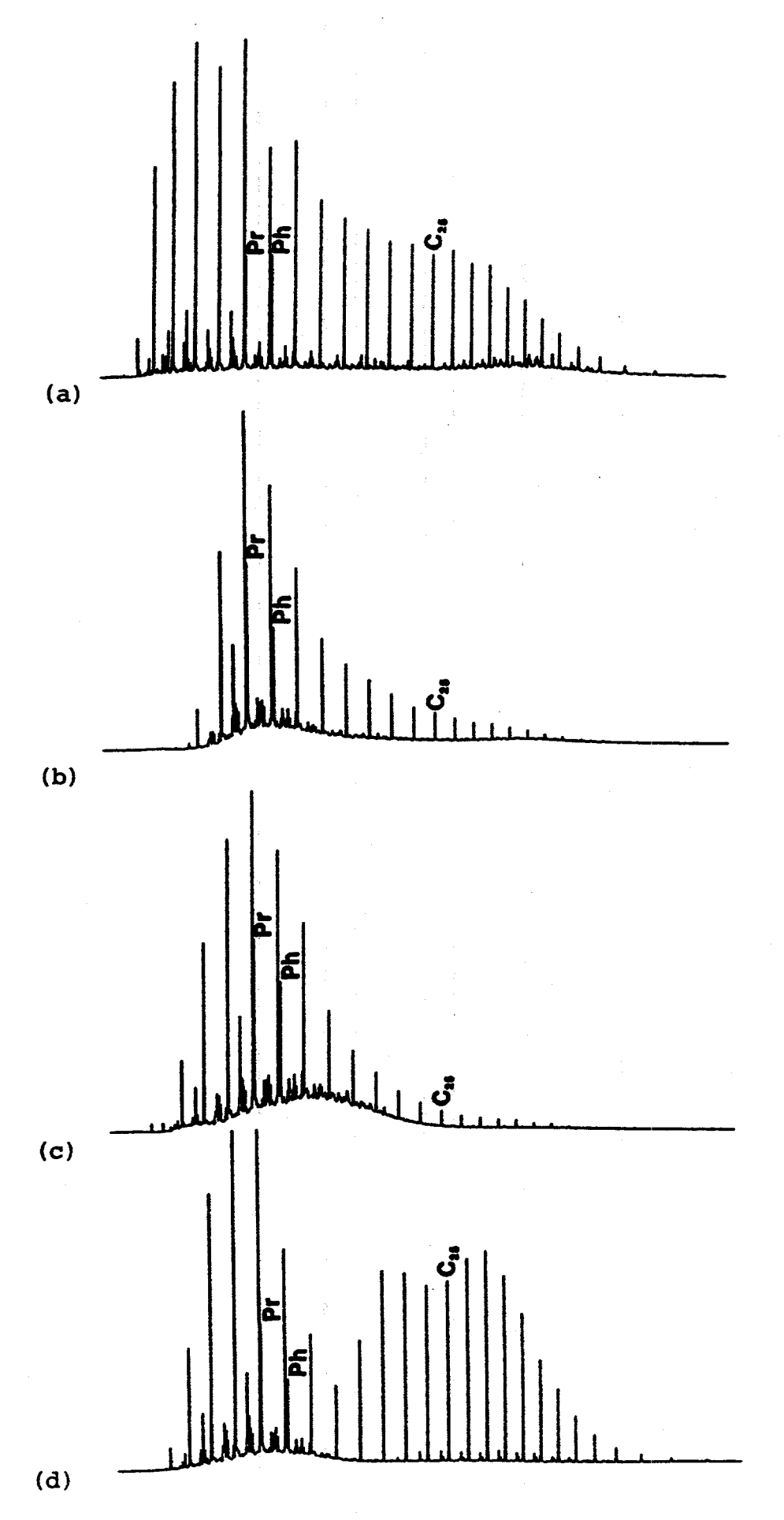


Figure 4. Representative gas chromatograms of saturated hydrocarbon fractions (a) Viola Limestone, (b) Sylvan Shale, (c) Springer Formation (d) Morrow Formation.

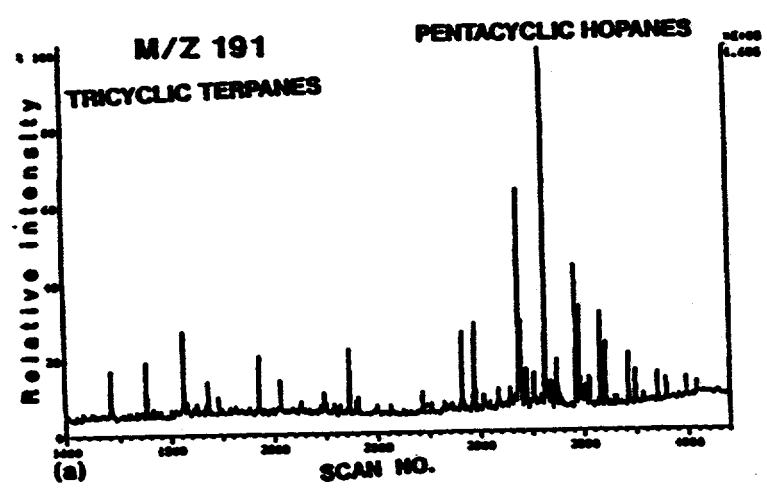


Fig. 5a. Typical distribution of terpanes (Group I) found in branched/cyclic fractions of Ordovician to Devonian oils from eastern and south eastern part of the Anadarko basin.

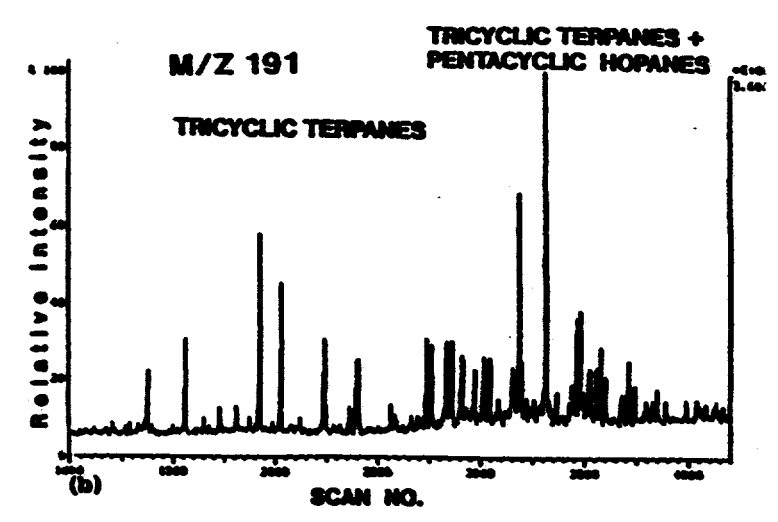


Fig. 5b. Terpane distribution of mixed tricyclic and pentacyclic types (GroupII found in branched/cyclic fractions of Devonian to Pennsylvanian oils.

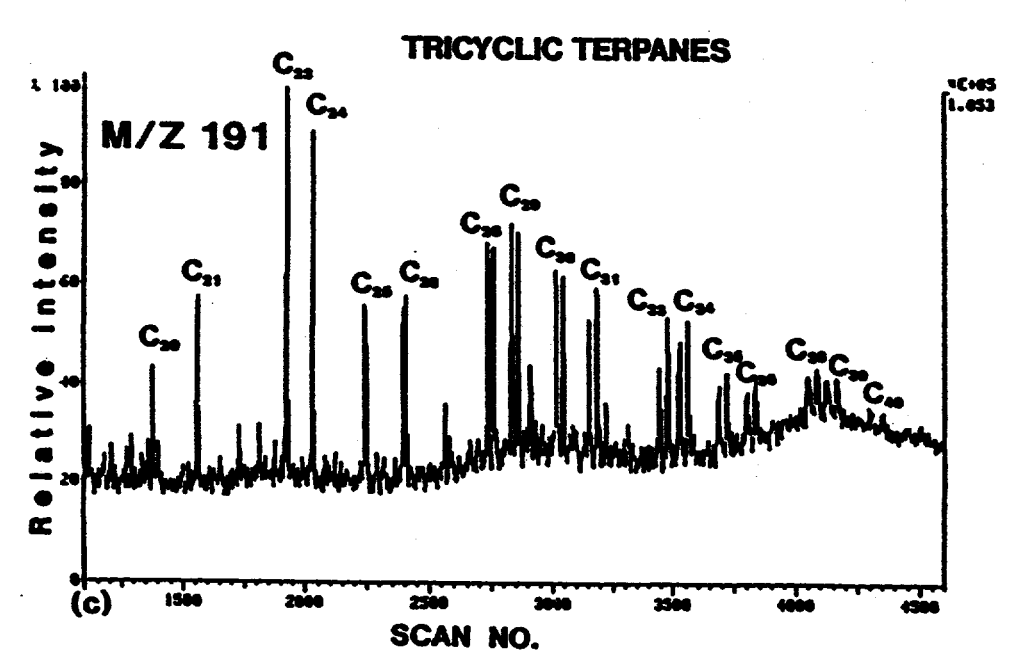


Fig. 5c. Characteristic distribution of extended tricyclic terpane series (Group III) found in branched/cyclic fractions of Pennsylvanian oils from East central part of the Anadarko basin.

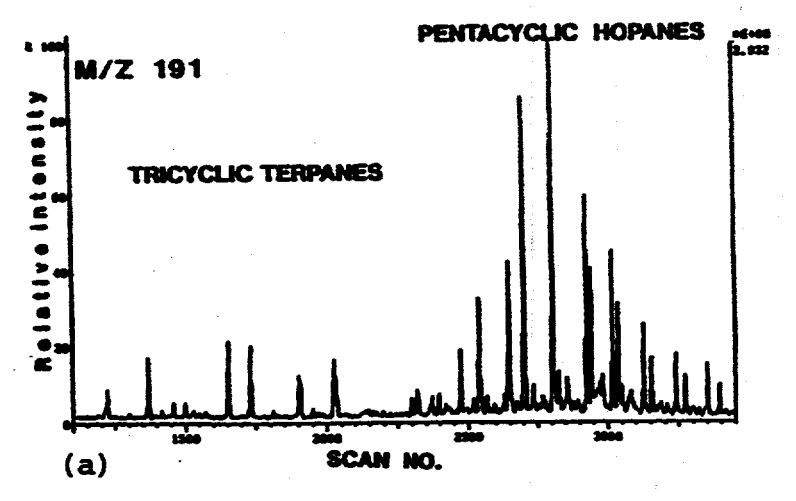


Fig. 6a. Typical distribution of terpanes found in the branched/ cyclic fractions of Viola Group extracts from south eastern part of the basin.

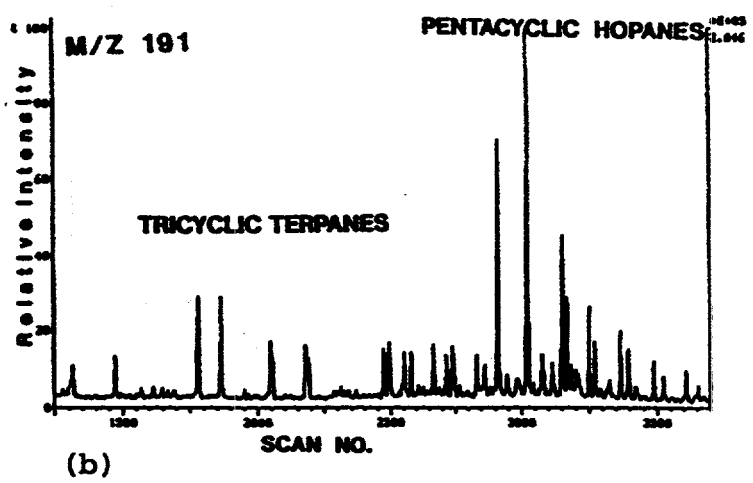


Fig. 6b. Typical distribution of terpanes found in the branched/cyclic fractions of Sylvan Shale from south eastern part of the basin.

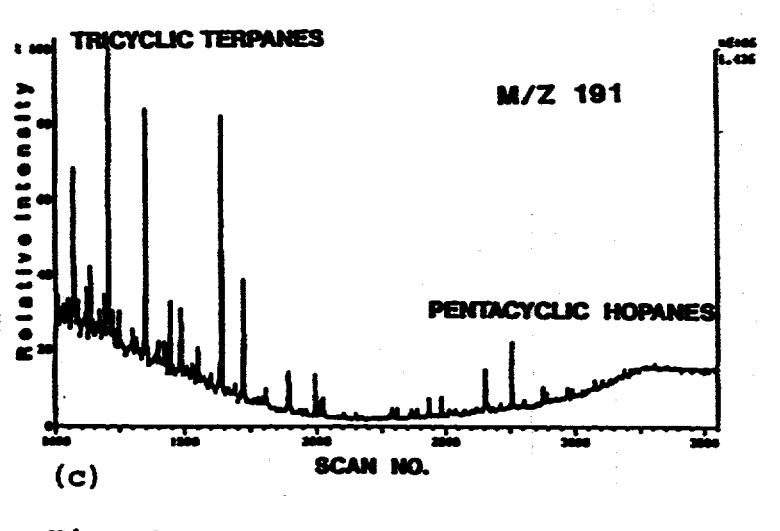


Fig. 6c. Typical terpane distribution, dominated by tricyclic terpanes up to $^{\rm C}_{26}$ found in the saturate fractions of Springer Formation extracts.

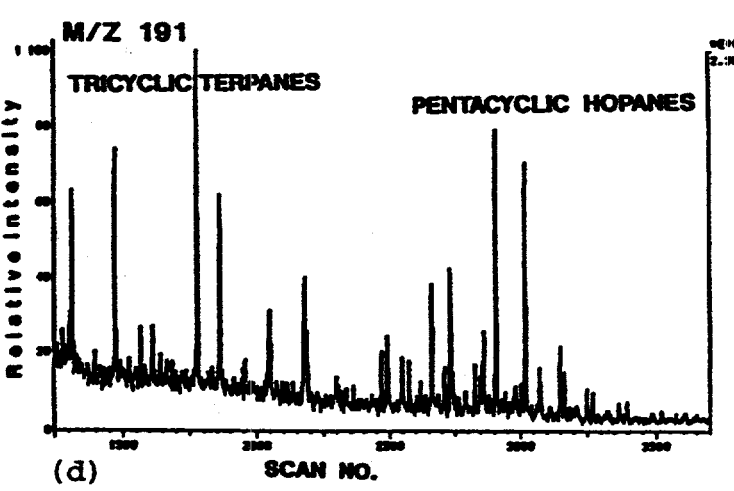


Fig. 6d. Typical distribution of terpanes showing the dominance of both tricyclic and pentacyclics found in the saturate fractions of Morrow Group extracts.

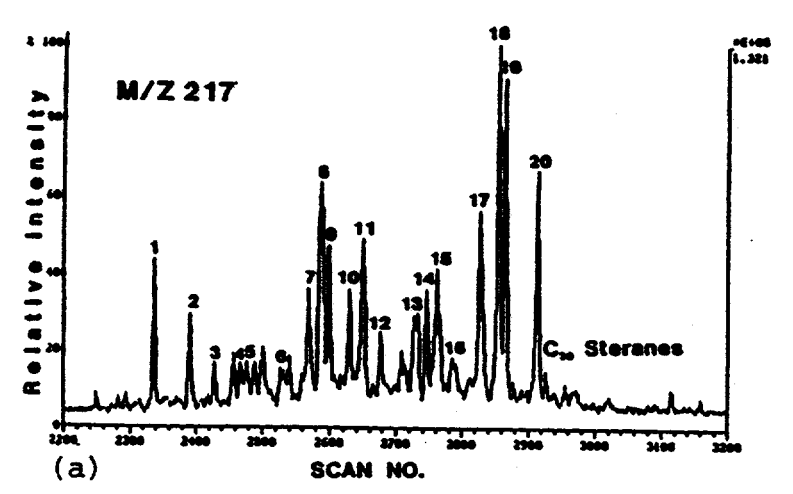


Fig. 7a. Typical distribution of steranes found in branched/cyclic fractions of oils from the Ordovician Viola reservoirs. Peak identities are listed in Table 1.

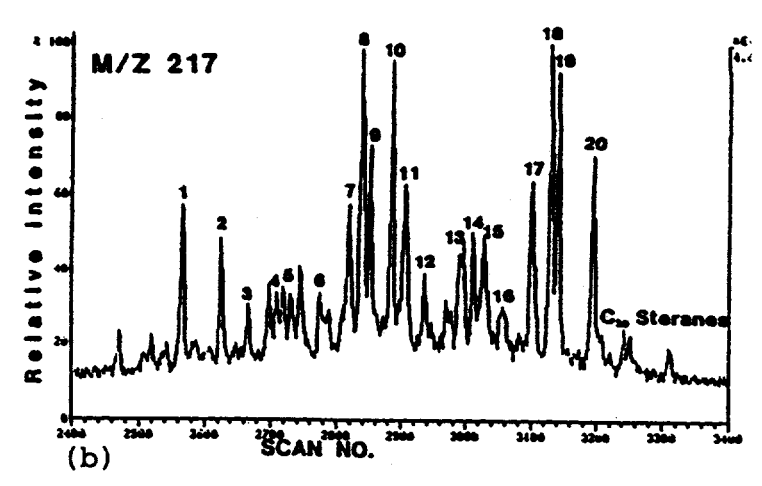


Fig. 7b. Typical distribution of steranes found in branched/cyclic fractions of Silurian/Devonian Hunton reservoirs. Peak identities are listed in Table 1.

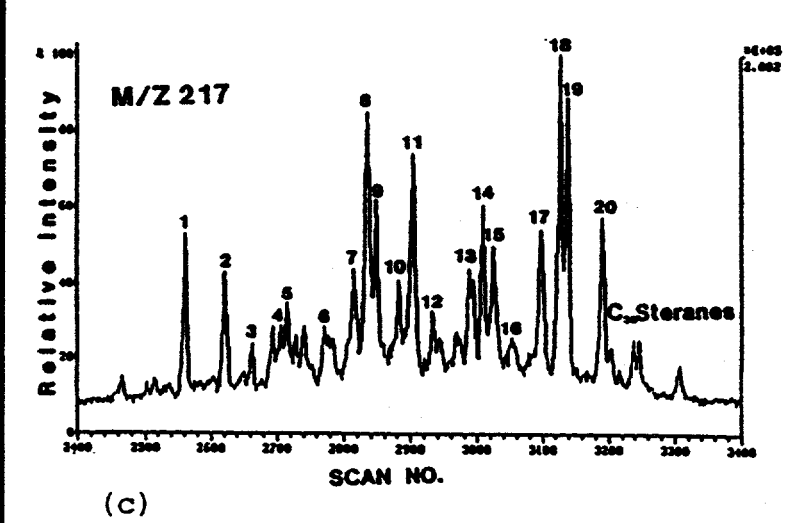


Fig. 7c. Typical distribution of steranes found in branched/cyclic fractions of Pennsylvanian oils. Peak identities are listed in Table 1.

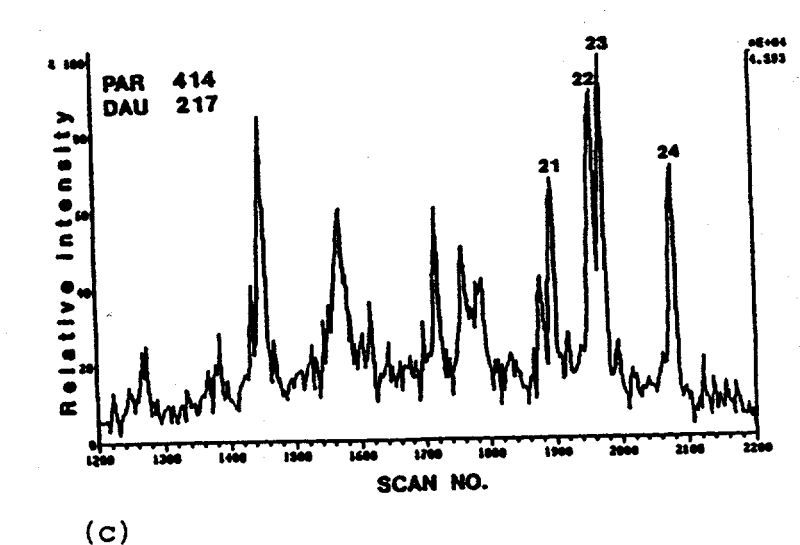


Fig. 7d. Partial chromatogram of the parent ion at m/z414 which produce the daughter ion at m/z 217, implying that the additional methyl group is on the side chain. The cmpounds have been tentatively identified as C₃₀-propyl steranes from Pennsylvanian oils. Peakidentities are listed in Table 1.

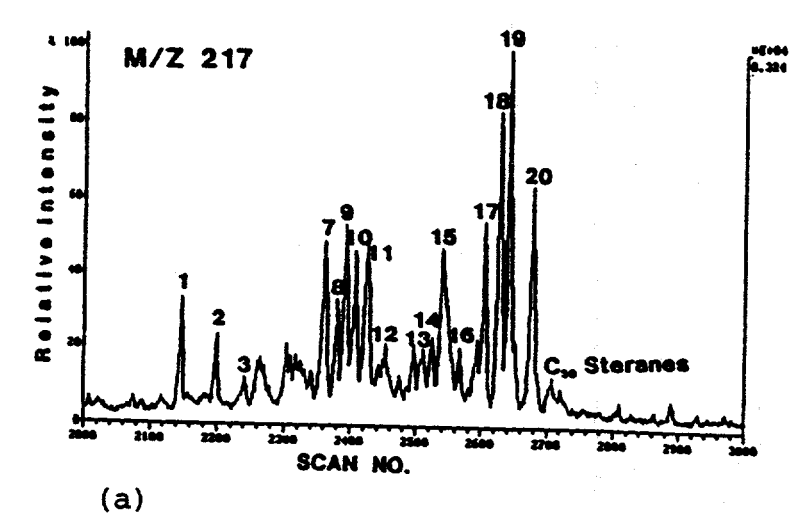


Fig. 8a. Typical distribution of steranes found in saturate fractions of Viola Group sediment extracts. Peak identities are listed in Table 1.

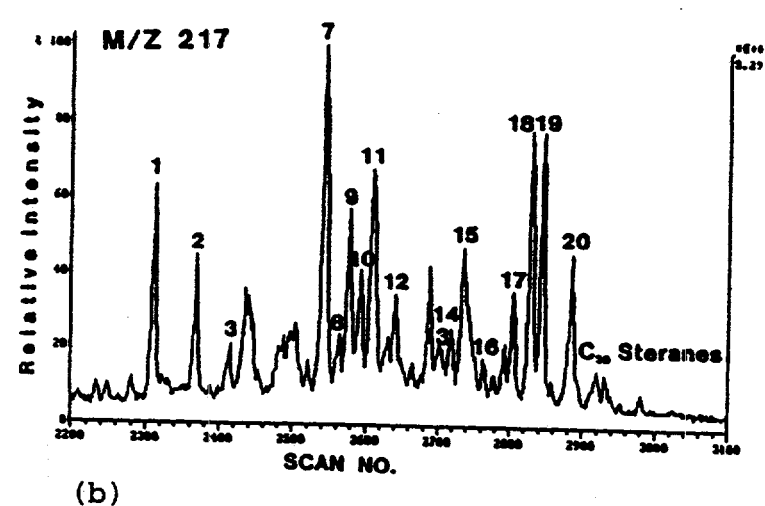


Fig. 8b. Typical distribution of steranes found in saturate fractions of Sylvan Shale extracts. Peak identities are listed in Table 1.

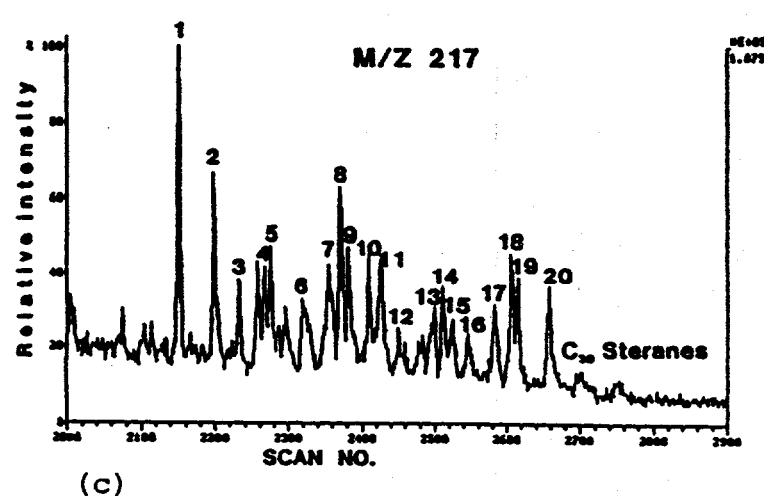


Fig. 8c. Typical distribution of steranes dominated by C₂₇ diasteranes found in saturate fractions of Springer Formation extracts. Peak identities are listed in Table 1.

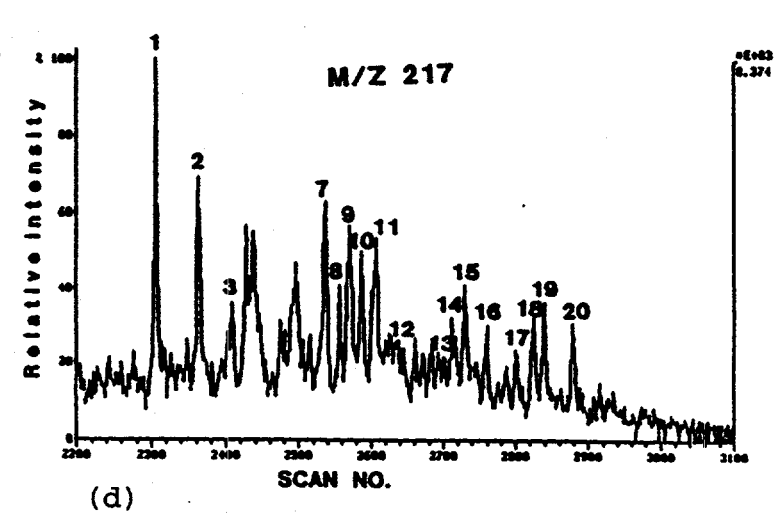
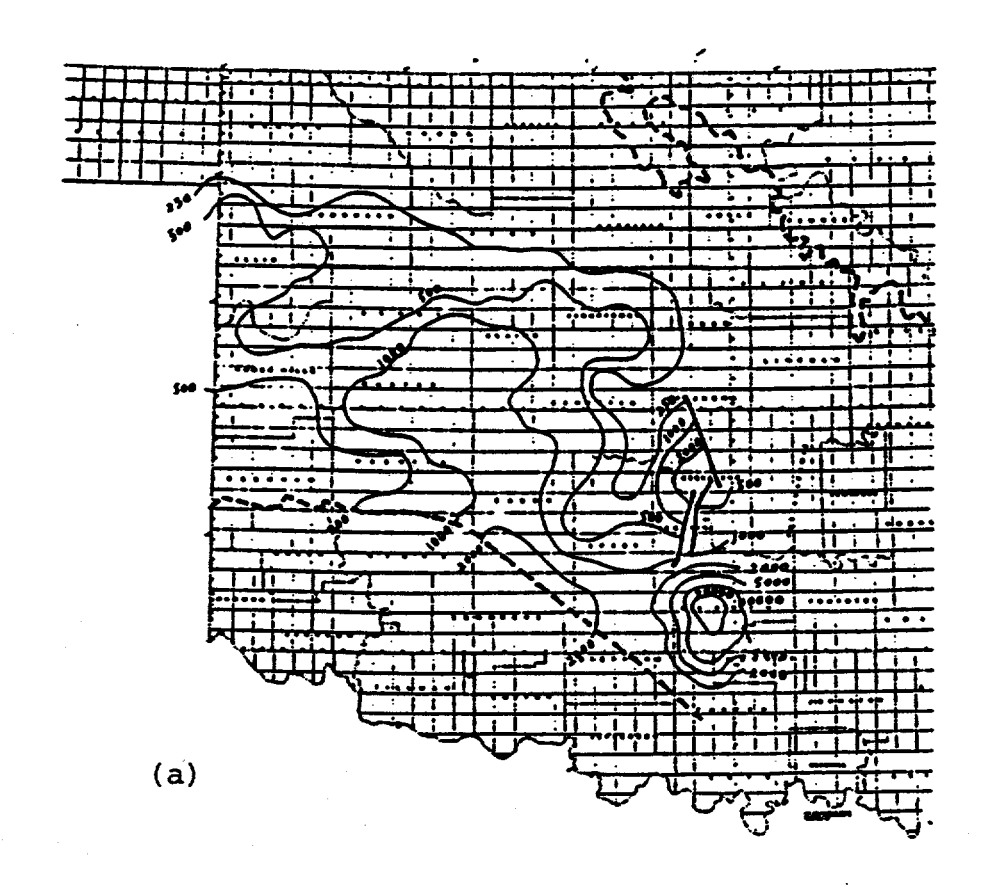


Fig. 8d. Typical distribution of steranes dominated by C_{27} diasteranes found in saturate fractions of Morrow Group sediment extracts. Peak identities are listed in Table 1.



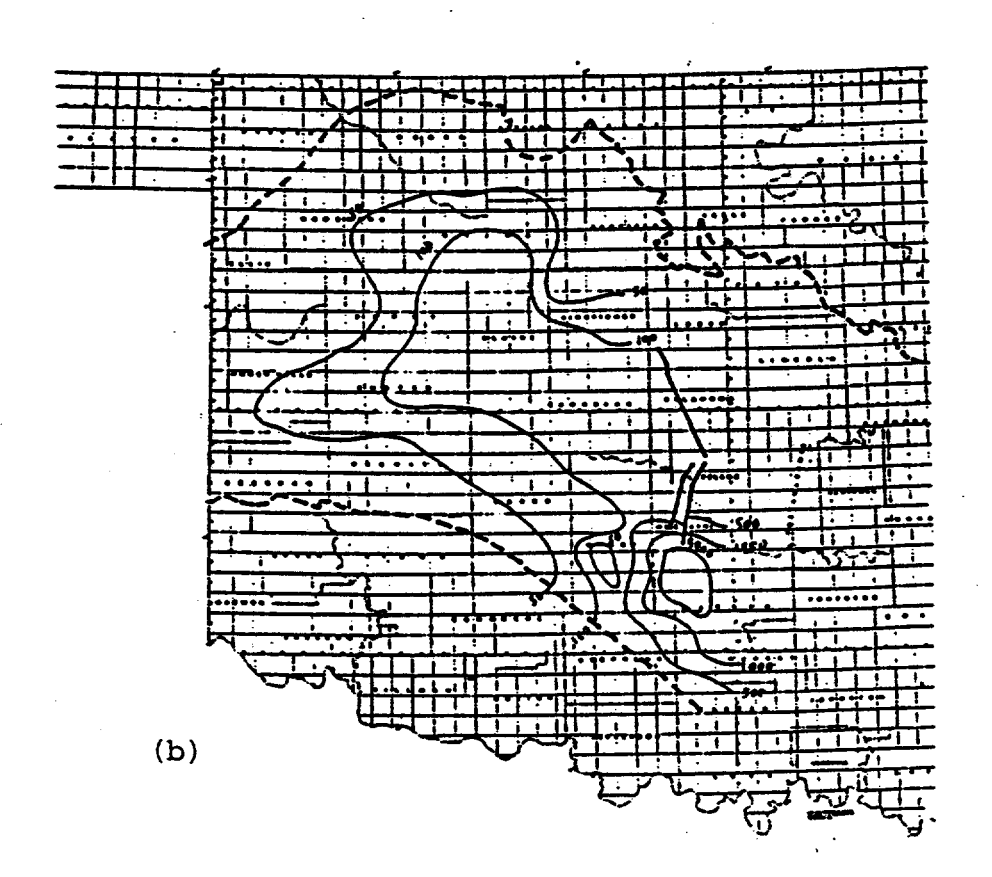
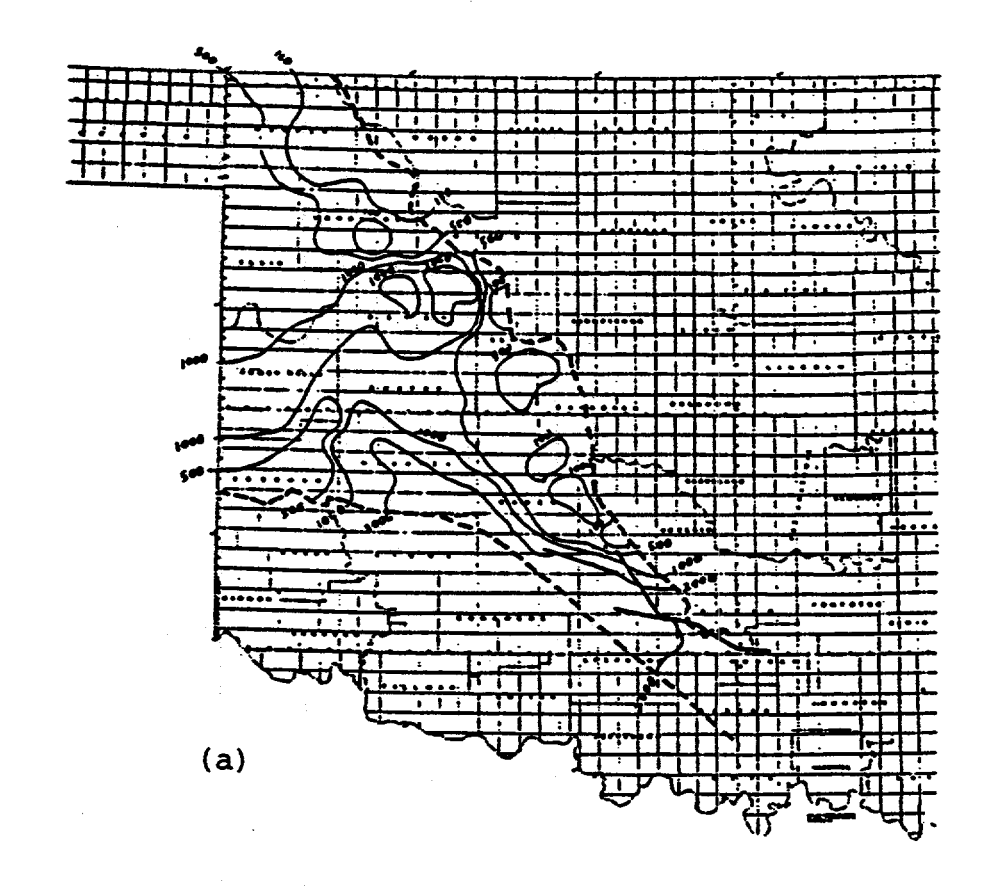


Figure 9. Petroleum Potential Index (PPI) map of: (a) Viola Group (b) Sylvan Shale.



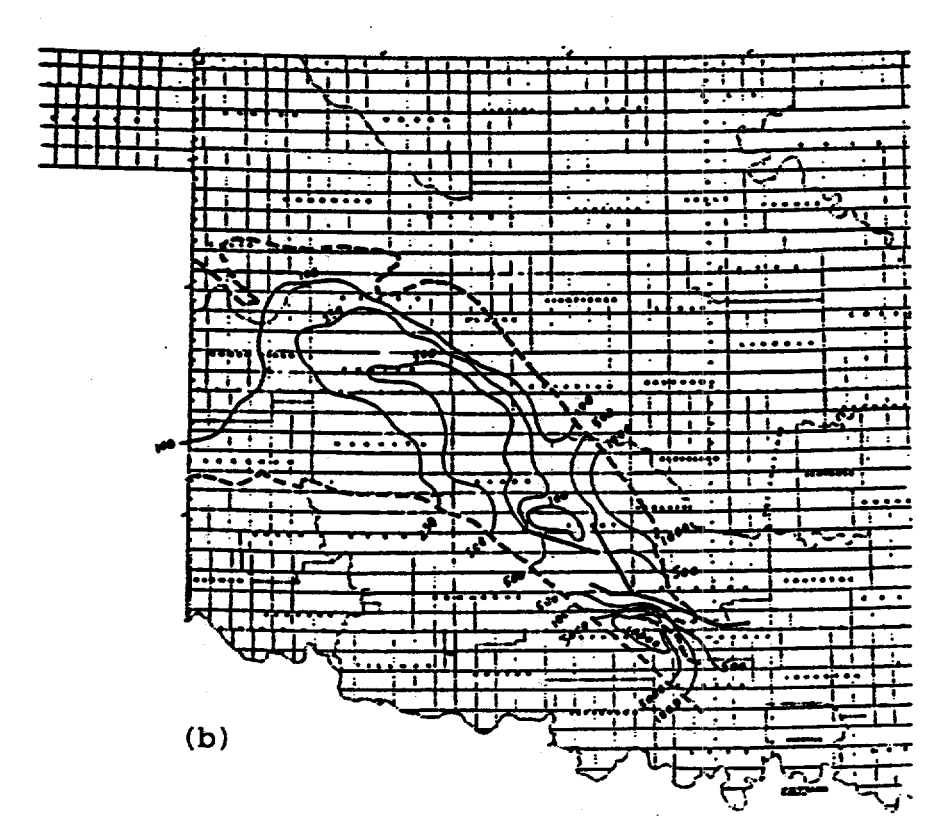


Figure 10. Petroleum Potential Index (PPI) map of : (a) Morrow Group (b) Springer Formation.

GEOCHEMISTRY AND ORIGIN OF REGIONAL DOLOMITES

Gilbert N. Hanson and William J. Meyers Department of Earth and Space Sciences SUNY Stony Brook

We are continuing to explore basic questions and new approaches to studying carbonate diagenesis related to the development of regional dolomite. Recent prime examples are: 1) the development of B isotopes and Pb isotopes for use in diagenetic studies, 2) the use of the U-Pb system to date unconformities, 3) the development of a number of detailed case histories in a range of stratigraphic ages and settings, 4) continued use and development of quantitative rock-water interaction modelling of trace elements and isotopes, 5) the development of analytical techniques and interpretations of trace anions and Na in dolomites, and 6) the application of hydrologic and thermodynamic models to dolomitization.

Our geochemical approaches are applied to rock suites that have been studied in great detail stratigraphically and petrographically, and have been well characterized by conventional geochemical parameters. We are studying carbonate strata of academic and economic interest, our earlier efforts were dominantly in Devonian and Mississippian carbonates, the most recent efforts are in Neogene carbonates. Studies of dolomitization in Neogene carbonates should be of interest because similar age carbonates are important reservoirs in other parts of the world. Furthermore, these are of scientific interest because of the relatively precise constraints on timing, paleotopography, sea-level history, and precursor mineralogy compared to Paleozoic examples, and are more like Paleozoic carbonates than are Pleistocene carbonates.

Pb Isotope Studies in Dolostones

These studies constitute the PhD. thesis of John Hoff. The goal is to use the Pb isotopic composition of carbonate rocks and minerals to constrain the origin of diagenetic fluids and constrain the absolute age of diagenetic events. To date, this research has concentrated on the origin of different dolomite generations within the Burlington-Keokuk Fms. (Mississippian) of Iowa, Illinois and Missouri and the timing of U-enrichment in dolostones from the Wahoo Fm. (Pennsylvanian), subsurface, Prudhoe Bay, Alaska.

In the mid-continent region dolomitized Paleozoic carbonates are host to Mississippi Valley-type (MVT) Pb-Zn deposits. Although the source of fluids responsible for MVT deposits remains uncertain, basinal brines have been proposed. Similar brines may also play an important role in the dolomitization of carbonate sequences. For example, trace element and isotope geochemistry suggest that dolomite II in the Burlington-Keokuk Fms. formed by the interaction of dolomite I with a brine (Banner et al., 1989; Cander et al., 1989).

Pb isotope data for the Burlington-Keokuk Fms. show that in almost all cases whole-rock dolostones are more radiogenic than dolomite separates. Whole-rock-dolomite pairs for some samples do not lie within error of isochrons of appropriate age for the rocks, suggesting that components of Pb within the whole-rocks have a different isotopic character than Pb in dolomite separates. Because, the dolostones are chemical in origin, this suggests that the Pb isotopic character of fluids changed during the diagenetic history of the Burlington-Keokuk Fms.

The Pb isotopic compositions of dolomites I and II are significantly different from those of MVT galenas, which precludes the dolomitizing fluid from being the fluid that formed MVT deposits. However, the similarity between the Pb isotopic composition of dolomite II and that found in oilfield brines, diagenetic galena and sedimentary rocks in the Mid-continent region is consistent with the formation of dolomite II by fluids that interacted with older sediments. The U-Pb data suggest that U was added to some dolostones during the last 5 Ma. This U enrichment was probably related to the exposure of the sequence to oxidized near surface fluids which are capable of mobilizing U. A similar mode of U enrichment appears to have occurred in the Wahoo Fm.

The Wahoo Fm. is a 60 to 90 meter thick sequence of limestones and dolostones deposited in an interior platform setting as a mosaic of lagoonal and shoal facies (Jameson, 1990a, 1990b). At Prudhoe Bay the Wahoo Fm. is buried to more than 3000 m and forms a giant hydrocarbon reservoir of the Lisburne Field. The sequence is overlain unconformably by the Kavik Shale (Upper Permian). The age of the Kavik Shale broadly constrains this bounding unconformity to be pre-Upper Permian and therefore this feature is commonly referred to as the PUPU.

450

A zone of extensively dolomitized rocks occurs just beneath the PUPU. These rocks have been termed "hot" dolostones because they are enriched in U (up to 55 ppm). Based on spatial relationships and trace element gradients away from the PUPU, dolomitization is thought to post-date formation of the unconformity (Jameson et al., 1988; Jameson, 1989a,b). The Pb in the dolostones exhibits a considerable spread in uranogenic Pb, but little spread in thorogenic Pb implying enrichment of U relative to Th. Induced fission track analysis (P. Swart, Univ. Miami) indicates that U is enriched in minor, non-carbonate phases (most likely authigenic clays). The relative enrichment of U is undoubtedly related to the greater mobility of U compared to Th at near-surface conditions. A regression of the Pb data yields an age of 263±40 Ma. The age and the uncertainty are comparable with the estimated time and duration of exposure of the PUPU. The lack of evidence for resetting of the Pb isotope system during burial dolomitization in the Permo-Triassic and development of an extensive unconformity in the Lower Cretaceous (Jameson, 1989a, 1990a) indicates that the Pb isotope system in carbonates is relatively robust to subsequent diagenesis.

Boron Isotopes in Carbonates

The development of boron isotopes as a geochemical tracer in carbonates constitutes the Ph.D. research of Gary Hemming. We have developed procedures for analysis so that reproducibility is better than $\pm 0.75^{\circ}/\infty$ (2σ) for less than 1 ng of B. We predict that the wide range of boron isotope compositions and boron abundances of various waters will allow boron isotope systematics in carbonates to characterize the fluids responsible for their precepitation. Seawater has consistent boron isotope composition $\delta^{11}B$ of ± 40 (relative to NBS 951) and abundances (4.5 ppm) independent of latitude or water depth (Spivack and Edmond, 1987). The first part of these studies was to evaluate the boron isotope composition of marine carbonates of diverse locations and types. It was found that marine carbonates independent of temperature, host organism or mineralogy have a small range in $\delta^{11}B + 19$ to ± 25 whereas they have a rather large range in abundances, 1 to 100 ppm (Hemming and Hanson, in review). It is suggested that the boron isotope composition of carbonates is controlled by pH and the isotopic composition of the fluid. pH determines the relative abundances of the B(OH)₃ and B(OH)₄1- species. At seawater temperatures there is a fractionation factor of 1.0194 between B(OH)₃ and B(OH)₄1- at 250C with only a small variation with temperature (Kakihana et al, 1977). It is concluded that only the B(OH)₄1- species is incorporated in the carbonate.

Carbonates and waters from several caves in Texas, and from Turner Falls, Oklahoma where extensive travertine deposits occur have been studied to evaluate boron systematics in carbonate-fresh water systems. The boron concentrations in both the water and mineral samples are low compared with modern marine carbonates. The isotopic composition of the water samples is about +18% oo. The abundance data indicate a similar distribution coefficient to that found for modern marine systems. The results of the modern freshwater carbonate study will be important to understanding the effects of freshwater diagenesis on ancient carbonates.

Mississippian (Waulsortian) marine cements were chosen for study because they are pristine based on oxygen and strontium isotopes (Douthit and Meyers, 1990). The boron isotopic composition of all samples fall within a relatively narrow range (0 to $+2.5^{\circ}/\infty$) whereas modern marine carbonates have values of +19 to $25^{\circ}/\infty$. Boron abundances range from 32 to 65 ppm, similar to that found in modern marine carbonates. Pristine Mississippian brachiopods, however, have boron isotope compositions of $+17^{\circ}/\infty$ with 20 to 40 ppm B which would suggest that B isotope composition of Mississippian seawater is lighter than modern seawater (+34 and $+40^{\circ}/\infty$ respectively), but not as different as the marine cements

might suggest. If this is the case, the isotopic composition of boron may be an important criterion for establishing whether a carbonate phase is pristine.

Dolomitization of Late Miocene Reef Complexes

An important component of our investigations into massive dolomites has been the study of diagenesis in late Miocene reef complexes in Mallorca, and a continuation of this work at Nijar, mainland Spain. These studies show that young Tertiary rocks are particularly attractive laboratories for diagenetic work because of the generally excellent timing constraints provided by Sr isotopes (e.g. Swart, et al., 1987), accurate knowledge of precursor mineralogies, and detailed eustatic sea-level curves (Haq, et. al, 1987). Upper Miocene reefs in these areas offer outstanding subjects because they are well preserved and well exposed, and their stratigraphy and facies have received detailed study, their paleotopographic setting is well known, and the lack of deeper-burial diagenesis reduces the number of applicable dolomitization models. On a broader scale, Late Miocene reef complexes of the western Mediterranean provide the most modern example of a large-scale, reef-rimmed evaporite basin (Messinian evaporites are several kms. thick), a common setting for ancient reefs with few Tertiary and no modern analogues. Furthermore, the dominantly progradational geometries, and Mediterranean setting of the reef complex make this system a more appropriate analogue for many ancient reef complexes in intracratonic basins than strongly aggradational high-relief oceanic pedestals and platforms.

The study of Mallorcan reefs constitutes the Ph.D. research of Erik Oswald. The major conclusion of Oswald's study is that Mediterranean Messinian evaporitic seawater was the dolomitizing solution of Messinian reefs in Mallorca. The obvious way to test this model is to investigate dolomitization of other reefs in the western Mediterranean, and this is the main objective of the Nijar study. Specifically, if the evaporitic Messinian model is correct, dolomites in reefs from the mainland, such as Nijar, should have distribution, timing, petrography, and geochemistry comparable to dolomites in Mallorcan reefs.

Dolomitization of the Seroe Domi Fm. Netherlands Antilles

Studies of the Miocene-Pleistocene Seroe Domi Fm. in Curacao consititutes the Ph.D. research of Bruce Fouke. The excellent exposures and well defined limestone-to-dolomite transition zones in the Seroe Domi Formation allow us to petrographically and geochemically describe the intermediate steps of dolomitization, and provide an opportunity in a natural setting to test and develop our concepts of water-rock dolomitization mechanisms. The rationale for this focus on limestone-dolomite transitions is that the complex processes of dolomitization can best be understood if both intermediate and end member dolomite and limestone components are thoroughly documented.

Burlington-Keokuk Fm.

We have developed the Mississippian Burlington-Keokuk Formation in Iowa, Illinois and Missouri as a natural laboratory and proving ground for new geochemical approaches, as illustrated by the current research on the B and Pb isotope systems. In addition to the extensive geochemical and petrographic work (Harris and Meyers, 1987; Banner, et al., 1988a&b; Cander, et al., 1989; Kaufman, et al., 1989; Grams, 1987; Kohrt, 1988; Choquette, et al., accepted; Prosky, 1989;). We are investigating the petrology of these rocks on two other fronts. Bibek Ghosh, for his M.S. research studied the microdolomite content and trace element geochemistry of crinoids. Ann Cox is reassessing the fluid inclusions, with particular emphasis on dolomite I.

The study of geochemistry of crinoids in the Burlington-Keokuk Fm. has shown that they have relatively low microdolomite contents, compared to similar facies of the same age in the Lake Valley Fm., suggesting a very active meteoric diagenetic system. Microdolomite contents and Mg contents of host calcite show a distinct regional trend of increasing microdolomite from north to south. Mass balance calculations suggest that Mg loss from crinoids could supply a significant amount of Mg for the dolostones. Covariation of Mg and Mn in host calcite in crinoids and modelling suggest that water-rock interaction, rather than mixing, was the dominant process affecting the crinoids.

Renewed investigations of fluid inclusions in Burlington-Keokuk dolomite I show that most of the fluid inclusions are single-phase inclusions. Inducing vapor bubbles has proven extremely difficult. Two-phase inclusions have salinities ranging from 8 to 18 wt.% while single-phase inclusions have salinities of about 20 wt.%. If these single-phase inclusions prove to be primary rather than necked two-phase inclusions, this will require dolomite I to have formed from fluids with salinities between gypsum and halite saturation at temperatures less than 60°C rather than the proposed mixed seawater and meteoric water. Rather, these data are consistent with these fluids having been marine evaporitic brines refluxed from younger Mississippian depositional systems, or warm saline basinal brines.

Diagenesis of the Carbonates in the Napier Range, Canning Basin Australia

The Ph.D. research of Bruce Ward is on the platform evolution and Devonian-through-Carboniferous diagenesis of the Frasnian platforms exposed in the southern half of the Napier range, Canning basin, Western Australia. The platform-margin and marginal-slope strata of the Devonian Reef Complexes of the Canning basin are notorious for their abundant marine calcite cements, oxide coatings, marine internal sediments, and calcareous cyanobacterial encrustations that fill neptunian fractures and large primary pores. Two groups and scales of processes are involved in marine-burial diagenesis. On a local scale, degradation of organic matter may play an important role in modifying porewaters and producing variable redox conditions. On a larger scale and dominant in large cavities and neptunian fractures, circulation of oxic near-normal seawater and reflux of saline seawater play an important role in the marine-burial diagenesis, and in modifications of large-pore waters in platform strata 100's of meters below the sediment water interface and millions of years after deposition of host limestone.

Analysis of SO₄2-, F1- and Cl1- in Dolomitic Rocks

Although there has been a fair amount of work on Na as a paleosalinity indicator of dolomitizing fluids (Humphrey, 1988 for summary), there has been very little use of anions. In combination with cation abundances and stable isotope data, the abundances of SO₄²-, Cl¹- and F¹-can be used to distinguish freshwater from seawater-derived brine origin of the potentially dolomitizing fluid. Although this information can also be obtained from fluid inclusion work, the direct analysis of these anions has several advantages. First, the analysis can be carried out on any type of dolomite crystals and dolomite cements, and second, it is possible to evaluate whether these anions are mostly present in fluid inclusions or incorporated in the dolomite crystals.

Willie Staudt a pre-Ph.D. student has developed a high precision technique for the analysis of these anions using Ion Chromatography. Initial results show that the Miocene dolomites from Spain interpreted to have formed from seawater evaporitic brines, generally have greater concentrations of Cl, and sulfate than "non- evaporitic" dolomites. A plot of Na abundances in the dolomites versus Cl concentrations shows good covariation with the regression line having a slope much less than one, the slope that would prevail if all Na and Cl were in halite or evaporitic brine inclusions. Thus most of the Na is probably incorporated in the dolomite lattice. Increasing concentrations of Na may reflect increasing sodium relative to calcium and magnesium in the dolomitizing solution.

Sulfate is an abundant anion in most proposed dolomitizing solutions. Sulfate concentrations in dolomites may be related to the relative abundance of sulfate relative to total dissolved carbon in dolomitizing solutions. The positive covariation of Na and sulfate in the Mallorcan samples suggests that sulfate is not derived from solid inclusions of gypsum and that both sodium and sulfate are related to their relative concentrations in the dolomitizing solution.

Future work will include dolomitic rocks that are well characterized by petrography and other geochemistry, and represent a variety of diagenetic environments. Candidates for this are the dolomites from Nijar and dolomites intercalated with Miocene evaporites on mainland Spain, the Burlington-Keokuk dolomites and the Seroe Domi dolomites.

Geochemical and Hydrological Models

As part of our effort to quantitatively understand regional massive dolomitization, we are carrying out two types of geochemical modelling and have begun hydrologic modelling. One type of geochemical modelling is a continuation of our water-rock interaction modelling (Banner and Hanson, 1990). A second involves solving the mass balance of regional-scale dolomitization, using equilibrium thermodynamics. In essence, we calculate the minimum amount of Mg-containing fluid necessary to dolomitize a carbonate sediment. Because fluid flow might be one of the principal controls on the rate of the dolomitization process, we have started to evaluate the hydrology of some dolomitization models.

In most scenarios a magnesium-bearing solution reacts with calcium carbonate to form dolomite:

$$Mg^{2+} + 2CaCO_3(s) --> CaMg(CO_3)_2 + Ca^{2+}$$
 [1]

The minimum volume (V_{min})needed for dolomitization can be calculated using mass balance by assuming that any Mg-solution entering the calcium carbonate sediment reaches thermodynamic equilibrium. Oswald and Schoonen (in review) have calculated V_{min} for reactions between seawater and seawater derived brines with platform carbonates. The conclusion is that brines in mixing-zone type circulation systems are very efficient, but that near-seawater salinities in reflux or Kohout circulation systems are very inefficient as dolomitizing fluids.

The hydrologic modeling involves evaluation of the salina-reflux model for dolomitization using flow modelling of Pekelemeer, Bonaire, Netherland Antilles. This was one of the first sites where modern dolomites were found (Deffeyes et al., 1965; Lucia, 1968). Before the International Salt Company built its solar plant in the mid 1970's, Pekelmeer was a hypersaline lake separated from the Caribbean Sea by a coral rubble ridge. The original model for the formation of dolomite in the muds of Pekelmeer involved a density-driven reflux of the hypersaline brine through the coral rubble ridge into the open sea (Deffeyes et al., 1965). It was predicted that there could be dolomite below the coral rubble ridge). However, Lucia (1968) studied cores from the coral rubble ridge, but found no dolomite.

To test this Liu and Martin evaluated whether or not hydrological systems such as Pekelmeer are more likely to be dominated by density reflux or evaporitic pumping. They conclude that in all scenarios the hydrology of hypersaline systems is dominated by evaporitic pumping. Only at low tide is there a period in which some of the lake water will flow in the direction of the sea. Because this period of reflux is relatively short (hours), the lake water will only penetrate the very top of the underlying sediments. Perhaps the only place where dolomite could form at slightly deeper levels is at the toe of the coral ridge.

REFERENCES CITED

- Banner, J.L., and Hanson, G.N.,1990, Calculation of simultaneous isotopic and trace element variations during water-rock interaction with applications to modeling carbonate diagenesis: Geochim. Cosmochim. Acta v. 54 3123-3137.
- Banner, J.L., Hanson, G.N., and Meyers, W.J., 1988a, Determination of intitial Sr isotope compositions of dolostones from the Burlington-Keokuk Fms. of Iowa, Illinois, and Missouri: constraints from cathodoluminescence and glauconite paragenesis: Jour. Sed. Pet., v. 58, p. 673-687.
- Banner, J.L., Hanson, G.N., and Meyers, W.J., 1988b, Rare earth element and Nd isotopic variations in regionally extensive dolomites from the Burlington-Keokuk Fm. (Mississippian): implications for REE mobility during carbonate diagenesis: Jour. Sed. Pet., v.58, p.415-432.
- Banner, J.L., Hanson, G.N., and Meyers, W.J., 1989, Water-rock interaction history of regionally extensive dolomites of the Burlington-Keokuk Formation (Mississippian): Isotopic evidence: in Shukla, V., and Baker, P.A., eds., Sedimentology and Geochemistry of Dolostones, SEPM Spec. Pub. 43, p. 97-114.

- Cander, H., Kaufman, J., Daniels, L., and Meyers, W.J., 1989, Regional dolomitization in Burlington-Keokuk Fms (Miss.), Illiniois, Missouri in Baker, P., and Shukla, V., (eds.) Concepts and Models of Dolomitization: SEPM Spec. Pub. 43, p. 129-144.
- Choquette, P.W., Cox, A., Meyers, W.J., accepted, Characteristics, distribution and origin of porosity in shelf dolomite: Burlington-Keokuk Formation (Mississippian), U.S. Midcontinent: J. Sed. Pet.
- Deffeyes, K. Lucia, F., Weyl, P., 1965, Dolomitization of Recent and Plio-Pleistocene sediments by marine evaporite waters on Bonaire, Netherlands Antilles: in Pray, L. and Murray, R. (eds.)

 Dolomitization and Limestone Diagenesis: SEPM Spec. Pub. 13, 71-80.
- Douthit, T., Hanson, G., Meyers, W., 1990 Structure in the secular variation of seawater 87Sr/86Sr for the Ivorian/Chadian (Osagean, Lower Carboniferous): AAPG Program and Abstracts, p.78
- Grams, J., 1987, Trace element variations in calcite cements, Burlington-Keokuk Fm.: Unpub. M.S. Thesis, SUNY Stony Brook, 193p.
- Haq, B.U., Hardenbol, J., Vail, P.R., 1987, Chronology of fluctuating sea levels since the Triassic: Science, v. 235, p. 1156-1166.
- Harris, D.C. and Meyers, W.J., 1987, Regional dolomitization of subtidal shelf carbonates: Burlington and Keokuk Fms. (Mississippian), Iowa and Illinois: in Marshall, J.D. (ed.) Diagenesis of Sedimentary Sequences, Geol. Soc. Spec. Pub. No. 36, p. 137-158.
- Hemming, N.G., Hanson, G.N., in review, Boron isotopic composition and concentration in modern marine carbonates: Geochim. et Cosmochim. Acta.
- **Humphrey, J.**, 1988, Late Pleistocene mixing zone dolomitization, southeastern Barbados, West Indies: Sedimentology, v.35, 327-348.
- Jameson, J., 1989a, Interactions between early and late diagenesis in reservoir formation, Lisburne Field, Prudhoe Bay, Alaska: AAPG Bull., v. 73, p. 367-368.
- Jameson, J., 1989b, Are petrographic textural criteria valid for determining timing of dolomitization? An example from the Wahoo Formation, Prudhoe Bay, Alaska: AAPG Bull., v. 73, p. 368.
- Jameson, J.J., 1990a, Cyclicity, facies and diagenesis of the Wahoo Formation, Prudhoe Bay, Alaska: AAPG Bull., v.74, 684.
- Jameson, J.J., 1990b, Reservoir description of the Lisburne Field, Prudhoe Bay, Alaska; AAPG Bull., v.74, 684.
- Jameson, J., Neuhart, D. and Wendlandt, R., 1988, Multiple stages of porosity development in the Wahoo Fm., Prudhoe Bay, Alaska: SEPM mid-year mtg. abs., v. 5, p. 27-28.
- Kakihana, H.; Kotaka, M.; Satoh, S.; Nomura, M.; and Okamoto, M., 1976, Fundamental studies on the ion exchange separation of boron isotopes, Bulletin of the Chemical Society of Japan, V. 50, p. 158-163.
- Kaufman, J., Cander, H.S., Daniels, L.D., and Meyers, W.J., 1988, Calcite cement stratigraphy and cementation history of the Burlington-Keokuk Fms. (Mississippian), Illinois and Missouri: Jour. Sed. Pet., v. 58, p. 312-326.
- Kohrt, K., 1988, Stable isotope compositions of Burlington-Keokuk crinoids: M.S. thesis, SUNY Stony Brook, N.Y., 270pp.
- Lucia F.J., 1968, Recent sediments and diagenesis of south Bonaire, N.A. J.S.P. 38, 845-858.
- Oswald, E. and Schoonen, M., in review, Dolomitizing seas in evaporitic basins: a model for pervasive dolomitization of platform carbonates: Jour. Sed. Pet.
- Prosky, J.L., 1989, Stoichiometry and trace element geochemsitry of Burlington-Keokuk dolomites: M.S. thesis, SUNY, Stony Brook.
- Spivak, A. J. and Edmund, J. M., 1987, Boron isotope exchange between seawater and the oceanic crust, Geochim. Cosmochim. Acta., V. 51, p. 1033-1043.
- Swart, P., Ruiz, J., Holmes, C., 1987, Use of Sr isotopes to constrain the timing and mode of dolomitization of upper Cenozoic sediments in a core from San Salvadore, Bahamas: Geology, v. 15, 262-265.

STABLE ISOTOPE SYTEMATICS OF BURIAL DIAGENENSIS IN THE ALBERTA DEEP BASIN: AN ION MICROPROBE STUDY

Lee R. Riciputi^{1,3}, David R. Cole², Warner H. Christie¹, Thomas M. Rosseel¹, and Hans Machel⁴

- ¹ Analytical Chemistry Division, ² Chemistry Division, Oak Ridge National Laboratory, Oak Ridge, TN, 37631
- ³ Department of Geological Sciences, University of Tennessee Knoxville, TN, 37996
- ⁴ Department of Geology, University of Alberta, Edmonton, Alberta, Canada

INTRODUCTION

The principle objective of this research is to use elemental and isotopic compositions coupled with detailed mineralogy and studies of fluid inclusions to quantify the mass transfer processes influencing porosity and permeability during burial diagenesis of carbonates and clastics in the Alberta Basin. Because the consequences of fluid-rock interactions are preserved over small distances - namely the dimensions encountered in pores, microfractures, or within the grains themselves (10s to 100s of microns) - it is desirable to use in-situ analysis techniques to resolve the inter- and intragrain chemical and isotopic variations in fine-grained, diagenetically altered samples. These variations are the result of a number of possible mechanisms such as recrystallization, fracture or pore-filling precipitation, and in some cases, diffusion (Fig. 1). Thus far our efforts have focused on microbeam analysis by secondary ion mass spectrometry (SIMS) techniques through the use of the new Cameca 4f ion microscope/ion microprobe. When used in microprobe mode, SIMS offers the possibility of quantitative measurement of both a wide variety of elements at the ppm level and isotopic ratios on spots of less than 20 microns in size, with preservation of spatial relations. SIMS also offers the ability to qualitatively map the distribution of elements over an area of up to 500x500 microns when used in scanning ion mode.

The majority of our initial efforts have been directed at developing quantitative techniques for the measurement of trace elements and stable isotopes in geologic media. Preliminary application of scanning ion imaging to map element distributions has been initiated on samples from the Upper Devonian Nisku Formation of the Alberta Basin as well as diagenetic sulfides from Cambrian black shales of China. These efforts as well as those in areas of technique development are briefly summarized below.

^{*} This research is sponsored by the U.S. Department of Energy, Office of Basic Energy Sciences under contract number DE-AC05-840R21400 with Martin Marietta Energy Systems, Inc.

QUANTITATIVE TRACE ELEMENT ANALYSIS

When properly calibrated, the ion probe allows in-situ, quantitative determination of trace element contents at the ppm level and below. Use of an O beam and collection of positive secondary ions eliminates most surface charging effects. The major problems are matrix effects and molecular interferences.

There is a lack of theoretical knowledge concerning the effects of different matrices on the ion formation process. As a result, it is necessary to empirically calibrate the ion probe using standards that have similar trace element chemistry as compared to the unknown to eliminate matrix effects. For geological applications, this requirement means that mineral standards that are homogeneous at the micron scale with respect to both the major and minor elements must be acquired and characterized for each type of mineral that is to be analyzed. Such standards are not readily available, as many standards that are homogeneous with respect to the major elements are zoned in trace element contents. Each potential standard must be characterized by analyzing multiple points (10 to 30) using the ion microprobe. If a mineral is found to be homogenous with respect to the trace elements, it then must be characterized using bulk analytical techniques such as instrumental neutron activation analysis (INAA) or inductively coupled plasma mass spectrometry (ICP-MS). We have currently found approximately 15 minerals (garnets, clinopyroxenes, apatites, feldspars, calcites, and dolomites) that are suitable for use as standards, and have finished preparing the bulk mineral splits for INAA and ICP-MS analysis.

The sputtering process produces positive, negative, and neutral ions. In addition, large numbers of molecular ions are also produced, which produce isobaric interferences at the same masses as the elemental ions (for instance, Ca⁴⁰O¹⁶ interferes with the Fe⁵⁶ peak). We have investigated a number of possible techniques to avoid the effect of molecular interferences. For masses that are lower than Ca, the high mass resolution capabilities of the Cameca 4f allow most interfering molecular ions to be avoided. However, at higher masses, the amount of mass resolution required reduces the effective ion transmission to levels that are too low to be useful. For higher masses, the wider energy distribution of elemental ions as compared to molecular ions can be used to reduce the amount of interference using high energy offsets. As higher energy ions are sampled, the relative contribution of molecular ions decreases. In many cases, the use of high energy offsets can effectively remove all molecular ions (Ray and Hart, 1982). In other situations, such as the analysis of the heavy rare earth elements, molecular interferences remain. interferences can be removed using systems of linear equations to deconvolve the peaks into their elemental and molecular components (Zinner and Crozaz, 1986). We have had some success using this technique for the analysis of REE in clinopyroxene, but we need better analyses on our standards to be certain. In theory, the use of very high offset energies should allow all molecular ions to be eliminated, although larger primary beam spots would be needed to offset the loss in intensity in the elemental ion signal (Schauer and Williams, 1990). The Cameca 4f is not equipped to handle offset energies larger than 125V, but we are currently modifying the instrument to allow use of higher offset energies for cases where small beam spots are not needed.

We are also investigating the use of doubly charged ions for trace element analysis. Although far fewer doubly charged ions are formed relative to singly charged ions, odd mass doubly charged ion peaks occur at half mass intervals (e.g., the doubly charged ion peak of

Rb⁸⁵ falls at mass 42.5), which should allow molecular ion interferences to be avoided and allow the use of little or no offset energy. Initial studies using doubly charged ions for the analysis of REE in clinopyroxene are encouraging, but preliminary results for Ti, V, and Rb in USGS whole rock glasses suggest that the formation of some doubly charged ions may be extremely sensitive to matrix variability.

We have had good success using energy offset techniques to calibrate elements that do not have large interfering molecular peaks in both clinopyroxene and a suite of glasses prepared from USGS whole rock powders (basalt to rhyolite in composition). We have demonstrated the linear response of the ion probe over several orders of magnitude of trace element contents, and the response appears to be fairly linear over the range of major element compositions in the silicate glasses (Fig. 2). This success suggests that once we have completed obtaining and analyzing our standards, we should have good success in analyzing the majority of trace elements in a variety of minerals.

STABLE ISOTOPE RATIO MEASUREMENTS

Isotope ratio measurements are the ultimate test of stability for an ion microprobe. Whereas precisions of 5% are quite acceptable for trace element analysis, precisions must be far better for isotope ratio measurements to be useful in natural geologic systems (at least 0.15%). The low abundances of the minor isotopes require long counting times to accumulate the needed counts to obtain high precisions, which requires that the primary beam intensity, magnet calibration and counting system remain very stable. In addition, the problems encountered in trace element analysis (charging of insulators, obtaining homogeneous standards to account for matrix effects, molecular interferences) are also present in using the ion probe for stable isotope analysis.

In spite of all these potential problems, we have demonstrated that the ion probe can obtain stable isotope ratios in conductors that are equal to the limits imposed by counting statistics, similar to results obtained using the Cameca 4f ion probe at Edinburgh (Valley and Graham, in press). We have analyzed $\delta^{18}O$ in a magnetite that is thought to be homogenous, using high mass resolution to eliminate molecular interferences. Over an analysis time of one hour using a beam spot of ~15 microns in diameter, approximately 1,000,000 counts of ¹⁸O can be obtained without overloading the counting system with respect to ¹⁶O. This yields a theoretical precision limit of 1 per mil, and our analyses of the same magnetite during any one day has similar precisions (Fig. 3). As can be seen, the accuracy of the instrument drifts from day to day due to variations in the instrument performance and aging of both the primary beam source and the electron multiplier and changes in sample geometry. However, careful monitoring of the day-to-day performance of the instrument using well-characterized standards will alleviate this problem. Our success with the magnetite suggests that we should be able to apply similar techniques to the analyses of S isotopes in conducting sulfides, and C isotopes in graphitic material.

ELEMENTAL IMAGING

In addition to spot analysis, the Cameca 4f can also be used to map the distribution of major, minor, and trace elements over areas as large as 500x500 microns when used in scanning ion image mode. Charging problems in insulators are partially offset by use of a

conductive coating and an O beam, and since the primary beam is constantly being rastered across the surface of the sample, charge build-up is inhibited. Both energy offset and high mass resolution techniques can be used to overcome molecular interferences.

Our preliminary efforts in the Alberta Basin have focused on the distribution of trace elements in dolomitized areas (Fig. 4). We have looked at several samples from the Upper Devonian Nisku Formation. The Nisku Formation in the subsurface of central Alberta contains pervasive dolomites that occur mainly as replacement of reefal limestone (Machel and Anderson, 1989). It is believed that dolomitization has been caused by (1) expulsion of burial compaction water, i.e., chemically modified seawater, and/or (2) thermal convection of formation fluids originally underlying or overlying the Nisku Formation. Elemental distributions are similar in the sections we have analyzed, wherein Mn, Fe, B, Na, and V are concentrated in the dolomite, and Sr in the calcite. No obvious intergrain zoning has been observed, although there is the suggestion in Figure 4 that select dolomites have high Fe cores. Comparisons of different generations of dolomitization have been hampered by lack of contacts between different types of dolomites, and the apparent subtle chemical variations between the different dolomites and calcites.

We have also imaged a diagenetic sulfide from the Daping deposit, Hunan Province of southern China. This deposit is one of several remarkably high-grade stratabound ores of Mo-, Ni-, and Fe-sulfides and arsenosulfides that occur discontinuously in lower Cambrian black shales in a 1600 km long belt from eastern Xunnan to Zhejiang (Coveney and Nansheng, 1991; Coveney et al., in press). These deposits may be time-correlative with other metalliferous black shales of Canada and Poland (Coveney and Nansheng, 1991). Imaging of phosphate nodules that has been partially replaced by sulfides revealed complex zonation across the mineral grains characterized by a variety of metal associations. In Figure 5, we show examples of images for Ni, Mo, As, and Ag in a phosphate nodule (lower right portion of image) that has been partially replaced by sulfides. Note the close spatial association of Ag and Mo, occurring in distinct bands separated by dolomite (light yellow-white zone). Note that Mo is a late-stage element, occurring at the edge of the nodule, outside of the Nirich band. Also note the correlation between As and Ag. These variations suggest that several pulses of fluid were involved in the formation of the deposit, and that cyclical variations in the fluid chemistry may have occurred.

SUMMARY AND FUTURE OUTLOOK

The results of preliminary studies suggest that the Cameca 4f ion microprobe/microscope will be a powerful tool for diagenetic studies. The elemental imaging capabilities provide a relatively rapid means to survey samples for gross elemental zoning, and for imaging textural variations in various types of dolomitized carbonates. The apparent subtle trace element variations between the different generations of dolomite and calcite will require quantitative spot analysis. The results of studies of silicate glasses and clinopyroxene suggest that calibration for trace element analysis (Rb, Sr, Fe, Mn, Mg, Ba, Na, and other potential elements) in carbonate should be relatively straightforward, once adequate standards have been obtained and documented. Bulk analyses of standard materials that have already been acquired will allow us to calibrate for some of these elements in the near future, and we plan to continue our search for other suitable carbonate standard material.

Successful analysis of O isotopes in magnetite suggests that similar success will probably be obtained for the analysis of S isotope ratios in sulfides, and possibly for C in bitumen. All three types of material will be studied in the Alberta Basin. In addition, diagenetic magnetites from the Lower Ordovician Arbuckle Group in southern Oklahoma (Elmore et al., 1987) will also be studied, as well as possible S isotope zoning in the sulfides from the China diagenetic sulfide deposit. It may also be possible to analyze C isotopes in carbonates using a negative O primary beam and analyzing positive secondary ions to control sample charging, but this possibility is yet to be explored.

REFERENCES

- Coveney, R.M., Jr., and Nansheng, C. (1991) Ni-Mo-PGE-Au-rich ores in Chinese black shales and speculations on possible analogues in the United States. Mineralium Deposita, 26:83-88.
- Coveney, R.M., Jr., Murowchick, J.B., Grauch, R.I., Nansheng, C., and Glascock, M.D. (in press) Field relations, origins, and resource implications for platiniferous Mo-Ni ores in black shales of south China. Journal of Mining and Exploration Geology.
- Elmore, R.D., Engel, M.H., Crawford, L., Nick, K., Imbus, S., and Sofer, Z. (1987) Evidence for a relationship between hydrocarbons and authigenic magnetite. Nature, 325:428-430.
- Machel, H.G., and Anderson, J.H. (1989) Pervasive subsurface dolomitization of the Nisku Formation in central Alberta. Journal of Sedimentary Petrology, 59:891-911.
- Ray, G., and Hart, S.R. (1982) Quantitative analysis of silicates by ion microprobe. International Journal of Mass Spectrometry and Ion Physics, 44:231-255.
- Schauer, S.N., and Williams, P. (1990) Elimination of cluster interferences in secondary ion mass spectrometry using extreme energy filtering. International Journal of Mass Spectrometry and Ion Processes, 103:21-29.
- Valley, J.W., and Graham, C.M. (in press) In microprobe analysis of oxygen isotope ratios in magnetites in granulite facies marbles: Diffusive exchange as a guide to cooling history. Contributions to Mineralogy and Petrology.
- Zinner, E., and Crozaz, G. (1986) A method for the quantitative measurement of rare earth elements in the ion microprobe. International Journal of Mass Spectrometry and Ion Processes, 69:17-38.

FIGURE CAPTIONS

- Figure 1: Schematic diagram illustrating possible chemical and isotopic exchange mechanisms occurring over a scale of 10's to 100's of microns in a fluid-rock system.
- Figure 2: Ion count ratio plotted versus elemental concentration ratio for a set of glasses made from USGS whole rock standard powders (48 to 75 wt% SiO₂) showing generally linear response of the ion probe. All elemental ion intensities are ratiod to the Si ion intensity, and elemental concentrations are ratioed to the Si content.
- Figure 3: Isotopic composition of δ^{18} O in magnetite analyzed on three different days over a period of three months. The plotted δ^{18} O have not been corrected for instrumental fractionation. The error bars are 1 per mil, and the average isotope ratios for each day are plotted as a straight line. Note that the internal precision is better than 1 per mil, although the instrumental fractionation varies from day to day due to changes in instrumental focusing parameters and aging of the ion source and detector system. Analyses were made using a primary $^+$ Cs beam of 0.8 to 1.5 nA and total analysis time was approximately 50 minutes. The beam size was $^-$ 15 microns, but using a combination of contrast and field apertures, only ions from the central 8 microns of the beam spot were analyzed. The magnetite sample analyzed is from the Adirondack Mountains, and was provided by J. Valley of the University of Wisconsin.
- Figure 4: Elemental image maps of dolomitized limestones from cores of the Nisku Formation (depth = 2441m) of the Alberta Basin. The imaged field is 250x250 microns. Imaged elements are (clockwise from the upper right corner) B, V, Fe, and Mg. The color scale is total ion counts. The B, V, and Fe are all concentrated in the dolomite, with the possible suggestion of Fe-rich cores.
- Figure 5: Elemental image maps of sulfide replacing a phosphate nodule (nodule lies in the lower right hand half of each image) from Cambrian black shales of Southern China. Each imaged field is 250x250 microns, and image maps are Ni, Mo, As, and Ag from top to bottom. Position of line scans are indicated by dark lines, and the left hand side of the line scan is the top of the imaged picture. Numbers along the base of the line scan are pixels, and each pixel corresponds to roughly 1 um. Note the cyclic nature of the Ni, As, and Ag zoning. Mo, which lies outside of the last Ni-rich band, was apparently a late-stage element. This sample was provided by James Murowchick, University of Missouri-Kansas City.

Figure 1. Schematic of fluid-rock interaction processes

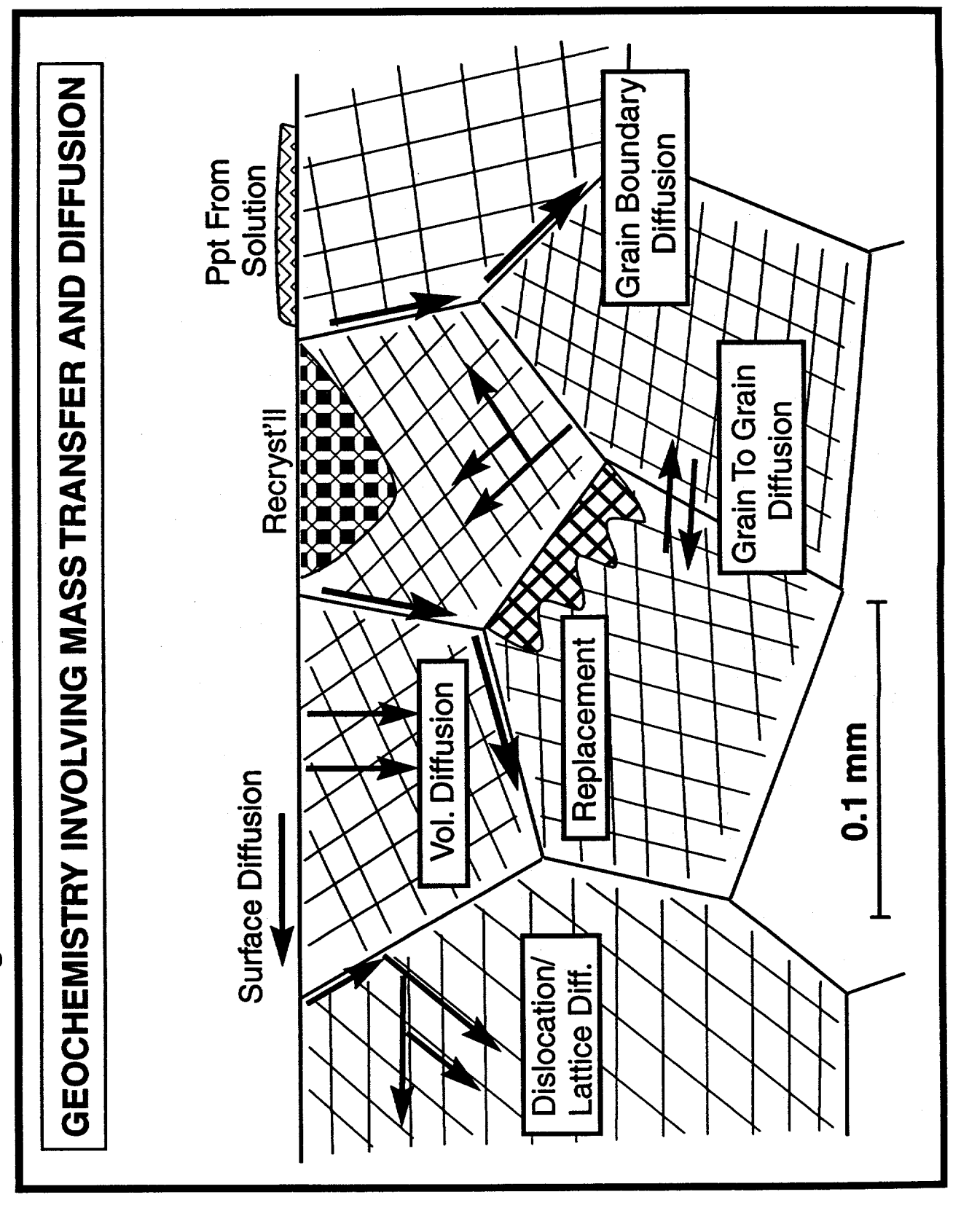
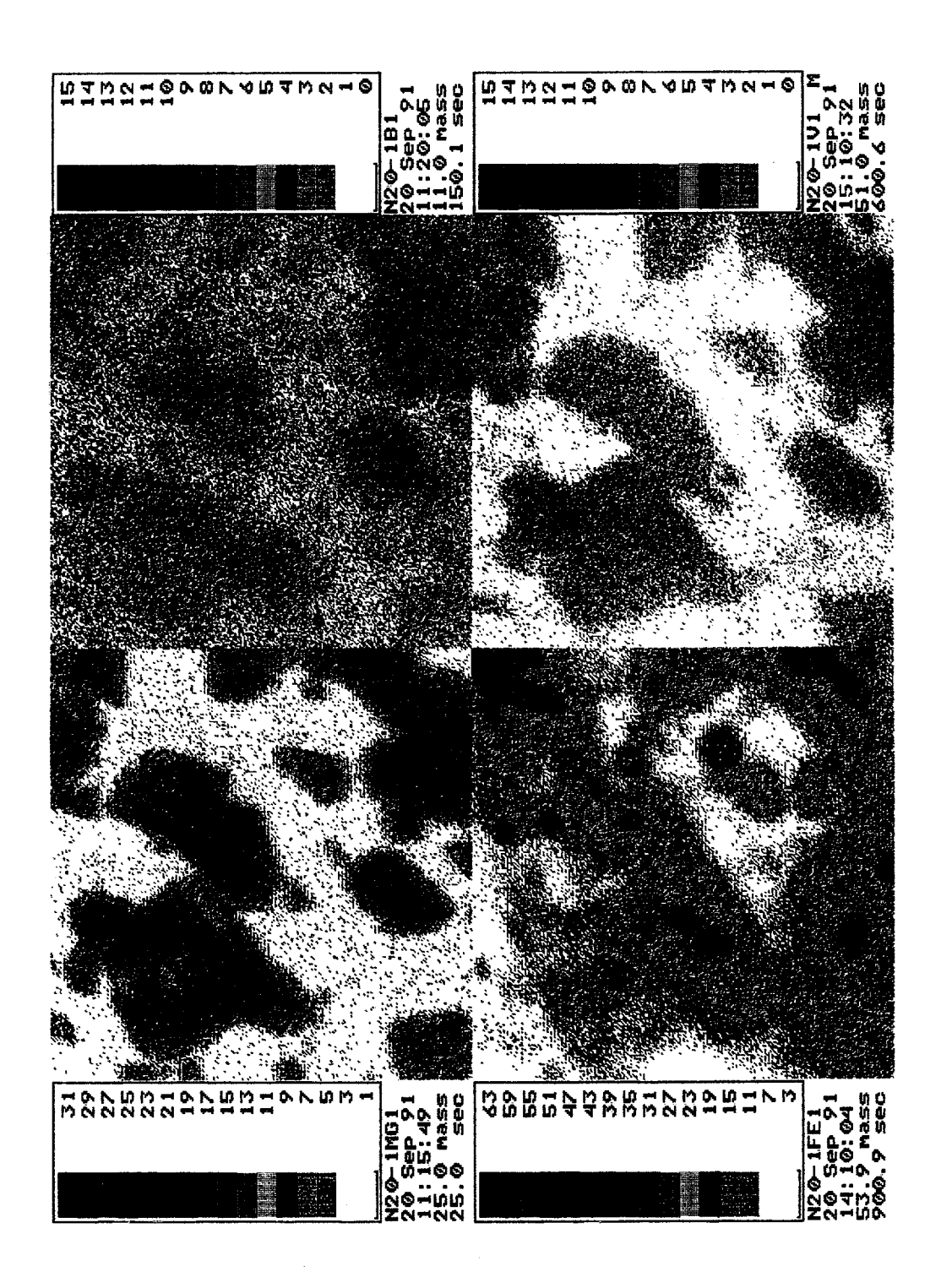
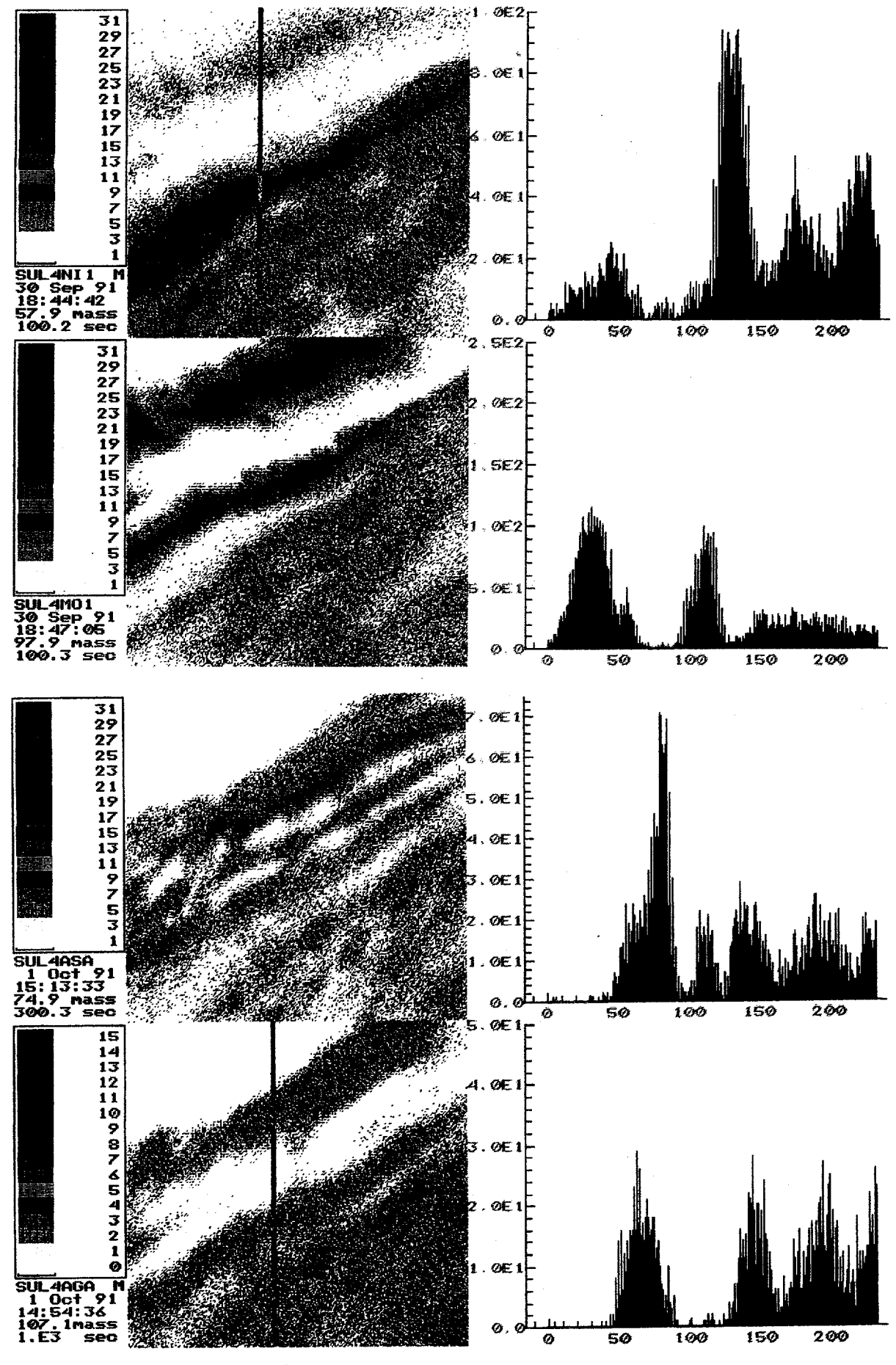


Figure 2: Plots of Ion Intensity ratios vs. elemental concentration ratio M+1/Si Internetry Retto Rb Ba 0.5 5 0.3 W Concentration M/Si 0.2 2 W Concentration MSI 0.05 M+1/9l Internity Ratio 0.6 W Concentration M/SI W Concentration M/Si

Figure 3: Oxygen isotope ratios in magnetite 9 -2 0 φ នុ Measured 180/160 ratio relative to SMOW, uncorrected

175





4.3

Mechano-Chemical Self-Organization and Nonlinear Dynamics in Sedimentary Basins

Peter Ortoleva

Departments of Chemistry and Geological Sciences
Indiana University
Bloomington, IN 47405

The central theme of this project is that the reaction, transport and mechanical (RTM) processes affect each other so strongly that basin diagenesis takes on a qualitatively different behavior than what would be predicted by the analysis of the participating processes separately.

In Figs. 1 and 2 we see schematic basin cross-sections that emphasize a few of the diagenetic phenomena born of the strong coupling of RTM processes. Basin diagenesis allows for a great richness of phenomena including (Fig. 1) the genesis of a (stratum localized) basal seal, dynamic transbasinal top seal, fault related side seals, episodic fluid release and smaller scale compartmentation within and adjacent to the basin-scale overpressured region. Furthermore, (Fig. 2) fingered reaction fronts and upwardly migrating petroleum and auto-localized petroleum (through petroleum-induced porosity preservation) can develop.

The phenomena of Figs 1 and 2 arise through feedback loops in the RTM process network. Examples of feedback loops are given in Figs. 3-5. The feedback loop of Fig. 3 yields flow self-focusing that destabilizes a planar reaction front (such as a redox or dolomitization front) to the formation of fingering. In Fig. 4 we see a feedback loop associated with the coupled dynamics of fluid overpressuring and hydrofracturing that can lead to the episodic release of fluids from depth. Clearly such phenomena can only be understood in terms of the coupled RTM dynamics.

Organic fluids and reactions are of central interest in obtaining a full understanding of diagenesis. Complex feedback coupling relations between organic and inorganic reactions and transport and mechanical processes underlie key aspects of petroleum migration and trapping. Consider the process coupling flow chart of Fig. 5. The observation that some inorganic diagenesis (notably pressure solution and fracture growth and healing) can take place in petroleum saturated rocks under some conditions (stress, temperature and organic chemistry) indicates that the RTM dynamics of a basin is a delicate

577<u>.</u> balance of effects that can be best understood via an integrated research approach.

Two conditions necessary for temporally oscillatory, spatially organized and other behavior are nonlinearity in the dependence of the rate of participating processes and displacement from thermodynamic equilibrium. These conditions are obtained in the sedimentary basin. Nonlinear systems have been extensively studied over the last two decades and, more recently, in the context of geological RTM systems (Ortoleva et al., 1987, 1990; Ortoleva, 1991a,b; Dewers and Ortoleva, 1988, 1991). A partial list of the nonlinear phenomena that have been identified to date is the following (Dewers and Ortoleva, 1988; Ortoleva, 1991a,b; Ortoleva and Dewers, 1992).

- 1. Oscillatory intra-crystal zoning in calcite (Ortoleva, 1990, 1991, 1992; Reeder et al., 1990).
- 2. Repetitive episodic fluid release from depth see Fig. 1 (Dewers and Ortoleva, 1991a; Ortoleva and Al-Shaieb, 1992).
- 3. Diagenetically differentiated marl/limestone bedding (Ricken, 1986; Dewers and Ortoleva, 1991b; Ortoleva et al., 1991).
- 4. Differentiated compaction/cementation bands in sandstones (Dewers and Ortoleva, 1990a-d, 1992).
- 5. Stylolite arrays (Ricken, 1986; Dewers and Ortoleva, 1990a-d, 1991, 1992).
- 6. Reaction front fingering (Chadam et al., 1986, 1988, 1990; Chen and Ortoleva, 1990a,b, 1992; Chen et al., 1990, 1991).
- 7. Oscillatory and fingered petroleum migration (Chen et al., 1990; Park et al., 1990; Ghaith et al., 1990).
- 8. Concretion growth through pressure of crystallization (Dewers and Ortoleva, 1990e).

Our approach to these problems is to develop quantitative RTM models and analyze them by simulating the models on computers. As a result we can identify phenomena that can take place and the range of conditions (basin tectonics and thermal history, sedimentology and mineralogy, and texture) favorable for their existence.

Technical challenges one encounters in such modeling studies are due to the enormity of the calculations. To meet them we are using homogenization theory, adaptive spatial gridding, specially designed linear solvers (preconditioned conjugate gradient-squared) and efficient procedures for handling systems of general chemistry. With this and parallel computation we are making the simulation of basin diagenesis in two and three spatial dimensions feasible.

Specific preliminary results obtained in the first 6 months of this three year project are as follows:

- 1. During subsidence and burial there can exist a front rising through the incoming sediment pile as suggested in Fig.1; in a range of conditions, this compaction/overpressuring/hydrofracturing front can become oscillatory and result in a series of fluid release episodes.
- 2. Arrays of centimeter scale diagenetically differentiated structures (such as stylolites and diagenetic bedding) in systems of 100 meter to suprakilometer scale present a challenging problem for numerical analysis; standard numerical techniques would require so many grid points as to make calculations unfeasible. In our studies we take a computational homogenization approach. Our results demonstrate that this approach will be a major step in the simulation of small scale (diagenetic or sedimentary) heterogeneity in basin dynamics. We find that the interplay of long and short scales provides the basis of key elements of basin diagenesis.
- 3. A number of technical problems had to be solved in order to carry out the simulation of a basin in two and three spatial dimensions. Work to date has produced (a) a moving finite element code to solve the poro-elasticity problem, (b) the design of parallelizable algorithms for the simulation of homogenization problems and (c) a preliminary three dimensional RTM basin simulator.

The work in progress indicated in item 3 above shall enable us to complete the studies of items 1 and 2 above and to extend these studies in year 2. Emphasis in year 2 will be on the spatial localization (in two and three dimensions) of episodic fluid release and the analysis of the multiple-scale phenomena associated with stylolites and diagenetic bedding and the kilometer scale migration and trapping of fluids. A multiple mineral poro-elastic rock rheology, and pressure solution model including the effects of the coupling of organic fluids migration and storage to pressure solution will also be developed. As a result of the latter, petroleum may become auto-localized to porosity-preserving pools as suggested in Fig. 2. From results obtained so far, we believe that important new insights are obtained by considering a basin undergoing diagenesis to be a strongly coupled nonlinear dynamical system.

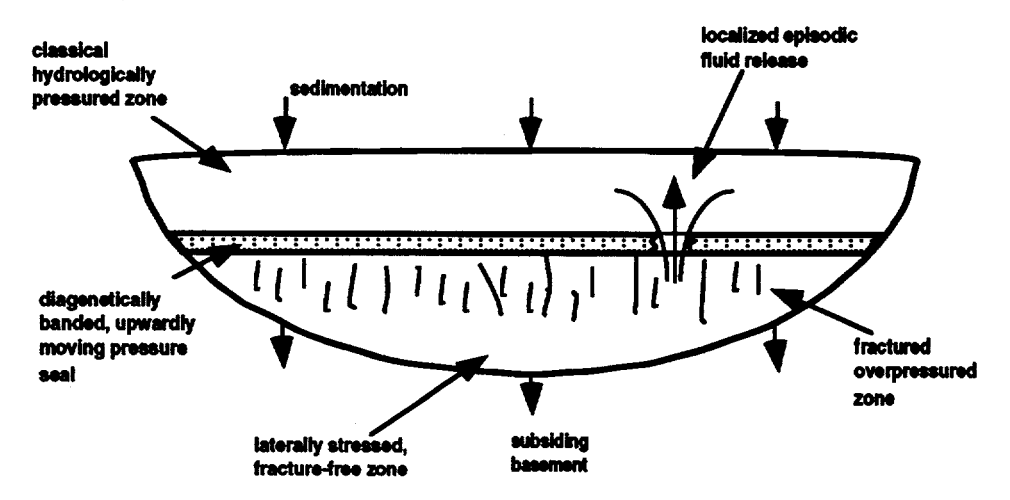


Fig. 1 Sedimentation leads to compaction in the normally pressured (classical) hydrologically pressured zone; at sufficient depth of burial, pressure solution can lead to diagenetically banded, low permeability rock (pressure seal) and create underlying overpressure ("geopressure"). As a result of the overpressure, hydraulic fracturing can occur resulting in local release of fluid in a series of episodes. At greater depth horizontal stresses tend to approach the vertical lithostatic stress and hydro-fracturing is thereby repressed.

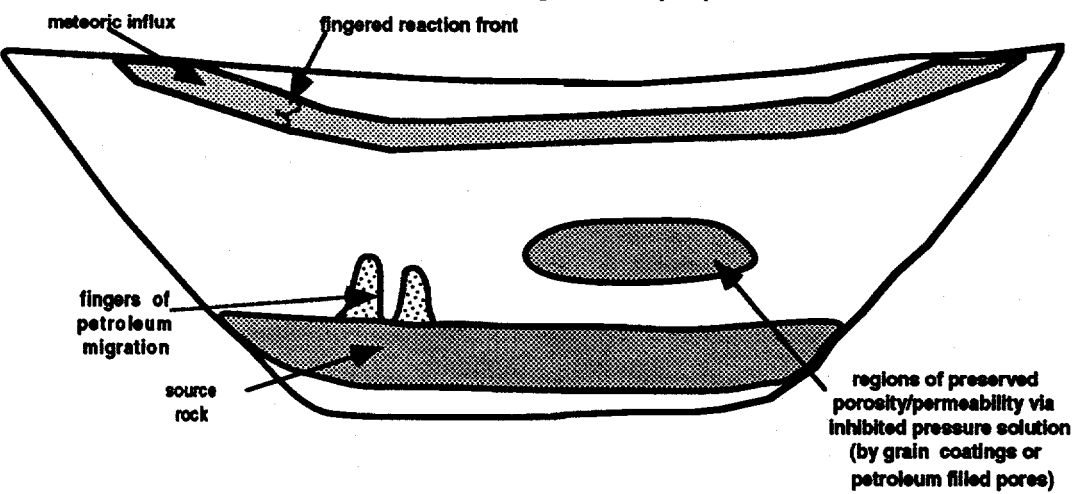


Fig. 2 Schematic cross-section of a basin suggesting other types of phenomena that could arise through well established physico-chemical diagenetic processes.

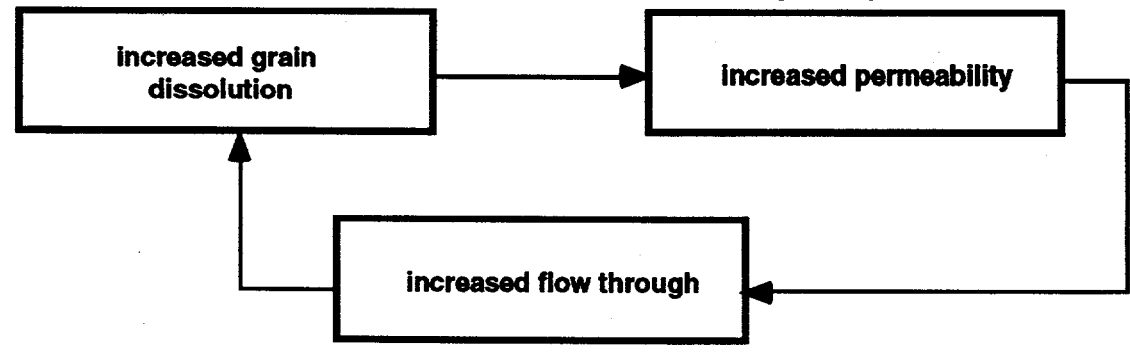
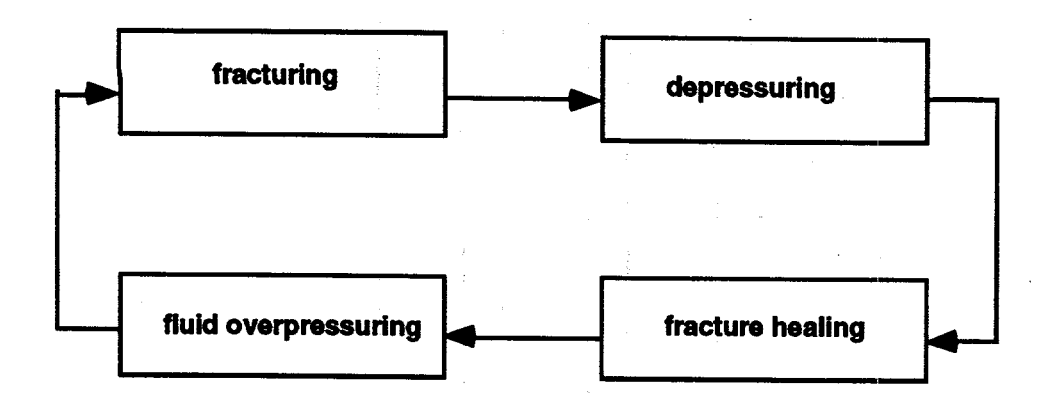


Fig. 3 Flow self-focusing feedback loop arising from the coupling of flow and dissolution through the texture dependence of the permeability.



1925

Fig. 4 Oscillatory, episodic fluid release cycle due to coupled fracturing, fluid flow and fracture healing dynamics.

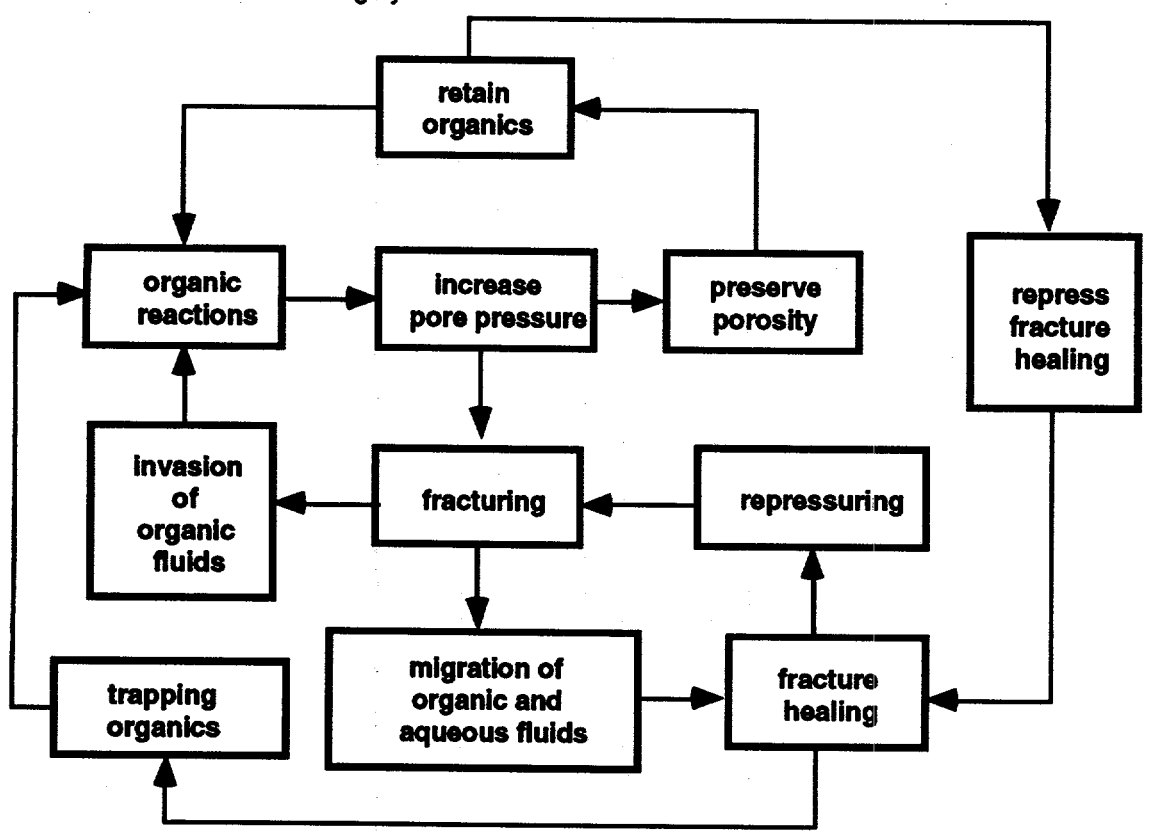


Fig. 5 Coupling of organic and inorganic reactions, transport and fracturing and pressure solution can sustain nonlinear feedback that results in episodic petroleum migration and the petroleum mediated development of petroleum reservoirs.

DEVELOPMENT OF AN EXPERIMENTAL DATA BASE AND THEORIES FOR PREDICTION OF THERMODYNAMIC PROPERTIES OF AQUEOUS ELECTROLYTES AND NONELECTROLYTES OF GEOCHEMICAL SIGNIFICANCE AT SUPERCRITICAL TEMPERATURES AND PRESSURES

Robert H. Wood, Lubomir Hnedkovsky, and Ching Lung Lin

Department of Chemistry and Biochemistry University of Delaware Newark, DE 19716

and

Everett L. Shock Department of Earth and Planetary Sciences Washington University St.Louis, MO 63130

INTRODUCTION

A detailed analysis of the processes that lead to the formation, migration, and accumulation of petroleum hydrocarbons is of vital economic and strategic importance. So too is the study of processes which govern the transport and deposition of metals and other inorganic species in sedimentary basins and in hydrothermal systems. Consideration of stable and metastable equilibria involving these aqueous species, minerals, gases, and condensed phases (solid and liquid) can lead to a more comprehensive understanding of a wide variety of geochemical processes, but requires accurate thermodynamic data for aqueous species at high pressures and temperatures. The long-term goals of this research are to create an experimental database and set of theoretical models which will allow accurate prediction of the thermodynamic properties of any aqueous solution component of significance to geochemical processes from normal surface conditions to the temperatures and pressures at which crustal rocks begin to melt. As a first step towards this goal we are measuring volumes and heat capacities of aqueous solutions of $\rm H_2S$, $\rm CO_2$, $\rm CH_4$, $\rm NH_3$, $\rm H_3BO_3$, and $\rm CH_3COOH$, species of great geochemical significance. The second goal is to use this vastly expanded data base to both test existing theories and predictive methods and to develop new and highly refined theoretical approaches. As a result of our measurements the available high temperature calorimetric and volumetric data on aqueous nonelectrolytes will be roughly tripled. The free energies at any temperature and pressure are readily calculated from the well known values of enthalpies and free energies at 298.15 K and 1 bar, together with heat capacities and volumes at all T and P. Thus, the present measurements will yield more accurate values for free energies of these species from 25°C to ~430°C.

An undertaking of this type overlaps the field of physical chemistry and geochemistry. The success of this project depends upon the interdisciplinary combination of the expertise of three of us (RHW, LH, and CLL) in making these types of high temperature measurements and using physical chemical theories to model the results, together with the expertise of the other author (ELS) in developing geochemically applicable models for thermodynamic properties, fitting experimental data, and making extrapolations to higher temperatures and pressures, and finally applying the calculated thermodynamic properties to studies of the consequences of fluid rock interactions.

EXPERIMENTAL MEASUREMENTS

Before starting measurements on these solutions, it was convenient to first find methods of storing and dispensing aqueous solutions of the solute in such a way that the concentration didn't change rapidly with time. The $\rm H_2S$ and $\rm CO_2$ were stored in PVC pipes under a pressure of about 5 atm with the solutions being contained in an inner, aluminized mylar bag and expelled from the container by pumping water into the outer chamber of the vessel, thereby expelling the solution from inside the mylar bag. For methane, pressures of 100 bar are necessary, so we used a stainless steel bomb with a separator that moves up and down within the bomb to separate the aqueous methane solution from the driving fluid.

Heat capacity measurements will be measured with the flow, heat capacity apparatus developed previously (Biggerstaff et al., 1988; Carter and Wood, 1991). This apparatus measures the change in electric power necessary to keep the same temperature rise when switching from pure water to an aqueous solution in the flow stream. Recently this apparatus has been used to measure the heat

capacities of aqueous electrolytes at pressures to 335 MPa and temperatures to and 425°C (Carter, R. W., Ph.D. thesis, in preparation).

The densities have been measured with a vibrating tube densimeter described previously (Majer et al., 1991). Briefly, the densimeter measures the density of the aqueous solution relative to the density of pure water at the same temperature and pressure by measuring the period of a vibrating tube filled with the solution. The apparatus is calibrated using pure water and helium gas under pressure. The difference in density between pure water and a solution can be measured with an accuracy of about $\pm 0.5\%$ and with a sensitivity of about 10^{-4} g/cm³.

RESULTS

The results of some of the volumetric measurements are given in Figures 1-3. The results show apparent molar volumes which are roughly proportional to the compressibility of pure water which peaks near 400°C at 28 MPa. This same behavior was observed in earlier measurements in this laboratory on argon, ethylene and xenon (Biggerstaff and Wood, 1988) and in exploratory measurements on CO_2 at high temperatures (Crovetto et al., 1990, 1991). This new volumetric data will allow reasonable extrapolation of the experimental solubilities of these gases at saturation pressure to high pressures. Solubilities of these gases have been measured up to about 350°C and the accuracy of the measurements is quite good up to 250°C, but the measurements get much more difficult and less accurate above this temperature. The heat capacity data will allow confirmation of these solubility results and calculation of the free energy of the aqueous species up to 425°C with pressures to 350 bar by integration of the heat capacity and volume results.

In addition, reasonable extrapolation to higher temperatures and pressures are possible.

THEORETICAL MODELS

The recent increases in computing power now allow a whole new approach to the prediction of the properties of very high temperature aqueous solutions. Given a law of the forces between the atoms in the molecules of the solution, one can integrate Newton's laws of motion for these forces for say 300 molecules, allow them to equilibrate at any temperature desired, and by appropriate averaging of the properties calculate all of the thermodynamic properties for this model system. Of course the model compounds are not the real world, but the models for these species are becoming more and more accurate and by fitting the models to experimental data at lower temperatures, one can then extrapolate these models of the forces between atoms to estimate the properties of real solutions. The sensitivity of the predictions to the model parameters can also be assessed. The extrapolations have the advantage that the forces between atoms in the real world are independent of temperature.

We are primarily interested in the partial molar free energies of these gases at temperatures to 1000°C. The advantage of this kind of calculation is that it can be done at any temperature and pressure without any "experimental" problems. In a sense these are experimental results but in a model universe, that is, not the real universe.

One problem with these measurements is there have not been reliable ways to estimate the numerical accuracy with which free energies can be calculated by

this procedure. Our first step in this project was to develop methods for estimating the systematic error due to the lag of the system configuration behind the Hamiltonian (Wood, 1991), and the systematic error due to the use of finite samples of configuration space in calculating the free energy (Wood and Müehlbauer, 1991).

The results of the calculations on the solubility of model methane in model water will be presented.

DISCUSSION

The volumetric measurements for aqueous nonelectrolytes described above permit revision of data and methods used to calculate thermodynamic properties of these species in fluid-driven geochemical processes. We are presently pursuing two approaches to these revisions. First, the revised Helgeson-Kirkham-Flowers (HKF) equations of state adopted by Shock et al. (1989) for aqueous nonelectrolytes are being used to regress the new data and obtain revised equation-of-state parameters. These parameters will allow improvements in the accuracy of predicted thermodynamic data calculated with the revised HKF equation throughout crustal conditions. Revised parameters will be presented in a format which will allow easy updating of the data files for the SUPCRT92 program recently made available to the geochemical community. These revisions should help resolve some existing inconsistencies in nonelectrolyte properties as described below. Secondly, the new experimental data will be used to develop a new equation of state for geochemical calculations involving aqueous nonelectrolytes based on the density of $\rm H_2O$ rather than on its dielectric constant. Such an equation of state should be more intrinsically appealing as it will eliminate the need to evaluate effective Born coefficients which imply that formally neutral aqueous species have fractional charges. However, only if it retains and enhances predictive power will such an equation of state be as useful as the revised HKF equations for geochemical calculations. Therefore, considerable effort will go toward constructing correlations to estimate data for the multitude of nonelectrolytes (inorganic and organic) involved in geochemical processes for which experimental data may never be collected.

An example of the utility of the data already collected can be illustrated by considering aqueous CO_2 . As shown in Figure 4 there is considerable divergence of calculated values of log K for carbonic acid dissociation (curves) and those determined experimentally (symbols) at pressures other than the vapor-liquid saturation pressures for H_2O (Psat). The curves in Figure 4 were calculated with equations, data and parameters from Shock et al. (1989). Part of the problem has been revealed by the lack of agreement between predicted values of V_2° for CO_2 and those measured as described above. Apparently, the magnitude of the effective Born coefficient obtained by Shock et al. (1989) by regression of CO_2 solubility data together with the Psat data in Figure 4 is too low. New regression results indicate that this coefficient should be at least an order of magnitude greater. These results help to identify the problem, but the complete solution will require the heat capacity measurements currently underway.

Meanwhile, other lines of evidence confirm that the calculations shown in Figure 4 should be revised. Many metamorphic petrologists have conducted experiments to determine the effects of changing the mole fraction of $\rm CO_2$ in $\rm CO_2$ -H₂O fluids on the stabilities of mineral assemblages. The data collected at the lowest mole fractions of $\rm CO_2$, combined with thermodynamic data for minerals, H₂O

and other aqueous species, allow retrieval of well-constrained estimates of log K for carbonic acid dissociation at supercritical conditions (Bvhlke and Shock, 1990; and in prep.). These values of log K, which extend temperatures above 600°C and pressures to 7 kb, connect smoothly with Read's data shown in Figure 4. Combined regression of these log K estimates with the volumetric and calorimetric data obtained in the present project will allow improved geochemical calculations with a new set of HKF parameters. As a result, it may be possible to reconcile differences in calculation methods and conceptual approaches to $\rm CO_2$ -H₂O fluids taken by aqueous geochemists and metamorphic petrologists. Applications of these results include studies of $\rm CO_2$ speciation in fluid inclusions, generation of gold-quartz veins in the Mother Lode of California, albite/carbonate metasomatism by sodium bicarbonate fluids, and many other metamorphic-hydrothermal processes.

REFERENCES

Biggerstaff, D. R., White, D. E. and Wood, R. H. (1988) Apparent molar heat capacities of aqueous argon, ethylene, and xenon at temperatures up to 720 K and pressures to 33 MPa. <u>J. Phys. Chem.</u> 92, 1994-2000.

Burlke, J. K. and Shock, E. L. (1990) Carbonic acid dissociation in aqueous metamorphic fluids. (abs.) Geol. Soc. Amer. Abstracts with Programs 22, A348.

Carter, R. W. and Wood, R. H. (1991) Calibration and sample measurement techniques for flow heat capacity calorimeters. J. Chem. Thermodyn. in press.

Carter, R. W. Ph.D. Thesis, in preparation.

Crovetto, R., Wood, R. H. and Majer, V. (1990) Densities of $\{\times CO_2 + (1-\times)H_2O\}$ with $\times < 0.014$ at supercritical conditions. Molar volumes, partial molar volumes of CO_2 at infinite dilution, and excess molar volumes. J. Chem. Thermodynamics 22, 231-243.

Crovetto, R., Wood, R. H. and Majer, V. (1991) Revised densities of dilute aqueous CO_2 mixtures of $\{xCO_2 + (1-x)H_2O\}$ with x < 0.014 at supercritical conditions. Molar volume, partial molar volume of CO_2 at infinite dilution, and excess volumes, by R. Crovetto, R. H. Wood and V. Majer, <u>J. Chem. Thermodynamics</u>, in press.

Majer, V., Crovetto, R. and Wood, R. H. (1991) A new version of vibrating-tube flow densimeter for measuring up to 730 K. <u>J. Chem. Thermodynamics</u> 23, 333-344.

Shock, E. L., Helgeson, H. C., and Sverjensky, D. A. (1989) Calculation of the thermodynamic and transport properties of aqueous species at high pressures and temperatures: Standard partial molal properties of inorganic neutral species Geochim, Cosmochim, Acta 53, 2157-2183.

Wood, R. H. and Muehlbauer, W. C. F. (1991) Systematic errors in free energy perturbation calculations due to finite sample size: Sample-size hysteresis. <u>J. Phys. Chem.</u> **95**, 6670-75.

Wood, R. H. (1991) Estimation of errors in free energy calculations due to the lag between the Hamiltonian and the system configuration. \underline{J} . Phys. Chem. 95, 4838-42.

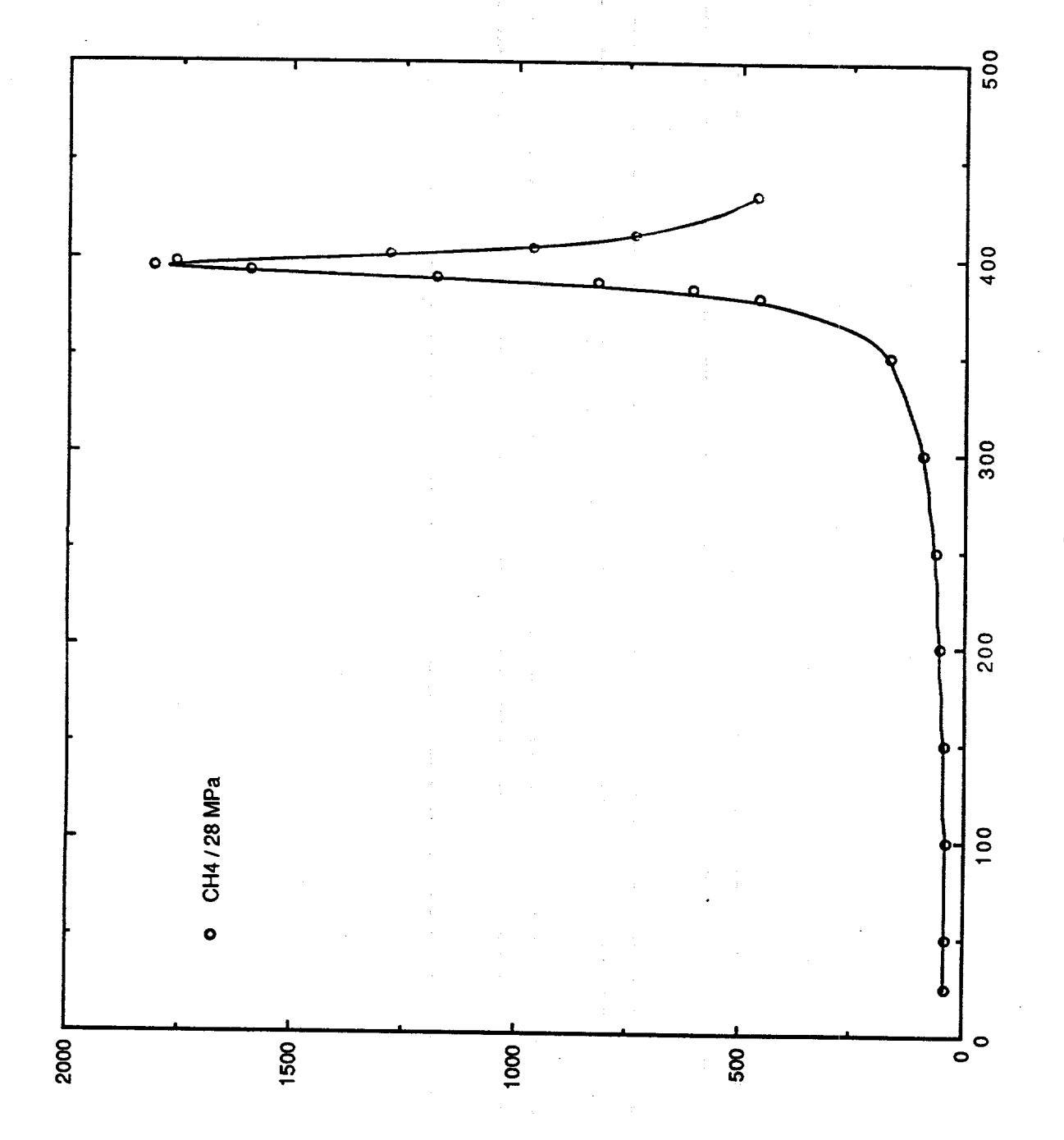


Figure 1. Apparent molar volume of $\text{CH}_4(\text{aq})$, 0.113 mol/kg) at 28 MPa vs. temperature.

apparent molar volume

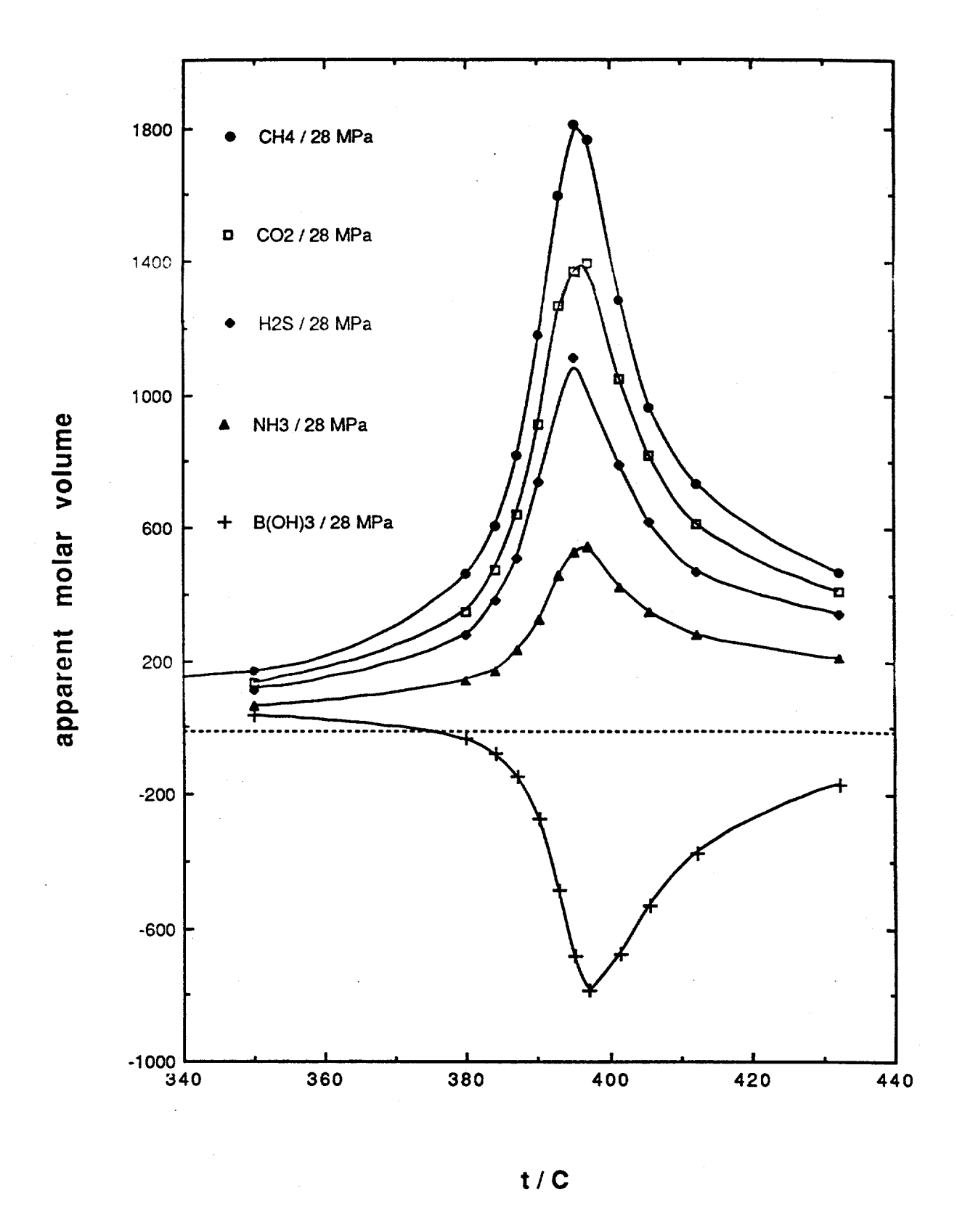
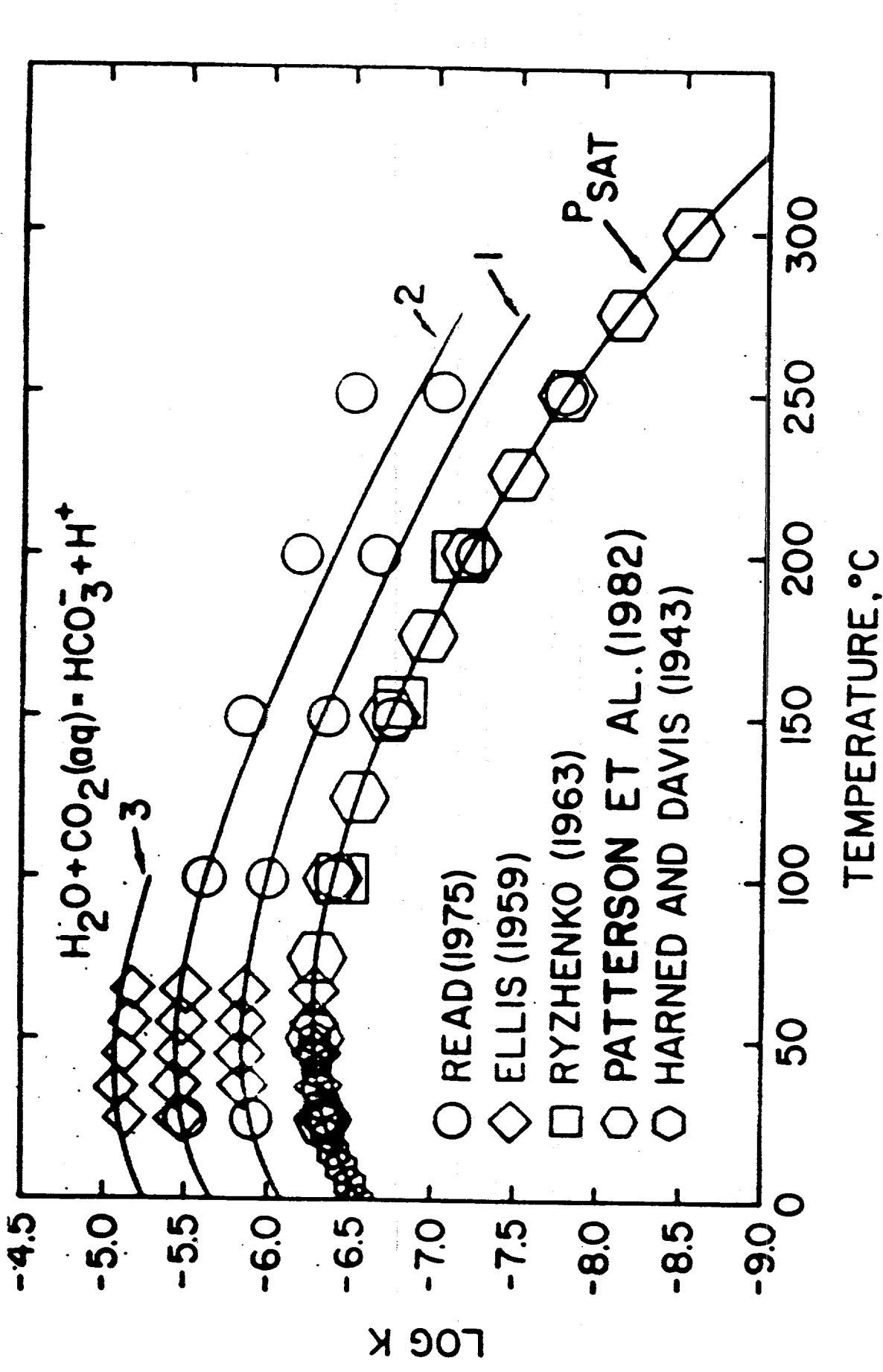


Figure 2. Apparent molar volume of CH_4 (aq, 0.113 mol/kg), CO_2 (aq, 0.115 mol/kg), H_2S (aq., 0.235 mol/kg), NH_3 (aq, 0.2 mol/kg), and $B(OH)_3$ (aq, 0.2 mol/kg) at 28 MPa vs. temperature.



function of temperature and pressure. The lines are the predictions of Shock Figure 3. Log [K], the logarithm of the acid dissociation constant as a et al. (1989) at 3 kbar, 2 kbar, 1 kbar, and Psat.

190

GEOCHEMISTRY OF CRUSTAL PROCESSES TO HIGH TEMPERATURES AND PRESSURES

SUBPROJECT:

THE SOLUBILITY OF CALCITE AND DOLOMITE TO TEMPERATURES OF 300 °C AND PRESSURES OF 1.3 KBARS*

D. R. Cole, D. J. Wesolowski, and S. E. Drummond

Chemistry Division
Oak Ridge National Laboratory
Oak Ridge, TN 37831-6110

Highly accurate measurements of the solubilities of calcite and dolomite are needed in order to model diagenesis and the development of secondary porosity in sedimentary basins because (1) both are common diagenetic phases, and (2) the dolomitization of limestone involves a ~14.2% volume reduction. Equilibrium constants have been determined for the principle reactions that control the solubility of calcite and dolomite in hydrothermal solutions:

$$CaCO_3 + H_2O + CO_2 \neq Ca^{2+} + 2HCO_3^{-}$$

1/2CaMg(CO₃)₂ +H₂O +CO₂ \neq 1/2Ca²⁺ + 1/2Mg²⁺ + 2HCO₃

at temperatures up to $300 \,^{\circ}\text{C}$ (± $0.1 \,^{\circ}\text{C}$) and pressures of 300, 800, and 1300 bars (± 1 bar). Two types of experiments were conducted in gold-bag rocking autoclaves (see Table 1). In one case, a co-solubility approach was used wherein equal molar proportions of calcite and dolomite were reacted with H_2O and CO_2 . It was necessary to adopt this approach because one cannot measure the solubility of dolomite by itself due to its incongruent dissolution behavior (except at or below $50\,^{\circ}\text{C}$). Because the crystalline solution between calcite and dolomite is negligible below $300\,^{\circ}\text{C}$ (Anovitz and Essene, 1989), the solubilities of both minerals are determined from a single experiment by measuring the ΣCa , ΣMg , and ΣCO_2 in solution. In this approach, $Ca^{2+} + Mg^{2+}$ are in stoichiometric proportion to HCO_3 so that we need not measure the HCO_3 concentration. The second type of experiment involved the reaction of calcite with H_2O and CO_2 . It was assumed that the Ca^{2+} concentration was in stoichiometric proportion to the HCO_3 .

Approximately one gram of solid (calcite + dolomite; calcite only) was reacted with water ranging in mass from 250 to 300 gms for durations of between 2 and 60 days at a given P and T. Total CO₂ concentrations were varied from approximately 0.05 to 1.0 m.

^{*}Research sponsored by the Division of Engineering and Geosciences, Office of Basic Energy Sciences, U.S. Department of Energy under contract DE-AC05-84OR21400 with Martin Marietta Energy Systems, Inc.

The cation concentrations were measured by either ion chromatography or atomic absorption spectroscopy, and ΣCO_2 was determined by acid/base titration. Analytical precisions for Ca^{2+} and Mg^{2+} were on the order of 1 to 1.5% and ΣCO_2 measurements are good to about $\pm 1\%$. The ionic strengths ranged from a low of 0.0008 to 0.07. Two criteria were used to demonstrate that equilibrium had been attained--(1) establishment of steady state concentrations of Ca^{2+} and Mg^{2+} as a function of time at a given P and T, and (2) reversal of each experiment by ramping up and down pressure at a constant temperature.

Treatment of the data to generate log K values for the reactions given above involved the use of NaCl(aq) as a model substance. This approach was taken because: (1) the ionic strengths in the experiments were very low, less then 0.07, (2) the Debye-Hückel slopes at low ionic strengths are controlled by the ions, and (3) data for NaCl is of high quality for the P, T, and I ranges of the experiments. We assumed the following: $\gamma_{CO_2} = 1$, $\gamma_{HCO_3} = \gamma_{\pm NaCl}$, $\gamma_{Ca^{2+}} = \gamma_{\pm NaCl}^4$ (calcite only), and $\gamma_{Ca^{2+}}^{0.5} \cdot \gamma_{Mg^{2+}}^{0.5} = \gamma_{\pm NaCl}^4$ (calcite/dolomite experiments). Data for $\gamma_{\pm NaCl}$ and $\alpha_{H_{2O}}$ were taken from Pitzer et al. (1984). The log K values at infinite dilution for calcite and dolomite are shown in Figs. 1 and 2, respectively. These data exhibit systematic retrograde behavior with non-zero heat capacities for the reactions. The curves are derived from least-squares fits to all the data as a function of T and density of water at each P and T. By ramping up (triangles, circles) and down (squares, inverted triangles) pressure at a fixed temperature, we have reversed these experiments to within approximately 10%. Clearly, dolomite solubility is less than calcite. At 300 bars, log K_{calcite} values range from -4.45 at $50\,^{\circ}$ C to -10.19 at $300\,^{\circ}$ C whereas log K_{dolomite} values range from -4.73 to -10.67 for the same temperature interval. Extrapolated log K values for calcite to low pressure conditions (1/v) agree well with calcite data given by Ellis (1959) and Plummer and Busenberg (1982). An increase in pressure results in an increase in solubility and this effect becomes more pronounced with increasing temperatures. For example, an increase of 1000 bars leads to an increase in solubility of calcite or dolomite by factors of about 6 at 100 °C and nearly 80 at 300 °C. This non-linear behavior can best be normalized by a function that relates the log K values with the density of water. Examples of this behavior are given in Figs. 3 and 4 for 100° and 200°C, respectively. Note that the straight lines on these figures are derived from the best fits of all the data. The non-linear behavior indicates that pressure changes in sedimentary basins containing carbonate may play an important role in porosity development and accompanying fluid migration.

REFERENCES

- Anovitz, L. M. and Essence, E. J. (1987) Phase equilibria in the system CaCO₃-MgCO₃-FeCO₃. J. Petrol. 28, 389-414.
- Ellis, A. J. (1959) The solubility of calcite in carbon dioxide solutions. Amer. J. Sci. 257, 354-365.
- Plummer, L. N. and Busenberg, E. (1982) The solubilities of calcite, aragonite, and vaterite in CO₂-H₂O solutions between 0 and 90 °C, and an evaluation of the aqueous model for the system CaCO₃-CO₂-H₂O. Geochim. Cosmochim. Acta 46, 1011-1040.

Pitzer, K. S., Peiper, J. C. and Busey, R. H. (1984) Thermodynamic properties of aqueous sodium chloride solutions. J. Phys. Chem. Ref. Data. 13, 1-101.

FIGURE CAPTIONS

- 1. Log of the equilibrium constant (K) for calcite reacted with H₂O and CO₂ plotted against log T (°K) for data from both the co-solubility and calcite-only experiments at 300, 800, and 1300 bars. Curves represent the least-squares best fits through all calcite data. The l/v curve is an extrapolation to liquid/vapor pressures from a fit to our high pressure data. Triangles and circles represent experiments coming from under saturation for co-solubility and calcite-only runs, respectively. Squares and inverted triangles represent experiments coming from over saturation for co-solubility and calcite runs, respectively.
- 2. Log of the equilibrium constant (K) for dolomite reacted with H₂O and CO₂ from cosolubility experiments at 300, 800, and 1300 bars. Curves represent the least-squares best fits through all dolomite data. Symbols are the same as described for Fig. 1.
- 3. Log K values for calcite and dolomite plotted against log density of water at 100 °C. Symbols are the same as described for Fig. 1.
- 4. Log K values for calcite and dolomite plotted against log density of water at 200 °C. Symbols are the same as described for Fig. 1.

EXPERIMENTAL CONDITIONS

CO-SOLUBILITY:

Temperature(°C): 50

50, 100, 150, 200, 250, 300

Pressure(bars) :

300, 800, 1300

CO₂ Concentration:

0.0476 to 0.932 m; I = 0.0008 to 0.05

Duration:

20 to 140 days(for reversal at const. T)

CALCITE ONLY

30, 50, 100, 150, 200, 250

Pressure(bars) :

Temperature(°C):

300, 800, 1300

CO₂ Concentration:

0.105; 0.697 m; I = 0.0025 to 0.07

Duration:

170 to 200 days(for reversal at const. T)

Figure 1

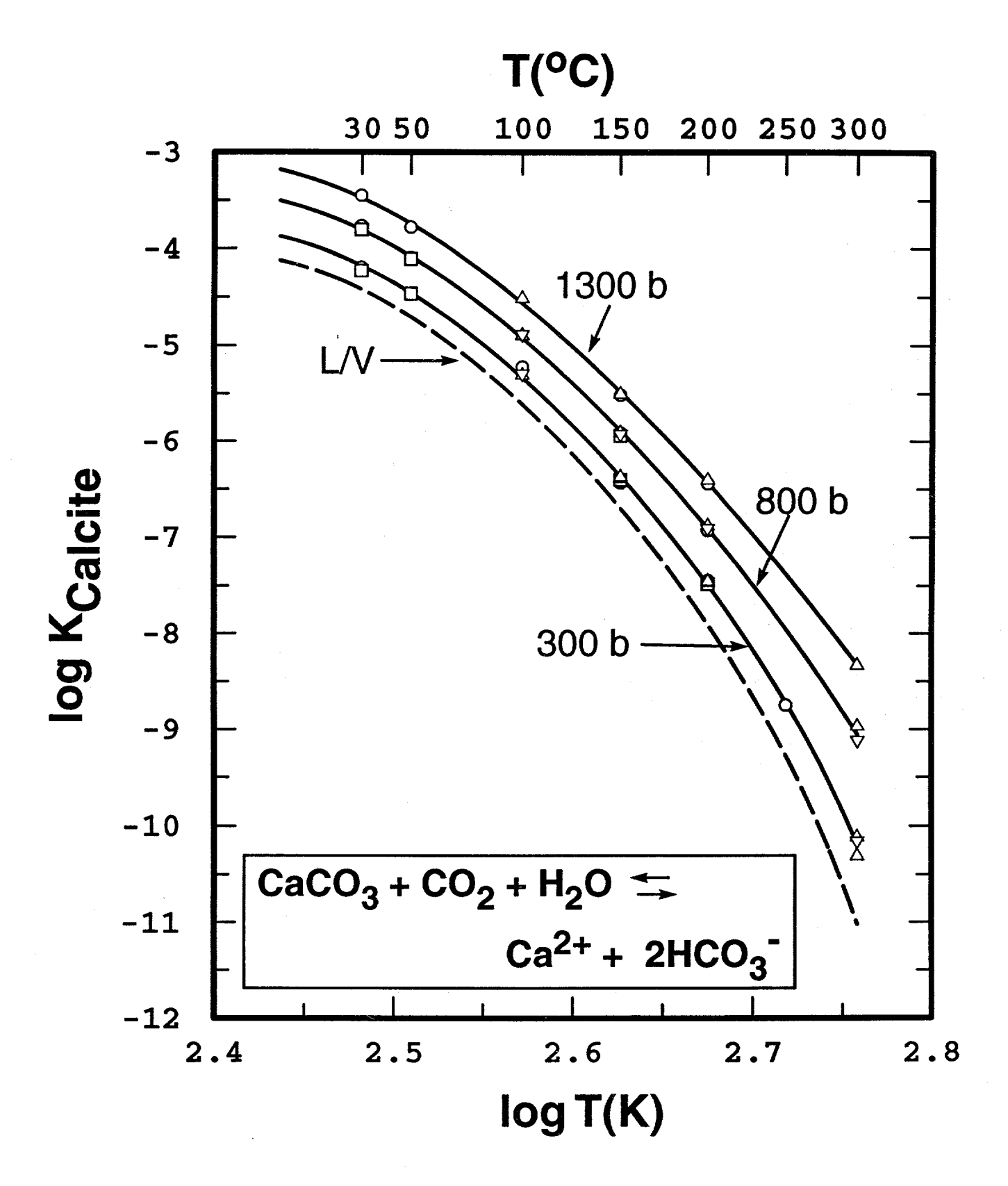


Figure 2

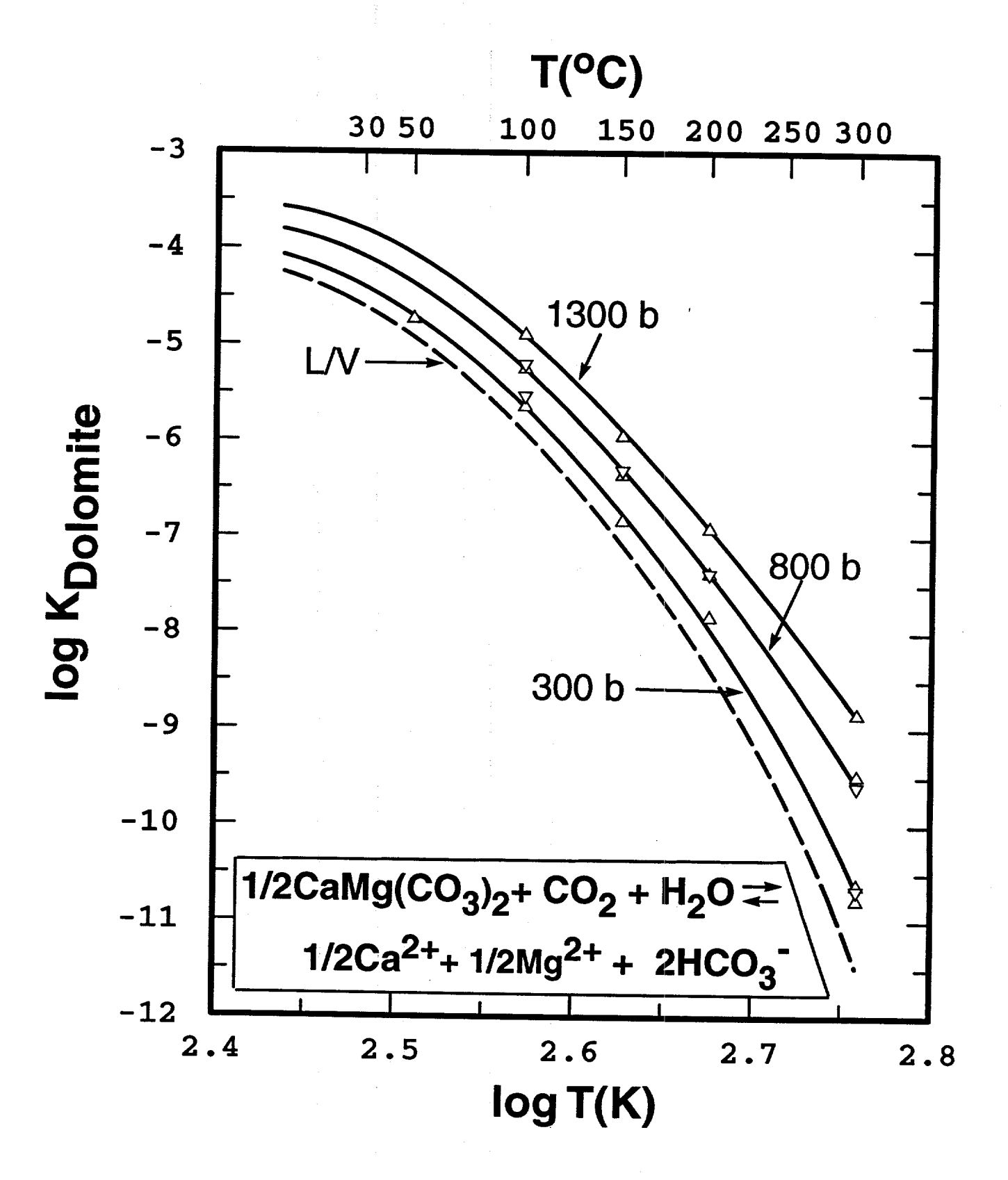


Figure 3

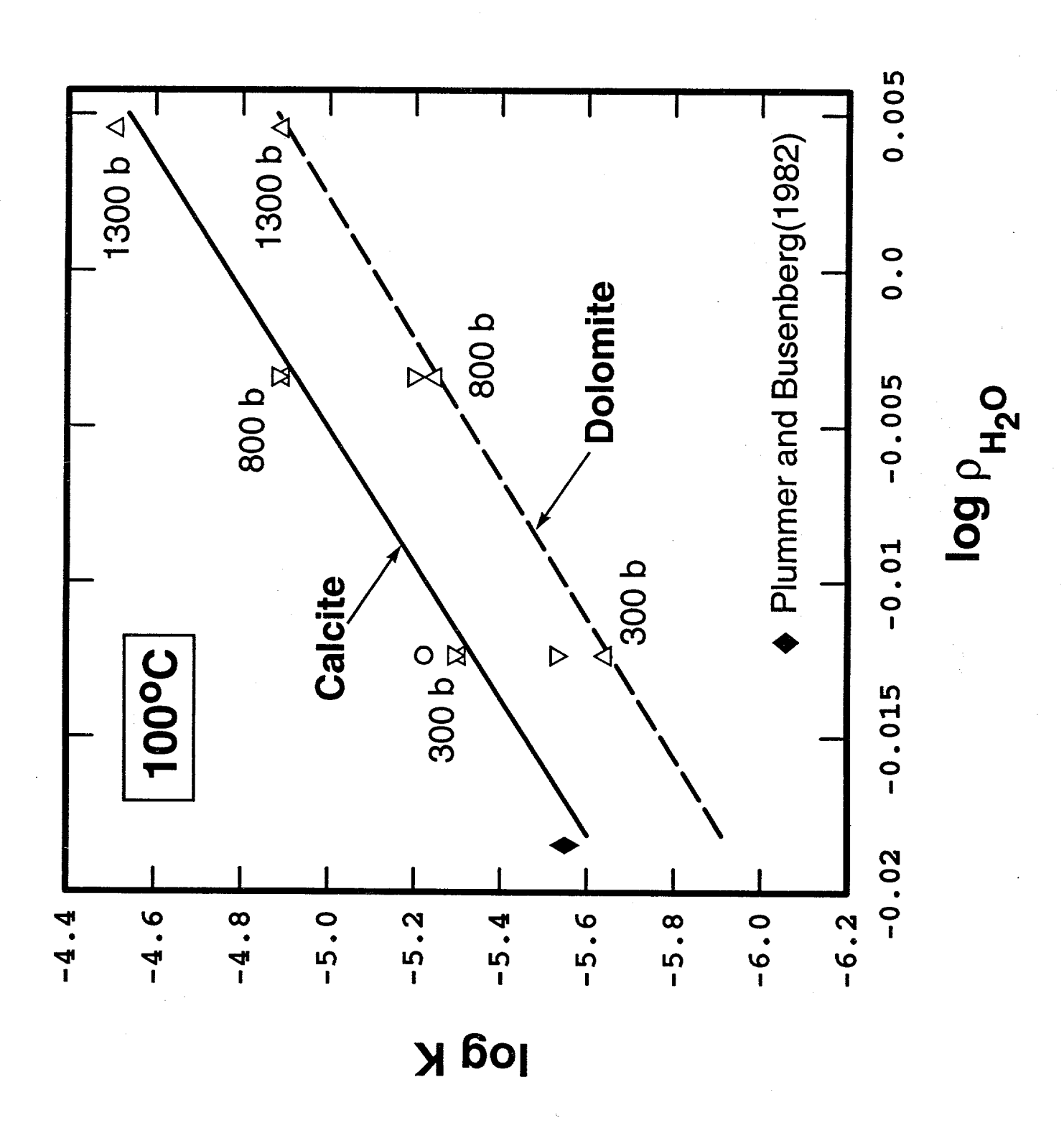
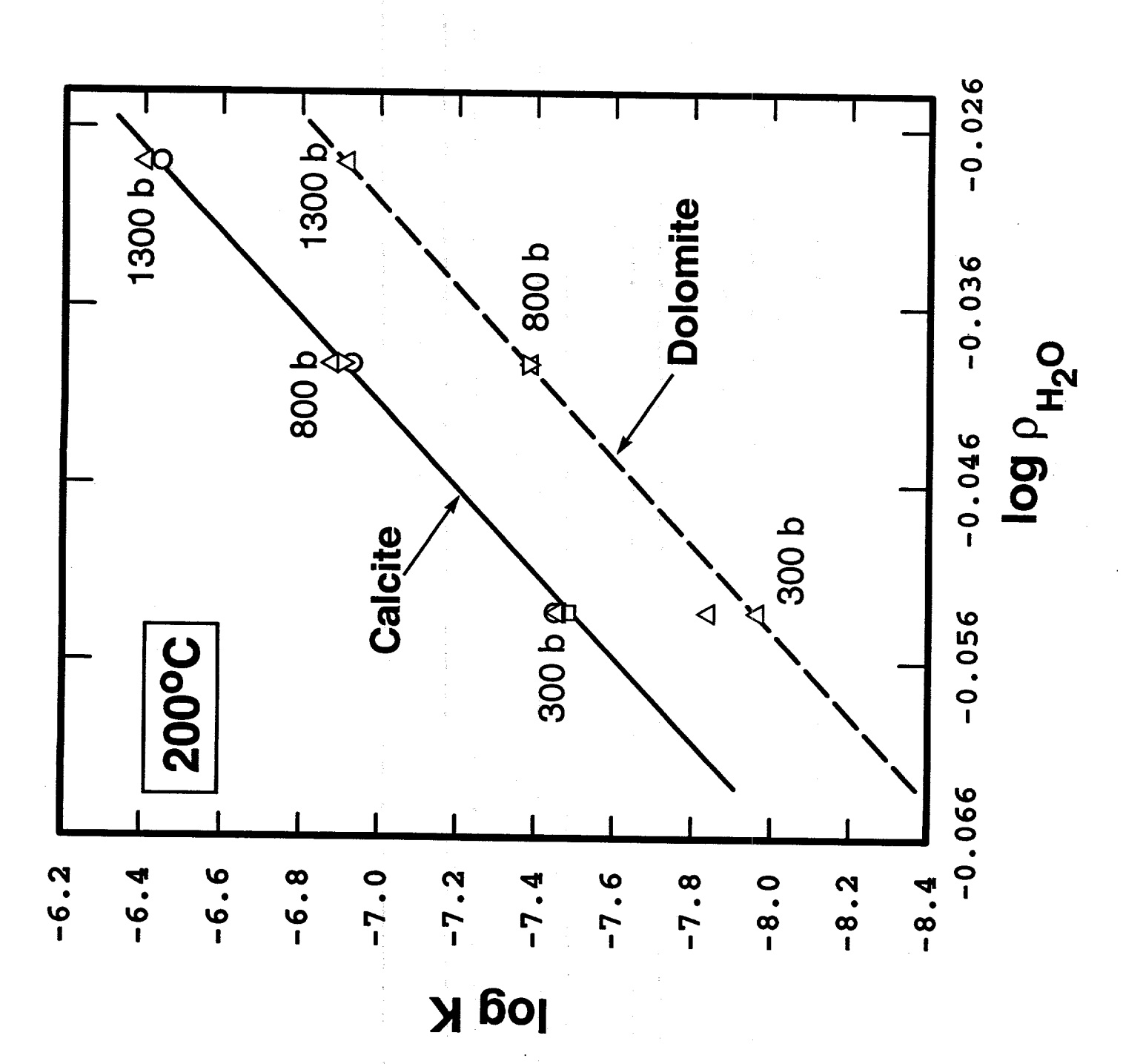


Figure 4



GEOCHEMISTRY OF CRUSTAL PROCESSES TO HIGH TEMPERATURES AND PRESSURES SUBPROJECT:

THE GEOCHEMISTRY OF ALUMINUM IN SEDIMENTARY BASIN BRINES*

David J. Wesolowski and Donald A. Palmer

Chemistry Division
Oak Ridge National Laboratory
Oak Ridge, TN 37831-6110

INTRODUCTION

The need for a quantitative understanding of the geochemistry of aluminum in natural systems is obvious. Aluminum is the third most abundant element in the Earth's crust (after oxygen and silicon) and the predominant rock and soil minerals are aluminosilicates. Many of the active Earth processes of interest geoscientists, such as weathering and soil geothermal contaminant transport, sedimentary diagenesis, alteration, and ore formation, are influenced by fluid buffering and permeability changes due to interaction of aluminum silicates, oxides and hydroxides with circulating aqueous fluids. thermodynamic properties of many aluminous minerals are very well known and progress is being made in modelling the nonideality of their solid solutions. However, the aqueous chemistry of dissolved aluminum remains a controversial subject, due to the slow kinetics dissolution and precipitation of aluminous phases, persistence of polymeric species in aqueous solutions to low total aluminum concentrations, and the extremely low equilibrium solubility of aluminum minerals at near-neutral pH.

The stable oxidation state of aluminum in all crustal regimes is Al(III). However, the small radius and high charge of Al³⁺ cause it to undergo a variety of hydrolysis and complexation reactions in natural and experimental aqueous solutions which can alter its activity, and therefore solubility, by many orders of magnitude. The most fundamental of these reactions are the products of interaction of aluminum with the aqueous medium itself:

$$xA1^{3+} + yH_2O = Al_x(OH)_y^{(3x-y)} + yH^+$$

Species have been identified with (x,y) values ranging from (1,0), the bare aluminum ion, to (13,32), the well known "Keggin" dodecahedral cage structure similar to metatungstate (BAES and

This research is sponsored by the U.S. Dept. of Energy, Office of Basic Energy Sciences under contract number DE-AC05-840R21400 with Martin Marietta Energy Systems, Inc. Portions of this subproject received supplemental support from the Office of Conservation and Renewable Energy, Division of Geothermal Technology Development.

MESMER, 1976; WESOLOWSKI et al., 1984). Each of these species, in turn, can react with organic and inorganic ligands to form stable complexes. However, in natural systems in which the total aluminum concentration in solution is limited by the solubility of aluminum oxides, hydroxides and silicates, the monomeric species, $Al(OH)_y^{3-y}$ with y=0-4, and their complexes with common natural ligands, are the dominant aqueous aluminum species.

The purpose of this research is to quantitatively and unambiguously determine the monomeric speciation of aluminum in natural waters over a wide range of solution compositions and temperatures. The thermodynamic properties at infinite dilution and the activity coefficients of the $Al(OH)_y^{3-y}$ ions, their formation constants, and their complexation by organic and inorganic ligands are obtained from solubility measurements, potentiometric titrations and spectroscopic techniques. This communication summarizes the results of studies of the solubility of gibbsite, $Al(OH)_3$, complexation of Al^{3+} by acetate and of $Al(OH)_4$ by a synthetic organic ligand, Bis-Tris, and potentiometric measurements of the formation constants of $Al(OH)^{2+}$ in basic and acidic brines over a wide range of temperatures and salinities.

GIBBSITE SOLUBILITY

1.) The system $Na^+-K^+-Cl^--OH^--Al(OH)_4^-$ to $100^{\circ}C$.

The solubility of gibbsite has been measured in a large number of solutions in the system Na-K-Cl-OH-Al(OH), from 6.4 to 80°C and 0.01 to 5.0 molal ionic strength (WESOLOWSKI, 1991). The aluminum concentration in the experimental solutions was determined by ion chromatography and the hydroxide ion concentration by difference. The results in NaCl and NaOH media, shown in Figure 1, have been coupled with the data of RUSSELL et al. (1955), Figure 2, and modeled using the Pitzer ion interaction treatment. An eight parameter expression (represented by the solid curves in Figures 1 and 2) for the molal concentration quotient of the reaction $Al(OH)_4 = Al(OH)_3 + OH$ was derived by least-squares regression of these results, which was also found to precisely describe our results in KOH and NaCl+KCl media within the experimental error. This expression adequately describes the more reliable literature data on the solubility of gibbsite in NaOH and KOH media to 100°C and up to 20 molal ionic strength, generally within ±0.1 log units. this expression, the equilibrium constant at infinite dilution, logK, and the stoichiometric molal activity coefficient ratio, $\log(\gamma OH^{-}/\gamma Al(OH)_{4})$, can be evaluated over the range 0-100°C and 0-12 molal ionic strength at 1 bar with a precision of approximately ± 0.02 log units. Standard thermodynamic properties of the reaction at 25°C and 1 bar are $logK_4 = 1.143 \pm 0.006$, $\Delta H^0 = -$ 22.5 \pm 0.3 kJ/mol, $\Delta S^{\circ} = -54 \pm 1$ J/K/mol and $\Delta C_{p}^{\circ} = -148 \pm 6$ J/K/mol. From these quantities and the standard thermodynamic properties of gibbsite, the values of ΔG_f° , ΔH_f° and S° of $[Al(OH)_4]_{(aq)}$ at 25°C and 1 bar are computed to be $-1305.6 \pm 1.2 \text{ kJ/mol}$, $-1500.6 \pm 1.5 \text{ kJ/mol}$ and 111.4 J/K/mol, respectively. Approximate values of the pure

electrolyte parameters β^0 , β^1 and C^{ϕ} for NaAl(OH), and KAl(OH), as well as the mixing parameters for aluminate ion with OH, OH + Na, and OH + K were also obtained (WESOLOWSKI, 1991). These results represent the only comprehensive data set on the behavior of the aluminate anion in Na+-K+-Cl brines in the temperature and composition range of common diagenetic processes in active sedimentary basins.

2.) The system $Al^{3+}-H^{3+}-Na^{3+}-Cl^{-}$ to 80°C.

The solubility of gibbsite in aqueous solutions was measured at ten ionic strengths made up of NaCl, HCl, and AlCl $_3$ at 30, 50 and 70°C with the initial acidity controlled by addition of HCl (PALMER and WESOLOWSKI, 1991). The results are shown in Figure 3. The aluminum concentration was determined by ion chromatography, while the final equilibrium pH was measured at temperature. evidence for aluminum chloride complexation was found by comparing solubility experiments in the presence of varying concentrations of sodium trifluoromethanesulfonate and sodium chloride at 50 °C and ca. five molal ionic strength. The equilibrium quotients for the reaction $Al(OH)_3 + 3H^{\dagger} = Al^{3+} + 3H_2O$ were modeled using both an empirical equation including the Debye-Hückel term and the Pitzer ion interaction treatment which incorporated the relevant single electrolyte and mixing interaction parameters currently available in the literature. In the latter treatment only four independent variables, including $\theta_{\rm AlNa}$, $\Psi_{\rm AlNaCl}$ and two terms describing the equilibrium constant at infinite dilution, were independent variables, including needed to fit the data well within the projected experimental error. In general, these new equilibrium quotients differ markedly from results of all but the most recently published solubility studies (Figure 4), including the work of NAGY and LASAGA (1991), who used our starting material for reversed solubility measurements at 80°C and low ionic strength.

The equilibrium constant for the reaction at infinite dilution, logK, and the stoichiometric molal activity coefficient ratio, log[$(\gamma Al^{3+})/(\gamma H^{\dagger})^3$], can be evaluated over the range 0-100°C and 0-5 molal ionic strength at 1 bar with a precision of \pm 0.08 log units. Standard thermodynamic values for the reaction at 25°C and 1 bar are logK = 7.735 \pm 0.057, ΔH° = -105.6 \pm 2.9 kJ/mol, ΔS° = 206 \pm 9 J/K/mol and ΔC_p° = 13 \pm 11 J/K/mol. From these values and the standard thermodynamic properties of gibbsite, values of ΔG_f° , ΔH_f° and S° of Al^{3+} (aq) at 25°C and 1 bar of -487.7 \pm 1.5 kJ/mol, -540.9 kJ/ mol, and -346 J/K/mol, respectively, have been calculated.

3.) Gibbsite solubility in pH buffer solutions at 50°C and 0.1 molal NaCl.

In order to determine the stepwise formation constants of the aluminum hydroxide species, the solubility of gibbsite in the near-neutral pH range was studied in pH buffers. Preliminary results

of this study have been reported by PALMER and WESOLOWSKI (1990). A temperature of 50°C was chosen so as to allow fairly rapid kinetics and minimize experimental problems. The ionic strength was fixed at 0.1 molal with NaCl to eliminate ambiguities with respect to activity coefficients, yet allow extrapolation to infinite dilution. Because our results in acidic and basic solutions indicated lower equilibrium gibbsite solubilities than those reported by MAY et al. (1975) by as much as 0.5 log units, we decided to duplicate their experimental conditions. authors used acetate, Bis-Tris and Tris buffers. MESMER, et al. (1989) have reported the molal dissociation constants of acetic acid in NaCl brines at elevated temperatures, but similar information was not available for Bis-Tris and Tris, so we first studied their dissociation in NaCl media at elevated temperatures (PALMER and WESOLOWSKI, 1987; WESOLOWSKI and PALMER, 1989). developing quantitative ion chromatographic techniques analyzing aqueous solutions containing several thousand to less than 1 part per billion total aluminum, we produced the results shown in Figure 5. (Throughout the discussion below, "pH" is formally defined as the negative logarithm of the molal hydrogen ion concentration). The solid curves represent the molalities of Al3+ and Al(OH), in equilibrium with gibbsite at these conditions derived from our work in acidic and basic media described above.

It is immediately obvious that the results in acetate and Bis-Tris buffers are not consistent with the results discussed above or the data in Tris buffers. MAY et al (1975) observed a similar discontinuity at pH 6 (the transition from his Bis-Tris to Tris buffer runs) and attributed this observation to a change in the nature of the solid phase. However, analysis of our results as a function of total buffer concentration (0.01 to 0.001 molal buffer concentrations were used in these experiments) revealed that acetate forms a strong complex with Al³⁺ and Bis-Tris strongly complexes Al(OH). Our solubility data indicated a formation constant for AlAc²⁺ of 10^{2.08} and a constant of 10^{2.61} for the Bis-Tris-aluminate complex. The acetate interaction with Al³⁺ has been confirmed by potentiometry (BELL, et al., this issue) and the Bis-Tris-aluminate complex was confirmed by additional solubility and Raman spectroscopic studies (WESOLOWSKI et al., 1990).

In Figure 6, the solubility of gibbsite is corrected for the effects of these complexes, and some additional measurements in Tris buffers are plotted as well. The contribution of $Al(OH)^{2+}$ to the solubility curve determined from potentiometry (see below) at these conditions is also shown in Figure 6. In Figure 7, the concentrations of all known aluminum species (i.e. Al^{3+} , $Al(OH)^{2+}$, $Al(OH)^{4}$, $AlAc^{2+}$ and $Al(OH)^{4}$ [Bis-Tris]) have been subtracted from the measured solubility. Theses species quantitatively account for the solubility of gibbsite measured in this study within the experimental error of \pm 0.1 log units, with the exception of a small positive anomaly in the "pH" 5-6 range. This anomaly must be due to an additional species, probably $Al(OH)^{+}_{2}$ or $Al(OH)^{\circ}_{3}$. Resolution of this question will await the results of the potentiometric studies discussed below.

202

POTENTIOMETRIC STUDIES OF THE HYDROLYSIS OF Al3+ IN NaCl BRINES

The hydrolysis of Al^{3+} in NaCl brines is now being studied by potentiometric titrations in our hydrogen-electrode concentration cell to temperatures of 150°C in 0-5 molal NaCl solutions. Solutions of HCl+NaCl are equilibrated under the same hydrogen pressure in the two compartments of the cell, which are fitted with matched Pt-H2 electrodes and connected by a porous teflon liquid junction. A solution of HCl+AlCl3+NaCl of the same ionic strength is added to the test compartment using a positive displacement pump, and the Al3+ is then titrated with NaOH+NaCl from another pump. The extent of hydrolysis in 0.1 molal NaCl solutions to 100°C is plotted as n in Figure 8. This quantity is an algebraic representation of the extent of hydrolysis, defined as the number of bound hydroxide ions divided by the total aluminum. The shapes and spacings of these curves as a function of "pH" and total metal concentration can be modelled to determine the stoichiometry of $Al_{x}(OH)^{3x-y}_{y}$ present in the solutions. At values of \bar{n} of 0.2 or less, the only species identified is Al(OH)2+. At higher degrees of hydrolysis, polymeric species begin to appear, even at the submillimolal aluminum concentrations employed in these studies. The molal formation constant of the reaction $Al^{3+} + H_2O = Al(OH)^{2+}$ + H extracted from these results is plotted as a function of reciprocal temperature in Figure 9. It has been shown above that these results are consistent with the gibbsite solubility measurements at 50°C. Also plotted in Figure 9 are values for the same reaction reported by KUBOTA (1956) and BROWN et al. (1985). These values agree with our result at 25°C within 0.02 log units. Experiments are now under way in 1.0 molal NaCl solutions.

SUMMARY

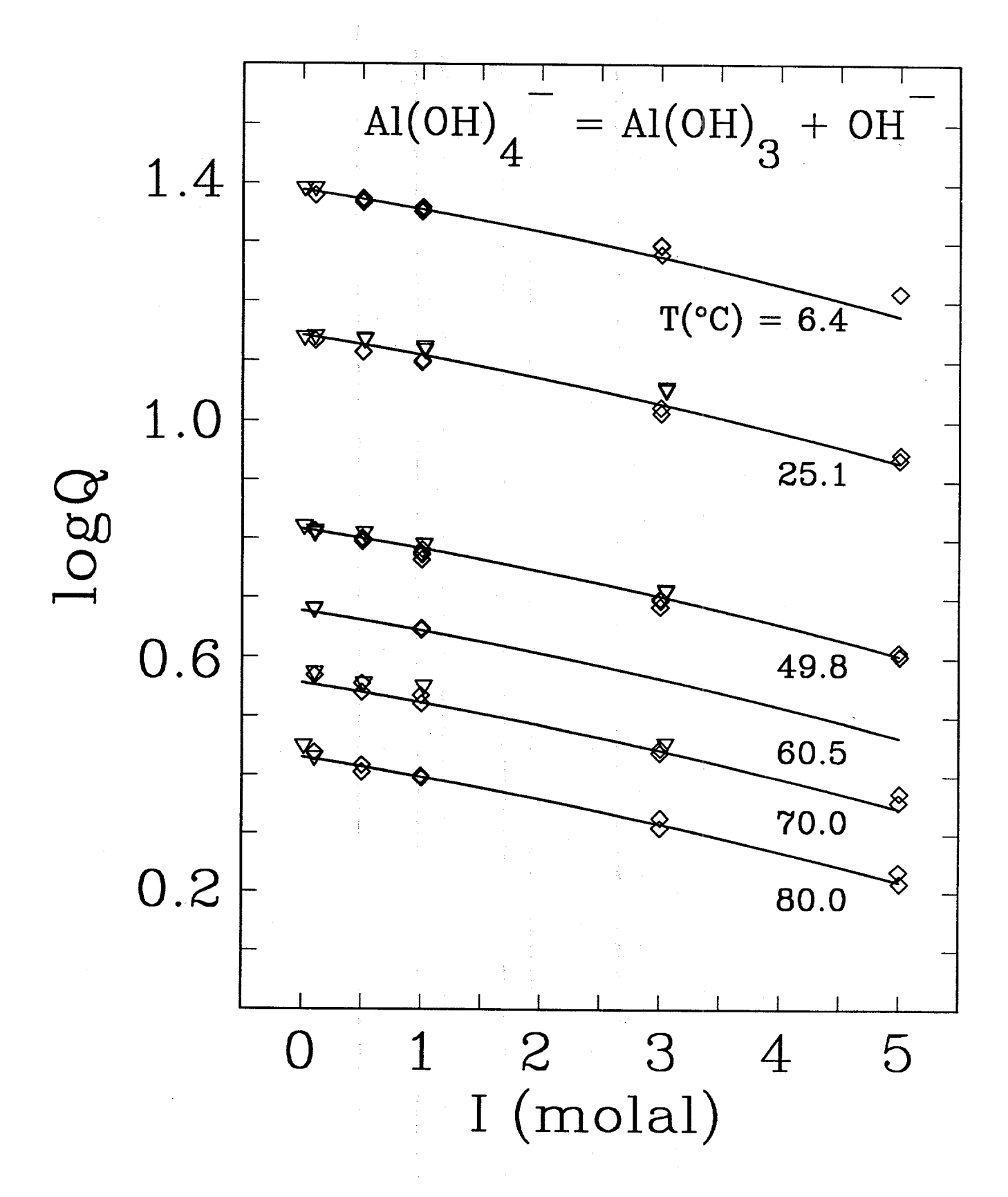
We are well on our way to a quantitative understanding of the aqueous chemistry of aluminum at the temperatures and salinities common to sedimentary basins. The thermodynamic properties and activity coefficients of Al3+, Al(OH)2+ and Al(OH)4, as well as their relative stability boundaries can now be readily calculated in high salinity brines to 100°C. Our current efforts will be extended to include potentiometric hydrolysis studies to 150°C and 5 molal ionic strength and additional solubility measurements as time We will attempt to measure boehmite, AlOOH, solubility allows. hydrogen-electrode with direct "Hq" measurement in our concentration cell. A new flowing potentiometric cell is now under development which will allow determination of the pressure coefficients of hydrolysis reactions to 1 kb, a critical need for modelling deep basinal brines and geopressured zones.

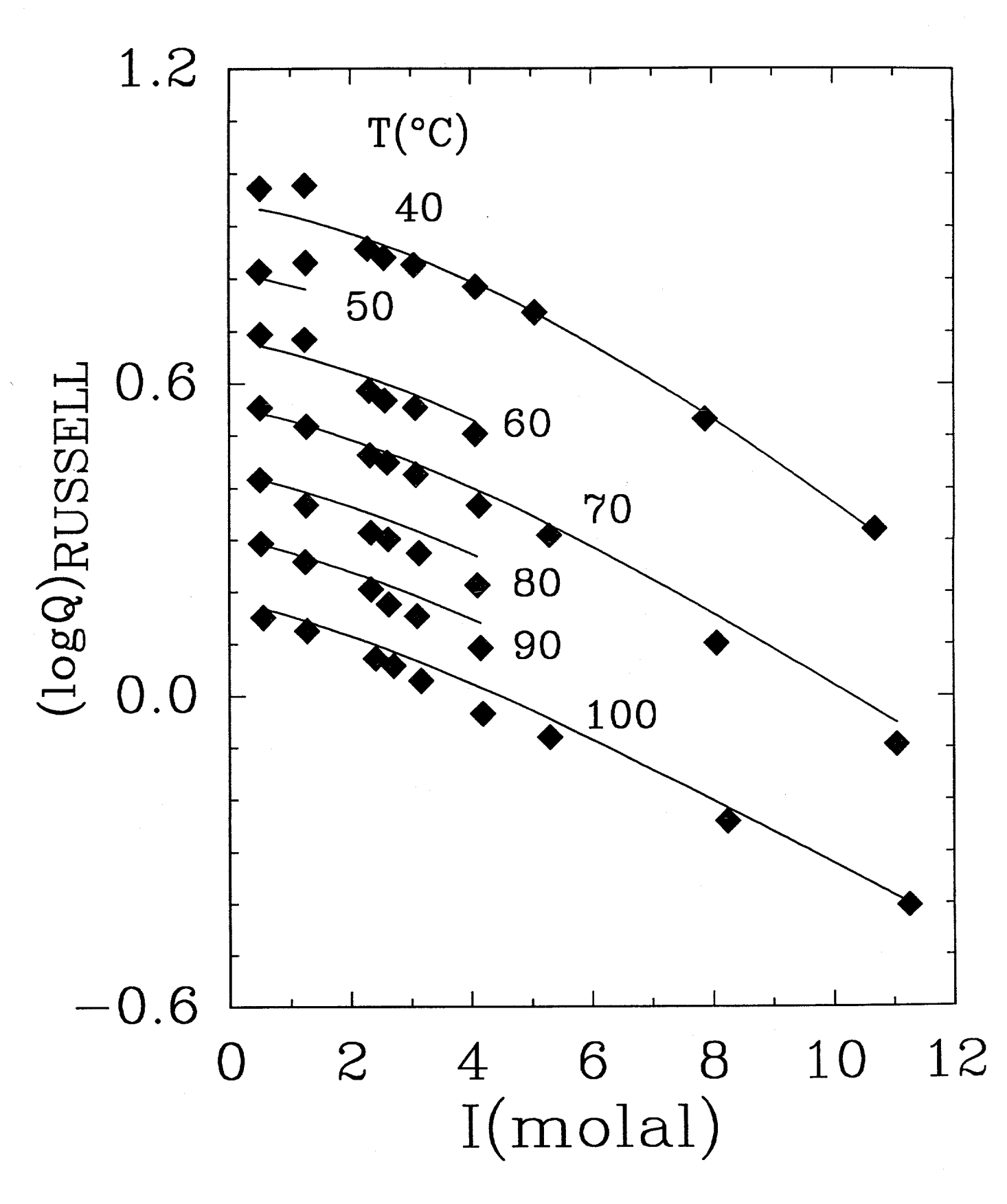
REFERENCES

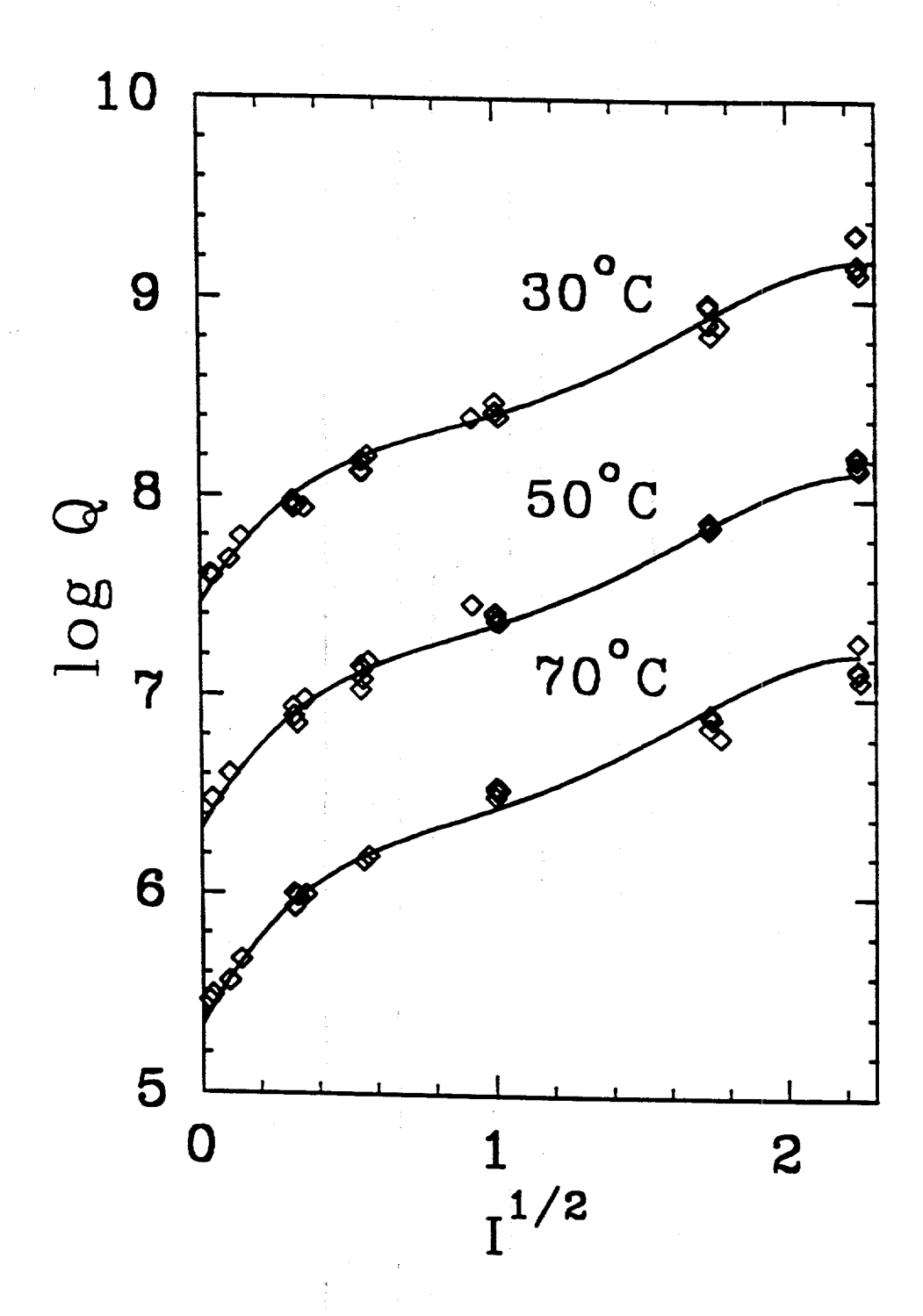
- BAES C.F. Jr. and MESMER R.E. (1976) The Hydrolysis of Cations, John Wiley and Sons, New York, 489 p.
- BROWN, P.L., SYLVA, R.N., BATLEY, G.E. AND ELLIS, J. (1985) The hydrolysis of metal ions. Part 8. Aluminum (III), J. Chem. Soc. Dalton Trans., 1967-1970.
- KUBOTA, H. (1956) Properties and volumetric determination of aluminum ion, Ph.D. Dissertation, Univ. of Wisconsin, Diss. Abstr. 16, 864.
- MAY H. M., HELMKE P. A. and JACKSON M. L. (1979) Gibbsite solubility and thermodynamic properties of hydroxy-aluminum ions in aqueous solution at 25 C. Geochim. Cosmochim. Acta 43, 861-868.
- MESMER, R.E., PATTERSON, C.S., BUSEY, R.H. and HOLMES, H.F. (1989) Ionization of Acetic Acid in NaCl(aq) media: A potentiometric study to 573 K and 130 bar, J. Phys. Chem. 93, 7483-7490.
- NAGY K.L. and LASAGA A.C. (1991) Dissolution and precipitation kinetics of gibbsite at 80°C and pH 3: The dependence on solution saturation state. Geochim. Cosmochim. Acta (In Press).
- PALMER D.A. and WESOLOWSKI D. (1987) Acid association quotients of tris(hydroxymethyl)aminomethane in aqueous NaCl media to 200°C, J. Solution. Chem. 16, 571-581.
- PALMER D.A. and WESOLOWSKI D.J., (1990) The solubility of gibbsite in aqueous sodium chloride solutions, In *Properties of Water and Steam* (ed.s M. PICHAL and O. SIFNER), Proceedings of the 11th International Conference, Hemisphere Publishing Corp., New York, 412-418.
- PALMER, D.A. and WESOLOWSKI, D.J., (1991) Aluminum speciation and equilibria in aqueous solution. Part II. The solubility of gibbsite in acidic sodium chloride solutions from 30 to 70°C, Geochim. Cosmochim. Acta (In Press).
- RUSSELL A.S., EDWARDS J.D. and TAYLOR C.S. (1955) Solubility and density of hydrated aluminas in NaOH solutions, *Journal of Metals* 7, 1123-1128.
- WESOLOWSKI, D.J., (1991) Aluminum speciation and equilibria in aqueous solution. Part I. The solubility of gibbsite in the system Na-K-Al(OH) $_4$ -OH-Cl from 0 to 100°C, Geochim. Cosmochim. Acta (In Press).
- WESOLOWSKI D.J. and PALMER D.A. (1989) Acid association quotients of Bis-tris in aqueous sodium chloride media to 125°C, J. Solution Chem. 18, 545-559.
- WESOLOWSKI D., DRUMMOND S.E., MESMER R.E. and OHMOTO H. (1984) Hydrolysis equilibria of tungsten(VI) in aqueous sodium chloride solutions to 300°C, Inorg. Chem. 23, 1120-1132.
- WESOLOWSKI D.J., PALMER D.A. and BEGUN G.M. (1990) Complexation of aluminate anion by Bis-tris in aqueous media at 25-50°C. J. Solution Chem. 19, 159-173.

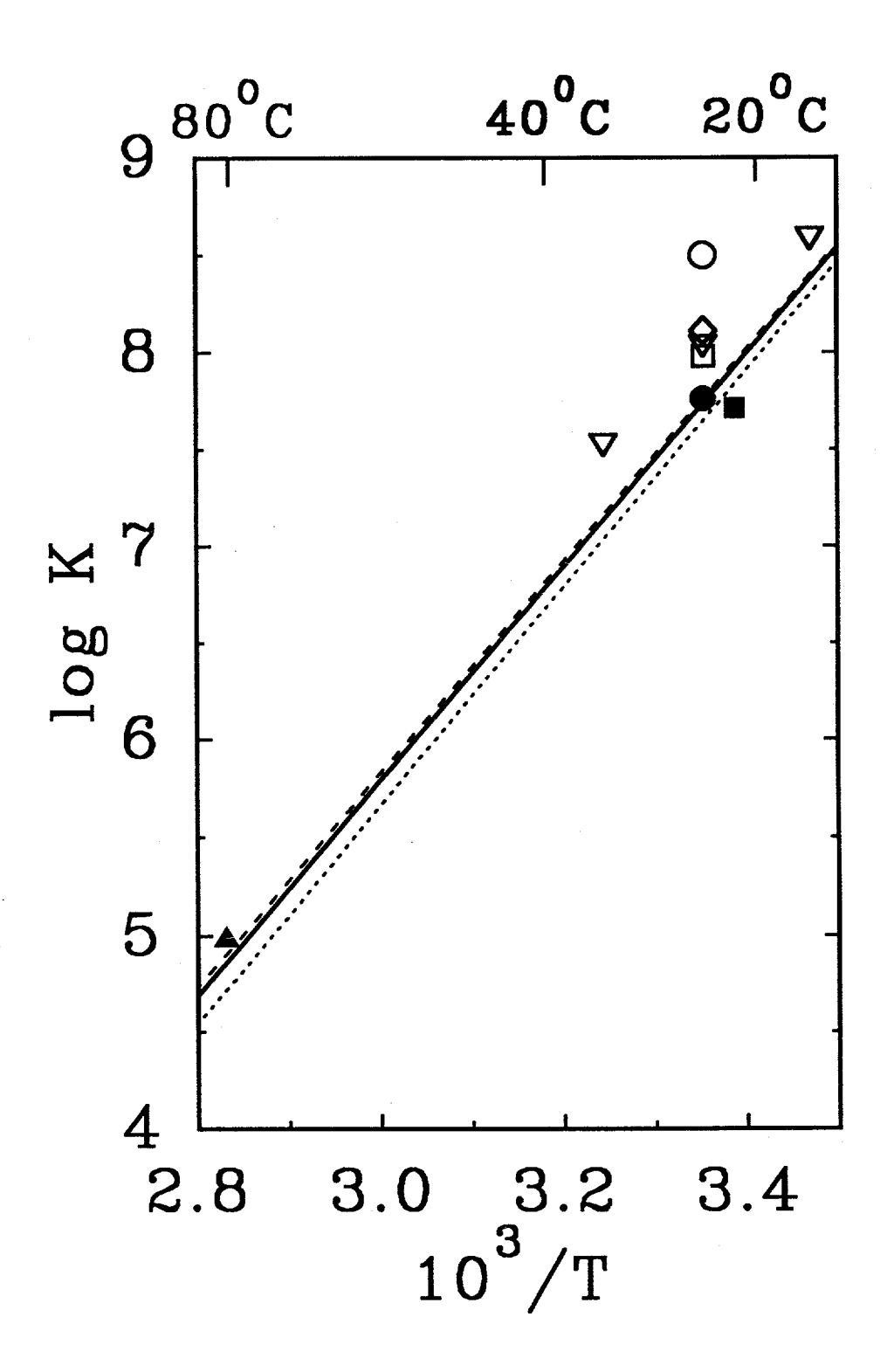
FIGURE CAPTIONS

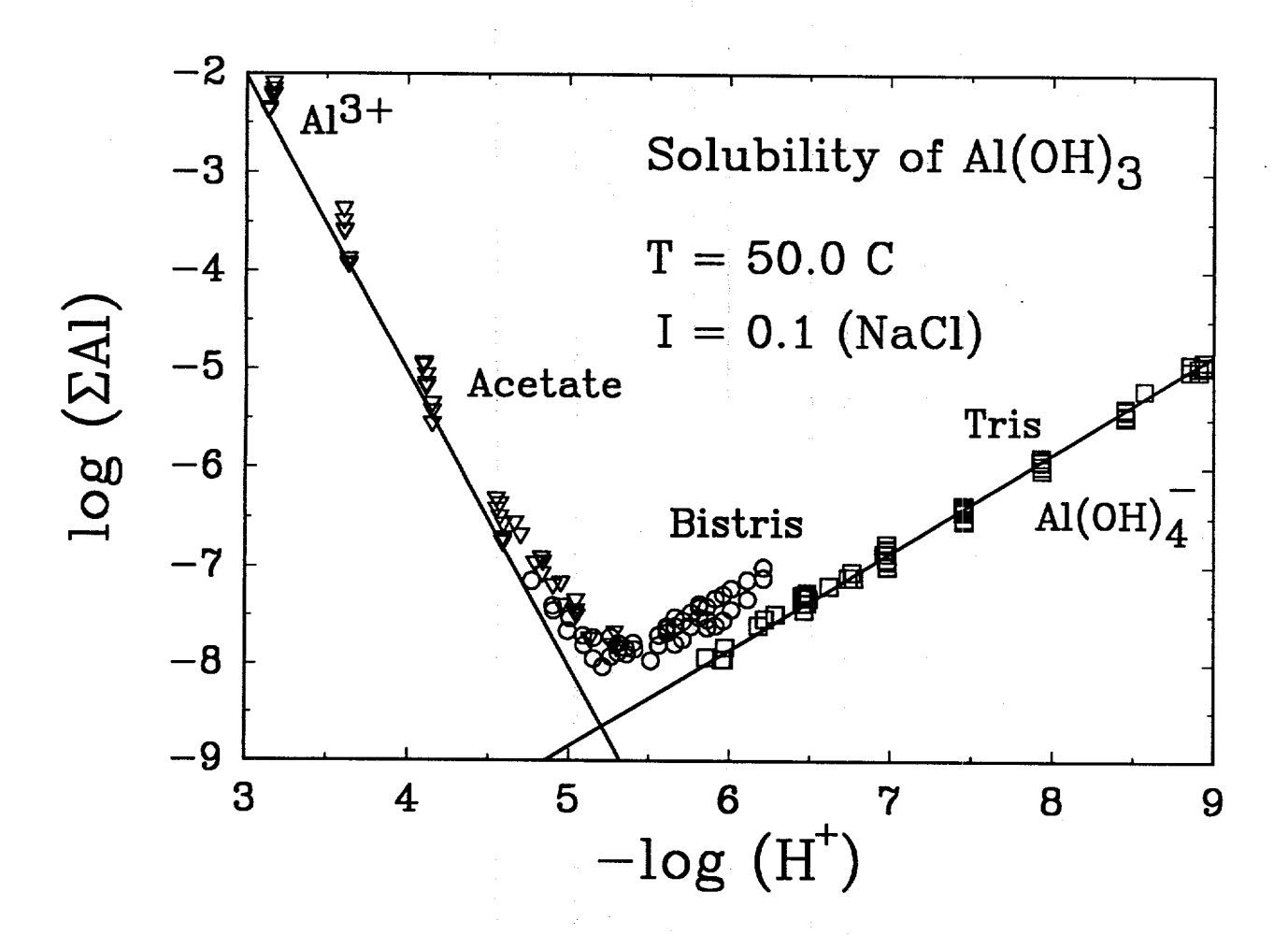
- Figure 1. Molal equilibrium quotients $(Q = mOH^-/mAl(OH)_4^-)$ for the reaction $Al(OH)_4^- = Al(OH)_3^- + OH^-$ in NaCl + NaOH + NaAl(OH)_4 solutions (\diamondsuit) , and NaOH + NaAl(OH)_4 solutions (\triangledown) as a function of temperature and ionic strength obtained in this study. The solid curves are the computed values for the chloride-bearing solutions from the Pitzer ion interaction model.
- Figure 2. Data of RUSSELL et al. (1955) for the reaction $Al(OH)_4^- = Al(OH)_3 + OH^-$ compared with the values computed from the fit (solid lines).
- Figure 3. Molal formation quotients $(Q = mAl^{3+}/[mH^{+}]^{3})$ for the reaction $Al(OH)_{3} + 3H^{+} = Al^{3+} + 3H_{2}O$ obtained in this study. The solid curves were computed from the Pitzer ion interaction model.
- Figure 4. The temperature dependence of log K for the reaction $Al(OH)_3 + 3H^+ \Rightarrow Al^{3+} + 3H_2O$ (solid and dashed lines, various fits). The symbols denote various literature values for this equilibrium summarized by PALMER and WESOLOWSKI (1991).
- Figure 5. Log total aluminum molality of solutions in equilibrium with gibbsite at the conditions indicated. The different symbols denote the buffers used (triangles = acetate, circles = Bis-Tris, and squares = Tris buffer). The solid lines are the concentrations of Al^{3+} and $Al(OH)_4^{-}$ in equilibrium with gibbsite computed from our work in strong acid and strong base.
- Figure 6. Log total aluminum in equilibrium with gibbsite corrected for specific interactions with the buffers. The curve for $Al(OH)^{2+}$ was obtained from the potentiometric studies discussed in the text.
- Figure 7. Residual plot of observed calculated log total aluminum molality in equilibrium with gibbsite at 50°C, 0.1 molal NaCl.
- Figure 8. Results of potentiometric titrations of Al^{3+} solutions with OH^- as a function of total metal concentration, temperature and pH (see text).
- Figure 9. Molal equilibrium quotients $(Q_{1,1} = mH^{+}mAl(OH)^{2+}/mAl^{3+})$ for the reaction $Al^{3+} + H_2O = Al(OH)^{2+} + H^{+}$ in 0.1 m NaCl computed from the data in Figure 8 (see text).

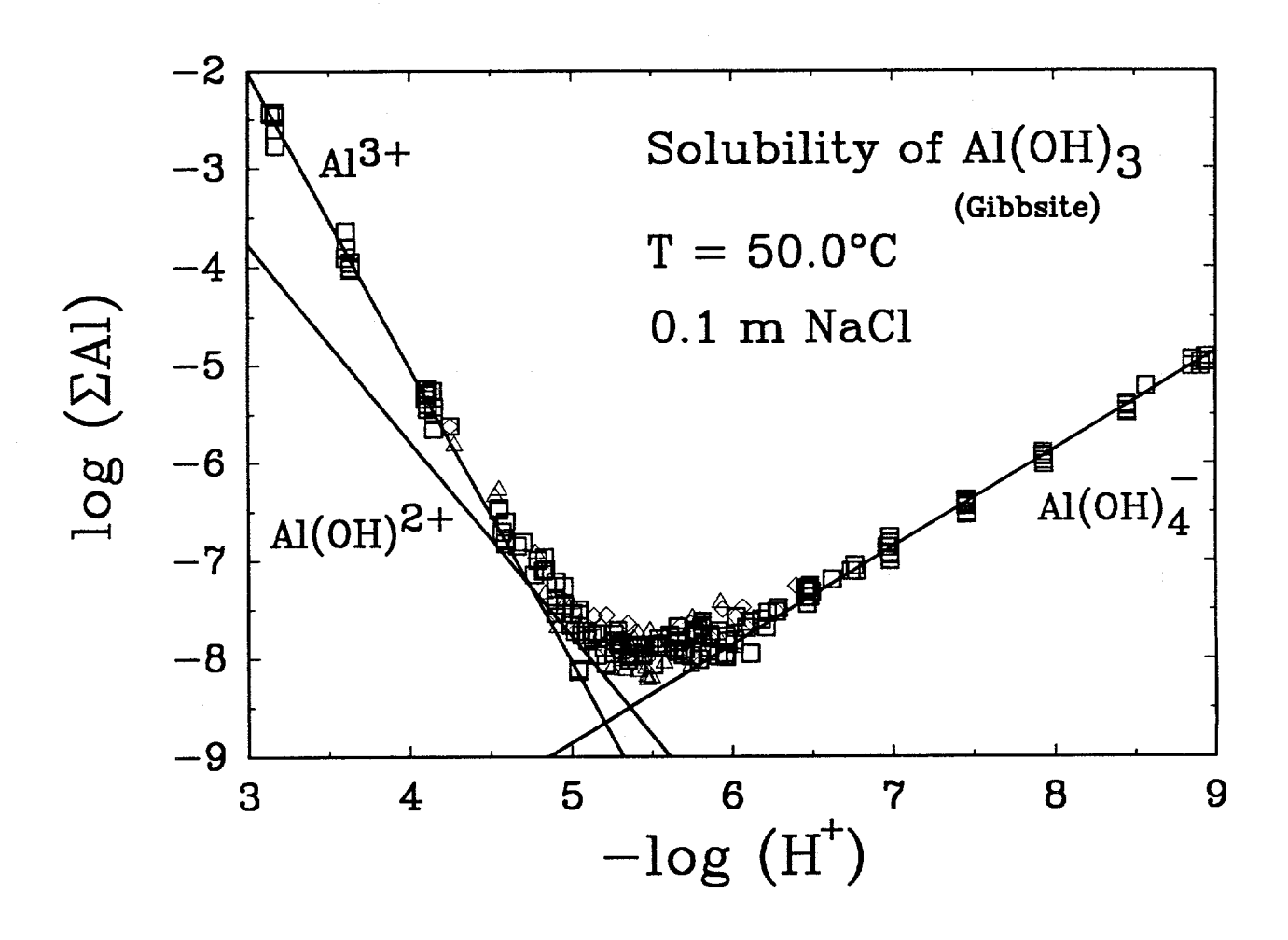












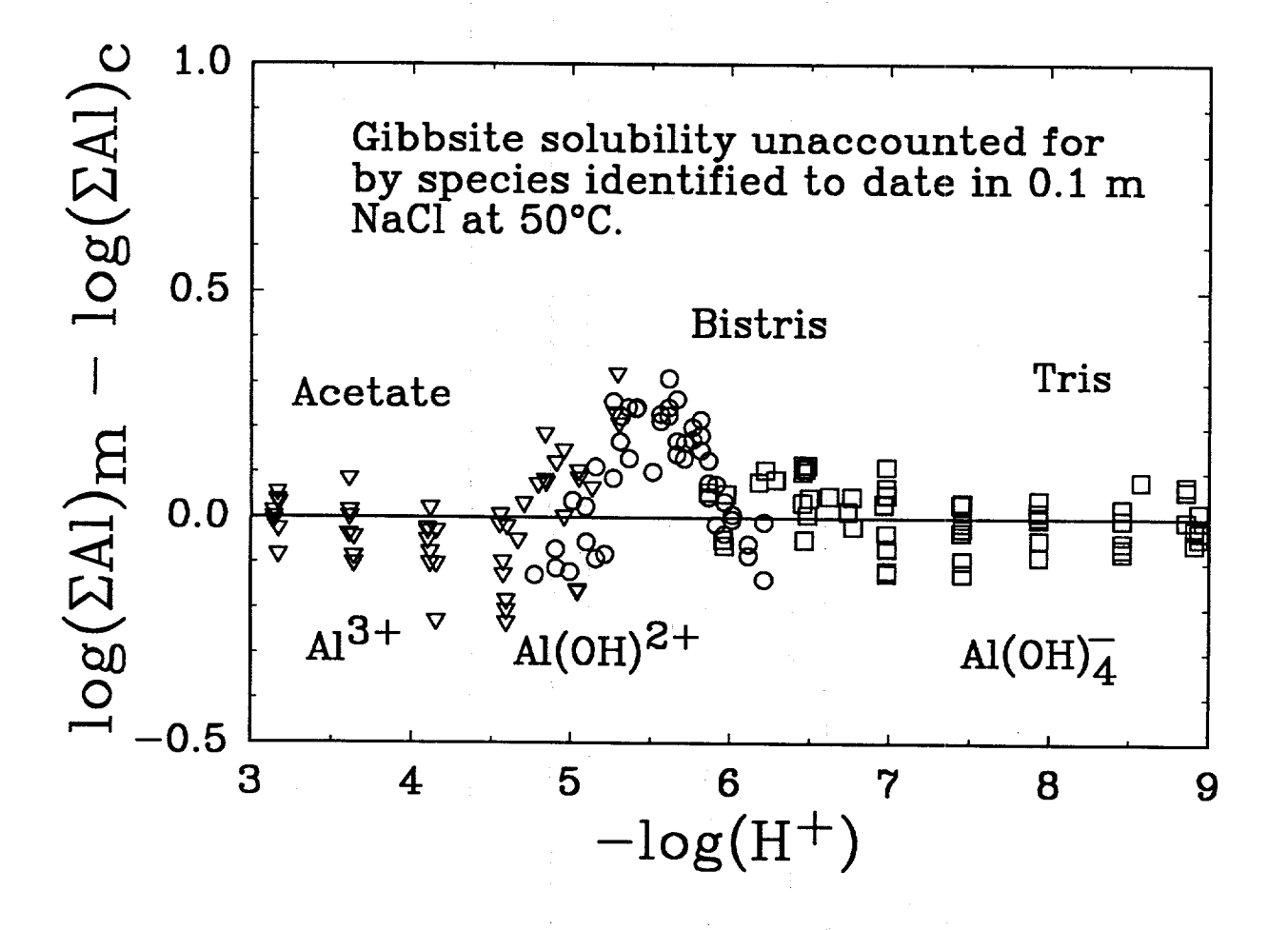
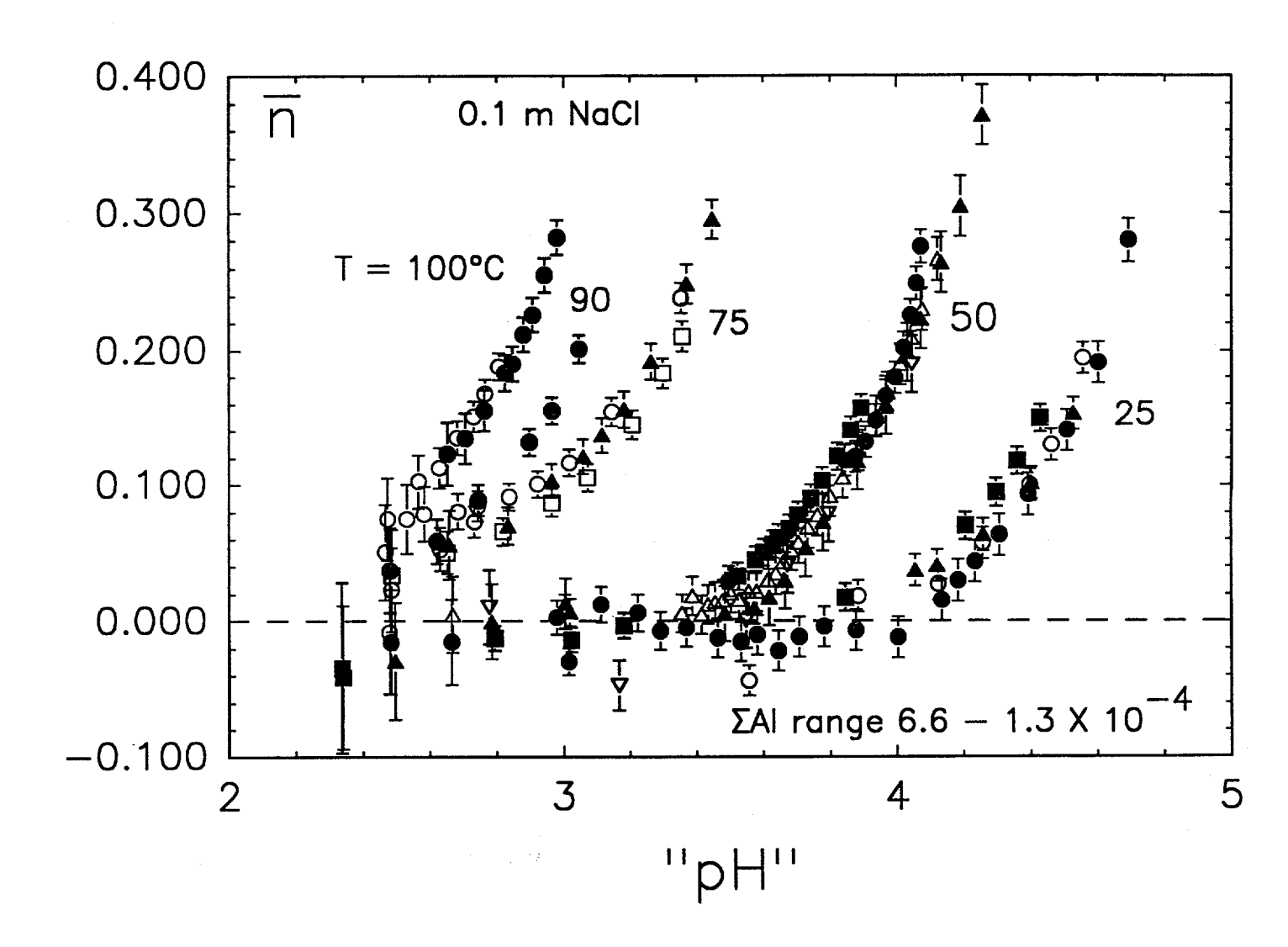
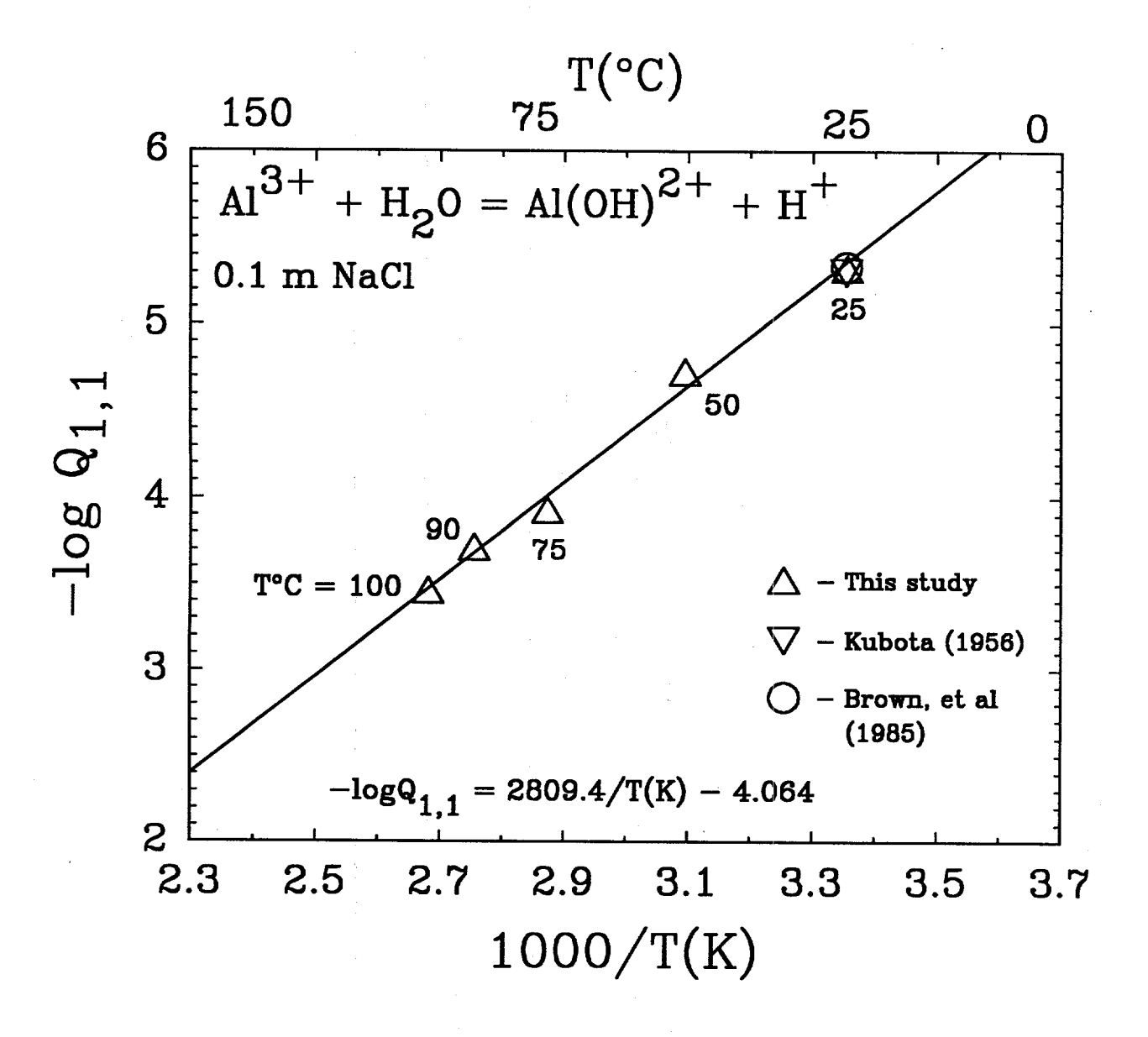


FIGURE 8





STABILITY OF NATURAL GAS IN THE DEEP SUBSURFACE

Colin Barker, University of Tulsa

The deeper parts of many U.S. basins are still poorly explored (and in that sense are frontier areas), so it is important to project our understanding of oil and gas generation and survival into these deeper settings. Some sedimentary sections are more than 50,000 ft (15,240 m) deep and no well in any sedimentary basin has been drilled below 31,500 ft (9,600 m). This poses a major problem because the standard methods of organic geochemistry rely on analyzing rock and fluid samples - and there are no samples from areas not yet drilled. Even in areas where deep wells have been drilled there are still serious problems of gas loss, or gas contamination, during sample retrieval. Because gases are so important in many aspects of energy exploration and exploitation, reliable techniques for establishing gas composition are essential. The value of natural gas is often diminished by the presence of non-flammable or environmentally hazardous components such as carbon dioxide and hydrogen sulfide. While it is possible to calculate the composition of deep gas thermodynamically it is still important to analyze what is actually present in the deep subsurface. One way to get this information is from the analysis of gas trapped in fluid inclusions. Fluid inclusions are defects (usually microscopic) that have encapsulated some of the gases and liquids present in the vicinity of the growing crystal. They may develop during mineral growth ("primary"), but can also form later by rehealing of fractures or in other ways ("secondary"), so that the contents of the inclusions may represent samples of the fluids that surrounded the crystal at various stages of growth. Analysis of gases in fluid inclusions poses a difficult problem. Any method that involves the combined contents of a large number of inclusions will give data for an unknown mixture of primaries and secondaries. For example, crushing the host mineral will release gases from both primaries and secondaries. In addition, crushing generates many new superclean fracture surfaces that remove gases by adsorption and change the overall composition. Separate analysis of each individual inclusion seems to offer the only way of getting compositional information for the primaries without contamination.

We have designed and built a dual mass spectrometer ("DMS") system to analyze gases in individual fluid inclusions (Barker and Smith, 1986; Barker and Underwood, 1991). It uses two UTI 100C quadrupole mass spectrometers operating in parallel. Minerals containing fluid inclusions are heated in a vacuum system that forms the inlet to the DMS system. On heating, phase relationships in the inclusions may change in such a way that the pressure of the contents increases rapidly, ruptures the host mineral, and releases the gases for analysis. Examination of the detailed shape of a burst shows that the full peak width at 95% of maximum response is slightly greater than 25 msec. Thus the problem of analyzing the volatile contents of each individual fluid inclusion reduces to one of getting a complete analysis within the 25 msec time constraint established by an individual burst. Most quadrupole mass spectrometers require about 100 msec/mass spaectrum. Since the UTI 100C instruments can scan from 1 to 300 amu in 75 msec, a mass range from 2-70 can be scanned in under 20 msec. The addition of a second mass spectrometer in parallel makes it possible to double the mass range to include 70-140 amu, or to include any mass range up to 300 amu. Background noise has been reduced by a pulse-triggering device that is phase-locked to the AC power line. Mass spectrometer analog output is

digitized and recorded on 9-track tape so that subsequent off-line processing with the Post Aquisition Data REduction ("PADRE") software provides essentially unlimited time for data evaluation.

Analytical data can be displayed as a mass spectrum for each individual fluid inclusion (AB of Figure 1), or the compositional data for all of the inclusions analyzed (or any subset) can be displayed on a ternary diagram with user-specified corners. This is a potentially useful way of showing whether more than one population of inclusions is present. It may also provide a check on the accuracy of the analyses by showing the scatter of the points. Often points will plot along a line showing mixing. Any size range can be isolated and displayed separately, and this size information is very useful in eliminating data from very small inclusions where background noise is a significant part of the response.

In addition to displaying compositional data for the fluid inclusions, it is possible to monitor the release of any particular gas by plotting a continuous trace showing the response at a given mass number as a function of temperature (XY of Figure 1). Water can be treated like any other gas and over the time scale of a bursting inclusion adsorption does not seem to be a problem. This is confirmed by detailed examination of burst shapes, especially for the pumpdown segments. These show that the shape is essentially the same for methane (which is not likely to be adsorbed) as for water and hydrogen sulfide.

A wide variety of geological samples has been analyzed in order to understand the capabilities and limitations of the analytical system, and also to help constrain the composition of deep gas. Recent results from these studies include:

- (1) Smackover formation: The Jurassic Smackover formation (and underlying Norphlet) are major petroleum plays in the Gulf Coast. We have analyzed a variety of calcite cements that are currently about 20,000 ft (6,096 m) deep. Fluid inclusion gases show a wide range of gas compositions and include water, methane, hydrogen sulfide, and carbon dioxide (Figure 2). Hydrogen sulfide is often a major component and some of the inclusions contain elemental sulfur. Relative amounts of the various components vary within individual samples and there are major differences with sample depth in the wells.
- (2) Ghost Rocks Melange, Alaska: Quartz samples now at the surface in the Ghost Rocks melange, Kodiak, Alaska appear to have crystallized at approximately 90,000 ft (27,430 m) (P.Vrolick, pc). Some of these samples are extremely methane rich and have individual inclusions containing virtually no water. Intermediate methane-water compositions produce prominant mixing lines on ternary diagrams (Figure 3) (Barker and Sullivan, 1989). The subducting plate leads to very low geothermal gradients and causes rapid burial so that although these samples crystallized at great depth the oil window, and presumably gas survival, is pushed very deep. Samples analyzed from subduction complexes in Barbados and the Olympic Peninsula, Washington contain only traces of methane, if any. None of the subducted samples contained sulfur gases.
- (3) Evaporites: Evaporites have been suggested as potential sites for nuclear waste storage. We have analyzed gases in inclusions in both domal and bedded salts from the Gulf Coast (10 samples) and the Palo Duro basin, Texas (7 samples) respectively (Patton,1989). Gas compositions are generally similar with water dominating. However, no higher hydrocarbons were observed in

domal salts whereas they were seen occasionally in bedded salts. Five of the 17 samples contained appreciable methane. Many of the inclusions in salt are large (one could be seen with the naked eye) and contained more water than the mass spectrometer could handle. The large inclusion bursts saturate the analog-to digital converter and give spurious information that is eliminated by the data-handling program.

- (4) Quartz overgrowths: Overgrowths are important in petroleum reservoir rocks because their fluid inclusions sample the fluids present at various times during reservoir development and filling. Unfortunately, most inclusions in the materials studied were very small and close to the analytical limits, but information on methane content (that is needed for interpreting microscopically observed phase relationships) was obtained (Eadington, et al, 1990; Eadington, et al, 1991).
- (5) Bald Eagle Formation: A suite of samples from the Bald Eagle Formation, cental Pennsylvania, the underlying Reedsville shale, and the overlying Juniata Formation were run in cooperation with A. Lacazette (Penn. State Univ.). Quartz was analyzed from all units together with calcites from the Bald Eagle. The quartz from the organic-rich, black, marine Reedsville shale contained mainly methane with little water and no higher hydrocarbons. Microscopic examination showed large, clear, single-phase gas inclusions. In the overlying Bald Eagle formation inclusions in the calcite and quartz contained water with variable but minor quantities of methane, while the quartz from the Juniata breccia had inclusions with water but no methane. This suggests that methane was available (probably from the Reedsville shale) at the time tectonism produced the horizontal fractures in the Bald Eagle Formation. Interestingly it has been suggested that tectonism also lead to brecciation of the Juniata formation, but no methane was incorporated into fluid inclusions there.

REFERENCES

- Barker, C. and Smith, M.P., 1986. Analysis of gases in individual fluid inclusions in natural minerals: Analytical Chemistry, v.58, p.1330-1333.
- Barker, C. and Sullivan, G., 1989. Analysis of gases in individual fluid inclusions in minerals from the Kodiak accretionary complex, Alaska: paper presented at PACROFI II, Virginia Polytechnic Institute and State University, Blacksburg, Virginia.
- Barker, C. and Underwood, W. D., 1991. Analysis of gases in individual fluid inclusions in natural minerals using a dual mass spectrometer system: In review.
- Eadington, P., Barker, C., and Underwood, W., 1990. Thermal history from fluid inclusions and maturity measurements: Measuring the effect of volatiles: Poster presentation, APEA Conference, Darwin, Australia.
- Eadington, P., Barker, C., and Underwood, W., 1991. Hydrocarbon fluid history of reservoir and aquifer rocks: CSIRO (Australia), NERDDP Project 1251. 88pp.
- Patton, B. D., 1989. A reconnaissance survey of gases in fluid inclusions in natural salts: Masters Thesis, University of Tulsa, 201pp.

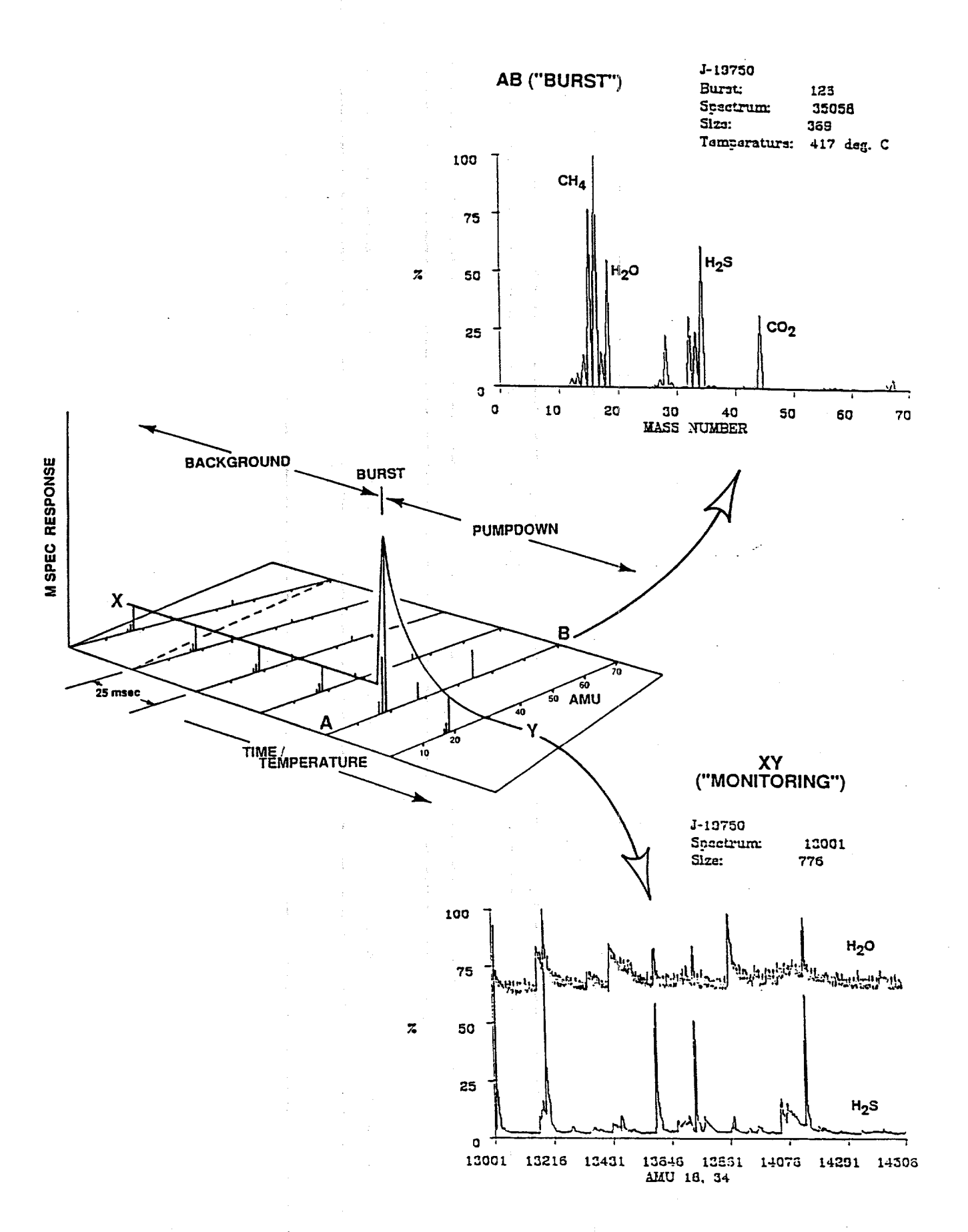


Figure 1: (Center) Schematic diagram showing the scanning of sequential mass spectra through time; (Top) Mass spectrum corresponding to an individual fluid inclusion burst; (Bottom) Release of water and hydrogen sulfide as a function of time showing bursting inclusions over approximately one minute.

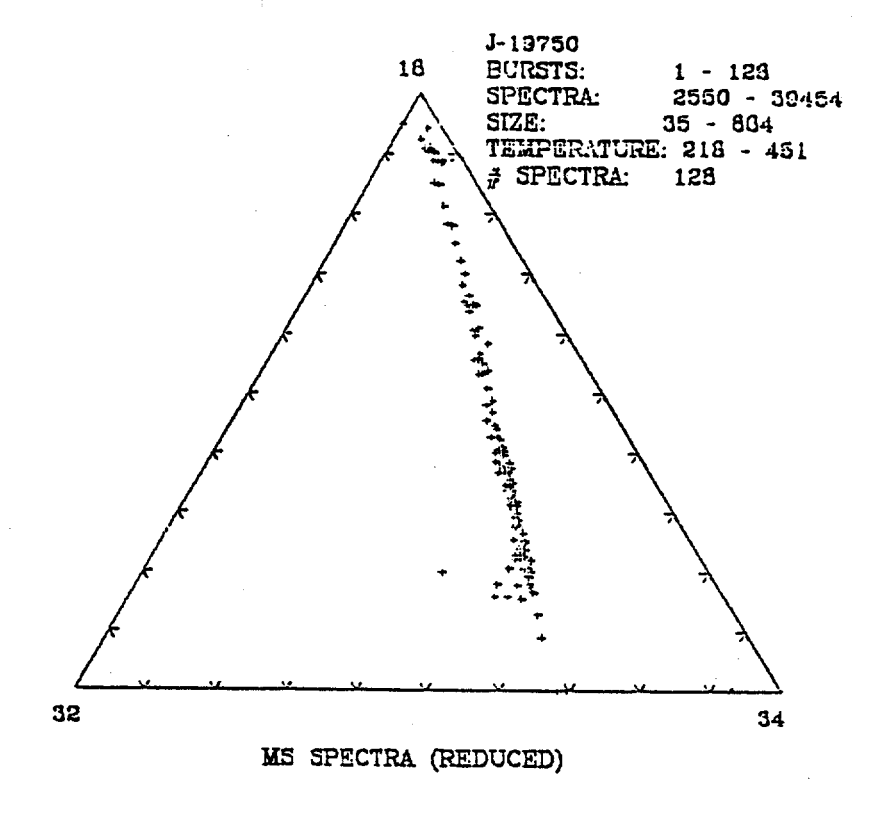


Figure 2: Ternary diagram showing gas compositions for 126 individual fluid inclusions in a calcite cement from the Smackover Formation at 19,750 ft. (6,020 m) The data show a mixing line between water (18) and hydrogen sulfide (32/34).

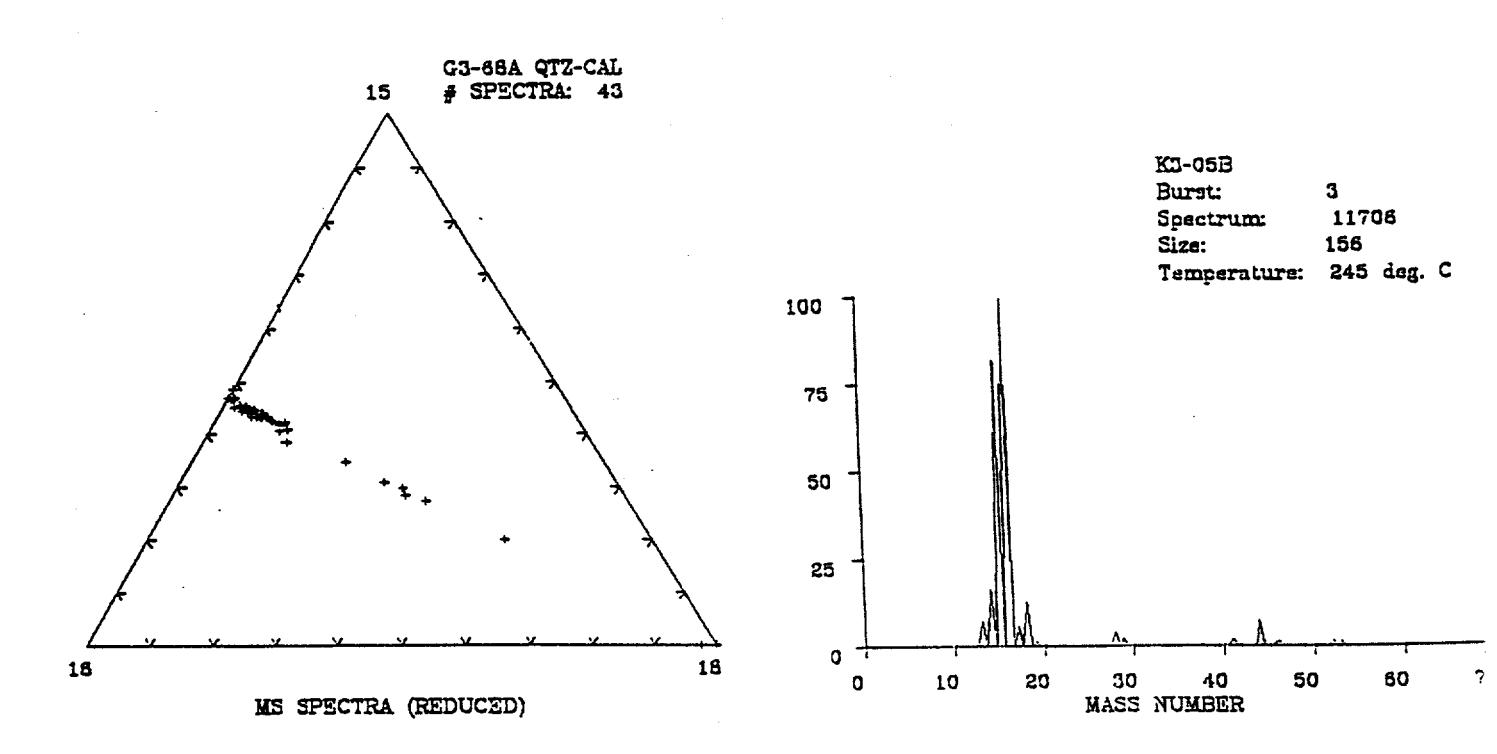


Figure 3: Compositions of gases in fluid inclusions in quartz samples from the Ghost Rocks melange, Kodiak, Alaska. (Left) Data for 43 individual inclusions showing a mixing line corresponding to variable methane/water ratios. (Right) Mass spectrum from an individual methane-rich fluid inclusion